THE UNIVERSITY
of EDINBURGH

Improved Uncertainty Analysis For Tidal Energy Project Development

Sunny Shah

April 2018

This thesis is submitted in partial fulfilment of the requirements for the award of an Engineering Doctorate, jointly awarded by the University of Edinburgh, the University of Exeter and the University of Strathclyde.
The work presented has been conducted under the industrial supervision of Black & Veatch Ltd. as a project within the Industrial Doctoral Centre for Offshore Renewable Energy (IDCORE).

THE UNIVERSITY
of EDINBURGH

Declaration

I declare that this thesis has been composed solely by myself and that it has not been submitted, either in whole or in part, in any previous application for a degree. Except where otherwise acknowledged, the work presented is entirely my own.

Sunny Shah

April 2018

Lay Summary

High investment risk is a key barrier to the commercialisation of the nascent tidal energy sector. An increase in investor confidence can unlock funding for early arrays, the lessons from which can provide further de-risking, leading to further investment. Investment decisions are based not only on the most likely expectations of a project's performance, but also on the likelihood of performance deviations. The likelihood of deviations is quantified using uncertainty analysis. This thesis recommends improvements to commonly used uncertainty analysis methods for quantifying the uncertainty in a tidal energy project's key investment metrics; energy yield, levelised cost of energy (LCOE) and internal rate of return (IRR). The potential for the commonly used methods to lead to misinformed investment decisions being made is demonstrated. Simpler solutions, which still provide an improved accuracy in uncertainty estimates, are also suggested for cases where the use of the most accurate method is not practical. The overall result is an increased confidence in the uncertainty estimates for key investment metrics used to appraise the financial viability of tidal energy projects.

Abstract

High investment risk is a key barrier to the commercialisation of the nascent tidal energy sector. An increase in investor confidence can unlock funding for early arrays, the lessons from which can provide further de-risking, leading to further investment. This thesis focussed on increasing investor confidence by improving the uncertainty analysis methods used to quantify the overall uncertainty in key investment decision metrics; energy yield, levelised cost of energy (LCOE) and internal rate of return (IRR).

A Monte Carlo Analysis (MCA) framework for tidal energy annual yield uncertainty analysis was developed and compared to the currently recommended ISO-GUM method. It was shown that key assumptions implicit in ISO-GUM are inaccurate for most realistic projects. Crucially, the resultant error provides an overly optimistic view of a project's P90 energy yield. By modelling a range of realistic projects, it was shown that the ISO-GUM P90 yield overestimate exceeds 2% for a maximum resource uncertainty between 4% and 11%, depending on the project, with increasing uncertainty leading to larger errors. It is difficult to judge accurately where within that range a given case crosses the 2% error threshold, as it is a complex function of numerous project specific variables. This undermines confidence in ISO-GUM results, even in cases where the method may be acceptable, because it is not possible to deduce the validity for a particular project *a priori*. MCA does not make the same assumptions and provides consistently

accurate results. A modification to the standard ISO-GUM process was also proposed as a simpler alternative to MCA, with an improvement in results compared to the standard method, but the residual error would still remain unquantified.

A generic cost modelling tool for probabilistic discounted cashflow analysis using MCA was also developed. The tool accepts user specified uncertainty distributions in a multitude of flexibly defined input variables defining a project's CapEx, OpEx, yield and finances to produce distributions representing uncertainty in LCOE and IRR. It was compared to commonly used deterministic methods for a realistic tidal energy project. MCA provides highly resolved results compared to the point estimates from deterministic methods. The improved decision support provided by MCA was demonstrated and the scope for misinterpreting the deterministic outputs was highlighted. The significance of several common cost modelling assumptions was tested and the difference between probabilistic and deterministic sensitivity analysis was highlighted. A probability weighted deterministic method was suggested and shown to provide useful indicative results at a reduced effort compared to MCA. Finally, the impact of the ISO-GUM P90 yield error on the P90 LCOE and IRR was quantified for several cases by propagating the ISO-GUM and MCA yield uncertainty distributions through the cost model.

MCA propagates input distributions through the functional relationship between the inputs and outputs. For any application, this reduces the unquantified approximations in the results compared to the simpler methods considered. This leads to not only more accurate results, but also a higher confidence in the results. The use of MCA is therefore recommended for annual yield and financial performance uncertainty analysis for tidal energy projects.

Acknowledgements

I am incredibly grateful to everyone whose input has made this thesis possible.

I would like to start by thanking my always helpful supervisors; Dr. Philipp Thies, Prof. Tom Bruce, Dr. Claire Cohen, Dr. Hannah Buckland, Dr. Scott Couch and Dr. Evangelos Boulougouris.

I would also like to thank the industrial partners involved in this project. The initial period with Marine Current Turbines (MCT) set the project off in the right direction. It was sad to see MCT's demise but I'm grateful to Mr. Andy Baldock for giving me the opportunity to continue my research with Black & Veatch (BV). It has been a pleasure and a privilege to work with BV, and I look forward to joining the team in 2018.

I thank my family for encouraging me to follow my interests and for strongly supporting my endeavours.

Last but not least, I'd like to thank my peers at the Industrial Doctoral Centre for Offshore Renewable Energy (IDCORE). We have been through a lot together and I look forward to crossing paths again, as colleagues and as friends.

Contents

List of Tables

List of Figures

List of Abbreviations

ADCP	Accoustic doppler current profiler
BV	Black and Veatch
CDF	Cumulative distribution function
CfD	Contract for difference
CLT	Central limit theorem
DCF	Discounted cash flow
DSCR	Debt service coverage ratio
EBITDA	Earnings before interest, tax and debt amortisation
FV	Future value
GUI	Graphical user interface
ICDF	Inverse cumulative distribution function
IRR	Internal rate of return
ISO-GUM	ISO-guide to the expression of uncertainty in measurement
KS	Kolmogorov-Smirnov
LCOE	Levelised cost of energy
MCA	Monte Carlo analysis
NPV	Net present value
PDF	Probability density function
ROI	Return on investment
PV	Present value
RNG	Random number generator
ROCs	Renewable obligations certificates

Chapter 1

Introduction

1.1 Low Carbon Electricity in the UK

A reliable and affordable supply of energy is critical for the survival and advancement of modern society. Electricity is an increasingly important part of the energy mix due to the increasing electrification of energy intensive applications, such as transport and heating (Energy UK, 2016; Baruah et al., 2014). Renewable sources of electricity are particularly important given the global ambitions to limit the global warming to no more than 2°C above pre-industrial levels, as defined in the Paris Agreement in 2015 (European Commission, 2015).

UK Government statistics on electricity consumption show an annual demand of 303 TWh in 2015 and a record 24.6% of this electricity was produced from renewable sources (Figure 1.1) (BEIS, 2016*a*). Electricity consumption was 17.9% of the total annual energy consumption. The UK is committed at an EU level to produce 15% of its energy from renewable sources by 2020 (DECC, 2011).

As defined in the Climate Change Act, the UK has a long term target to

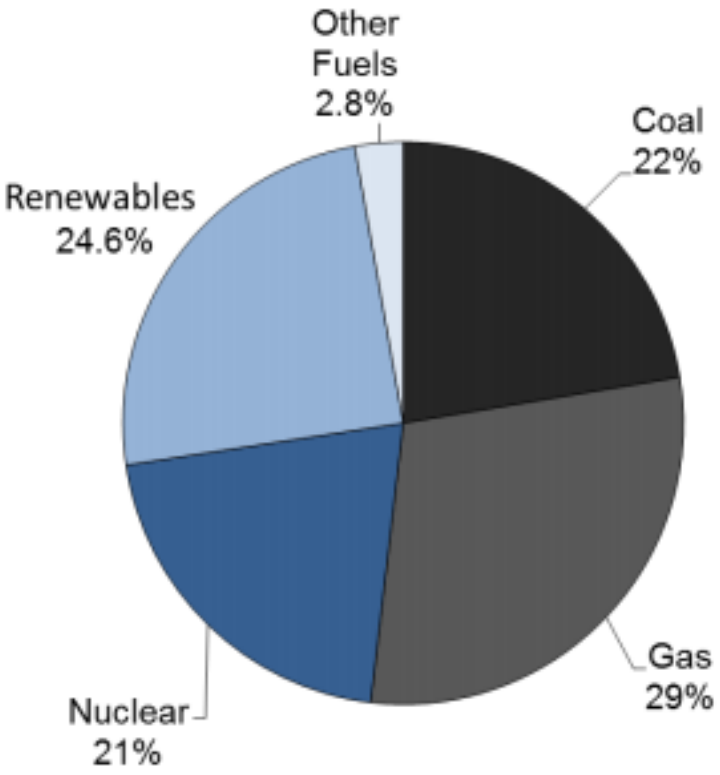

Figure 1.1: Sources of electricity supplied in the UK in 2015

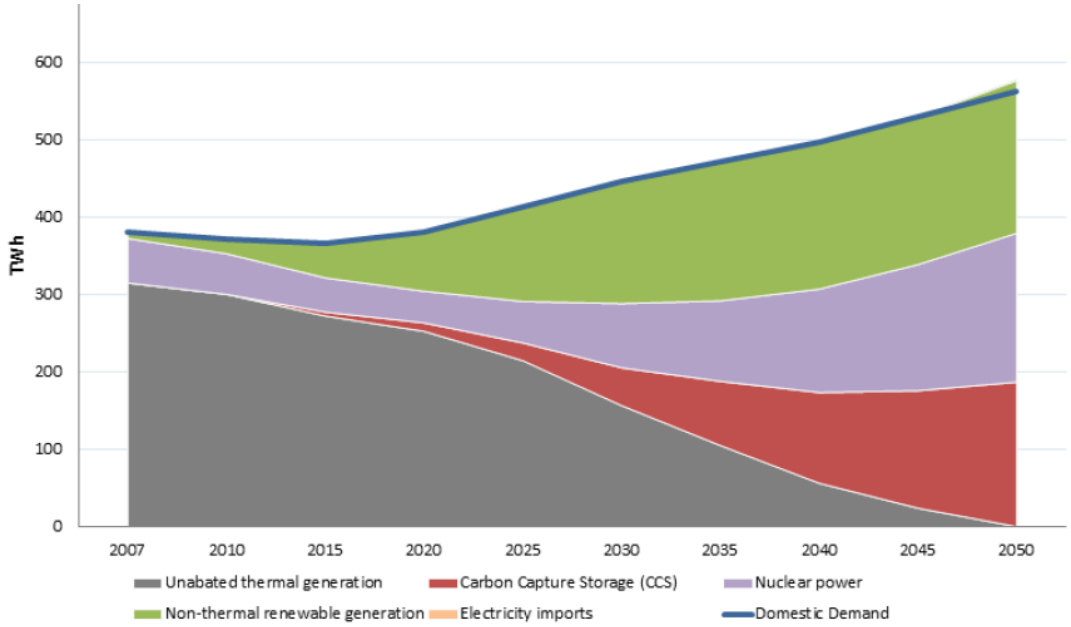

Figure 1.2: A possible electricity mix pathway up to 2050 to meet UK's carbon emission reduction commitments (Data generated using DECC 2050 calculator).

reduce greenhouse gas emissions by at least 80% by the year 2050, relative to a 1990 baseline (Parliament of the United Kingdom, 2008). Figure 1.2 shows a possible progression of the UK electricity mix up to 2050 that allows the UK to meet its obligations. Note the significant dependency on carbon capture and storage and nuclear energy. Failure of either of these two technologies for technical or political reasons would require an even greater contribution from renewable sources. Decarbonisation of electricity is a crucial part of the UK's long term strategy to meet these goals, in conjunction with other pathways, such as improved efficiency (Committee on Climate Change, 2016).

1.2 Global Context for Marine Renewables

Marine renewable energy refers to energy available for extraction from the seas. Five main technologies are in consideration at the present time for the exploitation of marine renewable energy (Borthwick, 2016):

1. Wave energy: exploitation of kinetic and/or potential energy available in ocean waves;
2. Tidal stream energy: exploitation of kinetic energy in the accelerated flow of seawater through narrow channels and around headlands;
3. Tidal range energy: exploitation of potential energy available in the rise and fall of tidal waters;
4. Ocean thermal energy: exploitation of the difference in temperature between deep cold seawater and warm surface water;
5. Salinity gradient energy: exploitation of energy available in the difference between salt concentrations (e.g. seawater and fresh river water in estuaries).

Note that offshore wind is sometimes considered as a source of marine renewable energy but is excluded in the definition above as it exploits space at sea, rather than energy available from the seawater itself. Futhermore, only wave and tidal technologies are discussed further as the other technologies are currently at a earlier stage of development.

The global theoretical generation potential from wave and tidal energy has been estimated as 32,000 TWh/year and 26,000 TWh/year respectively (Krewitt et al., 2009). Whilst the technically feasible resource is lower, the clear potential for marine energy to play a significant role in the future energy mix is illustrated

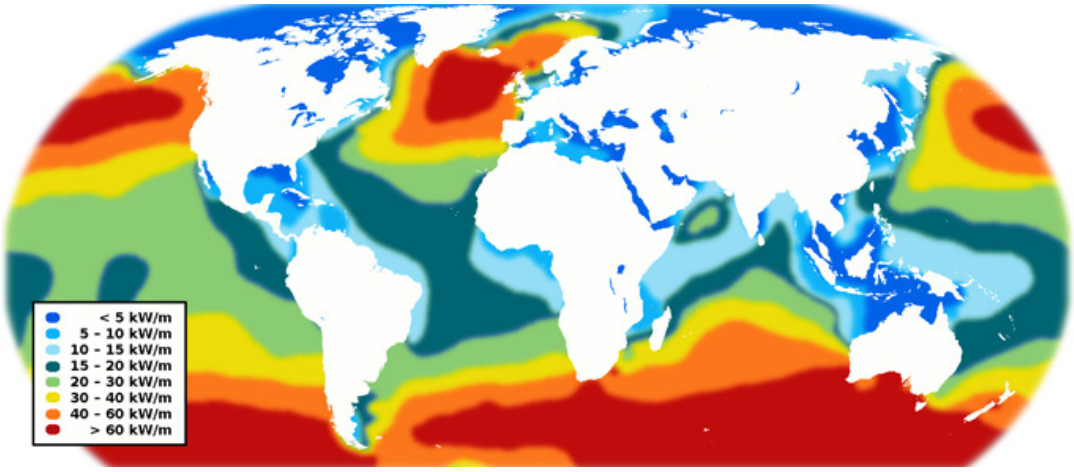

Figure 1.3: Map of global theoretical wave resource. Note the high power density close to the UK landmass (Albatern, 2017).

by comparing this potential to the global electricity consumption in 2016 of c. 20,000 TWh (European Environment Agency, 2016).

The level of support for the commercialisation of marine energy technologies varies greatly between countries around the world. The UK has a very high concentration of marine energy resource (Figures 1.3-1.5) and there has been a high level of political support for the sector historically. This has resulted in a high number of technology and project developers being based in the UK (Figure 1.6).

However, the sector faces significant challenges as it progresses towards commercialisation. The technology is yet to be proven to operate reliably at scale and over long periods of time; a prerequisite for commercial success. This is required to be achieved against a backdrop of reducing political support and increasing competition from drastic cost reductions in offshore wind energy (KPMG, 2017; Bloomberg New Energy Finance, 2017*a*).

Tidal stream and range technologies are more commercially advanced than

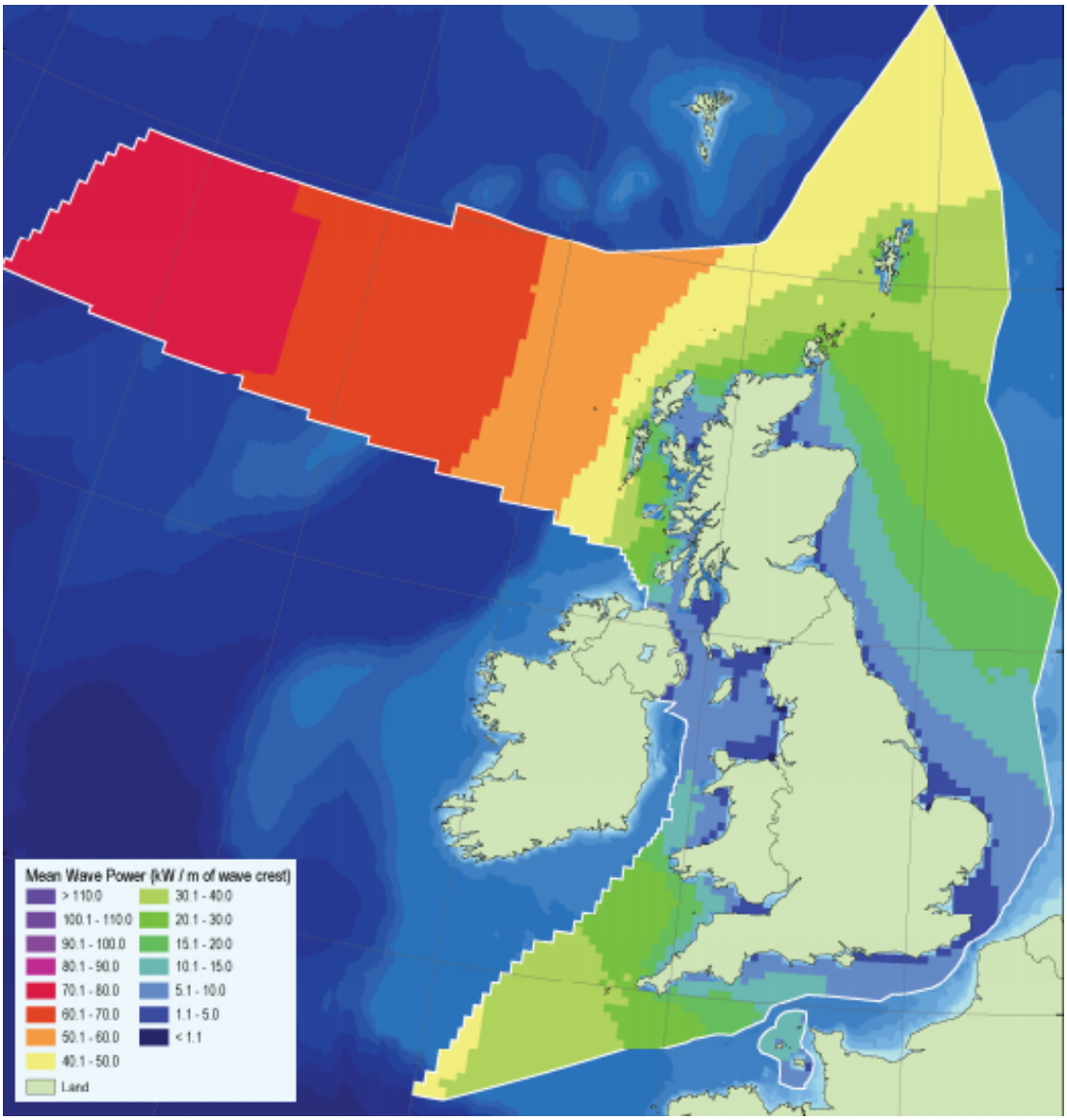

Figure 1.4: Map of UK's annual mean wave power (ABPmer et al., 2008). Reproduced from http://www.renewables-atlas.info/ Crown Copyright.

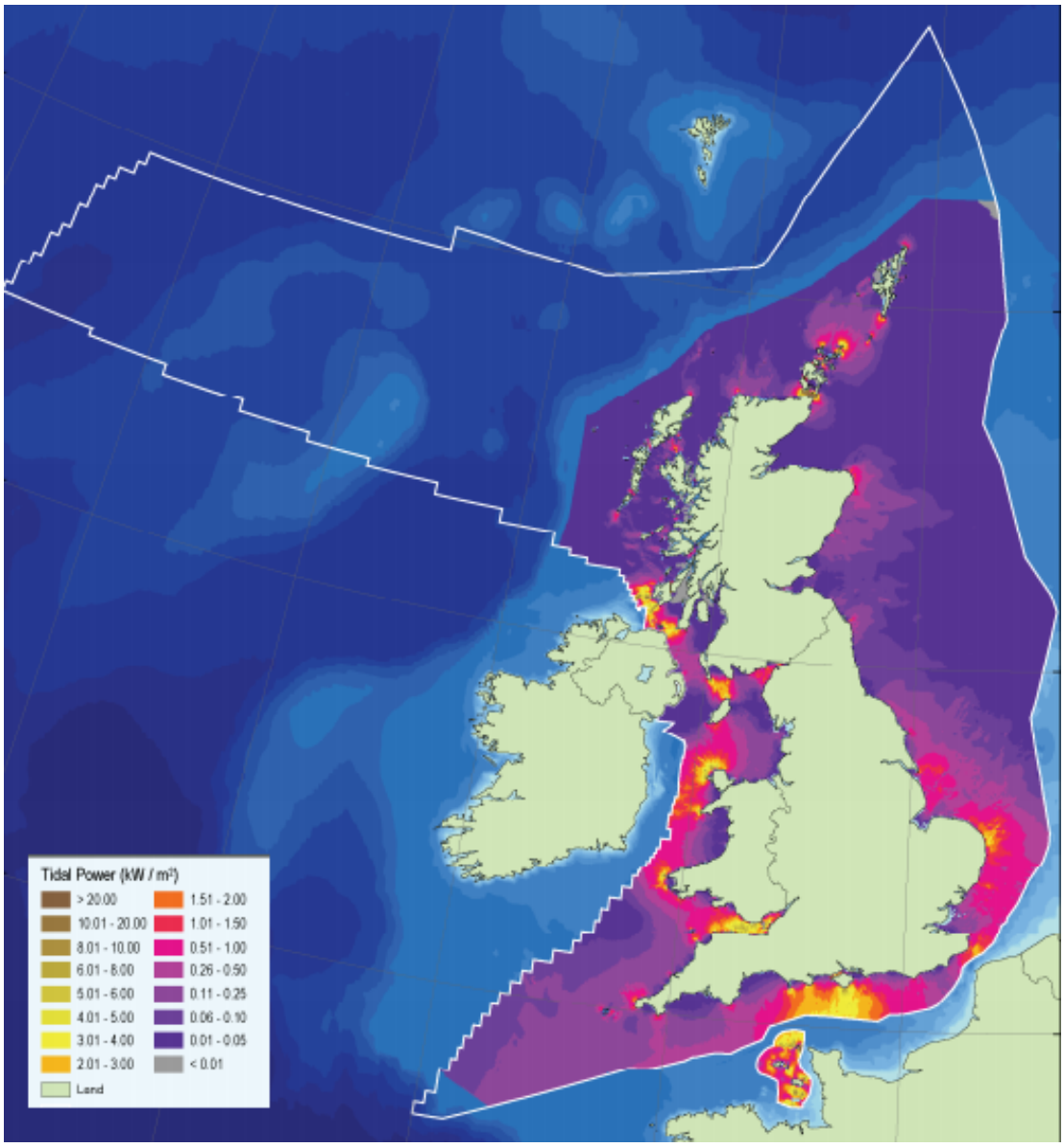

Figure 1.5: Map of UK's mean spring tidal power (ABPmer et al., 2008). Reproduced from http://www.renewables-atlas.info/ Crown Copyright.

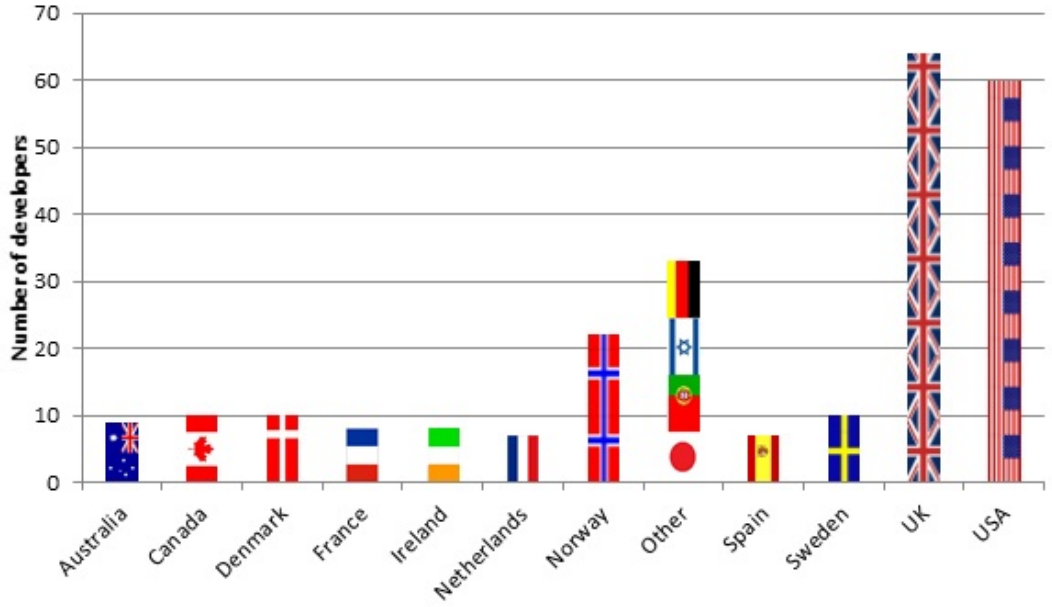

Figure 1.6: Nationality of marine energy device developers (Figure produced using analysis of data from the European Marine Energy Centre)

wave energy devices. Indeed, a commercially funded tidal stream project, MeyGen, is in operation with the next development phase close to reaching financial close and a tidal range project, Swansea Bay Lagoon, is also in the latter stages of financing (Smith et al., 2017). With increasing interest from the financial community, the uncertainty in forecasts related to tidal projects' performance is under greater scrutiny than wave energy projects, which are at a more experimental stage (Bloomberg New Energy Finance, 2017*a*). Whilst there are significant environmental uncertainties associated with tidal range projects, the technological uncertainties are lower; for example, due to transferable technology and experience from hydro projects (Poyry, 2014; Bloomberg New Energy Finance, 2017*b*). This thesis therefore focusses mostly on improving uncertainty analysis for tidal stream applications. Unless otherwise specified, 'tidal' henceforth refers to tidal stream energy only.

1.3 Rationale for Tidal Stream Energy

Tidal stream energy is recognised by the UK government as offering great future potential for decarbonisation of the country's energy mix (DECC, 2011). The perceived potential of tidal energy is due to the large available indigenous resource, reduction in exposure to volatile global energy markets, development of a skilled workforce and supply chain and relatively high public acceptance (Walker, 2011). Tidal energy in particular benefits from being highly predictable and the UK having one of the largest tidal resources in the world (RenewableUK, 2013; World Energy Council, 2016; IRENA, 2014).

It is difficult to quantify accurately the total potential deployment capacity for tidal projects, and estimates have varied greatly over the years (Iyer, 2011). It is currently thought that the UK can, in theory, generate 95 TWh/year from a total installed capacity of 32 GW of tidal stream projects (The Crown Estate, 2012). The practical capacity will inevitably be lower due to constraints such as environmental impact, disruption to other sea users and grid availability (Carbon Trust, 2011*b*). However, even with the pessimistic assumption of 2.8 GW installed capacity adopted by Carbon Trust (2006*b*), there is clear potential for significant contribution to the future energy mix.

The UK depended on energy imports to meet 37.4% of its primary energy demand in 2015, including from countries in the Middle East and Russia (Eurostat, 2017). This increases the country's exposure to geopolitical instability. Furthermore, 53% of UK's electricity was produced from fossil fuels (coal, natural gas and oil). This exposes the country to volatility in the global markets. The reduction of oil production from OPEC countries in 2016 causing higher oil prices and the closure of a North Sea gas pipeline in 2017 causing higher gas prices are two recent examples of such volatility (CNBC, 2017; Financial Times, 2017). Increasing

the contribution of indigenous energy sources, such as tidal energy, reduces this exposure and has a value greater than the value of the energy itself.

The UK has a highly skilled workforce and supply chain servicing the tidal energy sector (RenewableUK, 2017). This presents an opportunity to develop the local economies and also for the export of products and services to global growing markets. This is particularly important in the context of declining manufacturing jobs in the UK.

Tidal energy enjoys a high level of public acceptance, particularly in comparison to onshore wind energy (BEIS, 2016*b*). Projects can therefore be developed with lower opposition and this is another reason why tidal energy presents a good opportunity for contributing towards UK's renewable energy targets.

The development of tidal energy farms is therefore important from an environmental, industrial, political and social perspective. The specific focus of this thesis on improving uncertainty analysis for tidal energy project development is justified next.

1.4 Current Barriers to Commercialisation of Tidal Energy

Whilst the potential deployment capacity for tidal energy is vast, there is very little deployment at present. The total grid connected capacity of tidal stream devices operating in the UK at the end of 2016 was less than 10 MW (OES, 2017). With the exception of the commercially financed 6 MW array for the MeyGen project, deployments to date have been mostly for development and

testing purposes. A further 12 MW of capacity is under construction in Europe in 2017 (Ocean Energy Europe, 2017).

Over a decade of research, development and testing has resulted in a good understanding of the resource, device performance, marine operations and socio-environmental impacts, as summarised by Uihlein and Magagna (2016). However, it has not proved sufficient to attract the volume of investors and supply chain partners necessary for commercialisation. Many of the reasons for the current status of the sector being behind expectations can ultimately be attributed to high uncertainties withholding potential investors, as outlined below.

Sixteen years ago, Garrad Hassan (2001) estimated that 7.5 GW of capacity would be installed in the UK by 2010. This expectation was adjusted in 2006 to 'up to several gigawatts' of deployment in Europe by 2020, a large share of which 'could be in the UK' (Carbon Trust, 2006*b*). There are many such examples of the sector and individual companies not being able to deliver on overly ambitious targets. A culture of over-promising and under-delivering undermines confidence in the sector and is arguably one of the reasons why large multinationals and utilities such as Siemens, Alstom and Scottish Power withdrew from the sector after a brief period of active engagement (World Energy Council, 2016; Bloomberg, 2014). All participants in a survey of previous investors in marine energy companies indicated that they were unlikely to invest again in the near future (Leete et al., 2013).

Like other forms of renewable energy, tidal energy projects require long term investments. Such investments can only be made with confidence in a stable and supportive policy environment. The UK government has provided the most attractive market for tidal energy projects to date by offering high subsidies and numerous grants (HIE, 2016). Nonetheless, political risk was still cited as a major

risk factor in the survey of investors (Leete et al., 2013). The removal of ring-fencing of funds for wave and tidal energy projects in the contract for difference (CfD) budget allocations in 2016 is an example of a policy risk being manifested (ReNews, 2016)[1]. This change makes it substantially more difficult for a wave or tidal energy project to win a contract for the subsidy because it is required to directly compete on cost with offshore wind projects.

The high cost of tidal energy at present is also a barrier. The fact that only one project successfully reached financial close when five renewable obligation certificates (ROCs) per MWh (roughly equivalent to £300) were available suggests that the cost of energy was at least that high (Atlantis Resources, 2017) [2]. Conversely, the offshore wind industry delivered multiple large projects supported by 2 ROCs (UK Trade & Investment, 2015). Furthermore, the lifetime cost of a project is dependent on factors such as construction delays, reliability and maintenance issues which are difficult to confidently quantify due to the lack of operational experience at present. This uncertainty worsens the investment case.

In summary, the industry is characterised by high levels of uncertainty stemming from technical and external factors. Developers find themselves in a challenging situation whereby many of the issues can only be addressed by experience, but experience cannot be gained without investment. For example, cost reductions require scaling to benefit from learning effects and economies of scale. But scaling cannot be done without large investments. Large investments cannot be made until costs are low enough, and the risks well understood (Deloitte, 2014). Political support can help break the cycle, but current unstable policy

[1]CfD is the current UK mechanism for subsidising renewable energy projects whereby the operator is paid the difference between an agreed strike price and the prevalent wholesale electricity price to provide a long term stable cashflow

[2]ROC was the previous UK subsidy mechanism before CfD where an operator was provided an agreed number of certificates of fixed value

adds further to the uncertainty. Indeed, high uncertainty has been identified as a major barrier to the commercialisation of the nascent sector (RenewableUK, 2013). High uncertainties lead to higher borrowing costs, or investors look for alternative investment opportunities (The World Bank, 2012).

The need for risk reduction is recognised by the sector and much work has been carried out recently to address specific technical, environmental and socio-economic factors (Wyatt, 2014; Uihlein and Magagna, 2016; MeyGen, 2017). This thesis focusses instead on improving the uncertainty analysis methods used to quantify the holistic uncertainty in investment decision metrics such as LCOE and IRR.

1.5 Increased Confidence Through Improved Uncertainty Analysis

A demonstrable improvement in the accuracy of uncertainty estimates would allow investment decisions to be made with higher confidence. An increase in investor confidence can unlock funding for more early arrays, the lessons from which can provide further reduction in perceived risk, leading to further investment. Whilst it is by no means the only route to risk reduction, it is relatively unexplored to date and has the potential to improve the investment case for tidal energy.

Poor uncertainty analysis can lead to poor decisions being made, even if the best methodologies are used in all other processes. In other words, the choice of uncertainty analysis method can alter the decision metrics, with all other parameters being equal. It is therefore important to ensure that the improvements being pursued in other areas are not undermined by the uncertainty analysis process, and the best possible decision support is made available to investors.

1.6 Research Motivation

This research project was initially proposed by Marine Current Turbines, a leading technology developer, with the primary motivation being an improved understanding of project performance uncertainties. This would allow the company to offer suitably structured performance warranties with confidence by understanding the likelihood of adverse performance (and therefore claims) as a result of uncertainties in the resource assessment and turbine performance in service.

However, the research direction changed significantly after 9 months due to Marine Current Turbines ceasing operations. The project was then continued under the supervision of Black and Veatch, an engineering consultancy.

Black and Veatch had an interest in not only the turbine performance uncertainty but also the holistic project development cycle. This was due to the company having a range of clients ranging from technology developers to funders and governments. Research outputs that could be applied generically to any technology type were more important than highly specific analysis of a particular turbine type.

An overarching motivation for both companies was a desire to facilitate investment into the sector. Both companies viewed a thorough appraisal of current uncertainty analysis methods and alternatives as a currently neglected area of research that could provide much needed confidence to potential investors.

1.7 Aim, Objectives and Scope

1.7.1 Aim and Objectives

The aim of this thesis is to increase investor confidence in uncertainty estimates for tidal energy investments. More specifically, this is achieved through improvement in annual yield uncertainty analysis and financial performance uncertainty analysis.

For both of the applications mentioned in the aim, improvement in the uncertainty analysis is achieved by:

- Identifying and appraising currently used methodologies for uncertainty analysis, and possible alternatives with scope for improved results;
- Identifying, and where necessary, developing tools to implement the uncertainty analysis methods identified;
- Quantifying differences in results derived from these methods by use of realistic case studies;
- Identifying and appraising reasons for observed differences in results;
- Recommending the most suitable methods with consideration of accuracy in results, and also their practical applicability in an industrial context.

1.7.2 Scope

The scope of this thesis was selected to be yield and financial performance analysis because the outputs of these processes provide the key investment decision metrics; annual yield estimate, levelised cost of energy (LCOE) and internal rate

of return (IRR) [3]. The scope selection was also guided by the industrial input to this project.

The thesis focuses on tidal stream technology, but many aspects are equally applicable to other technologies, and in some instances this is highlighted. Where required, it is assumed that projects are located in the UK market, but most discussions are market agnostic.

The identification and quantification of uncertainties is a large subject area in itself. This thesis focuses largely on the accurate processing of the uncertainties once they are quantified. This is justified on the basis that this research is industrially focussed for engineering consultancy applications. In this context, it is acceptable and commonplace for expert judgement and pragmatism to be used to quantify uncertainties in parameters that are not otherwise easily quantified.

1.8 Thesis Structure

The thesis is structured in 6 chapters. Chapter 2 provides the necessary theoretical foundation and outlines generic uncertainty analysis methods that are later used for specific applications.

Chapter 4 focusses on uncertainty analysis for a project's annual yield estimates. The suitability of two alternative methods for uncertainty analysis is compared by applying them to a range of realistic projects and with consideration of the equivalent practice in the more established wind energy sector.

Chapter 5 focusses on uncertainty analysis for a project's financial performance.

[3] LCOE is a technology agnostic measure of breakeven cost of energy and IRR is the return on investment in a projec. Detailed definitions of these terms and further technical considerations are provided in Section 4.2

A generic and flexible stochastic cost model is developed and the results for a representative case study are compared to simpler commonly used methods.

Chapter 6 links the models developed in preceding chapters. The annual yield uncertainty calculated by the models in Chapter 4 is fed into the cost model in Chapter 5 to determine the resultant exposure to error in key project performance metrics.

The thesis concludes with a general discussion and by highlighting the contribution to knowledge provided and its industrial impact. The themes and results presented earlier are drawn together to derive the final conclusions and to identify the limitations.

Figure 1.7 shows a flowchart of the thesis structure. Note that Chapter 4 and Chapter 5 cover topics that are quite distinct. They are presented in such a way that they can be read independently by including the chapter specific results and discussion within each chapter. This structure then logically leads the narrative to the analysis in Chapter 6, which relies on an understanding of the concepts in Chapter 4 and Chapter 5.

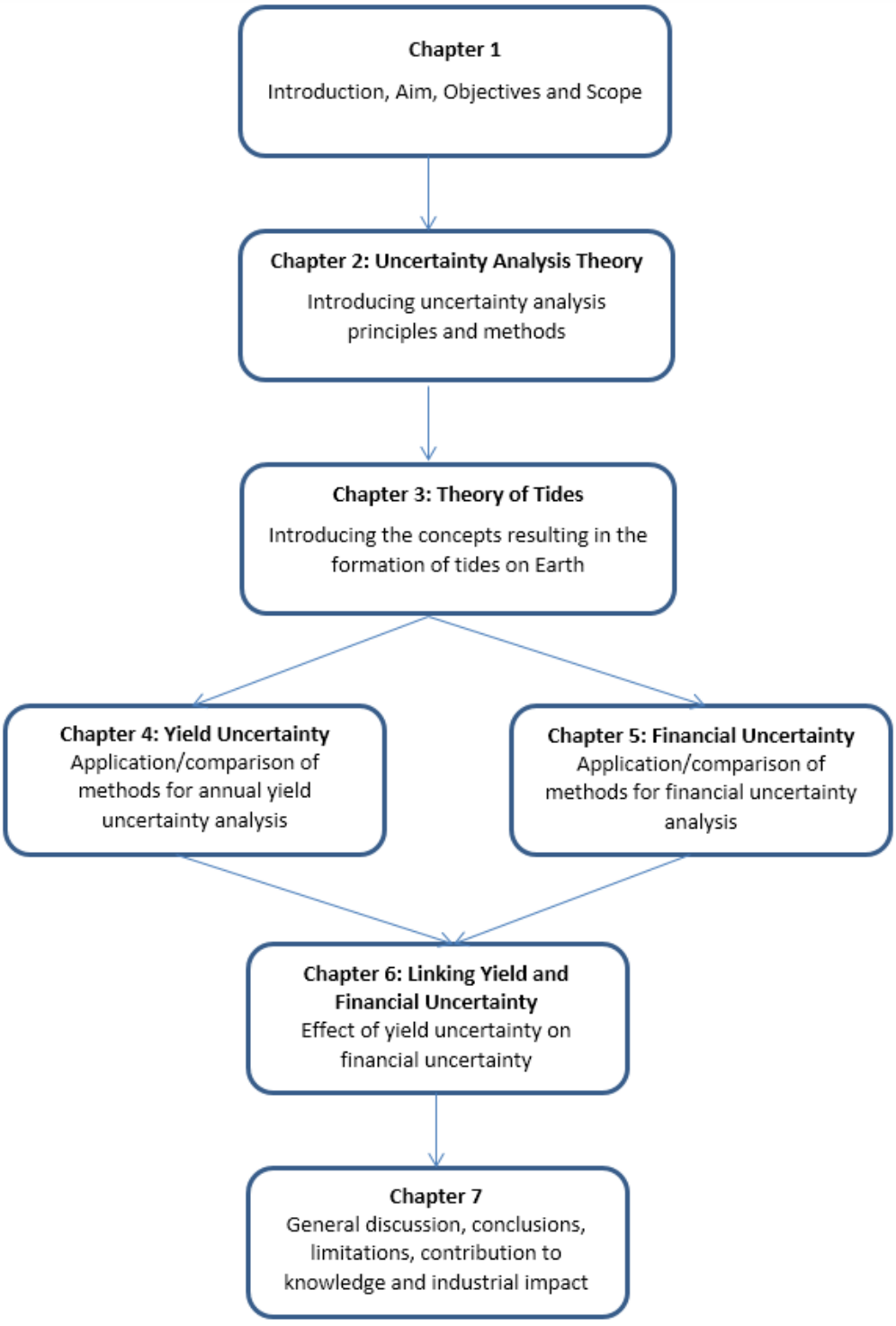

Figure 1.7: Flowchart of thesis structure

Chapter 2

Uncertainty Analysis Theory

2.1 Introduction

Uncertainty is inherent in almost all facets of life, but is particularly high when estimating future occurrences and/or events with little precedence. In brief, it results from insufficient information, incorrect assumptions, natural variability and indeterministic human behaviour (Loucks et al., 2005). Uncertainty analysis techniques are used to relate the uncertainties in variables affecting an outcome to the resulting uncertainty in the final outcome. This allows statements to be made about the likelihood of particular outcomes and also the plausible deviations from it. This information is essential for making decisions with confidence under uncertainty. Nonetheless, a robust appraisal of the uncertainties is often neglected in practice (Goldstein, 2016).

The tidal energy sector requires developers and investors to estimate time dependent parameters based on limited previous experience. As a result of the sector's immaturity, there is little empirical data, imperfect knowledge and there is considerable exposure to natural variation, such as weather. As such, both

design and investment decisions in the sector are made under very high levels of uncertainty. Good uncertainty analysis is therefore crucial for the sector because any estimates provided without indication of the associated uncertainty are not only incomplete, but can also be misleading.

Uncertainty analysis is a broad term, but generally it involves identifying all individual sources of uncertainty affecting an outcome, quantifying the uncertainty in each variable and finally propagating the uncertainties to compute the uncertainty on the final outcome (Magnusson, 1997). As justified in the thesis scope (Section 1.7.2), it was generally assumed that the relevant uncertainties have been identified and quantified. The focus therefore was on the uncertainty propagation. References such as Sullivan (2015) and Smith (2014) are recommended for the uncertainty quantification theory.

The aim of this chapter was to generically cover the theoretical foundation of probability, statistics and uncertainty analysis methods that were then applied to relevant applications in following chapters. Note that concepts relevant only to a particular application were covered in the appropriate chapters. Some key terms were defined and a description of the uncertainty analysis methods being considered was provided.

2.2 Probability and Statistical Sampling

2.2.1 Background on Probability

Probability is the mathematical framework for describing events with an uncertain outcome. It is related to statistics but distinct in that probability is concerned with predicting the likelihood of a future occurrence whereas statistics is used to infer from past events.

A fundamental concept underpinning probability theory is sample space. It represents a collection of all possible outcomes in a random experiment, where an experiment is a broadly defined term which may range from a lab test to a computer simulation (Ash, 2008). An event is a subset of the sample space and may consist of single condition (e.g. rolling a six on a die) or more complex conditions (e.g. rolling a number greater than 4 or rolling the same number three times in a row). A union of events A and B is a set consisting of A or B or both whereas an intersection of A and B consists of both A and B. Events in a sample space that have no common points can be referred to as mutually exclusive (e.g. a head and a tail outcome in a single coin toss). For a discrete sample space, the sum of probabilities of all events is equal to 1 and the probability of event x is $p(x)$.

Since the experiment is random, its outcome cannot be specified exactly before it is performed but probability can be used to describe the various outcomes. The frequentist interpretation of probability states that the observed frequency of occurrence of event A should converge towards the probability of occurrence of A as the number of repetitions of the experiments increases (Hansen, 2005). The probability measure is not given objectively by the experiment in Bayesian interpretation because it also reflects the knowledge available before conducting

the experiment. The two interpretations are fundamentally different and only the frequentist interpretation is applied in this thesis.

A random variable can be used to refer to the unrealised outcome of a random experiment. The value of the variable is described stochastically by a probability distribution and the particular value of the variable within the sample space is only known after the experiment is complete. The distribution describing the random variable is therefore the probability measure describing it. The distribution may be binary, continuous and/or multivariate.

2.2.2 Background on Statistical Sampling

Sampling is a fundamental aspect of statistics and its requirements stem from the fact that it is not practical to study every individual in a population or every event in a sample space. A representative subset of the population, a sample, is therefore selected and the method of sampling used affects the chosen sample. Data derived from a sample are treated statistically to infer information about the population and to understand the confidence in the inference (Sudman, 1976).

The size of the random sample and the nature of the population affects the probability of drawing a conclusion that is erroneous. In general, the larger the sample, the higher the statistical rigour of the inference and ability to detect small differences in the sample. The random error in a sample stems from the fact that two samples of the same size from the same population will not necessarily be identical. A smaller random error gives higher confidence that the sample is representative of the population or that differences observed in the population are not due to random variation.

Random sampling can be carried out in the physical domain (e.g. sampling human

population) and also numerically for computer simulations. Random Number Generators (RNGs) are used to produce a sample of random numbers using a computer. Psuedo-RNGs are typically used for computational random sampling because it is difficult for computers to a generate truly random sequence given that a computer programs work on the basis of following prescriptive algorithms (Haahr and Cherry, 1999). Psuedo-RNGs therefore use mathematic formulae or pre-calculated tables to generate the psuedo-random sequences. This is simpler and more computational efficient than using a true RNG based on randomness in the physical world and the outputs also have the benefit of being reproducible. Given its fundamentally deterministic nature, psuedo-RNGs have a periodicity after which the sequence will be repeated but the periodicity is sufficiently long for its effect to be negligible for most practical purposes (Haahr and Cherry, 1999). Whilst the psuedo-RNG will typically generate a sample with uniformally distributed values between 0 and 1, techniques such as inverse transform sampling can be used to transform the uniform sequence into a random sample from a different type of distribution (Wicklin, 2013). This is discussed in more detail in Section 2.4.3.

2.3 Uncertainty Definitions

2.3.1 Uncertainty, Risk and Error

The terms ‘error’ and ‘risk’ are often used interchangeably with ‘uncertainty’. However, it is important to distinguish the differences between the terms at the outset. There is considerable variation in the definitions of the terms between sources and in particular, in relation to the application (Goldstein, 2016). The following definitions are used in this thesis and the primary application of the terms is to outcomes of measurements and model estimates.

Error

The error in a measurement or calculation is the difference between the individual result and the true value. In theory, the true value cannot be known. However, in practice, a reference value (such as manufacturer brochure or published data table) can be used in certain cases (Ellison and Williams, 2012). A known error can be used to apply a correction to the result and any unknown error is a source of uncertainty.

Uncertainty

Uncertainty is the indefiniteness in a measurement or calculation (NASA, 2015). It results from a lack of knowledge and is characterised by a probability distribution, range or interval. It cannot generally be used to correct the original result.

Risk

Risk is differentiated from uncertainty as an outcome with not only an associated likelihood of occurrence, but also a consequence (Shermon, 2016). An outcome with high uncertainty and low consequence may have comparable risk to an alternative outcome with low uncertainty and high consequence.

2.3.2 Probabilistic Representation of Uncertainty

Figure 2.1 shows the representation of uncertainty using a probability distribution. It can be used to illustrate the definitions below that are discussed throughout this thesis. Only sufficient detail to support the narrative is presented. Further details on the basic theory can be found in textbooks, such as Holický (2013).

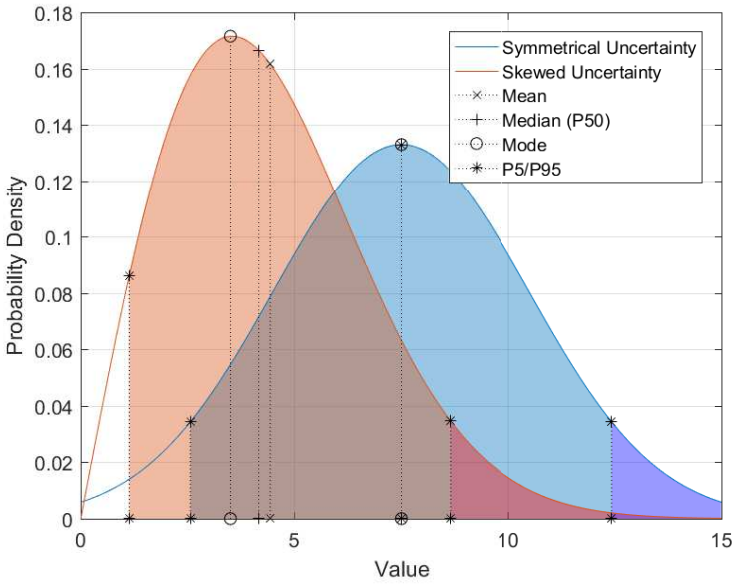

(a) PDF

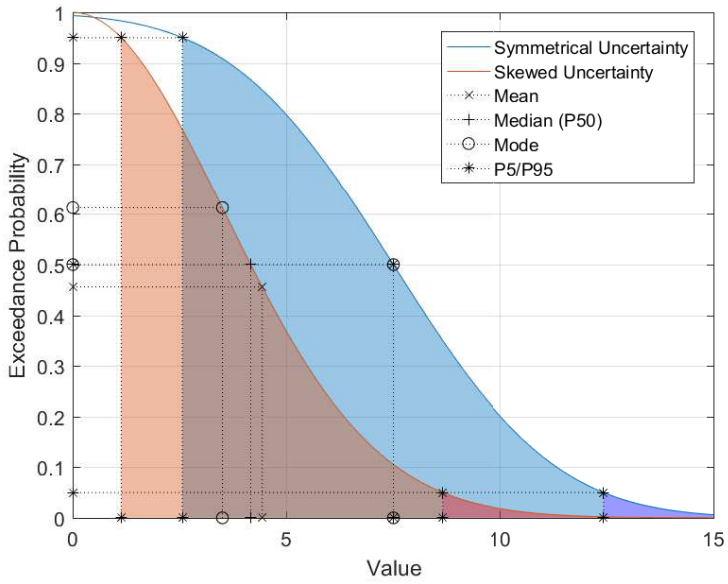

(b) ICDF

Figure 2.1: Probabilistic representation of uncertainty. Note the difference in the mean, mode and median value for the skewed distribution. Also note that the area bounded by the P5 and P95 (shaded light) represents the range for a 90% confidence level and the entire area including the dark shading shows the P95 (single sided 95% confidence interval).

Probability Distribution

A probability distribution links each outcome in an event with its probability of occurrence. Probability distributions can be discrete or continuous. Discrete distributions have a fixed set of possible outcomes (such as results of a coin toss), whereas an outcome in a continuous distribution can assume any value within a range (such as height of an animal). Only continuous distributions are required for the considerations in this thesis. A probability density function (PDF) is the mathematical function that defines the probability distribution. It provides the probability density of a particular outcome. The cumulative distribution function (CDF) is the integral of the PDF, and is therefore the area under the PDF curve. It gives the probability that the outcome is smaller than or equal to the value at which it is evaluated. The inverse cumulative distribution function (ICDF) provides the value associated with a particular cumulative probability.

Mean, Median and Mode Values

The mean, median and mode values can be used to assess the base case. The three values are identical for a symmetrical distribution, but the mode is lower than the median and the median is lower than the mean for a distribution which is skewed to the right, as seen in Figure 2.1.

Minimum and Maximum Values

Minimum and maximum values are used to assess the best and worst case. The range is the difference between the maximum and minimum. However, many distributions have infinite tails so the theoretical minimum and maximum value cannot be quantified. Also, the extreme values with near-zero probability are less

interesting practically than a more likely extreme case, but the magnitude of the range can indicate the total uncertainty present.

Standard Deviation and Confidence Intervals

The standard deviation is a measure of the spread in a given distribution. A large standard deviation implies a higher spread, and therefore a wider distribution. Standard deviation is defined mathematically as:

$$\sigma = \sqrt{\frac{1}{N}\sum_{i=1}^{N}(x_i - \mu)^2} \tag{2.1}$$

where σ is the standard deviation, x_i represents the value of each outcome in the event, μ is the mean outcome and N is the total number of outcomes in the event. A standard deviation representing the uncertainty in a parameter is known as the standard uncertainty.

A confidence interval indicates the probability (confidence level) that an outcome lies within a particular range. For example, a confidence interval of $\pm$ 1 unit with a 90% confidence level indicates that there is a 90% chance of the outcome being within 1 unit of the mean (symmetrical distribution assumed). Figure 2.1 provides an example of a 90% confidence interval.

Percentiles and Exceedance Probability

The n^{th} percentile of a distribution is the value for which n% of the sample is smaller. Conversely, n^{th} exceedance probability, Pn, is the value for which n% of the sample is larger (Dobos et al., 2012). Therefore the 5^{th} percentile of a distribution is equal to the P95 value. There is a 5% probability of a sampled

value being smaller or a 95% probability of the sampled value being greater. By definition then, the P50 is equal to the median.

Note that percentile and exceedance probability are sometimes used interchangeably in literature and in practice, i.e. 5^{th} percentile and P5 may refer to the same value. The distinction defined above is observed throughout this thesis. Furthermore, a high Pn (P95 or similar) is sometimes used to represent the pessimistic case regardless of context. This approach is only consistent with the definition above for cases where the low end of the distribution represents the unfavourable outcome. For example the P95 of a profit distribution represents the pessimistic case because low profit is undesirable. However, the P95, defined as above, for a cost distribution represents the optimistic case. Always representing the pessimistic case by a high Pn therefore requires inverting the mathematical definition depending on the context. In this thesis, an approach that is mathematically consistent with the above definition is used. Therefore, the P95 (or similar) value may represent the optimistic or the pessimistic case for a variable.

Deterministic Values

When insufficient information is available to define a distribution, deterministic values with undefined confidence intervals can be considered. Single point, static values are used and it is implicitly assumed that there is no probability of a different outcome.

2.3.3 Commonly Used Uncertainty Distributions

Four commonly used distributions for representing uncertainty are introduced below and presented in Figure 2.2. These distributions are chosen because they

are suitable for subjective assignment and most routinely found to be used in practice. Distributions typically defined by fitting to empirical data (such as Weibull) are not considered because such data is not used in this study.

Normal Distribution

A Normal (Gaussian) distribution (Figure 2.2a) is defined by its mean and standard deviation. It is a symmetrical distribution with equal likelihood of occurrence above and below the mean and about 68% of the outcomes are within 1 standard deviation of the mean. The PDF is defined as:

$$P(x) = \frac{e^{\frac{-(x-\mu)^2}{(2\sigma^2)}}}{\sigma\sqrt{2\pi}} \tag{2.2}$$

where x is an outcome, μ is the mean and σ is the standard deviation.

It can accurately represent a very wide range of parameters because it describes many random phenomena, and due to the effects of the central limit theorem (CLT). The CLT states that the sum of a large number of independent distributions leads to an approximately normal distribution irrespective of the nature of the underlying distributions (Cowan, 1998).

An example of the Normal distribution being used in the tidal energy sector is for the representation of uncertainty in measurement of flow velocity and electrical losses in array cables. The symmetrical shape and infinite tails of this distribution make it particularly suitable for representing these uncertainties.

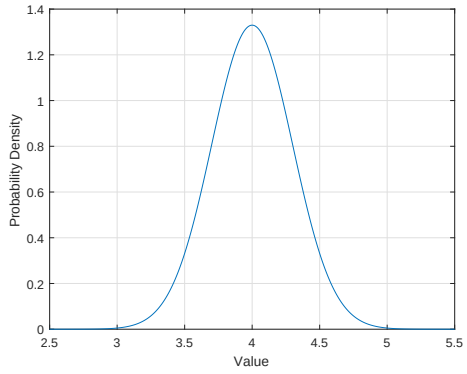

(a) Normal - Mean=4, Std Dev=0.3

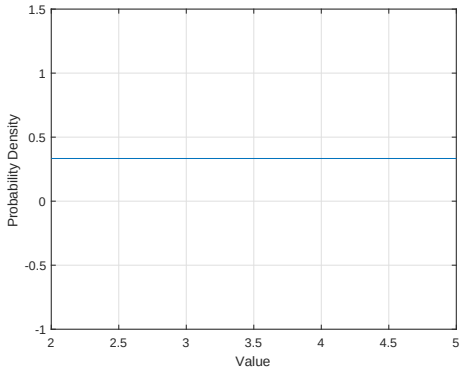

(b) Uniform - Min=2, Max=5

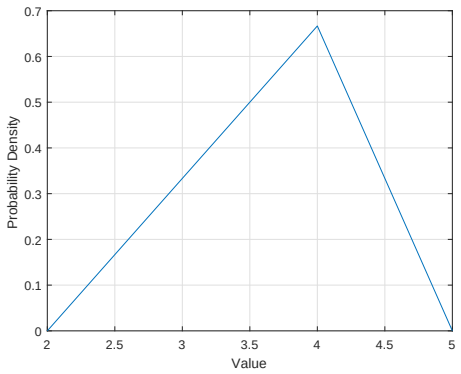

(c) Triangular - Min=2, Mode=4, Max=5

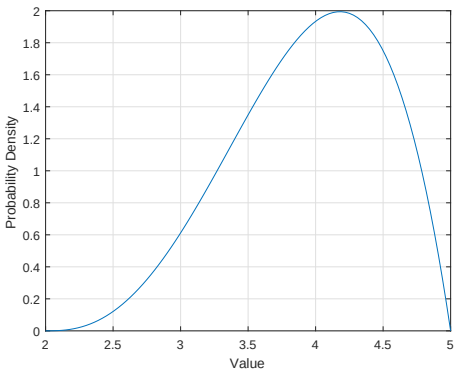

(d) PERT - Min=2, Mode=4, Max=5

Figure 2.2: Representing uncertainty using different types of probability distributions

Uniform Distribution

In a uniform (rectangular) distribution, all values within a specified range have an equal probability of occurring (Figure 2.2b). The PDF is defined as:

$$P(x) = \frac{1}{c-a} \text{ for } a \leq x \leq c \tag{2.3}$$

where a and c are the minimum and maximum respectively.

It is most appropriate to use when the range of outcomes is known, but no outcome is more likely to occur than the other. The rolling of a single die is an example where a uniform distribution provides an appropriate representation. An example relevant to the tidal energy sector is when assumptions must be made for capital expenditure based on a preliminary quote from a supplier. The cost may be provided as a range depending on the final structure of the contract and there is no expectation of a most likely final cost within that range.

Triangular Distribution

A triangular distribution (Figure 2.2c) is defined by the minimum, maximum and mode values. It may also be defined by low and high percentiles, rather than the minimum and maximum values. There is a linear reduction in likelihood from the mode towards the two tails, but the distribution does not necessarily have to be symmetrical. The PDF is defined as:

$$P(x) = \frac{2(x-a)}{(b-a)(c-a)} \text{ for } a \leq x < b \tag{2.4}$$

$$P(x) = \frac{2(c-x)}{(c-b)(c-a)} \text{ for } b \leq x \leq c \tag{2.5}$$

where a, b and c are the minimum, mode and maximum respectively.

The Triangular distribution is especially useful for cases where the relationship between variables in known (intuitively or through experience) but sufficient data is not available to infer statistical properties with confidence. Furthermore, it is useful for representing situations where the mode is biased towards the minimum or maximum value by specifying a skew. There is a gradual reduction in the likelihood of occurrence towards the tails (due to the linear decrease) compared to a Normal distribution or a PERT distribution (explained next). Appropriate uses of the Triangular distribution include project management applications where the critical path of a project is assessment by assigning Triangular distributions to each activity, or for capital expenditure estimation for industrial projects (such as tidal energy investments).

PERT Distribution

A PERT distribution (Figure 2.2d) is also defined by the minimum, maximum and mode values, or by the percentiles. In contrast to the triangular distribution, however, the tapering of likelihood towards the tails is not linear. A PERT distribution provides a higher density of occurrences closer to the mode than a triangular distribution defined using the same parameters. A symmetrical PERT distribution is similar, though not numerically identical, to a Normal distribution. PERT distributions can be more useful in some applications than Normal distributions because it is more intuitive to subjectively define the minimum, mode and maximum than a standard deviation, and because skews can also be represented easily.

The PERT distribution is a form of the Beta Distribution. The Beta distribution

PDF is defined as:

$$P(x) = \frac{x^{\alpha-1}(1-x)^{\beta-1}}{B(\alpha,\beta)} \tag{2.6}$$

where α and β are Beta distribution shape parameters (Equations 2.8 and 2.9) and B, the Beta function, is as defined in Equation 2.10. The PERT distribution is a particular case of the Beta distribution such that (Buchsbaum, 2012):

$$mean = \frac{a+4b+c}{6} \tag{2.7}$$

where a is the minimum, b is the mode and c is the distribution maximum. This constraint reduces the possible distributions such that:

$$\alpha = \frac{4b+c-5a}{c-a} \tag{2.8}$$

$$\beta = \frac{5c-a-4b}{c-a} \tag{2.9}$$

$$B(\alpha,\beta) = \int_0^1 x^{\alpha-1}(1-t)^{\beta-1}dt \text{ for } \alpha,\beta > 0 \tag{2.10}$$

This allows the Beta equivalent PERT distribution to be defined using the intuitively specified minimum, mode and maximum values.

The PERT distribution has similar applications to the Triangular distribution as both are defined using the same level of inputs. The PERT distribution is more appropriate than the Triangular distribution for cases where a steeper reduction in likelihood of occurrence towards the tail is more representative than a linear decrease.

2.4 Uncertainty Analysis Methods

The uncertainty propagation process can begin once the input parameters affecting the outcome (output) have been identified and the uncertainty in each is quantified. In general, the input uncertainties are propagated through the functional relationship between the inputs and outputs to compute the uncertainty on the output variable. The most suitable method for a given application depends on the quality of the input uncertainty data and the nature of the functional relationship. The level of confidence required in the outputs and the resources available for the task are also considerations when choosing the most suitable method, as discussed below.

Three uncertainty propagation methods are described below; deterministic (simple and weighted), ISO-guide to the expression of uncertainty in measurement (ISO-GUM) and Monte Carlo analysis (MCA). Each of these methods is either the most commonly used method for the applications considered in the thesis, or is considered to offer an improvement over the established method. Discussions specific to the particular applications and their comparisons are presented in Chapters 4-6. Only the generic concepts that are common to all chapters are introduced here.

In addition, the First and Second Order Reliability Methods typically used for structural and mechanical reliability analyses are also introduced as there are some common parallels with the applications in consideration in this thesis.

2.4.1 Deterministic Methods

A deterministic (static) method solves the functional relationship between the input variables and the output using single point estimates for each input, thus

giving a single point deterministic output. In its simplest form, a deterministic analysis may be carried out using the central values for each variable (P50 or mean). However, this does not necessarily result in the P50 or mean output, and it does not provide any information on the uncertainty in the output.

Some knowledge of the uncertainty may be gained by rerunning the static analysis for different points. For example, an optimistic/pessimistic output value can be calculated using optimistic/pessimistic input values respectively. However, it does not account for the interdependence between the inputs such as the fact that it is unlikely for the worst case outcome for each input variable to occur simultaneously if they are independent and uncorrelated (Palisade Corporation, 2017*b*). This type of analysis only provides a few discrete snapshots of the full range of outcomes, and the associated probabilities of occurrence are unquantified. However, a deterministic analysis may be the only option available if there is insufficient information available to assign probability distributions to input variables with confidence. Furthermore, it is also valuable for scenario analysis where discrete values for inputs are known. Finally, it is a very simple process compared to the other methods described next, and for some applications, a rough and quick method is most appropriate (Uusitalo et al., 2015).

A probability weighted static analysis may be carried out for improved results if the distribution of input uncertainties is known, or at least the likelihood of occurrence for a particular magnitude of deviation is known. The magnitude of the deviation can be weighted according to its likelihood of occurrence as:

$$x_P = x_{mean} \pm (deviation \times likelihood) \tag{2.11}$$

where x_P is the probability weighted deterministic value of the input variable and x_{mean} is the mean. For example, if there is a 50% likelihood for a 2 unit deviation

from a mean of 5 units, the probability weighted deterministic values would be $5 \pm (0.5 \text{ x } 2) = 4$ and 6.

The functional relationship can be solved for the probability weighted deterministic input values to derive the probability weighted deterministic output value. Finally, a deterministic sensitivity analysis can be used to understand major variables with most significant impact on the final output. This is done by sequentially varying one variable by a fixed (deterministic) amount whilst keeping all other variables constant and recording the impact on solution (CRAN-R, 2018).

2.4.2 ISO-Guide to the Expression of Uncertainty in Measurement (ISO-GUM)

The calculus of small changes can be applied to a function linking several input variables with an output variable to estimate the uncertainty bounds on the output variable due to uncertainty in the inputs. For a quantity y that is a function of x_1, x_2, $\cdots$ x_n:

$$y = f(x_1, x_2, \cdots x_n) \tag{2.12}$$

The change in y due to changes in x_i can be expressed as (Harvard University, 2007):

$$\delta y = \frac{\partial f}{\partial x_1}\delta x_1 + \frac{\partial f}{\partial x_2}\delta x_2 + \cdots + \frac{\partial f}{\partial x_n}\delta x_n \tag{2.13}$$

JCGM (2008a) provides a generic analytical framework for the probabilistic propagation of uncertainties based on equation 2.13. The process is described below with a particular emphasis on the approximations and assumptions required to reduce the complexity to a suitable level for practical applications.

Input Uncertainties

As noted in Section 1.7.2, it is assumed in this thesis that the uncertainty in each relevant variable has been appropriately quantified already. However, there are some limitations with ISO-GUM regarding the input uncertainties that are worth noting.

Firstly, the uncertainty distributions must be assumed to be symmetrical. Whilst it is possible to model asymmetrical uncertainties, it is more difficult and the authors of the guidance recommend the use of an alternative method, MCA (Section 2.4.3), in this case (JCGM, 2008*b*). Also, the uncertainties must be small in comparison to the central value of the inputs. Finally, the calculations are greatly simplified if it can be assumed that all uncertainties are independent and uncorrelated with each other, as discussed in the next subsection (JCGM, 2008*a*).

A most likely value and a standard deviation representing the uncertainty (standard uncertainty) in each variable should be available before beginning the process of uncertainty propagation.

Functional Model for Uncertainty Propagation

The function relating the input variables to the output must be defined. In most cases, the functional relationship is likely to be complex and may require making simplifying assumptions to define a functional model. For an output variable Y which depends on input variables x_i:

$$Y = f(x_1, x_2, \ldots, x_i) \tag{2.14}$$

If the standard uncertainty in the input variables is u_{x_i} then the standard uncertainty in Y, u_Y, is (JCGM, 2008*a*):

$$u_Y = \sqrt{\sum_{i=1}^{N} \left(\frac{\partial f}{\partial x_i}\right)^2 u_{x_i}^2 + 2\sum_{i=1}^{N-1}\sum_{j=i+1}^{N} \frac{\partial f}{\partial x_i}\frac{\partial f}{\partial x_j} u\left(x_i, x_j\right)} \tag{2.15}$$

where $u\left(x_i, x_j\right)$ is the covariance between x_i and x_j. If it is assumed that all variables are independent and uncorrelated (i.e. $u\left(x_i, x_j\right) = 0$), then Equation 2.15 is simplified to:

$$u_Y = \sqrt{\sum_{i=1}^{N} \left(\frac{\partial f}{\partial x_i}\right)^2 u_{x_i}^2} \tag{2.16}$$

It is assumed that the uncertainty in Y is validly represented by a Normal distribution. This is normally sufficiently accurate due to the CLT (see Section 2.3.3), but it may prove inaccurate if only a small number of uncertainties are present or if a few large non-Gaussian uncertainties are dominant (JCGM, 2008*a*). Assuming a Normal distribution, this means there is c. 68% probability of the true value, Y_{true}, being:

$$Y_{true} = Y_{mean} \pm u_Y \tag{2.17}$$

where Y_{mean} is the mean value of Y.

Note that Equation 2.16 is based on a first-order Taylor series approximation and may be inaccurate if the function, f, has significant non-linearity. This assumption is commonly made for a range of applications but there are also instances where it is shown to be invalid. Bertrand-Krajewski et al. (2011) illustrate several examples of both cases. The validity of this assumption for tidal energy applications is considered in Chapter 4.

The partial differential in Equation 2.16 is called a sensitivity coefficient as it represents the effect of changes in the input variables on the output variable. In

practice, the sensitivity coefficient may be easier to derive empirically using a perturbation analysis (Ó'Catháin et al., 2013):

$$\frac{\partial Y}{\partial x_i} = \frac{Y_{i,Pert} - Y}{x_{i,Pert} - x_i} \tag{2.18}$$

where $Y_{i,Pert}$ is the value resulting from solving the function in Equation 2.14 using a perturbed value of x_i, $x_{i,Pert}$. This approach assumes that the function is linear between the nominal value and the perturbed value.

Expanded Uncertainty

It may be necessary to specify the value of Y at a different probability interval than that represented in Equation 2.17, such as the P90. The additional metric that defines the uncertainty at a particular interval is called the expanded uncertainty. A coverage factor relating the standard deviation to the desired interval can be used to calculate the expanded uncertainty by making an assumption about the shape of the distribution:

$$U_Y = k \times u_Y \tag{2.19}$$

where U_Y is the expanded uncertainty, u_Y is the standard uncertainty and k is a coverage factor. The value of the coverage factor is determined by the assumed shape of the distribution and the interval of choice. The uncertainty in Y can therefore be expressed as $Y \pm u_Y$ for that interval. The coverage factor to derive the P90 from the standard deviation of a Normal distribution is 1.282 (Cowan, 1998).

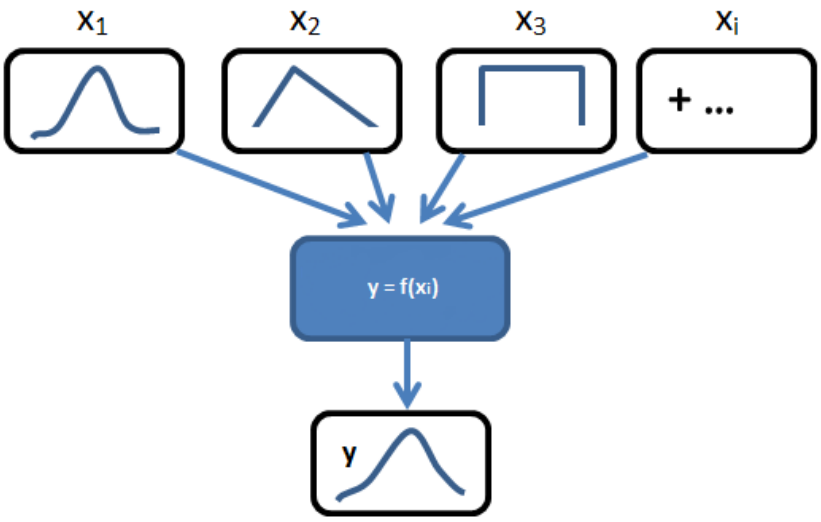

Figure 2.3: Generic MCA process flowchart where x_i are the input uncertainties in variables affecting a desired outcome, y is the resultant uncertainty in the outcome and $f(x_i)$ is the functional relationship between between the inputs and outputs.

2.4.3 Monte Carlo Analysis (MCA)

Monte Carlo analysis (MCA) is a numerical method for solving probabilistic problems that may be too complex for an analytical approach. The functional relationship between inputs and outputs is solved repeatedly using randomly generated numbers from each input uncertainty distribution (Palisade Corporation, 2010). It is effectively repeating the deterministic calculation many times, but the input values are defined stochastically. The resulting output for each iteration is recorded and the empirical distribution resulting from a large number of iterations represents the uncertainty in the output variable. The general process is illustrated in Figure 2.3.

The resultant distribution converges towards the analytical solution as the number of iterations increases. Typically, a sample size in the order of thousands to hundreds of thousands will be required, depending on the function being solved and the acceptable margin of inaccuracy (Palisade Corporation, 2010). The

number of simulations required also depends on the coverage probability required because a wider confidence interval requires a sufficiently high density of sampling in the lower likelihood endpoints of the distribution (i.e. tails). JCGM (2008*b*) recommends that the number of simulations is at least 10^4 times greater than $1/(1-p)$, where p is the coverage interval in decimals.

Given the requirement for high numbers of iterations, it is essential that the function can be solved sufficiently quickly to allow the required numbers of simulations to be completed in an acceptable time frame. The practicality of using MCA for a particular application is dictated by the complexity of the function, available computational power and time constraints. Some approximations can be made at expense of reliability in results to approximate the output distribution using a much smaller number of iterations (JCGM, 2008*b*). This method is not covered in further detail as none of the applications in this thesis required such an approach to be taken.

Provided that the application of MCA is practical for a given application, it overcomes many of the ISO-GUM limitations because it propagates the distributions through the functional relationship rather than the standard uncertainties. The benefits of MCA can be summarised as:

- Input distributions are not assumed to be symmetrical;
- It is not assumed that the functional model is linear;
- No assumptions are made regarding the shape of the output distribution.

The accuracy of MCA rests upon the assumption that the functional relationship assumed between the input and output parameters closes resembles the physical reality. Accurately defining this deterministic model is therefore a crucial step. Prior knowledge, empirical data from experimentation or first principles may be

used to define the model accurately. This step is highly specific to the intended application and is not discussed further in this generic section. The formation of the model for tidal energy yield uncertainty analysis is discussed in Chapter 4. Note that any errors in the model definition will be propagated through to the MCA outputs as a systematic error and any uncertainties in the model definition must be treated as an additional input uncertainty to the system.

The stochastic element is introduced next by assigning distributions to each input variable. This may be done subjectively in the absence of empirical data, or by using data fitting techniques if sufficient data is available. Numerical techniques such as Method of Maximum Likelihood, Method of Moments or Non-linear Optimisation are used to identify the most suitable distribution for a given dataset (Raychaudhuri, 2008). Goodness-of-Fit tests such as Chi-Squared and Kolmogorov-Smirnov test are used to confirm the accurate fitting of the empirical data to gain confidence in the chosen input distributions (Raychaudhuri, 2008).

The input distributions are sampled next to generate the input data for each iteration of MCA. A uniform sample with a range between 0 and 1 is produced using a RNG (as described in Section 2.2.2). The inverse transformation method can then be used to convert the uniform sample between 0 and 1 to a random sample from the distribution of interest. The method relies on knowledge of the CDF of the distribution and the fact that a CDF is by definition strictly increasing from 0 to 1 and continuous. The variate between 0 and 1 can be transformed monotonically to the lognormal CDF curve of the distribution of interest to generate the random value from that particular distribution (Wicklin, 2013). The method can be used to generate random numbers from truncated distributions (e.g. triangular), negative correlations can be applied between variables and can be used for discrete and continuous functions. However, a closed form inverse CDF is required for the transformation method to work and an iterative process such as Newton-Raphson may be necessary in this case (Raychaudhuri, 2008).

Each MCA simulation is run by solving the deterministic model using values from the random samples from each input distribution sequentially and storing the output values, which form the output sample. This sample can be subjected to various analysis analyses to gain insight. The mean and median output values can be calculated to gain indication of the expected outcomes. A histrogram may be produced to visualise the PDF of the output distribution and percentiles calculated to understand exceedence probabilities. Finally, distributions may be fitted to the output sample to calculate representative distribution statistics from the experiment and measures of good fit.

2.4.4 First and Second Order Reliability Methods (FORM and SORM)

Uncertainty analysis is used in reliability engineering to quantify the failure probability of a system in performance. This can help defining safety factors to ensure that probability of a state where the loads exceed the critical condition for failure is acceptably low and that the system is neither over nor under engineered (Bastidas-arteaga and Soubra, 2015). In a general form, a limit state function for failure can be defined as follows:

$$D_f = \left\{\mathbf{X} | g(\mathbf{X}) \leq 0\right\} \tag{2.20}$$

where D_f is the portion of the sample space D that is within the failure region, $g(\mathbf{X})$ is the system's performance function and $\mathbf{X}$ is a vector of random variables. Conversely, the safety region D_s is:

$$D_s = \left\{\mathbf{X} | g(\mathbf{X}) > 0\right\} \tag{2.21}$$

The boundary between D_s and D_f where $g(\mathbf{X}) = 0$ is known as the limit state surface.

The probability of failure P_f is defined as:

$$P_f = P[g(\mathbf{X}) \leq 0] = \int_{g(\mathbf{X})\leq 0} f_{\mathbf{x}}(\mathbf{x}) dx_1 \dots dx_n \tag{2.22}$$

Where $f_{\mathbf{x}}$ is the joint probability density function (PDF) of vector $\mathbf{x}$. Note that the limit state function can be linear or non-linear. The integral is multi-dimensional and difficult to evaluate so approximations are used in practice to simplify the integrand and approximate the integration boundary (Du, 2005). First Order Reliability Method (FORM) is used to evaluate Equation 2.22 when it can be validly represented by a linear approximation and Second Order Reliability Method (SORM) is used for highly non-linear limit state functions by using a second order approximation.

FORM uses the first order Taylor expansion to simplify the integrand. First, the random variables are transformed from the original random domain (hereby referred to as X-space) into a standard normal space (hereby referred to as U-space) where all the variables follow a normal distribution, have a mean of zero and standard deviation of 1. A Rosenblatt transformation is used to achieve this as the CDFs of the variables are constant before and after the process (Rosenblatt, 1952).

$$U_i = \Phi^{-1}[F_{x_i}(X_i)] \tag{2.23}$$

Where U_i is the transformed variable in the U-space whereas X_i is the original variable in the X-space and Φ is the Rosenblatt transformation. The integral after transformation is:

$$P_f = P[g(\mathbf{U}) \leq 0] = \int_{g(\mathbf{U})\leq 0} \phi_U(\mathbf{u}) d\mathbf{u} \tag{2.24}$$

Where $\phi(\mathbf{u})$ is the joint PDF of $\mathbf{U}$. The integral can also be expressed as follows because all variables are independent and uncorrelated and the point PDF is simply a product of all individual normal PDFs.

$$P_f = \int_{g(u_1,u_2,\ldots,u_n)\leq 0} \cdots \int \Pi_{i=1}^{n} \frac{1}{\sqrt{2\pi}} \exp(-\frac{1}{2}u_i^2) du_1 du_2 \ldots du_i \tag{2.25}$$

Next, the linear approximation is used on the integration boundary $g(\mathbf{U}) = 0$. The point at which the probability density is the highest is the optimal location for expansion because this results in the lowest loss in accuracy. This is because the function has the highest value at this point and it reduces significantly away from it due to the shape of the function. It is the shortest distance (in U-space) from the origin to the limit state ($g(\mathbf{U}) = 0$). A simple substitution into the Taylor expansion therefore then provides the linearised function.

SORM is similar to FORM except that the second order terms in the Taylor series are also used to expand the integral at the point of highest probability density. As a result, SORM is more accurate than FORM except for cases where the function is highly linear anyway. However, the inclusion of the second order derivative also results in SORM being significantly more inefficient than FORM (Du, 2005).

2.5 Summary

The presence of uncertainty in most decision processes, and the need to understand the resultant likelihood of deviations from a desired outcome were highlighted. Three commonly used methods for conducting uncertainty analyses were presented generically.

Deterministic methods are easy to implement, but outputs are of limited use as the probabilities of occurrences cannot be quantified. At worst, deterministic results

can be misleading if the underlying assumptions are not understood. ISO-GUM is an effective method for probabilistic uncertainty analysis provided that its limiting assumptions can be satisfied. It is used across a range of applications, but MCA may provide improvement in results if the ISO-GUM assumptions are not valid. The key benefit of MCA over all the other methods is that it requires the least number of unquantified approximations to be made. This is because it involves the propagation of distributions instead of propagation of uncertainties.

The most suitable method in practice depends on the nature of the functional relationship and the input uncertainties, the available computational resource, the tolerance for inaccuracy in results and the time available to derive results. The choice of optimal uncertainty analysis method with consideration of these criteria for different applications in tidal energy project development is considered in subsequent chapters of this thesis.

Chapter 3

Theory of Tides

3.1 Introduction

The cyclic rise and fall of seawater is a result of gravitational interactions between the Earth, Moon and Sun. However, there are many subtleties governing the periods and magnitudes of the tides, and the resultant flow of seawater. An understanding of these factors allows tides to be measured, modelled, predicted and therefore, exploited for energy extraction. This chapter introduces the theories underpinning our knowledge of the tides on Earth. Pugh (1987) provides a thorough explanation of the theory of tides and a succinct summary is provided below, with reference to additional sources where necessary.

3.2 Astronomical and Non-Harmonic Tidal Forces

The lunar tide is the most dominant tidal force, followed by the solar forcing and these are explained in detailed first.

The Moon exerts a gravitational pull on the Earth's surface that is a function of the relative masses and distances, as governed by the Newton's inverse square law:

$$F = \frac{Gm_e m_m}{d^2} \tag{3.1}$$

where F is the gravitational force being exerted, G is the gravitational constant, m_e and m_m are the masses of the Earth and Moon respectively and d is the distance between the centre of the Earth and the Moon. The same function also defines the forces exerted between the Earth and the other celestial bodies.

The points on the Earth that are closer to moon therefore experience a greater gravitational pull. This force is experienced by the Earth's land and water masses but the response of the ocean is considerably more noticeable because of its fluid properties. The gravitational pull on the Moon's side of the Earth is estimated to be 7% greater and assuming that there are no land masses or frictional losses, this would result in an approximately 50cm change in water depth due to the lunar forcing (University of Bristol, 2015). The water body also experiences an inward gravitational pull towards the centre of the Earth but this is relatively small and the tidal bulge Figure 3.1 is a result of the net force (Open University, 1989).

The rotation of the Earth's orbit also results in centrifugal forces that form a bulge on the opposite side of the Earth to the Moon (Figure 3.1). This is because the gravitational attraction is equal and opposite to the centrifugal force which results in the Earth and the Moon maintaining their orbits. However, the centrifugal force

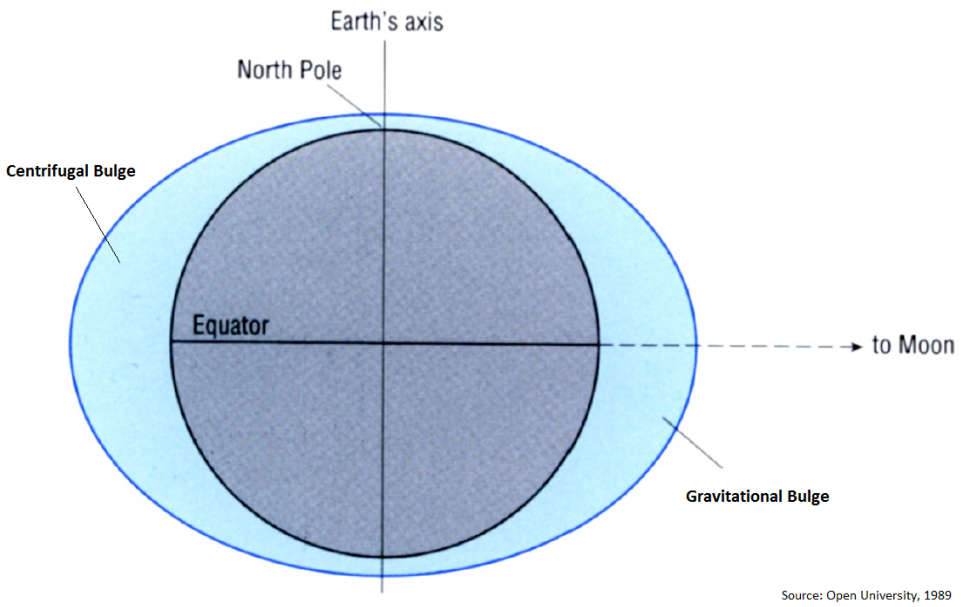

Figure 3.1: Gravitational attraction between Earth and Moon.

is larger than the gravitational force on the side of the Earth away from the Moon and this is the driver of the centrifugal bulge on Earth.

Finally, since the Earth rotates about its axis every 24 hours, each point on Earth experiences both bulges in a 24 hour period. The bulges correspond to the high tides and this explains the reason for most places on Earth experiences two high tides a day at roughly 12 hour intervals, with the precise period also affected by the Moon's advance during that period and other celestial bodies. The low tides are a result of the withdrawal of water towards the bulges and occur at the midpoint between the bulges where the gravitational pull of the Moon is at the lowest.

The solar tides follow the same principle but the magnitude of its impact is less than half of the lunar tides due to the significantly larger distance between the Earth and the Sun (NOAA, 2018). The superimposition of the solar and lunar influence is one of the factors for every subsequent tidal cycle being different to the last due to the variation in phase between the position of the Sun and the

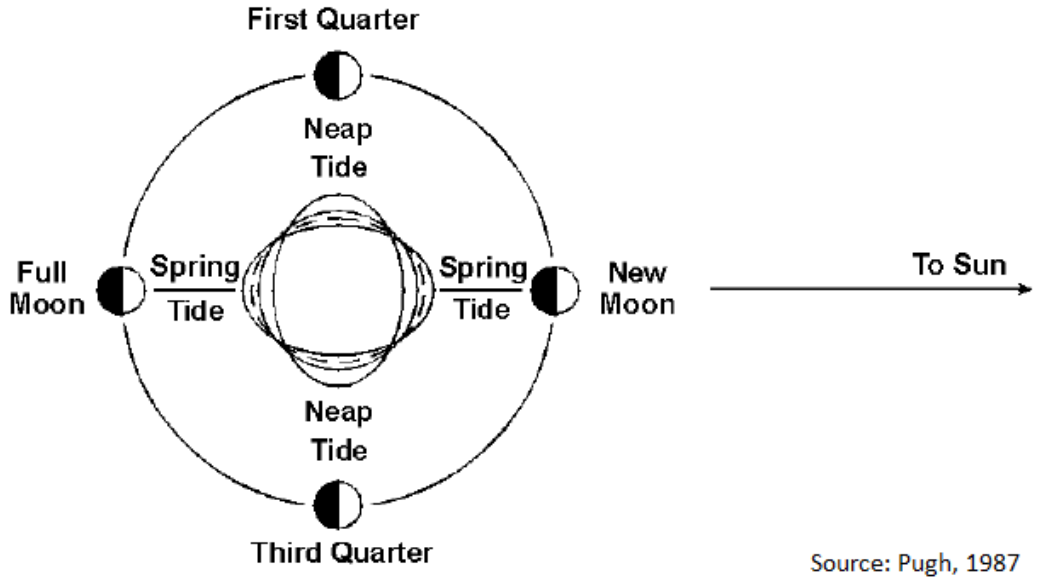

Figure 3.2: Position of the Sun and Moon resulting in formation of spring and neap tides.

Moon. The position of the Moon and Sun is aligned during full moon and new moon, leading to a high positive superimposition and this is the reason for spring tides being highest. Conversely, the neap tide is weak because the lunar and solar forces are at right angles to each other and have minimum reinforcing effects (Figure 3.2).

Furthermore, there are other astronomical variables linked to the Earth, Sun and Moon system which affect the tides. The orbits are elliptical and therefore the distance between the mass bodies varies over time. Similarly, the angle of the orbit also affects the production of the tides. The relative importance of each of these factors varies depending on the location on earth (Figure 3.3). Therefore the net effect of the forcing is not uniform across the surface of the Earth and this is one of the reasons why there is a variation in the tidal regimes around the

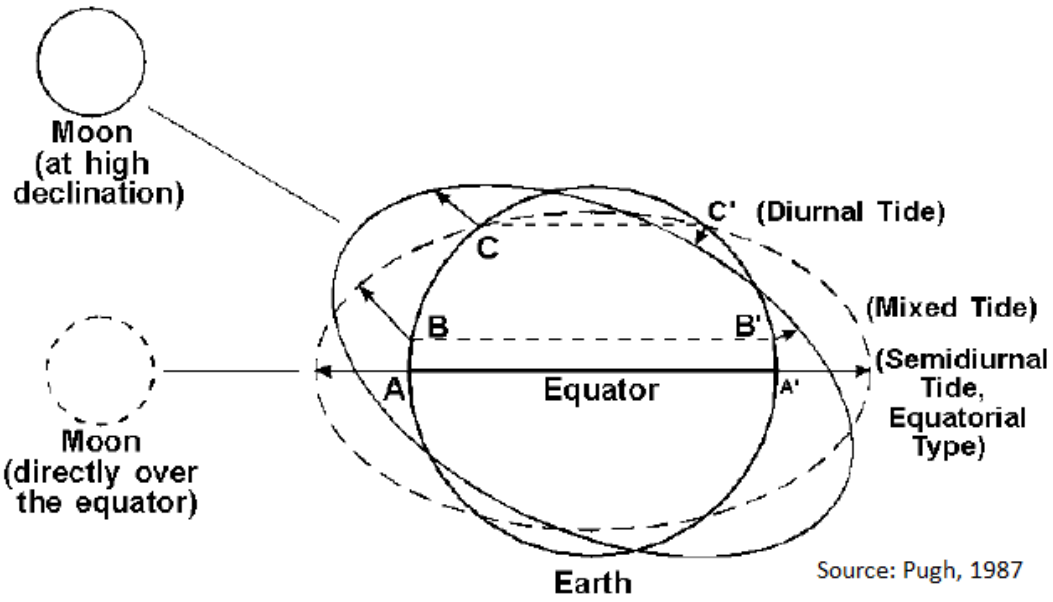

Figure 3.3: Position of the Sun and Moon resulting in formation of spring and neap tides.

world. The relative importance of these factors also varies over time for any given location.

The variations in tidal profile around the world due to the aforementioned factors can be classified into three main categories (Figure 3.4); diurnal tides, semi-diurnal tides and mixed tides. Diurnal tides are characterised by one high and one low tide in one tidal day and are typically found in Australia, Antarctica and the Gulf of Mexico (Pugh, 1987). On the other hand, a semi-diurnal profile is one where two roughly, but exactly identical, highs and lows are observed in one tidal day. Finally, mixed tides are said to occur where one large high and low tide is followed by a lower high and low tide, typically observed in the Pacific. Figure 3.5 shows the global variation in type of tides around the world.

The net tidal forcing can be resolved into a horizontal and vertical component (relative to the Earth's surface). The horizontal component, also known as the

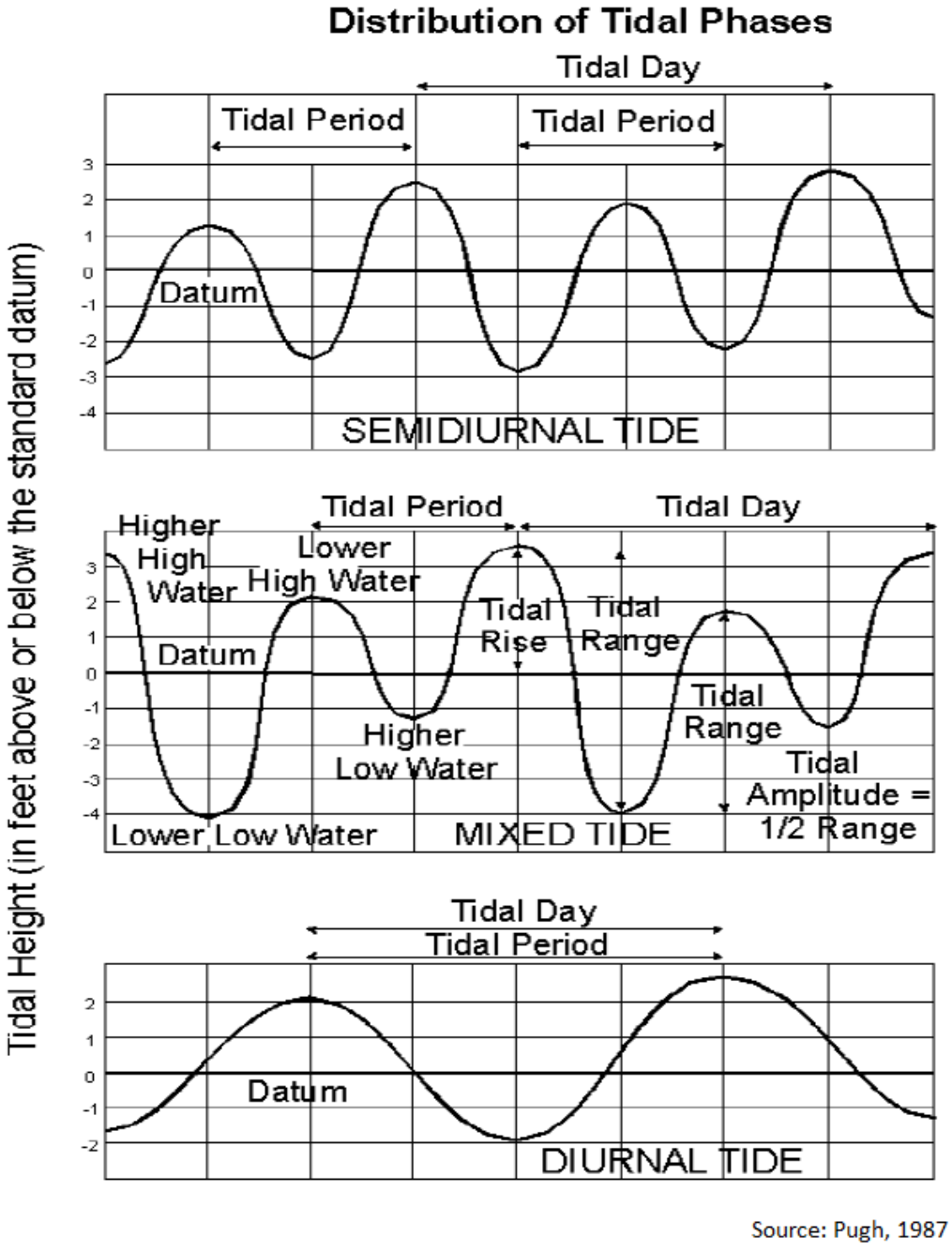

Figure 3.4: Tide level profile for three main types of tides

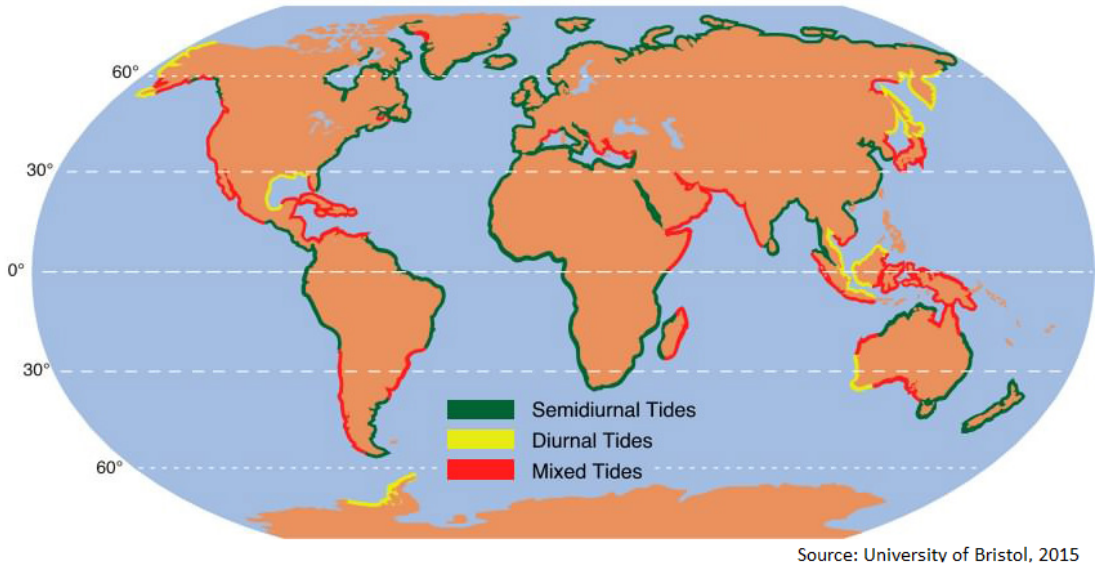

Figure 3.5: Variation in dominant type of tide around the world

tractive force, is not opposed by gravity and it forms the mechanism for the tidal movements because it causes the water particles to move in accordance with the net balances. The tidal forcing directly below the moon has no tractive component as the force only has a vertical component.

The above discussions allow the tidal effects to be fully understood in a case where the Earth is a sphere with no land mass and uniformly deep oceans, the distance and relative positions of the Earth, Moon and Sun are constants and there are no other forces affecting the motions. Whilst these assumptions can be used to gain a simple understanding of the major drivers in tidal forcing, in reality, further complexities must be considered to allow a fuller understanding. Further reasons than those already discussed for variation in timing and magnitude of the high and low tide over time and location are explained next.

The shape and depth of a tidal basin can result in resonance which alters the tidal characteristics in a region. This phenomenon can explain why certain locations experience drastically different tidal profiles despite small geographical difference, and thus an expectation of small tidal difference according to equilibrium tide

theory. For example, the East coast of Florida experiences semi-diurnal tides whilst the West coast experiences mixed tides due to the resonant basin (IHO, 2013). Resonance can also lead to significant amplication of the tidal height, for example in the Bristol Channel.

The tidal forcing resulting from the relative position of the Earth, Sun and Moon is known as the harmonic forcing. Other non-harmonic forces also govern the observed tide at a given location. These include environmental and atmospheric conditions.

Reducing depth leads to a rise in the height of the tidal wave, similar to wind waves approaching shallow waters. A constricting shoreline also has a similar effect. More locally, a channel linking two basins with differing tidal characteristics has its tides governed by the equilibrium conditions between dynamics of the two basins. Narrow constrictions or headlands also result in significant local flow acceleration effects, and often provide good sites for tidal energy extraction. Finally, at a highly local level, the bathymetry and presence of features such as boulders or reefs can result in significant turbulence and/or upflow of the tidal currents.

The change in atmospheric pressure due to passing weather systems can affect the tidal levels at a location, with low barometric pressure causing higher than expected tidal levels and vice versa. The wind conditions also affect the tidal levels and currents. Water has viscous properties and does not respond impulsively to forcing. The lag in response due to friction is also a non-harmonic effect, albeit with a relatively small impact.

3.3 Tidal Predictions

The harmonic component of tides is evidently deterministic and can therefore be predicted with high accuracy provided that sufficient knowledge of the tidal regime is available. This section discusses the method for predicting the tides and the data required in order to achieve this with accuracy.

Each of the factors affecting the tides discussed above can be represented generically as a cosine signal (Figure 3.6). The frequency and magnitude of the tidal forcing corresponding to each factor is governed by the fundamental physics. Each such factor is known as a tidal harmonic constituent and the superimposition of all harmonic constituents represents a full picture of the tidal harmonics at a location. If all harmonic constituents are known then the tide can be calculated deterministically for any time in the past or future. The process of resolving and extrapolating the harmonic constituents in time is known as harmonic analysis (Pawlowicz et al., 2002). The fundamentals of harmonic constituents are discussed first, followed by how to resolve them from a timeseries of tidal data.

The Principal Solar Semi-Diurnal harmonic constituent, S_2, corresponds to the position of the Sun whereas the Principal Lunar Semi-Diurnal harmonic constituent, M_2, corresponds to the position of the Moon (Hicks, 2006). Constituents are defined by the time taken to complete one tidal cycle, the period. The period for S_2 is 12 hours because it takes 12 hours for the principal solar tide to reach a peak from its previous peak. This corresponds to noon to midnight where the Sun is directly overhead or directly below the Earth, corresponding to the gravitational and centrifugal bulges observed in Figure 3.1. The M_2 period is 12.42 hours, which corresponds to the 24.48 hours taken by the Moon to return to same point over Earth. It is more common to represent the tidal harmonics by frequency (in degrees/hour) rather than period (in hours), which can be calculated

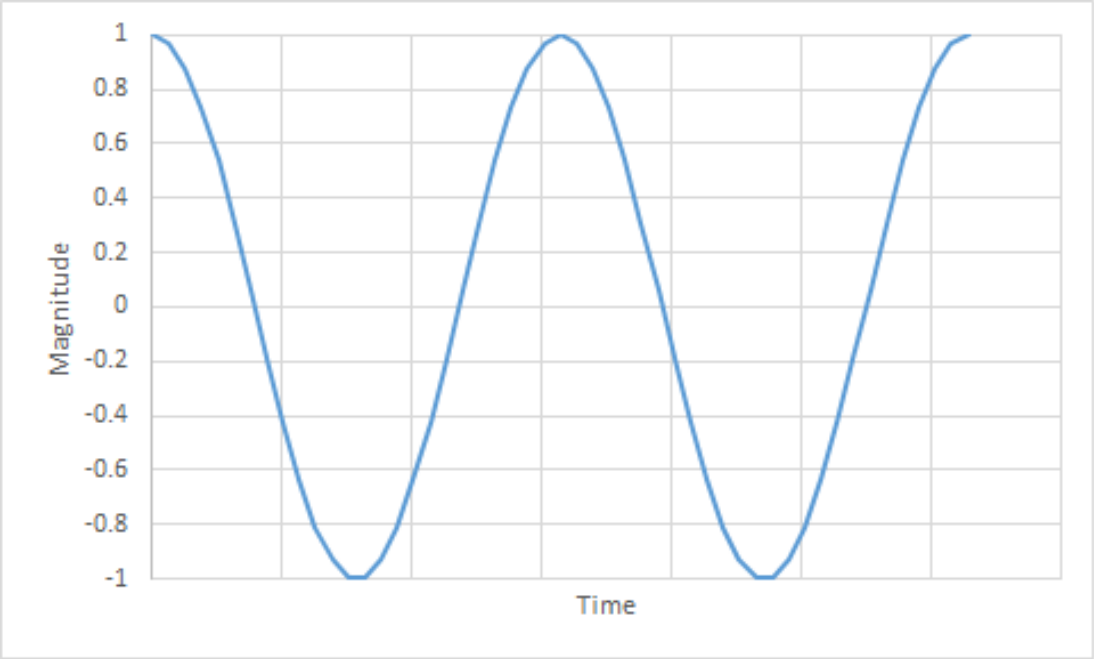

Figure 3.6: Generic representation of a tidal constituent

as follows:

$$Frequency = \frac{360}{period} \tag{3.2}$$

The frequency of S_2 and M_2 therefore is 30 degrees/hour and 29 degrees/hour, respectively. Figure 3.7 shows how these two tidal cycles with varying frequencies align to create spring and neap tides, where their superimposition is greatest and smallest, respectively.

Whilst there are a great number of tidal constituents in theory, a few key constituents (S_2 and M_2) are dominant and knowledge of these can be sufficient for practical applications. The Larger Lunar Elliptic constituent (N_2) and the Smaller Lunar Elliptic constituent (L_2) represent the change in distance of the Moon and the Sun to the Earth due to their elliptical orbits. The Principal Lunar Declinational constituent (O_1), the Principal Solar Declinational constituent (P_1) and the Luni-solar Declinational constituent (K_1) relate to the declination of the

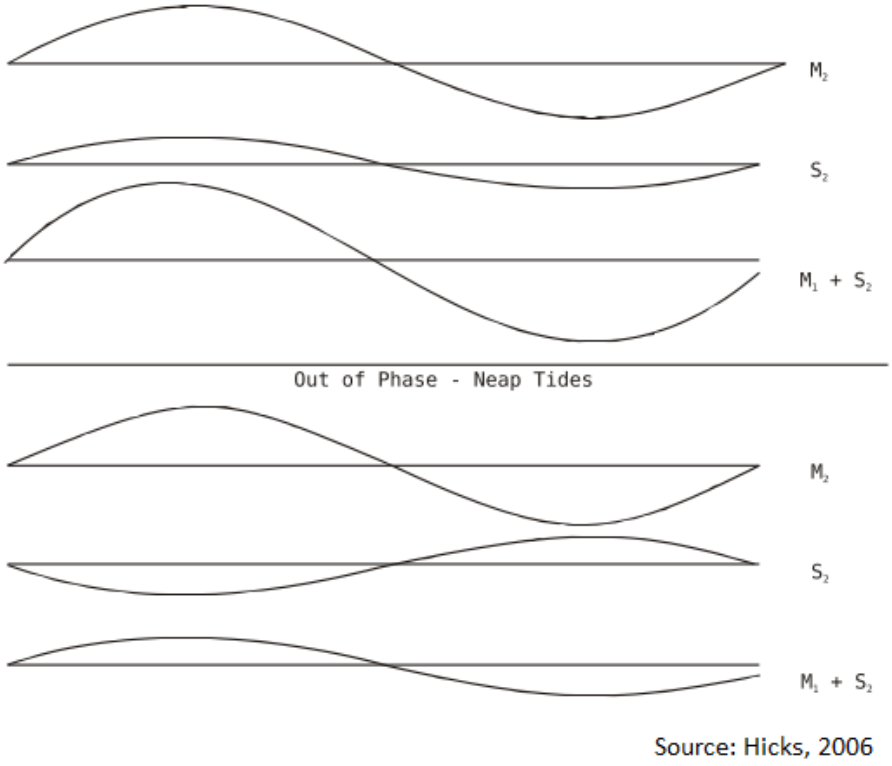

Figure 3.7: Superimposition of M_2 and S_2 tidal harmonic constituents leading to spring and neap tides

Moon and the Sun. Table 3.1 shows the relative magnitude and frequency of these tidal harmonic constituents.

Table 3.1: Summary statistics for key tidal harmonic constituents (Hicks, 2006)

Contituent	**Symbol**	**Relative Magnitude**	**Period (hrs.)**	**Frequency (degrees/hr)**
Principal Lunar	M2	1	12.42	28.99
Principal Solar	S2	0.46	12	30.00
Principal Lunar Declinational	O1	0.41	25.82	13.94
Luni-solar Declinational	K1	0.4	23.93	15.04
Larger Lunar Elliptic	N2	0.2	12.66	28.44
Principal Solar Declinational	P1	0.19	24.07	14.96
Smaller Lunar Elliptic	L2	0.03	12.19	29.53

Harmonic analysis is a mathematical process used to isolate individual harmonic constituents from a timeseries of tidal data, which is inherently a superimposition of all underlying harmonic constituents. As with any statistical process, the larger the dataset used for inference, the more accurate the results. However, a minimum of 30 days days of tidal data is sufficient to resolve the dominant harmonics (Hicks, 2006).

The aim of harmonic analysis is to identify the amplitude and phase of each harmonic constituent. Since actual measurements will include superimposition of tidal harmonics as well as non-harmonics, the results of harmonic analysis must be considered as estimates with an associated uncertainty, rather than deterministic parameters with a fixed 'true' value. Furthermore, the tidal timeseries would need

to be infinitely long to resolve all theoretical harmonics so there is an additional uncertainty associated with the length of data available in practical applications. The harmonic constituents derived from a given measurement location are unique to that particular location given the potential sensitivity of tidal characteristics to geographic location discussed earlier. Least squares fitting is used to resolve the harmonic parameters and once they are known, the tidal characteristics over time can be determined because the amplitude, frequency and phase are known.

3.4 Hydrodynamic Modelling of Tides

Hydrodynamic models are used to extrapolate the known tidal characteristics at a given location over space. The models extrapolate the input tidal data and boundary conditions across the modelling domain with respect to factors such as tidal forcing, bathymetry, atmospheric and environmental conditions IEC (2015). Hydrodynamic models can also be used calculate the effect of energy extraction on the natural undisturbed flow due to presence of tidal turbines. This includes local effects, such as wakes, and far field effects, such as flow diversion.

There are two types of hydrodynamic models; 2D and 3D. The 2D models solve depth averaged equations to produce depth averaged velocity outputs whereas 3D models consider the physics in all three dimensions to produce directional outputs, including the vertical profile of the flow. Some, or all, of the following data is also required for the resource assessment stage, depending on the project, in order to initiate the hydrodynamic model and/or supplement the raw model output; tidal heights, bathymetry, wind, wave, atmospheric pressure, salinity and turbulence.

3.5 Summary

An understanding of the underlying physics causing the formation of tides on Earth is important in order to accurately model it for exploitation of its energy potential. Tides are formed by the astronomical forces induced by the varying relative positions within the Earth, Moon and Sun system, the centrifugal forces caused by the rotation of the Earth and non-harmonic factors such as atmospheric pressure and local bathymetry. Harmonic analysis can be used to resolve the harmonic (astronomic) constituents from a measured timeseries in order to determine the past or future tidal characteristic at a measurement location. There is uncertainty in this determination due to the noise introduced by non-harmonic components in the measured data and also from any limitations in the length of the measured dataset with respect to the length required to fully resolve all dominant harmonics. The knowledge of the tides at a given location can be used in conjunction with a hydrodynamic model to extrapolate the tidal characteristic spatially from the measurement location to another location of interest. Energy extraction can also be modelled by using such models. Inevitably, additional uncertainty is introduced when hydrodynamic models are used owing to the modelling approximations introduced, imperfect knowledge of the underlying physics and amplification of uncertainties accumulated through the measurement and harmonic analysis phases.

Chapter 4

Yield Uncertainty Analysis

4.1 Introduction

The pre-construction annual energy yield estimate of a tidal energy project is an important investment decision metric. It is calculated using a project's long term site resource and the power performance characteristics of the technology used. Both sets of data are based on measurements, models and assumptions that are subject to uncertainty. The resultant uncertainty in the annual yield is a significant component of the overall risk profile of a typical tidal energy project (SI Ocean, 2013; Kutney et al., 2013). An increased confidence in this uncertainty estimate is one pathway to reducing perceived risk in the sector (OREC, 2015*b*).

The uncertainty in an annual yield estimate can be represented as a probability distribution (Figure 4.1). It is important for the investor to know not only the central expectation for a project's yield (and therefore revenue), but also the conservative case in order to appraise the risk involved in the investment. The P50 and P90 annual yield are useful metrics for this purpose, respectively (Ó'Catháin, 2012; OREC, 2015*b*). A project with a lower P50 yield may in fact be more

financeable than a similar project with a higher P50 yield if the P90/P50 ratio is higher, i.e. smaller likelihood of large deviation from the P50 (Figure 4.1). Based on evidence from the wind industry, a P90/P50 ratio between 0.8 to 0.9 is considered to be necessary in order to attract commercial project finance, with a higher ratio leading directly to a reduction in the cost of finance (Ó'Catháin, 2012; Economist, 2010).

The annual yield uncertainty distribution represents the aggregate effect of all the individual uncertainty sources affecting the yield of a project. The shape of the distribution, and therefore the P50 and P90 yield values, depends on the characteristics of the underlying individual uncertainties and the method used to combine the uncertainties. Both factors are discussed in this chapter, but the focus is on the latter aspect. User confidence and understanding of the process used to combine the yield uncertainties is as important as confidence in the quantification of individual uncertainties because the method of combining uncertainties has the potential to affect the results.

The ISO-guide to the expression of uncertainty in measurement (ISO-GUM) method (described generically in Section 2.4.2) has been recommended for tidal energy annual yield uncertainty analysis in a reference document for the industry (OREC, 2015*b*). Monte Carlo analysis (MCA) (described generically in Section 2.4.3) has also been noted as a suitable alternative if the assumptions implicit in ISO-GUM are not valid (Ó'Catháin et al., 2013; OREC, 2015*b*). However, a comprehensive proof of the validity of ISO-GUM for tidal energy yield uncertainty analysis has not been presented in the literature so far. Further investigation is therefore needed to understand any differences in ISO-GUM and MCA results, and if one method is more suitable than the other.

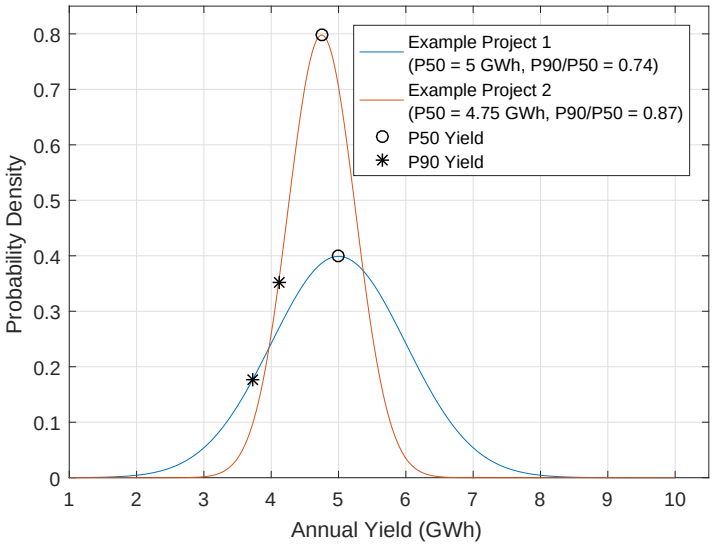

(a) PDF

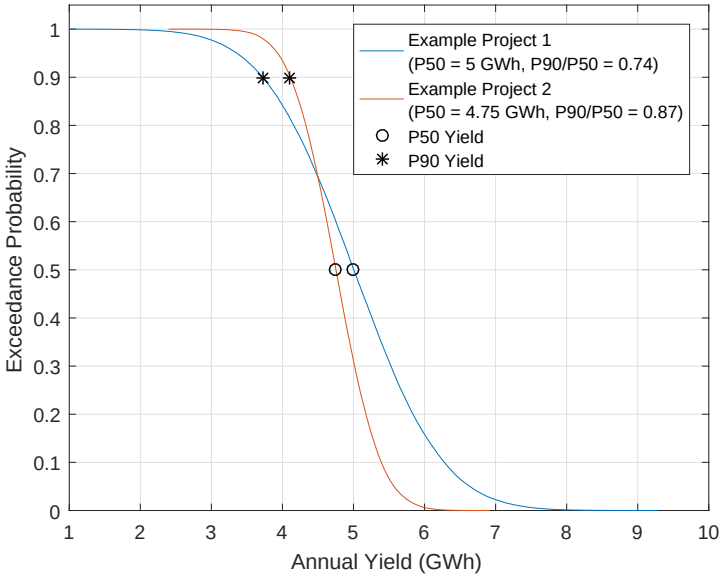

(b) ICDF

Figure 4.1: Annual yield uncertainty distributions for two example projects with differing P90/P50 yield ratios. Project 1 has a higher P50 yield, but may still be less attractive to an investor than Project 2, which has a higher P90 yield due to the lower uncertainty.

Chapter Outline

The aim of this chapter was to quantitatively assess the suitability of using ISO-GUM and MCA for combining annual yield uncertainties, and to recommend the most suitable method for tidal energy projects.

This was achieved by first making comparisons to the equivalent process used for wind projects in order to understand parallels and differences. A set of reference test cases representing a range of realistic tidal projects were then defined. Annual yield uncertainty for all cases was derived using ISO-GUM and MCA. Furthermore, a sensitivity analysis and other comparisons between the two methods were made to identify thresholds, caveats and limitations of their suitability for tidal energy annual yield uncertainty analysis.

The quantification of uncertainties was not considered in detail in this chapter, as per the explanation in Section 1.7.2, and also because guidance documentation on quantifying yield uncertainties has been published recently (OREC, 2015*b*). Furthermore, the quantification will naturally improve as experience and data is gathered by the sector.

4.2 Literature Review

4.2.1 Yield Assessment Process

The aim of the yield assessment process is to quantify the available tidal resource at a site of interest and to estimate the electricity that can be produced by a tidal farm at that location. Therefore, there are two parts to yield assessment; resource assessment and power performance assessment. This distinction between

resource, power performance and yield assessment is observed throughout the thesis. A succinct summary of these processes is provided below, with a particular focus on introducing the sources of uncertainty. The specific requirements for a project vary depending on the stage of development and size of the project, but the general steps that allow an understanding of the sources of uncertainty are generic.

Resource Assessment

A technical specification for the resource assessment process has been published by IEC (2015). The following description is based on this document, with additional references where necessary.

The directional flow velocity at a site must first be measured for a period of 35 to 90 days using an accoustic Doppler current profiler (ADCP). An ADCP measures the velocity profile of a flow across the water column by transmitting acoustic pings at a fixed frequency and measuring the Doppler shift in the reflected sound waves (RD Instruments, 2011). The aim of the measurement campaign is to capture enough tidal cycles to resolve the underlying harmonics caused by the relative positions of the earth, sun, moon and other celestial bodies that govern the tide (Pugh, 1987). A process called harmonic analysis is used to determine the amplitude and phase of the different tidal harmonics with known frequencies from the measured dataset (Codiga, 2011). Harmonic analysis uses least squares fitting to derive the harmonics. The minimum data requirement is related to the period containing at least one full spring-neap cycle. It is the minimum amount of data required to capture the most dominant tidal harmonics (Boon, 2004). The longer periods allow the less dominant, lower frequency harmonics to be captured, thus improving the accuracy of the understanding of the tide (Stiven et al., 2011). Harmonic analysis can then also be used to reconstruct a tidal velocity timeseries

for any past or future time period of interest from the set of resolved harmonics (temporal extrapolation).

Unless measurements are made at the turbine locations, the resource also needs to be extrapolated spatially. This is achieved through the use of hydrodynamic models. The models extrapolate the input data and boundary conditions across the modelling domain with respect to factors such as tidal forcing, bathymetry, atmospheric and environmental conditions. The hydrodynamic model is also required to calculate the effect of energy extraction on the natural undisturbed flow. This includes local effects, such as wakes, and far field effects, such as flow diversion. Modelling energy extraction is a requirement for projects larger than c. 10 MW or where the proposed energy extraction is greater than 2% of the theoretical undisturbed resource. There are two types of hydrodynamic models; 2D and 3D. The 2D models solve depth averaged equations to produce depth averaged velocity outputs whereas 3D models consider the physics in all three dimensions to produce directional outputs, including the vertical profile of the flow. Some, or all, of the following data is also required for the resource assessment stage, depending on the project, in order to initiate the hydrodynamic model and/or supplement the raw model output; tidal heights, bathymetry, wind, wave, atmospheric pressure, salinity and turbulence.

The key output of the resource assessment phase is a timeseries of tidal velocities at each turbine location over the period of interest.

The factors affecting the level of uncertainty in the resource assessment process outlined in IEC (2015) can be summarised as:

- Measurement period and location(s): longer period captures more of the prevalent tidal harmonics. More locations reduce spatial extrapolation and provide data points for model calibration/validation;

- Quality of measurements: instrument quality, consistency in measurements and continuity of data;
- Capability of models: e.g. 3D model does not require vertical extrapolation of the resource to derive a flow profile across the water column, which is an additional source of uncertainty if using a 2D model;
- Discretisation in space and time: higher resolution of model reduces approximations;
- Boundary conditions: Quality of model outputs are heavily dependent upon boundary conditions used.

The site measurement and spatial modelling uncertainties are noted as being more significant to the annual yield uncertainties than the temporal modelling in a qualitative analysis by Ó'Catháin (2012). A quantitative analysis for two case study sites by Kutney et al. (2013) also finds modelling uncertainties to be very significant and the importance of uncertainty in seawater salinity and temperature is shown to be less important. Note that Kutney et al. (2013), and also Stock-Williams et al. (2013), do not deem the measurement uncertainties to be significant enough for analysis in contradiction to the conclusion reached by Ó'Catháin (2012). This is because the former authors assume an instrument uncertainty quoted by the manufacturer and thus do not include the uncertainty added from operational factors such as directional accuracy due to presence of ferrous metals and station keeping in energetic flow, as considered by Ó'Catháin (2012).

Power Performance Assessment

The aim of the power performance assessment is to provide an energy yield estimate at the site of interest. It involves converting the site resource data

into a gross energy yield through the device power curve, and then into a net energy yield, through the accounting of performance losses.

The gross yield is calculated from the power curve and velocity data in the time domain or the frequency domain using Equations 4.1 and 4.2, respectively.

$$E_{gross} = \frac{t}{n} \sum_{i=1}^{n} f(v_i) \tag{4.1}$$

where E_{gross} is the gross yield, t is the hours in a year, n is the number of data points in the velocity timeseries and $f(v_i)$ is the function defining power output for a given velocity v_i.

$$E_{gross} = t \sum_{j=1}^{n_{bins}} f\left(v_j\right).p_j \tag{4.2}$$

where n_{bins} is the number of velocity bins in the power curve, p_j is the probability of the velocity being within the j$^{\text{th}}$ bin and $f(v_j)$ is the power output in the jth bin.

Note that IEC (2015) recommends the frequency domain method as the preferred approach for yield calculation. In a comparison of the frequency and time domain methods, Ó'Catháin et al. (2013) showed the latter method to be more accurate. This is to be expected because it does not require discretisation of the velocity data into bins, which is a source of numerical error. However, the difference in results from the two methods is reasonably small, and the frequency domain expression is more computationally efficient, particularly for large timeseries datasets.

IEC (2015) suggests that both a hub height and a rotor area-weighted velocity should be considered to reduce the vertical profile of the resource data from

multiple bins to a single value for use in Equations 4.1 or 4.2. No preferred approach is offered as the importance of vertical shear is not yet well established.

The net yield can be calculated by multiplying the performance losses by the gross yield estimated (Equation 4.3). A standardised taxonomy for yield losses has been proposed by OREC (2015*a*) and is presented in Table 4.1. Not all categories would be applicable to all projects. The losses may be quantified using physical testing (e.g. tank testing for performance losses), numerical modelling (e.g. reliability modelling for availability losses), existing datasets (e.g. manufacturer brochure for electrical losses) and expert opinion, where necessary (OREC, 2015*b*).

$$E_{Net} = E_{gross} \times Losses \tag{4.3}$$

Clearly, the power curve is a crucial part of the yield assessment process, in addition to the resource modelling. A technical specification for the measurement of a tidal turbine power curve has been published by IEC (2013) and is summarised below. This process is typically carried out by the device manufacturer. The output power curve can then be used by the project developer for calculating the expected yield at their site.

ADCPs are used to measure the undisturbed flow velocity upstream of the device. Power transducers are used to measure the turbine power output over a period that is concurrent with the upstream flow measurement. This allows the relationship between flow velocity and power output to be quantified. The 'method of bins' is used to discretise the measured dataset. More specifically, the 10 minute average of the power weighted velocity from each vertical ADCP bin and the corresponding average power are binned in 0.5 m/s velocity bins across the operational range of the turbine. The average of the values in each of the velocity bins defines the power curve for the turbine. Precise requirements for

Table 4.1: Taxonomy of yield loss categories proposed by OREC (2015*a*)

Loss Category	Sub-Category
1. Availability	1a. Marine energy converter
	1b. Environmental
	1c. Balance of plant
	1d. Grid
	1e. Site access and other force majeure events
	1f. Other
2. Resource Array Interactions	2a. Internal resource array interactions
	2b. External resource array interactions
	2c. Future external resource array interactions
3. Device Performance	3a. Power performance
	3b. Local resource characteristics
	3c. Hysteresis
	3d. Performance degradation
	3e. Other
4. Electrical	4a. Electrical losses
	4b. Facility parasitic consumption
5. Curtailment	5a. Operational management
	5b. Grid curtailment/constraint
	5c. Offtaker curtailment
	5d. Environmental curtailment
6. Other	6a. Resource metric - energy relationship
	6b. Water density
	6c. Other

the local characteristics of the test site, ADCP locations and power measurement equipment are stipulated to ensure standardisation of the process. The frequency, resolution and volume of data required across the operating range of the turbine for a test to be considered complete is also defined, and methods for extrapolating missing data are provided.

The power curve is defined by the manufacturer at a test site and there is an assumption the turbine performance will be similar when deployed at a different site. The effect of local effects such bathymetry, turbulence and directionality are noted as potentially having a significant impact on the measured power curve. However, no site specific adjustments are proposed to allow a test power curve to be applied to a different site due to a lack of understanding at present. Note that the equivalent international standard for the wind industry does propose such site specific adjustments, which is possible due to the higher level of understanding of the wind resource and turbine performance (IEC, 2005).

Factors affecting the uncertainties in power performance analysis process outlined in IEC (2013) can be summarised as:

- Data collection period: longer period provides higher statistical rigour and reduces need for extrapolation;
- Quality of measurements: includes measurement of electric power, current speed and quality of data acquisition system;
- Representativeness of test site to project site: results in uncertainty due to site conditions and sea conditions;
- Discretisation in space and time: size of vertical bins, velocity bins and averaging period;

- Capability of models: confidence in models for estimating losses such as availability, hydrodynamic interactions etc.

4.2.2 Breakdown of Yield Uncertainties

A standardised framework for the categorisation of marine energy yield uncertainties has also been proposed by OREC (2015*a*). The proposed breakdown of uncertainties, and the recommended process to quantify each uncertainty, is summarised in Table 4.2. The relative importance of each uncertainty category is considered by OREC (2015*d*) based on a literature review and the findings are also summarised in Table 4.2.

It is anticipated that developers will conduct analyses that conform to the categorisation outlined in Table 4.2. This will make comparisons between projects easier. This thesis assumes uncertainties are quantified according to the standard taxonomy. The site measurement, temporal variation and spatial variation uncertainties are referred to as the resource uncertainties because they represent the uncertainty on the velocity. The performance and loss uncertainties are referred to as the loss uncertainties for brevity.

Table 4.2: Taxonomy of yield uncertainty categories

Uncertainty Category	**Sub-Category (OREC, 2015*a*)**	**Quantification process (OREC, 2015*b*)**	**Importance (OREC, 2015*d*)**
1. Site Measurement	1a. Instrument Accuracy	Provided by device manufacturer	Low
	1b. Measurement Interference	Avoided by good practice and error-checking	Low
	1c. Short-term site data synthesis	Not specified	Low
	1d. Data quality and metadata	Guidance in IHO (2008) to be followed	Low
2. Temporal Variation	2a. Historic resource estimation	Guidance in IEC (2015)	Low/Medium
	2b. Future resource variability	Sensitivity analysis on different meteorological inputs to the resource model for non-astronomical variations	Medium/High for exposed site
	2c. Climate change	No evidence of a significant effect of climate change on future tidal currents	Low
3. Spatial Variation	3a. Model inputs	Validation of the 2D model	Medium

	3b. Horizontal and vertical extrapolation	Sensitivity analysis on model inputs or use of additional ADCP dataset	Medium/High (Horizontal) Low/Medium (Vertical)
4. Performance and Losses	4a. Availability	Sensitivity studies using stochastic availability model	Medium/High for early arrays
	4b. Resource-array interactions	Sensitivity analysis on wake parameters of hydrodynamic model	Low/Medium for small arrays, high for large
	4c. Device performance	Guidance in IEC (2013)	Medium
	4d. Electrical losses	Specified by manufacturers	Low
	4e. Performance degradation	Assumed impossible to quantify, but empirical data over time should provide guidance	Medium
	4f. Curtailment	Depends on the terms of the Power Performance Agreement (PPA)	Low

4.2.3 Yield Uncertainty Analysis Methods

Once the characteristics of the individual uncertainties affecting the annual yield are known, it is necessary to combine them to derive the net effect on the annual yield uncertainty. Two uncertainties in the resource estimate represented by a standard deviation of 5% each do not necessarily represent a 10% standard uncertainty in the resource because the uncertainties can be independent and therefore, uncorrelated. It is incorrect to simply sum uncorrelated uncertainties because it is unlikely for two extreme values to occur simultaneously (Figure 4.2). A method is therefore required to combine the uncertainties together in a manner that respects the inter-dependence of uncertainty sources.

Furthermore, a 5% standard uncertainty in the resource does not equate to a 5% uncertainty on the annual yield because the relation between resource and yield is defined by an indirect function of the power curve and performance losses, as explained in Section 4.2.1. A method is therefore required to propagate the resource uncertainty into the equivalent yield uncertainty.

It is mathematically difficult to propagate and combine the effect of individual uncertainties on the annual yield analytically (Ó'Catháin et al., 2013). A model is required to approximate the analytical solution. The accuracy of the method used to combine the individual uncertainties is therefore an important factor affecting the resulting combined yield uncertainty distribution, in addition to the nature of the individual uncertainties themselves.

As noted in Section 4.1, ISO-GUM and MCA are currently considered to be suitable methods for combining and propagating individual uncertainties in the yield assessment process to calculate the combined uncertainty on the annual yield estimate. OREC (2015*b*) concluded that ISO-GUM performance is adequate when compared to MCA but no details of the comparisons were provided.

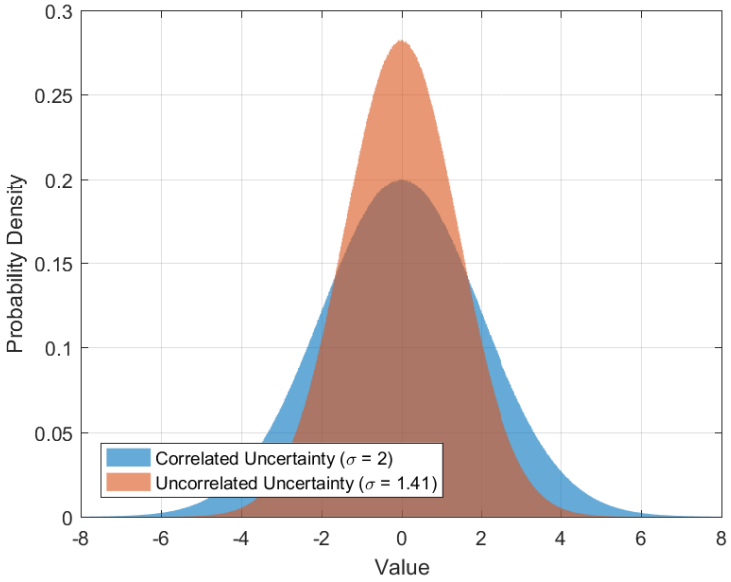

Figure 4.2: Sum of two correlated and uncorrelated distributions with standard deviation $(\sigma) = 1$. Note the lower σ when it is assumed that the uncertainties are uncorrelated.

Comparisons between ISO-GUM and MCA have been made in other more mature industries. MCA was shown to be more accurate for the applications in Yang et al. (2014), Theodorou et al. (2011) and Ha et al. (2014), whereas Azpurua et al. (2011) found no significant difference. Finally, Couto et al. (2013) tests a range of applications and also finds ISO-GUM unsuitable for some of them. Therefore, it is clear that ISO-GUM cannot be considered universally applicable. It should be noted that ISO-GUM is a widely used method for the wind industry (Derrick, 2009; Lackner et al., 2007; MEASNET, 2009) and its accuracy has been validated against operational data (Mortensen and Jørgensen, 2013; Natural Power, 2015).

4.3 Methodology

The process for applying ISO-GUM and MCA to the context of tidal energy yield uncertainty is presented below. The generic principles for the two methods are explained in Chapter 2. Note that the ISO-GUM methodology outlined below follows the guidance provided by OREC (2015*b*) exactly, and the same assumptions are applied. No specific guidance for the application of MCA for tidal energy yield uncertainty analysis could be found. Therefore, the methodology presented below was developed for this study, based on the generic principles.

It was assumed that the following information was available at the start of this process. A succinct description of the processes used to derive this information is provided in Section 4.2.1 and Section 4.2.2.

- Annual velocity timeseries for the site resource as per IEC (2015);
- Power curve for turbine and performance loss factors as per IEC (2013) and OREC (2015*b*);
- Uncertainty distributions for all applicable resource and loss uncertainties in Table 4.2, quantified as recommended in OREC (2015*b*).

The general process for combining the uncertainties is described in detail below and a flowchart of the processes for ISO-GUM and MCA is shown in Figures 4.3 and 4.4, respectively.

Note that the time domain method for yield calculation was used for this analysis (Equation 4.1). Since power curves are specified in velocity bins, as explained in Section 4.2.1, linear interpolation was used to calculate the power output for velocities between the bin edges. This approach was preferred over the less

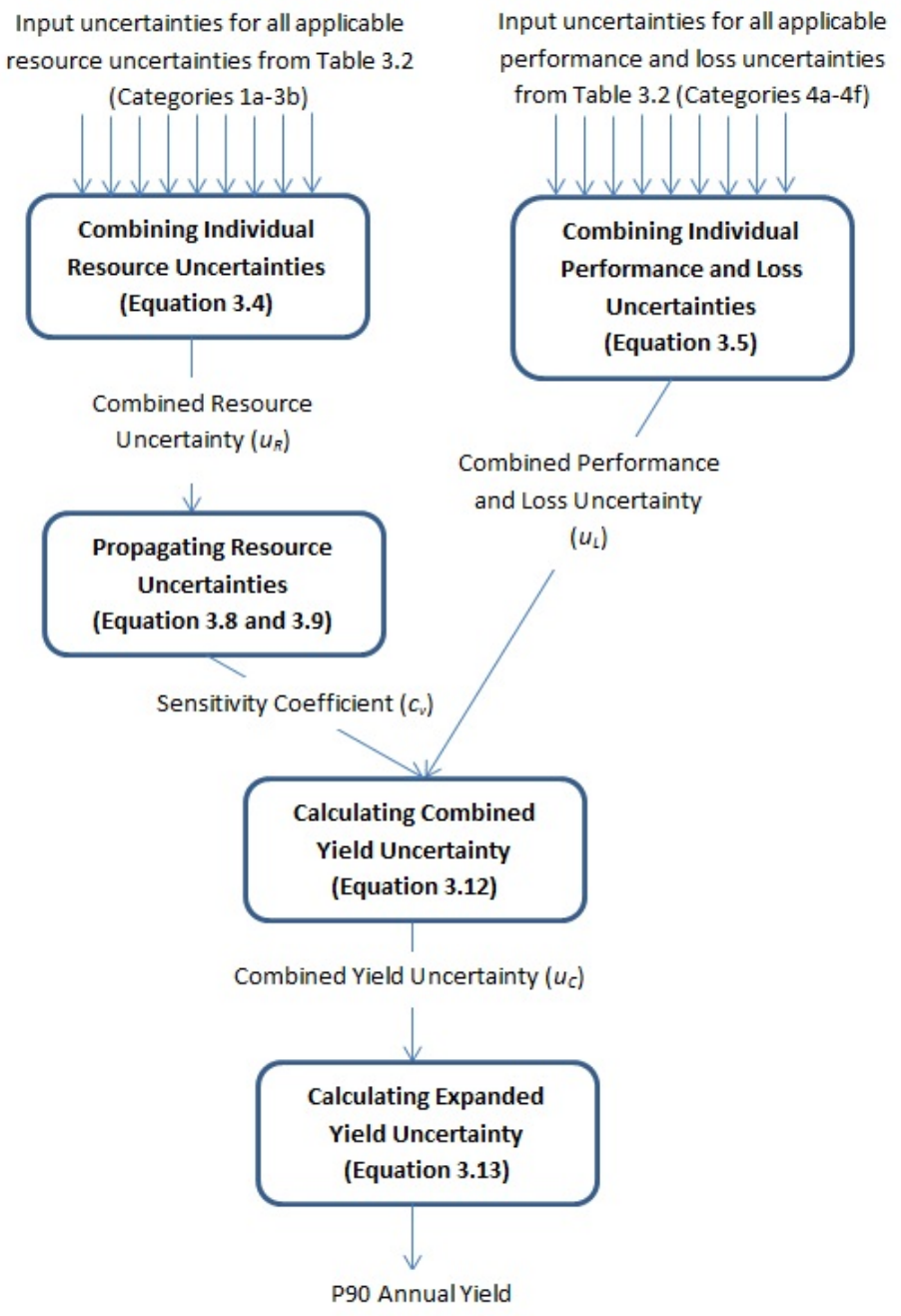

Figure 4.3: Flowchart of yield uncertainty analysis methodology using ISO-GUM. Each process in the analysis is shown inside boxes and the the process inputs/outputs are shown on the arrows.

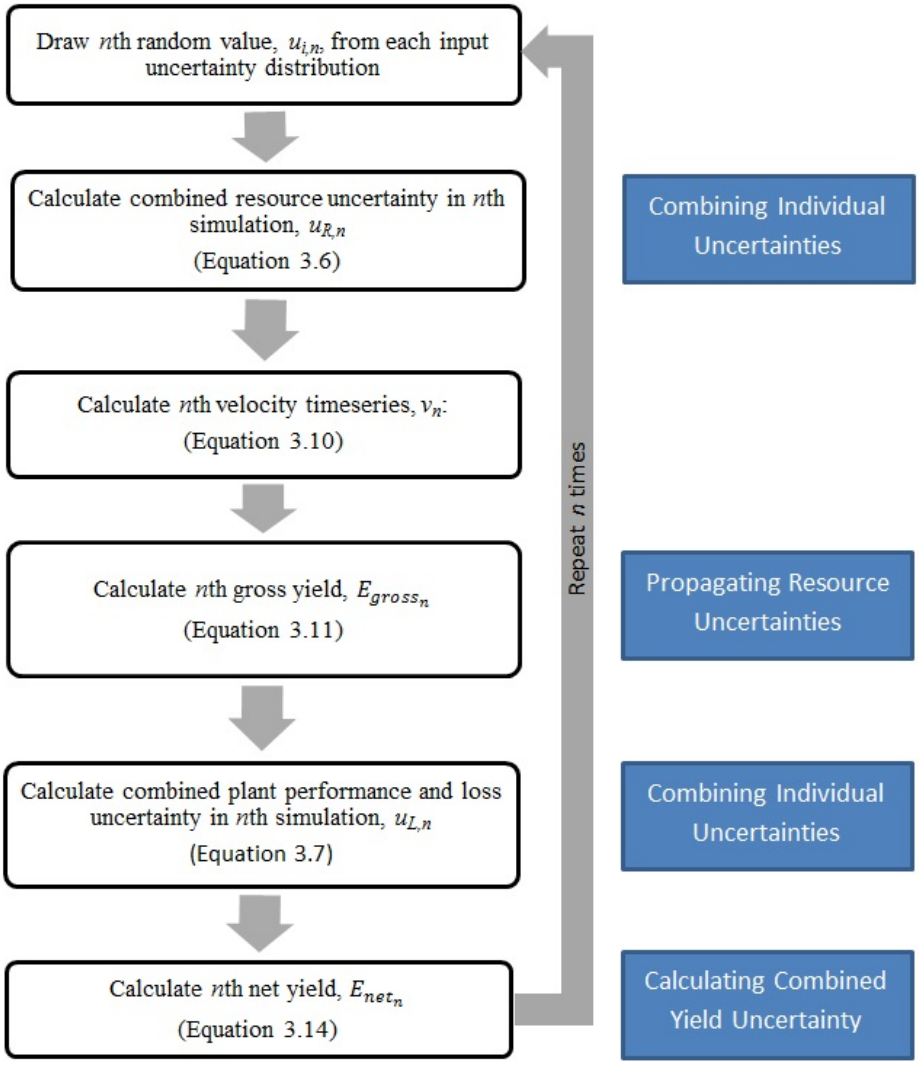

Figure 4.4: Flowchart of yield uncertainty analysis methodology using MCA. The blue boxes relate to the equivalent processes for ISO-GUM shown in Figure 4.3.

computationally demanding frequency domain method (Equation 4.2), or a non-interpolated time domain calculation, to avoid introduction of small numerical errors from the binning process which are not related to the topic of study.

4.3.1 Combining Individual Uncertainties

ISO-GUM

It is assumed that all of the individual uncertainties in Table 4.2 are Gaussian and uncorrelated (OREC, 2015*b*). The standard uncertainties of a number of variables with the same units may be summed in quadrature to calculate the combined standard uncertainty (JCGM, 2008*a*). Therefore, the standard uncertainty in the resource and losses, u_R and u_L, respectively, are calculated as:

$$u_R^2 = u_{1a}^2 + u_{1b}^2 + \cdots + u_{3b}^2 + u_{3c}^2 \tag{4.4}$$

$$u_L^2 = u_{4a}^2 + u_{4b}^2 + \cdots + u_{4f}^2 + u_{4g}^2 \tag{4.5}$$

where i in the standard uncertainty, u_i, corresponds to the labels of uncertainties in Table 4.2.

MCA

If n random numbers are drawn from each individual uncertainty distribution the combined uncertainty distribution sample is:

$$u_{R,n} = u_{1a,n} + u_{1b,n} + \cdots + u_{3b,n} + u_{3c,n} \tag{4.6}$$

$$u_{L,n} = u_{4a,n} + u_{4b,n} + \cdots + u_{4f,n} + u_{4g,n} \tag{4.7}$$

where the first half of the subscript (e.g. $1a$, $1b$ etc) corresponds to the labels of uncertainties in Table 4.2 and the n represents the n^{th} MCA simulation. The combined standard uncertainties, u_R and u_L, are the standard deviations of the combined distribution samples, $u_{R,n}$ and $u_{L,n}$, respectively. Note that it is quite simple to draw random numbers from input distributions that are correlated and/or non-Gaussian, but Gaussian uncertainties were initially assumed to allow a direct comparison to be made with ISO-GUM.

4.3.2 Propagating Resource Uncertainties

ISO-GUM

The uncertainties u_R and u_L cannot simply be summed in quadrature, as explained in Section 4.2.3. A sensitivity coefficient, c_v, representing the sensitivity of the annual yield to a change in velocity is required first to propagate the resource uncertainty to its yield equivalent value. As described in Section 2.4.2, ISO-GUM assumes that the functional relationship between the input and output variable is linear. Therefore, it is assumed that the resource-yield relation is linear (for small changes in resource) and c_v can effectively be calculated from the gradient of the resource-yield relation using Equation 4.8 (Ó'Catháin et al., 2013). The validity of the linearity assumption is tested in Section 4.4.

$$c_v = \frac{\left(\frac{E_{pert}}{E}\right) - 1}{\left(\frac{v_{pert}}{v}\right) - 1} \tag{4.8}$$

where v is the mean nominal velocity and E is the gross annual yield corresponding to the nominal annual velocity timeseries. The gross annual yield is calculated from the annual velocity timeseries using Equation 4.1. The nominal velocity is defined here as the velocity resulting from the resource assessment process

outlined in Section 4.2.1. v_{pert} is the perturbed mean velocity and E_{pert} is the corresponding perturbed gross annual yield. The perturbed velocity timeseries is derived by multiplying the nominal velocity timeseries by a small perturbation factor. A perturbation factor in the range of -3% to 3% is suggested in Ó'Catháin et al. (2013) and the use of an average c_v from perturbations of ±5% is suggested by OREC (2015*b*).

The c_v can be used to calculate the standard uncertainty in the yield due to the standard uncertainty in the resource, u_{E_R}:

$$u_{E_R} = c_v \times u_R \tag{4.9}$$

MCA

The resource-yield function is not assumed to be linear and is solved for each simulation, n, with the velocity timeseries multiplied by the combined resource uncertainty for that simulation, $u_{R,n}$ (Equation 4.10). Equation 4.11 is used to produce the gross annual yield uncertainty distribution due to resource uncertainty. Therefore any non-linearity will naturally be accounted for and propagated through to the yield uncertainty distribution.

$$v_{i,n} = v_i \times u_{R,n} \tag{4.10}$$

Where v_i is the nominal velocity timeseries derived from resource modelling, as described in Section 4.2.1 and i represents the data points in the timeseries.

$$E_{gross_n} = \frac{t}{m} \sum_{i=1}^{m} f(v_{i,n}) \tag{4.11}$$

where E_{gross_n} is the gross yield in the n^{th} simulation and m is the total number of datapoints in the annual velocity timeseries.

4.3.3 Calculating Combined Yield Uncertainty

ISO-GUM

The standard uncertainty in the annual yield due to the standard resource uncertainty, u_{E_R}, can be combined in quadrature with the standard loss uncertainties, u_L, to calculate the combined standard uncertainty in the annual yield, u_c:

$$u_c = \sqrt{u_{E_R}^2 + u_L^2} \tag{4.12}$$

As per the central limit theorem (CLT), it is assumed that the combined yield uncertainty distribution is also Gaussian (Ó'Catháin et al., 2013). The P90 yield can therefore be calculated from the P50 yield using a coverage factor of 1.282, as described in Section 2.4.2:

$$E_{Net_{P90}} = E_{Net_{P50}} - 1.282(u_c \times \ E_{Net_{P50}}) \tag{4.13}$$

where $E_{Net_{P50}}$ is the nominal net annual yield resulting from the unperturbed velocity timeseries and the nominal (most likely) loss assumptions. Note that the nominal net yield is equal to the P50 net yield because it is assumed that the yield uncertainty distribution is Gaussian and therefore the most likely (nominal) value is equal to the median (P50).

MCA

The combined loss uncertainties distribution sample, $u_{L,n}$, is multiplied by the gross annual yield distribution, E_{gross_n}, and the nominal losses assumed to calculate the combined yield uncertainty distribution, E_{net_n}:

$$E_{net_n} = \ E_{gross_n} \times Losses \times u_{L,n} \tag{4.14}$$

4.4 Comparing ISO-GUM and MCA

MCA repeatedly solves the functional relationship explicitly so its accuracy is simply a function of the number of simulations. Higher repetitions increases the density of sampling the analytical solution. The data presented in this study uses a highly converged simulation with 10^6 samples and is assumed to replicate the analytical solution very closely. The difference between MCA and ISO-GUM results is therefore referred to as the ISO-GUM error. It is important to note that this refers to the error introduced due to ISO-GUM, with all other assumptions being constant between the two methods. For example, any errors due to inaccuracies in the power curve etc affect ISO-GUM and MCA results equally and are not included in the error being considered here.

A number of different comparisons are presented below to thoroughly appraise the validity of the two methods for tidal energy yield uncertainty propagation. Realistic wind and tidal project annual yields were analysed first to understand differences in the linearity of the resource-yield functions to inform whether standard wind industry practices can be directly translated to the tidal energy context. Next, the stability of ISO-GUM results was tested over a number of linearisation ranges and the P90 yield was compared to MCA results for the tidal project. Finally, the analysis was repeated over an extensive range of plausible uncertainty magnitudes to highlight underlying reasons for divergence in results, and to identify thresholds on the validity of the methods.

4.4.1 Comparing Realistic Wind and Tidal Projects

There are many similarities in the principles of operation of wind and tidal turbines. As a result the sources of uncertainties are also similar, as can been by comparing Table 4.2 with the equivalent table for wind in DNV KEMA

(2013). However, the key uncertainties of significance are different due to the fundamental differences in the nature of the resource (Stock-Williams et al., 2013). For example, there is considerable uncertainty in the temporal modelling and vertical extrapolation of the wind resource (Clayton, 2016). Those uncertainties are low in tidal resource modelling due to the deterministic nature of the tides and data collection across the water column by ADCPs. Furthermore, there are considerable differences in the site velocity distribution and turbine power curves (as discussed later, and illustrated in Figures 4.5 and 4.8a). Since these two factors are critical to the yield assessment process, it is prudent to verify that the validity of ISO-GUM is maintained when applied to tidal projects. Representative conventional wind and tidal turbines were paired with representative long term wind and tidal site resource, respectively, to facilitate the comparison between ISO-GUM and MCA.

It is acknowledged that the methodology below is simpler than the standard approach applied in the wind industry. However, the methodology below is the direct equivalent of the current tidal industry recommendation. It is applied to allow a like-for-like comparison between wind and tidal projects.

Reference Tidal Project

A generic power curve was produced for a representative conventional tidal turbine. The defining characteristics of the turbine performance are summarised in Table 4.3 and the resulting power curve is shown in Figure 4.5a. Note that a generic power curve was used here instead of a real turbine power curve so that alternative power curves with variations in the defining characteristics could be produced easily for sensitivity analysis in Section 4.5. A cut-in velocity was not enforced as the effect of this on the annual yield is minimal and poses additional difficulty in producing the alternative power curves for sensitivity analysis.

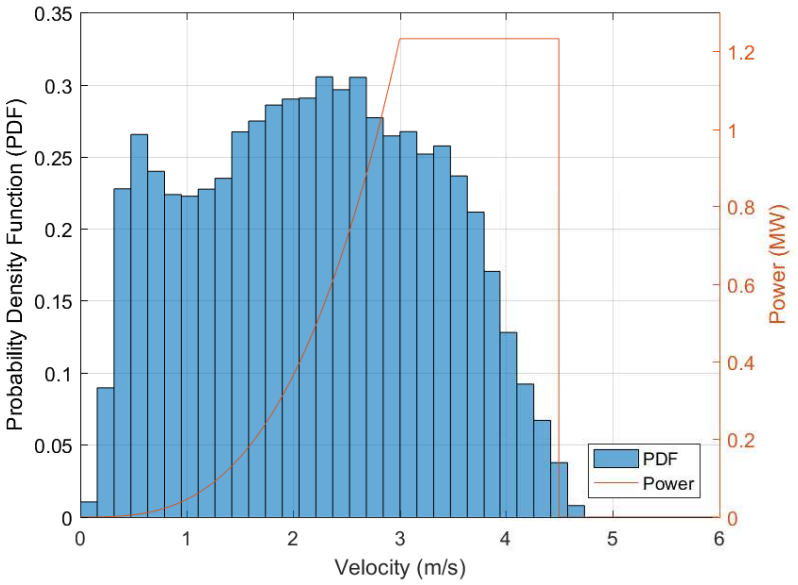

(a) Tidal Turbine

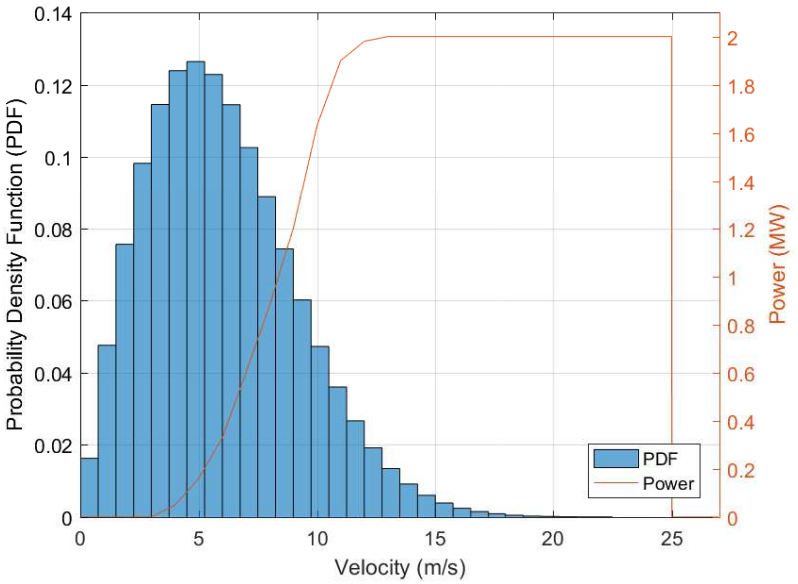

(b) Wind turbine

Figure 4.5: Representative wind and tidal turbine power curve and site resource.

Table 4.3: Defining characteristics of reference tidal turbine

Diameter (m)	Cp	Rated Velocity (m/s)	Cut-out Velocity (m/s)	Rated Power (MW)
18	0.35	3	4.5	1.2

Velocity timeseries data recorded by an ADCP at a site in the Pentland Firth, Scotland, was used as input velocity in this study (labelled ADCP1 in Figure 4.6). The characteristics of this measured dataset, Site 1, are summarised in Table 4.4. The raw data is processed as follows:

- Data from the top 5 m and bottom 10 m of the water column was removed to exclude data that is likely to be contaminated due to inherent principles of ADCP operation, such as sidelobe interference and surface wave interference (Stiven et al., 2011; RD Instruments, 2011);
- A power weighted depth averaged velocity across the rotor capture area was calculated as defined in IEC (2013). A rotor tip clearance of 10 m from the seabed was assumed to represent the height of the turbine support structure;
- Data was averaged over a 10 minute ensemble period to average out the effects of turbulence and high random error in single ADCP pings (RD Instruments, 2011);
- Harmonic analysis (described in Section 4.2.1) using UTide software (Codiga, 2011) was used to generate an annual velocity timeseries for the year 2017 from the post processed measured timeseries with a timestep of 10 minutes, referred to as the nominal resource.

A loss factor of 20% was chosen pragmatically for this study to derive the net yield. Note that the value of the loss factor is not significant because it affects ISO-GUM

Table 4.4: ADCP data specification for Site 1 (Pentland Firth)

Latitude/longitude (degrees)	58.66/-3.14
Measurement Period	17/02/13 to 23/03/13
Total Days Recorded	34
Ensemble Period (mins)	10
Pings Per Ensemble	1200

Figure 4.6: ADCP measurement locations

and MCA results equally and therefore does not affect the comparison. A factor was applied nonetheless because the uncertainty on the losses is considered in the study, so it is physically representative to also assume a value for the losses.

Reference Wind Project

A Vestas V90 2 MW wind turbine was considered in this analysis. It is a widely deployed model with a conventional rotor configuration and drivetrain architecture with a publically available power curve (Vestas, 2015). The representative site resource was assumed to have a Weibull distribution with k factor = 2 and a hub height mean velocity of 6 m/s, as assumed by the manufacturer to illustrate typical annual yield (Vestas, 2015). The k factor determines the shape of the distribution and the mean velocity defines the scale. The distribution characterises long term wind resource in the frequency domain. The statistical characterisation of wind resource using a Weibull distribution is described further in Seguro and Lambert (2000). The turbine power curve and site resource are shown in Figure 4.5b. Note that a 10% loss factor was assumed pragmatically to derive the net yield. It is lower than the value assumed for the tidal turbine because the yield loss due to availability, wakes etc. can be expected to be lower for a wind turbine. It is re-iterated that the precise value of the loss assumption is not important to the study results because the relative difference is of interest.

Validity of Linearity Assumption

As noted in Section 4.3.2, ISO-GUM assumes that there is a linear relation between change in velocity and change in yield for 'small changes'. Therefore, implicit in the validity of ISO-GUM is the assumption that the magnitude of resource uncertainty in the project under consideration is comparable to the

magnitude of the 'small change' over which the linearity assumption is valid. Figure 4.7 shows that the effect of change in resource on the annual yield is considerably more linear for the wind turbine than that for the tidal turbine for the same range of perturbations. Most importantly, the wind example displays a highly linear behaviour over the ± 20% perturbation range whereas the tidal example is notably non-linear (Figure 4.7b). It is considered that most realistic projects would have resource uncertainties within this range so the linear observation for the wind turbine suggests that the ISO-GUM linearity assumption is generally valid for wind projects. Indeed, only a small difference in yield uncertainty derived using ISO-GUM and MCA was found by Geer (2015) for a wind turbine. The higher non-linearity for the tidal turbine does not necessarily mean that ISO-GUM is invalid for tidal projects if the impact of assuming linearity anyway is small. The underlying reason for the tidal non-linearity is explained below first, and a study on the resultant impact under various circumstances follows afterwards.

The non-linearity in the tidal yield with change in perturbation can be explained by understanding the sources of non-linearity in the resource-yield relation. Consider a velocity below the rated velocity of a turbine. A slightly higher velocity will result in a higher yield compared to the nominal case (Figure 4.5). An increase in velocity at the rated velocity produces no increase in yield. An increase in velocity at the cut-out point causes a dramatic reduction in yield to zero. The precise function between annual yield and resource variation is the net effect of a variation over an annual timeseries of velocities. It is therefore defined by the relative positions of the resource frequency distribution and power curve. In general, a high occurrence of velocities much below the rated velocity results in a roughly linear increase in annual yield (as with wind turbine). A high proportion of occurrence close to the rated and cut-out velocity will lead to a non-linear change in yield with increasing perturbations (as with tidal turbine).

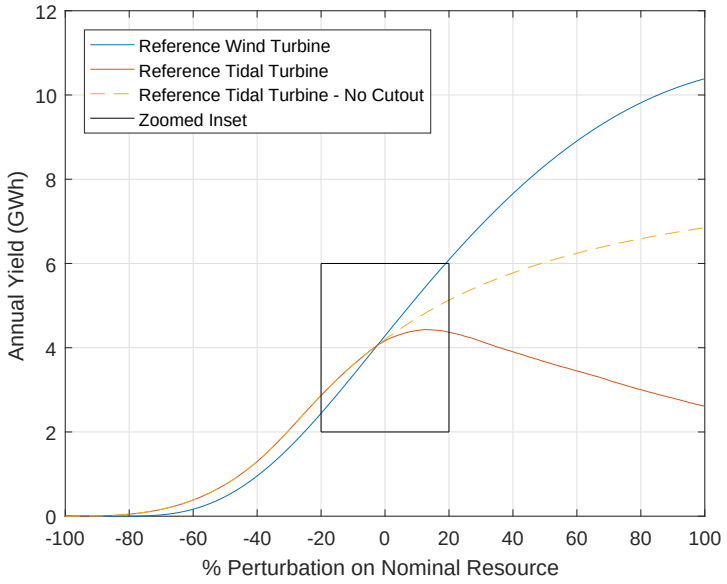

(a) ± 100% perturbations

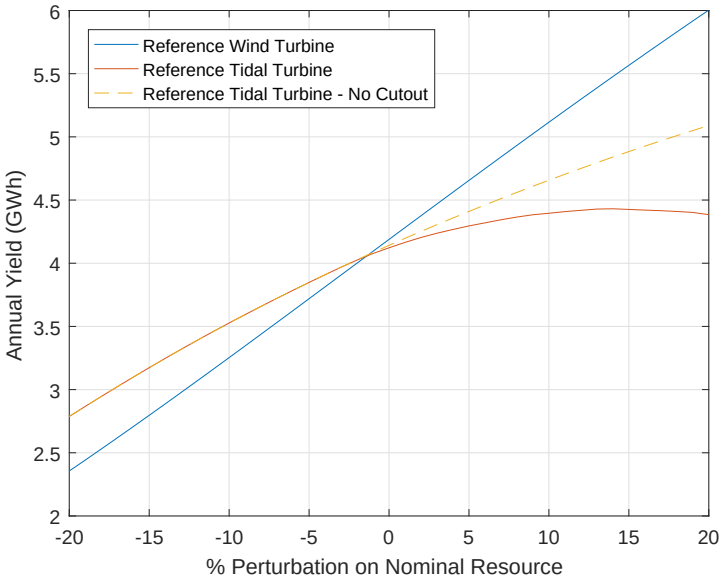

(b) Zoomed inset

Figure 4.7: Effect of resource perturbations on annual yield for reference wind and tidal turbines

To further illustrate this point, Figure 4.7 shows the resource-yield function for the same tidal turbine modelled without a cut-out velocity. This increases the linearity and the residual non-linearity can largely be attributed to the effect of the rated region of the power curve. Since the wind turbine has a much higher occurence of velocities in the lower part of the power curve, considerably larger perturbations on the nominal resource are required before the non-linear effects of the rated and cut-out regions become dominant.

Figure 4.8 shows that over 97% of the annual wind resource occurs below the rated velocity whereas less than 75% of the tidal resource is below rated velocity. The pre-rated velocities are responsible for approximately 90% and 45% of the annual yield for the wind and tidal turbines, respectively. A large perturbation of +20% pushes an additional 5% of the wind velocities and 15% of the tidal velocities above the rated velocity. More importantly, the large perturbation still does not result in a meaningful density of wind velocities occurring above the cut-out velocity whereas 10% of the tidal velocities cross this threshold. This explains the high sensitivity to the cut-out velocity observed in Figure 4.7. Note that a perturbation of 20% represents the P90 of a standard uncertainty of roughly 15%, i.e. a 90% probability of error in resource being smaller than 15%.

As shown in Figure 4.7, the linearity assumption is clearly valid for the wind turbine for standard uncertainties less than 15%. A different turbine model and site resource will alter the function somewhat, but the linearity assumption for wind energy should remain valid because the wind speed frequency distribution will always be highly skewed towards the minimum and the cut-out velocity of any turbine will always be considerably higher than the mean velocity. Therefore, the following analysis focusses only on the tidal turbine.

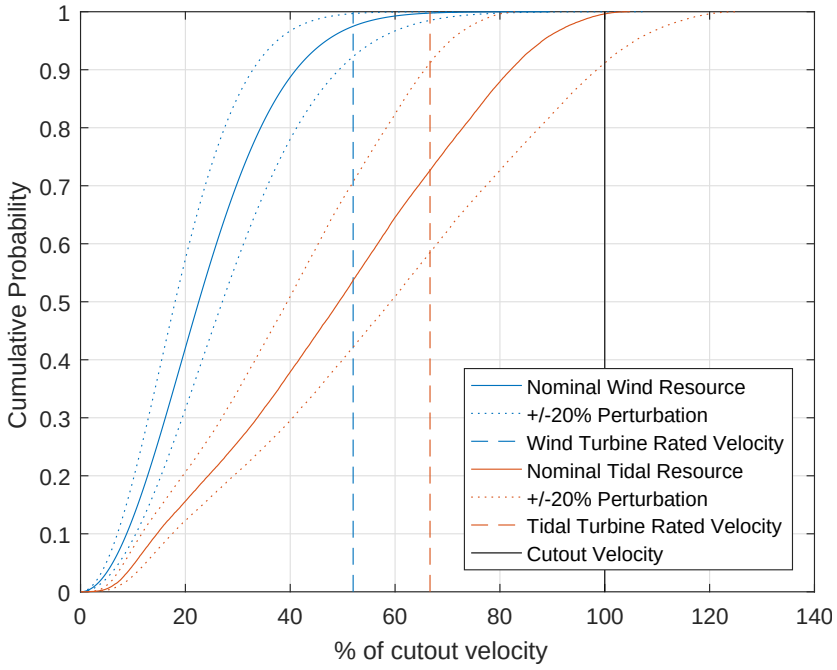

(a) CDF of normalised velocity occurrence

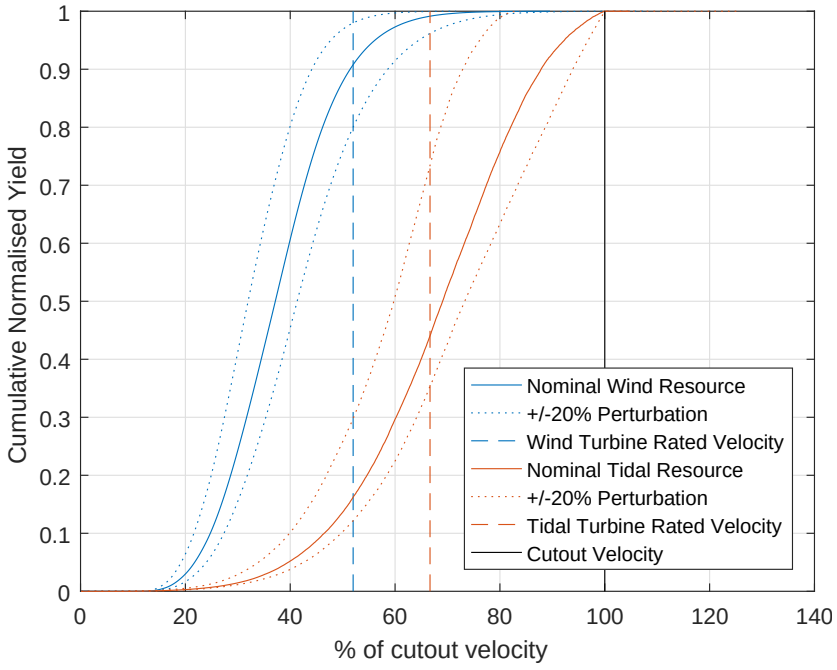

(b) CDF of normalised annual yield

Figure 4.8: Distribution of resource and yield relative to turbine rated and cut-out velocities for reference wind and tidal turbines. Note that the wind and tidal resource is normalised to the respective turbine cut-out velocities and the cumulative yield is normalised to the respective annual yields. This was done to facilitate comparisons between the wind and tidal cases which are quite different in absolute magnitudes.

4.4.2 Comparing ISO-GUM and MCA P90 Yield for Reference Tidal Project

ISO-GUM linearises the resource-yield function between the perturbation range used for linearisation in Equation 4.8. However, since the function is shown to be non-linear, the derived value of c_v can be expected to be dependent on the arbitrary perturbation range used for the analysis. Table 4.5 shows that there is some instability in c_v depending on the level of perturbation used and therefore also in the P90 yield. The impact of c_v instability on the P90 yield is magnified as the u_R increases.

It is therefore not advisable to use a generic c_v for a given site, irrespective of the exact resource uncertainty under consideration. A $\pm 2\%$ perturbation is used in the following analysis to highlight the exposure to inaccuracy if a generic compromise is used.

Figure 4.9 shows the linearised resource-yield function assumed by ISO-GUM with a c_v based on perturbations of $\pm 2\%$. The linearised function diverges significantly from the analytical solution ($\approx$ MCA solution), even for relatively small variations in the mean velocity. Consequently, ISO-GUM overestimates the P90 yield by 2.21% and 15.9% for standard resource uncertainties of 5% and 15%, respectively, for the reference case (Figure 4.10). There is better agreement at the P50 level, with ISO-GUM overestimating P50 yield by 0% and 0.78% for standard resource uncertainties of 5% and 15%, respectively. The yield uncertainty distribution is not Gaussian as assumed by ISO-GUM because it is truncated at the peak yield beyond which a higher resource results in a lower yield as the effect of turbine cut-out becomes more dominant. This results in a large overestimate of the P10 yield. However, in general the P50 and P90 (or similar) are of more interest than the P10 (or similar) from an investor's point of view.

Table 4.5: Effect of using a range of arbitrary perturbation levels on ISO-GUM model results

Pert.	**Description**	$\mathbf{c_v}$	**ISO-GUM P90 Yield (GWh)**		**Overestimate compared to MCA P90 (%)**	
			u_R=5%	u_R=15%	u_R=5%	u_R=15%
±5 %	As suggested in OREC (2015*b*)	0.986	3.90	3.38	2.05	15.30
-0.50%	As suggested in Ó'Catháin et al. (2013)	0.941	3.91	3.41	2.36	16.50
±2 %	Generically representative compromise	0.963	3.91	3.39	2.21	15.90

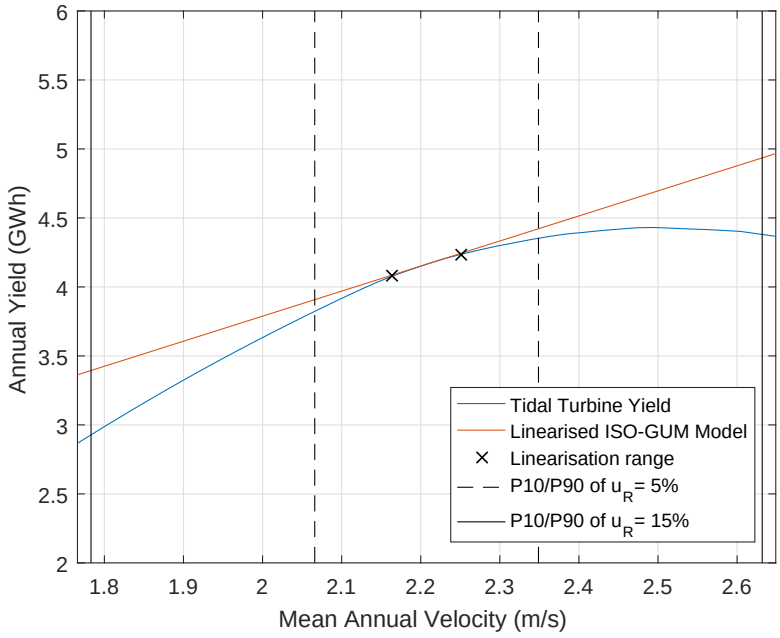

Figure 4.9: Comparing ISO-GUM linearisation with analytical resource-yield function. Note that a ±2% resource perturbation is used for linearisation.

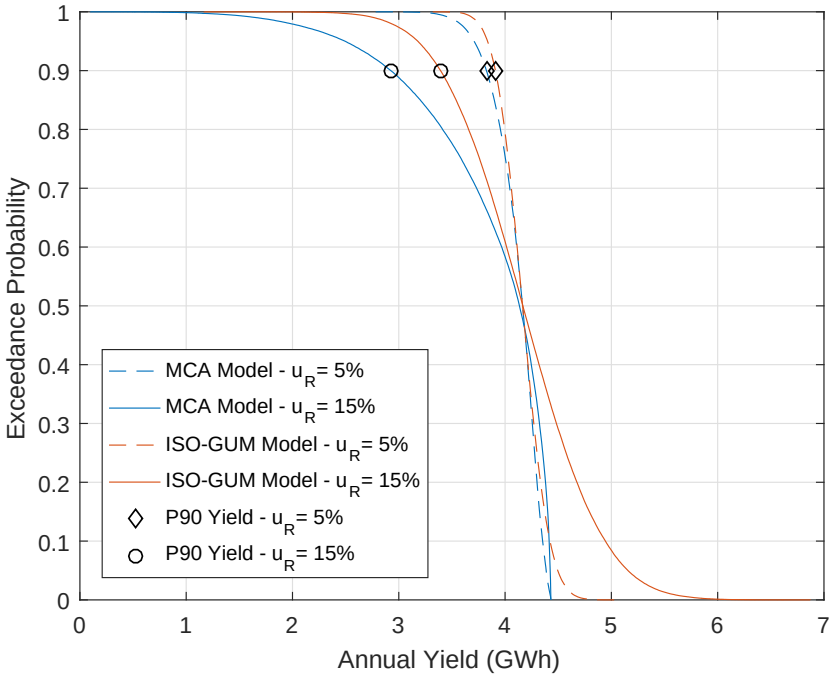

Figure 4.10: Annual yield uncertainty distributions due to resource uncertainty of 5% (dotted lines) and 15% (solid lines) for reference tidal project.

The skewed yield uncertainty distribution produced by MCA when only the resource uncertainties are accounted (Figure 4.10) becomes considerably more Gaussian due to the effects of the CLT when combined with the Gaussian loss uncertainty distribution (Figure 4.11). As a result, the agreement between the ISO-GUM and MCA estimates of the P90 yield improves. This effect is more pronounced when the loss uncertainty is higher. Whilst it may be intuitive to assume that a larger loss uncertainty will exaggerate the discrepancy in ISO-GUM and MCA results due to resource uncertainty, the contrary is true. This is because the loss uncertainty distribution is Gaussian and a larger uncertainty results in the skew of the annual yield distribution (due to resource uncertainty) becoming less dominant in the combined annual yield distribution. Table 4.6 shows the resultant decrease in ISO-GUM P90 yield error and increase in ISO-GUM P50 yield error with increasing loss uncertainty.

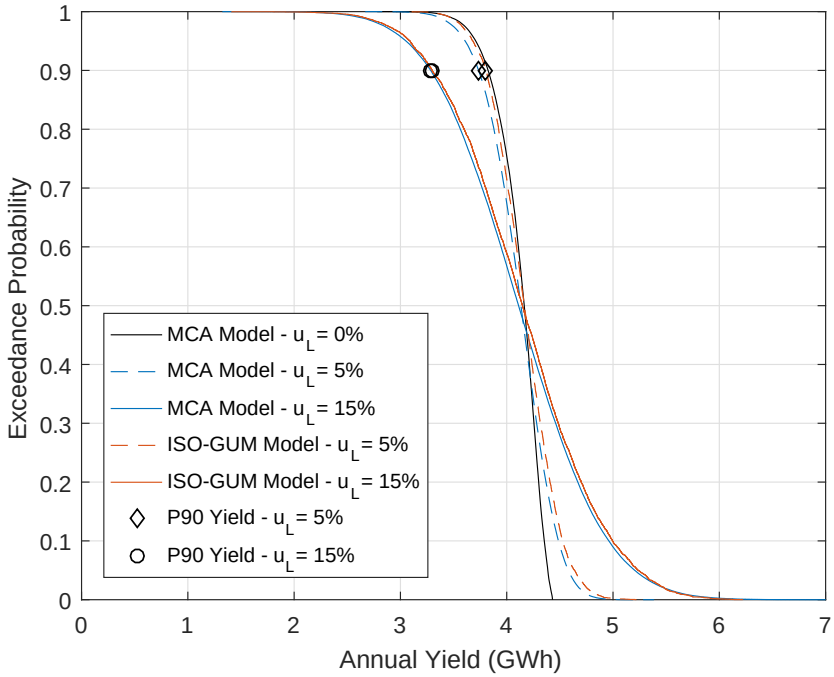

(a) $u_R = 5\%$ (Comparable to dotted lines in Figure 4.10)

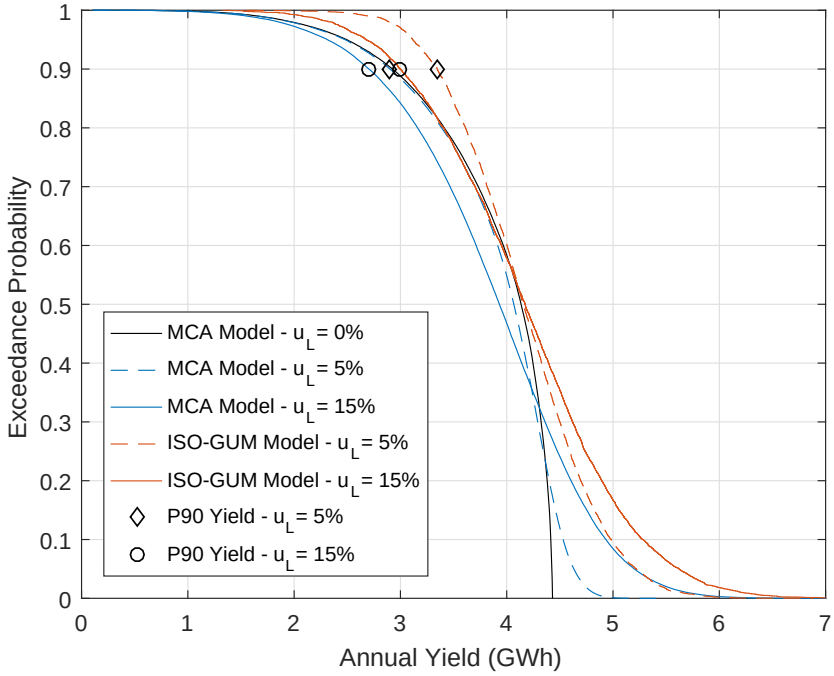

(b) $u_R = 15\%$ (Comparable to solid lines in Figure 4.10)

Figure 4.11: Combined annual yield uncertainty distributions for varying u_R and u_L, derived using ISO-GUM and MCA

Table 4.6: ISO-GUM P90 and P50 overestimate for varying u_R and u_L for reference tidal case.

	P90 Overestimate		**P50 Overestimate**	
	$u_R = 5\%$	$u_R = 15\%$	$u_R = 5\%$	$u_R = 15\%$
$u_L = 0\%$	2.21	15.90	0.00	0.78
$u_L = 5\%$	1.85	15.43	0.76	2.40
$u_L = 15\%$	1.19	12.84	1.25	5.95

4.4.3 Comparing ISO-GUM and MCA P90 Yield for a Range of Realistic Projects

The ISO-GUM and MCA P90 yields for the reference tidal project were compared for a range of uncertainty values to add granularity to the analysis in the previous section and to identify thresholds of validity. Standard uncertainties for u_R and u_L ranging from 0% to 15% in increments of 1% were analysed. This range is considered to cover the full range of uncertainties that may be encountered in realistic projects. The trends discussed in the previous section are still apparent in Figure 4.12a. For a given u_L, a higher u_R results in ISO-GUM overestimating the P90 yield by a larger amount as the linearised model gradient diverges further from the analytical value. For a given u_R, a higher u_L reduces the difference between ISO-GUM and MCA P90 yield slightly. A 2% overestimate in yield potentially erodes the profit margin of project by a large percentage and is therefore considered as a reasonable threshold beyond which the method may be deemed unsuitable for use by a developer or financier. This pragmatic assumption is also based on consideration of an estimate by Economist (2010) that a P90 difference of 2-8% can lead to a 0.5-0.75 percentage point difference in the cost of finance.

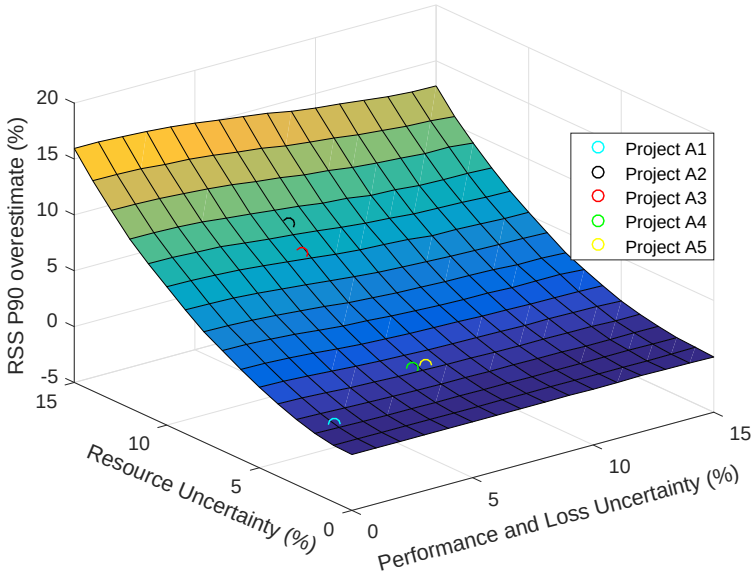

(a) Range of u_R and u_L

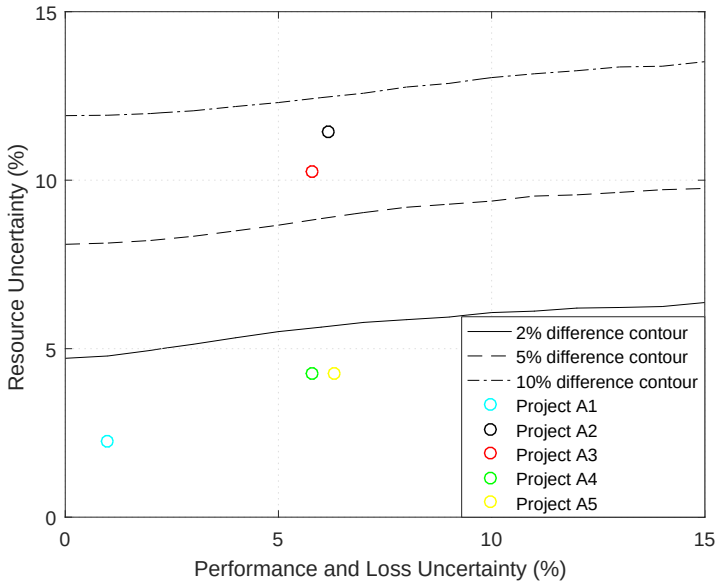

(b) Error threshold contours

Figure 4.12: Difference between ISO-GUM and MCA P90 yield for reference tidal project for range of uncertainty combinations and for specific standard uncertainties representing example projects in OREC (2015*b*). The example project characteristics are summarised in Table 4.7. A generic c_v based on a $\pm 2\%$ perturbation was used.

As shown in Figure 4.12b, a resource uncertainty of 5-6% will result in this threshold being exceeded irrespective of the loss uncertainty. The resource and performance loss uncertainties for a range of realistic projects has been quantified by OREC (2015*b*), and summarised in Table 4.7. Figure 4.12 and Table 4.7 show the overestimate in ISO-GUM P90 yield compared to MCA for these projects. Considerable difference is seen for the higher uncertainty projects when a generic c_v based on a ±2% perturbation is used.

4.5 Sensitivity Analysis

The results in the previous section are true for the specific case of the reference tidal project, but cannot be interpreted intuitively for a different project with a different turbine or resource. As such, the following section presents the sensitivity of the method accuracy to each of the variables that affect the position of the velocity frequency distribution relative to the power curve, and also to the perturbation level used to derive c_v. Variables considered that affect the power curve are turbine diameter, rated velocity, cut-out velocity and Cp. Variables considered that affect the site resource are the site location and year of consideration. The range of sensitivity test values, shown in Table 4.8, was chosen such that all realistic projects are encompassed within it. Furthermore, three perturbation ranges for calculating the c_v were considered in the sensitivity analysis; ±5%, ±2% and -0.5%, as in Table 4.5.

Figure 4.15 shows the variation in ISO-GUM P90 yield error over a range of resource uncertainties and turbine rated velocities. For a given rated velocity, the error increases with increasing resource uncertainty. For a given resource uncertainty, the error is generally larger for increasing rated velocities up to 3.4 m/s. This is because a higher rated velocity results in higher non-linearity of

Table 4.7: Example project characteristics (OREC, 2015*b*) and resulting ISO-GUM overestimate

Project	**Description**	$\mathbf{u_R}$(%)	$\mathbf{u_L}$(%)	**ISO-GUM overestimate (%)**
A1 Single turbine	1x 28 day ADCP record, warranted availability and turbine performance	2.24	1.00	0.43
A2 5-turbine array, minimal data	1x 28 day ADCP record, 2D hydrodynamic modelling, validated power curve, minimum performance and availability warranty	11.42	6.16	8.32
A3 5-turbine array, moderate data	As A2, but with 3D CFD modelling of resource and wake interactions	10.25	5.79	6.82
A4 5-turbine array, maximum data	As A3, but 90 day ADCP record and additional 30 day deployments for model validation	4.25	5.79	1.22
A5 10-turbine array	As A4, but larger turbine distance from ADCP location and blockage effects significant	4.25	6.30	1.09

Table 4.8: Summary of sensitivity test cases (varying parameter in italics). Note that the location of Sites 2 and 3 is shown on Figure 4.6, labelled as 'ADCP2'. The annual velocity timeseries for these sites is presented in Figure 4.14 and the specification of the ADCP datasets is summarised in Table 4.9.

Test	Sensitivity Test Variable	Diameter (m)	Cp	Rated Velocity (m/s)	Cut-out Velocity (m/s)	Site	Year
#00	Reference Case	18	0.35	3	4.5	1	2017
#01	Diameter	*15*	0.35	3	4.5	1	2017
#02		*16.5*	0.35	3	4.5	1	2017
#03	Cp	18	*0.3*	3	4.5	1	2017
#04		18	*0.4*	3	4.5	1	2017
#05	Rated Velocity (m/s)	18	0.35	*2.6*	4.5	1	2017
#06		18	0.35	*2.8*	4.5	1	2017
#07		18	0.35	*3.2*	4.5	1	2017
#08		18	0.35	*3.4*	4.5	1	2017
#09	Cut-out Velocity (m/s)	18	0.35	3	*4.1*	1	2017
#10		18	0.35	3	*4.3*	1	2017
#11		18	0.35	3	*4.7*	1	2017
#12		18	0.35	3	*4.9*	1	2017
#13	Site	18	0.35	3	4.5	*2*	2017
#14		18	0.35	3	4.5	*3*	2017
#15	Year	18	0.35	3	4.5	1	*2022*
#16		18	0.35	3	4.5	1	*2027*
#17		18	0.35	3	4.5	1	*2032*
#18		18	0.35	3	4.5	1	*2037*

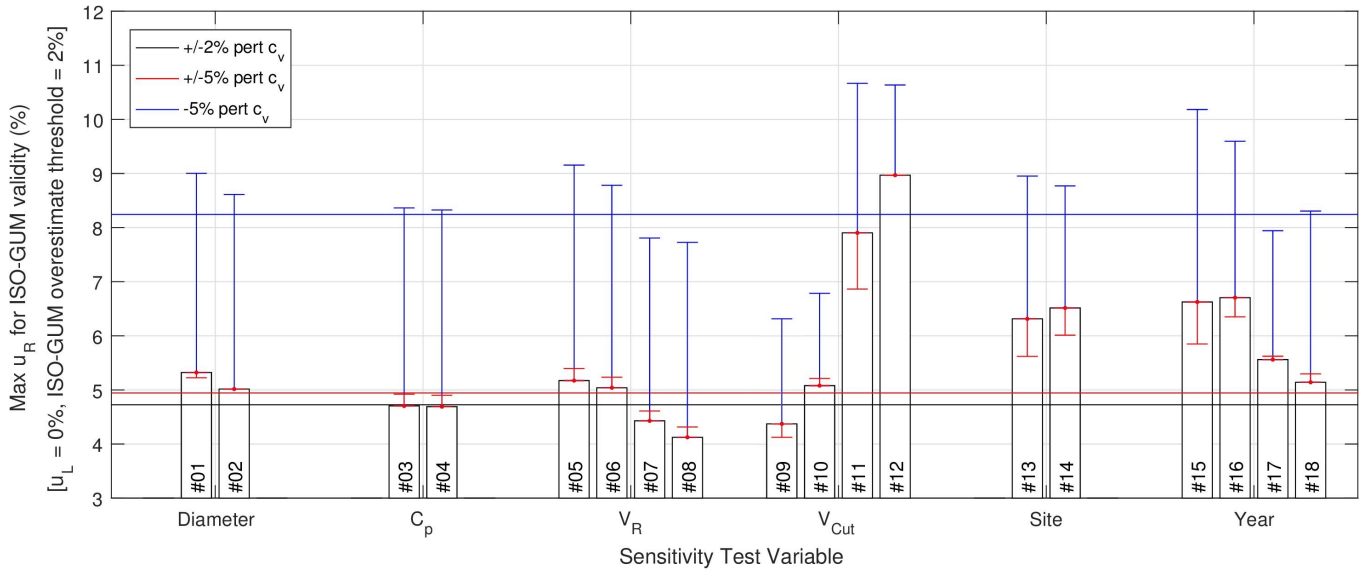

Figure 4.13: 2% ISO-GUM P90 yield error threshold uncertainties for reference project and sensitivity test cases using different c_v definitions. The rectangular bars show the sensitivity test cases using $\pm 2\%$ perturbation c_v and the error bars show the variation resulting from changing c_v perturbation for each case. The reference project values are shown as solid horizontal lines. The test variables are defined in Table 4.8.

Table 4.9: ADCP data specification for Site 2 and 3 (EMEC, 2014). The resource distribution is presented in Figure 4.14.

Location	Site 2	Site 3
Latitude/Longitude (degrees)	59.14/-2.81	59.16/-2.83
Measurement Period	19/03/05 to 21/04/05	18/08/05 to 28/09/05
Total Days Recorded	33	41
Ensemble Period (mins)	20	20

the resource-yield function due to a higher proportion of the velocity timeseries data being in the non-linear part of the power curve. Further increases in rated velocity reduces the error as the point of peak sensitivity shifts out of the non-linear power curve region. This statement is valid for this case, but the trends could be different if a different resource and/or cut-out velocity is considered. Figure 4.13 shows the trends for varying all sensitivity analysis variables.

The maximum resource uncertainty before a 2% ISO-GUM P90 yield error is reached is presented in Figure 4.13 for all sensitivity test cases. Note that the data is presented for a fixed loss uncertainty of 0% as the effect of varying u_L is comparatively small and intuitively interpreted because it is roughly linear, as observed in Figure 4.13.

Considerable difference in the accuracy of the ISO-GUM method is seen in the sensitivity analysis. The underlying reasons for trends observed for each sensitivity test parameter are described next, followed by an interpretation of the implications for tidal energy annual yield uncertainty analysis for a given project.

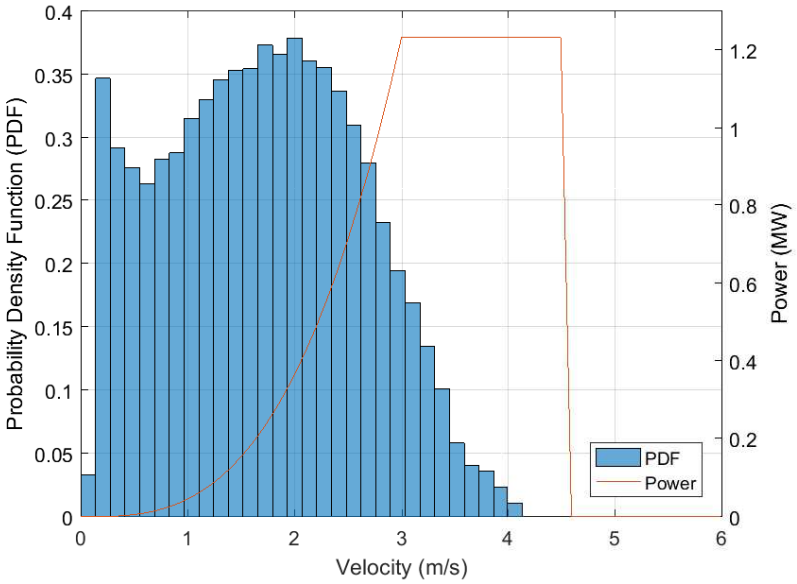

(a) Site 2

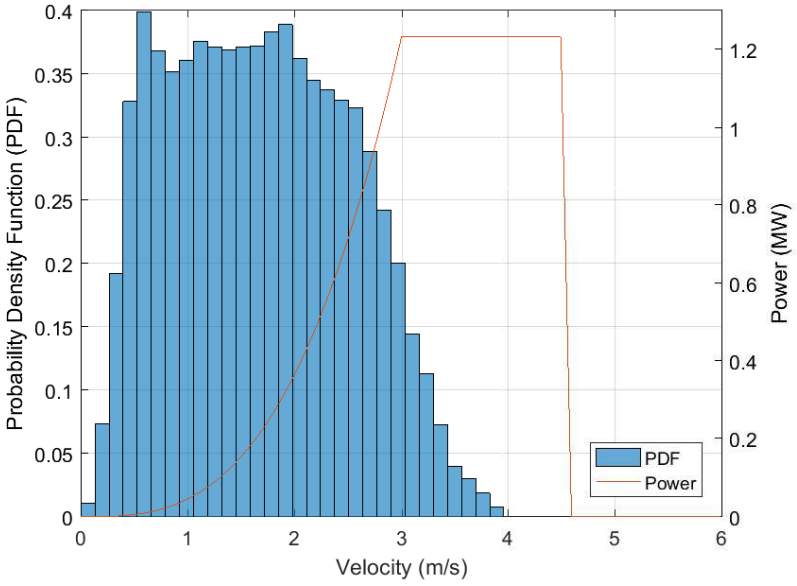

(b) Site 3

Figure 4.14: Representative tidal turbine power curve and site resource at Site 2 and 3, defined in Table 4.9. Note that the data presented shows an annual timeseries for year 2017 derived using the process outlined in Section 4.4.1.

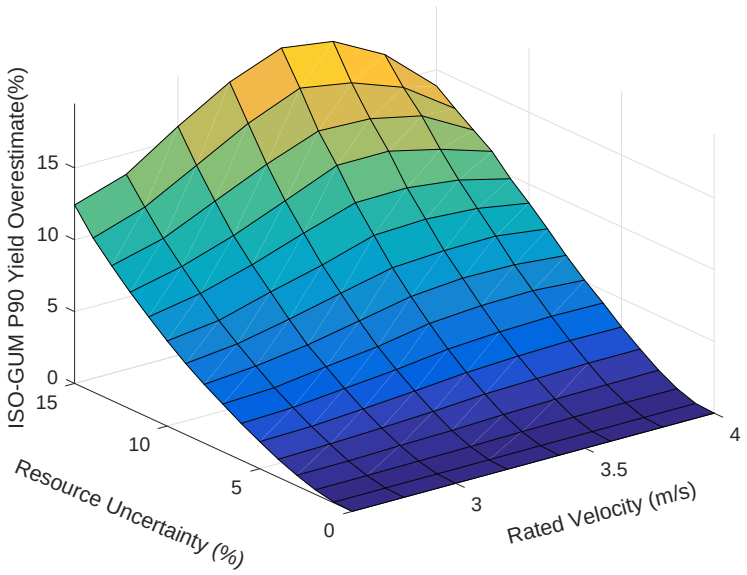

Figure 4.15: Sensitivity of ISO-GUM P90 yield error to variation in resource uncertainty and rated velocity. Note that these results are derived using a c_v derived from $\pm$2% perturbations. The resource uncertainty resulting in a 2% overestimate for all sensitivity test parameters, including the rated velocity, is presented in Figure 4.13.

Explanation of Trends

Increasing rotor diameter increases the ISO-GUM inaccuracy slightly. This is due to the higher swept area leading to higher power capture from a given flow rate. The difference is disproportionately larger at higher velocities because the power capture is a cubic function of the velocity. Therefore, there is a higher sensitivity to the higher end of the power curve, such as the occurrences close to the rated and cut-out velocities. These occurrences introduce the non-linearity that is the root cause of ISO-GUM inaccuracy, and increasing rotor diameter therefore increases ISO-GUM inaccuracy.

There is negligible sensitivity to variation in the C_P because it has a linear effect on the power capture across the velocity range. The change in C_P therefore does not impact the ISO-GUM accuracy.

The effect of varying rated velocity has already been discussed in detail previously in this section when describing Figure 4.15.

There is an increase in ISO-GUM accuracy with an increase in cut-out velocity. An increase in cut-out velocity reduces the non-linearity of the velocity-yield function because it reduces the occurrences of velocities crossing the cut-out threshold (a significant source of non-linearity) with all other parameters being equal.

ISO-GUM is more accurate for Sites 2 and 3 than it is for Site 1. This is because Site 1 has a higher resource, as can be seen by comparing Figure 4.5a and Figure 4.14. A lower resource results in a higher proportion of the yield being generated from the lower, more linear parts of the power curve, thus increasing ISO-GUM validity. ISO-GUM is slightly more accurate for Site 3 than for Site 2. The mean velocity for Site 2 and Site 3 is 1.71 m/s and 1.69 m/s, respectively.

The slightly lower resource at Site 3 may be the reason for the slightly higher accuracy, however it is not possible to declare this conclusively based on mean velocity only. This is because the frequency of occurrences of a slightly higher velocity site could in theory be such that the resultant velocity-yield function is more linear than that of an alternative site with a lower mean velocity (i.e. if there is a high concentration of low velocities with a long high velocity tail).

Finally, considerable sensitivity is observed with a variation in year of operation. The effect of lower frequency tidal harmonics causes some variation in the annual resource at the same site dependent on the year of operation. As shown in Table 4.10, year 2022 and 2027 have a similar annual mean velocity and year 2032 and 2037 have a similar annual mean velocity, but it is higher than the former years. As with the variation in resource due to site location, the result of the higher resource is a higher ISO-GUM error due to higher non-linearity in the resource-yield function.

Table 4.10: Mean annual velocity for each year considered in the sensitivity test

Sensitivity Test	Analysis Year	Mean Annual Velocity (m/s)
#15	2022	2.123
#16	2027	2.121
#17	2032	2.197
#18	2037	2.199

In addition to the variation in the assumed values for the sensitivity test variables, Figure 4.13 also shows the sensitivity of ISO-GUM accuracy to a variation in the perturbation used to derive the c_v. In general, using a -5% perturbation results in a significant difference compared to the reference perturbation of ±2%. The difference resulting from using a ±5% perturbation is also notable, but smaller. These variations are due to the numerical error introduced when linearising

the various resource-yield functions under the varying linearisation assumptions. Given that the observed variations are not related to underlying physical reasons (as with the previous explanations), it is not accurate to make general statements regarding the validity of ISO-GUM in relation to the choice of perturbation factor for a particular variation in project parameters.

Implications of Sensitivity Test Results

It is possible to make qualitative statements about the accuracy of ISO-GUM for variations in project parameters, as done in the previous section. However, it is not simple to quantitatively estimate the accuracy of ISO-GUM for a particular combination of project parameters. The analysis above quantifies the error for variations in one parameter whilst keeping other parameters constant. There are a very large number of feasible combinations of project parameters beyond those analysed here and the results here cannot be intuitively extrapolated to a similar, but unanalysed case. This is because the ISO-GUM accuracy is a result of the compound effect of various physical and numerical phenomenon. For example, simply considering the resource for year 2022 instead of the reference year 2017 allows an approximately 40% higher resource uncertainty for the 2% error threshold to be reached. This may be because the 2017 mean annual velocity is 4% higher and therefore there is a higher density of velocities in the non-linear region of the power curve. However, the differences observed are often due to the numerical error in the ISO-GUM assumption rather than due to a physical reason. This is evident in the fact that the threshold u_R for any given test case varies considerably depending on the perturbation used. Furthermore, the trends observed for a particular sensitivity test variable are not necessarily consistent when a c_v using a different perturbation level is used. For example tests #11 and #12 have a similar maximum allowable u_R with a c_v based on a -5% perturbation,

but there is a considerable difference between the two when a ±5% perturbation is used instead.

Crucially, the ISO-GUM validity threshold of 2% error is exceeded for almost all sensitivity cases for resource uncertainties less than 12%, which is not an extreme value. Given the above, it may be possible to understand pragmatically the relative accuracy of ISO-GUM for a given project based on its relative parameters (e.g. low resource relative to high cut-out should result in relatively high accuracy), but a significant doubt would remain over the magnitude of the error in the analysis and whether it is acceptable in absolute terms. A detailed comparison, as presented here, requires considerable effort and is unlikely to be feasible for commercial project decisions. This is particularly true given that the use of MCA requires less effort and provides consistently accurate results.

4.6 Custom Sensitivity Coefficient

As seen in Figure 4.9, the resource-yield function is highly non-linear. As described in Section 4.3.2, ISO-GUM uses a small perturbation about the nominal resource to fit a linear function for deriving the sensitivity coefficient, c_v. Given the non-linearity in the analytical resource-yield function, this results in the fitted linear function diverging significantly from the analytical function for deviations from the nominal resource that are much larger than perturbation used for linearisation. If the P90 yield is of interest, then it is proposed that a custom c_v is calculated using a perturbation equal to the P90 of the resource uncertainty, u_R, under consideration.

Figure 4.16 shows the difference in the resulting linearised function when the P90 of u_R is used. The custom c_v derived with this approach was used to calculate the P90 yield for the reference tidal project in Section 4.4. Figure 4.17 shows

the result and they can be compared to the results in Figure 4.10, which use a generically representative c_v derived using a ±2% perturbation. There is a significant reduction in the difference between the MCA and ISO-GUM P90 yield. Note that closest agreement between MCA and ISO-GUM occurs at the P90 level because the c_v is customised for accuracy in the P90 result. Table 4.11 shows the Figure 4.17 results numerically and is comparable to Table 4.5, which shows the equivalent results for a range of arbitrary perturbation levels from literature. Table 4.12 shows the P90 yield ISO-GUM overestimate using the custom c_v approach for the 5 example projects defined by OREC (2015*b*). It is comparable to Table 4.7, which uses the generically representative ±2% perturbation to derive the c_v. In all cases, note the significant reduction in the ISO-GUM P90 yield error.

Table 4.11: Effect of using custom perturbation levels on ISO-GUM model results

Pert.	**Description**	**c_v**	**ISO-GUM P90 Yield (GWh)**		**Overestimate compared to MCA P90 (%)**	
			u_R=5%	u_R=15%	u_R=5%	u_R15%
-6.41%	P90 of $u_R = 5$ %	1.281	3.82	3.14	-0.01	7.23
-19.20%	P90 of $u_R = 15$ %	1.545	3.75	2.93	-1.86	0.02

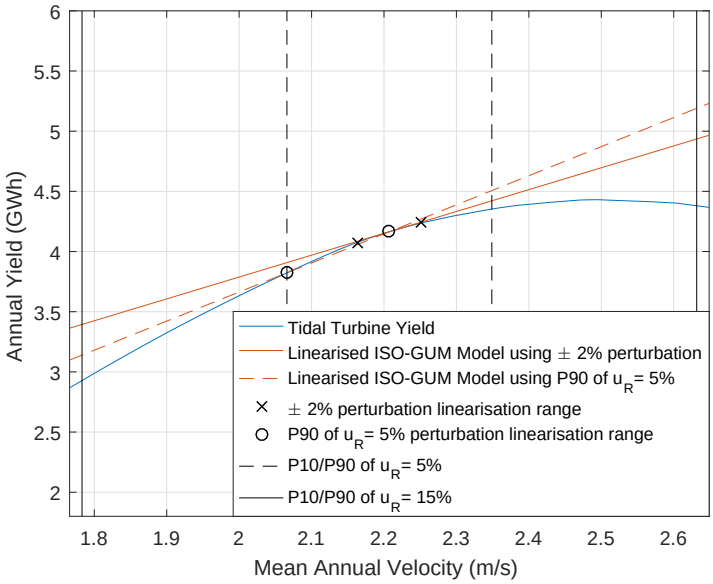

(a) Using P90 of $u_R = 5\%$ for linearisation

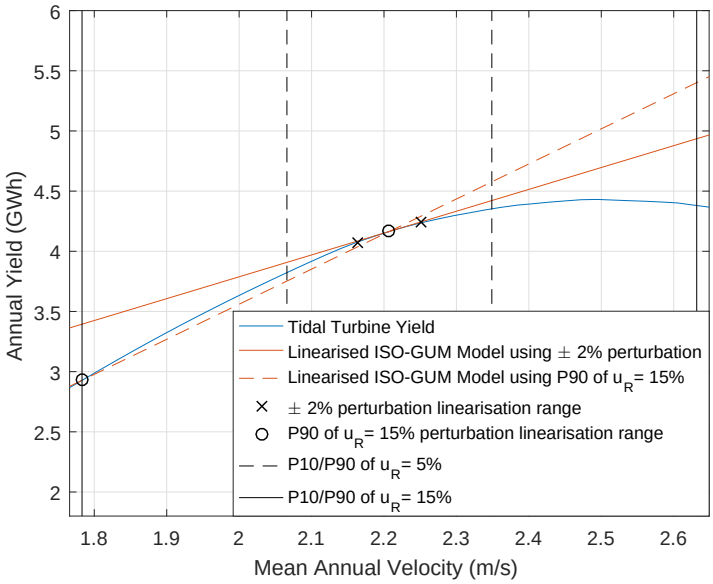

(b) Using P90 of $u_R = 15\%$ for linearisation

Figure 4.16: Comparing analytical resource-yield function with ISO-GUM linearisation using a generically representative ±2% perturbation and a custom perturbation equal to the P90 of the u_R.

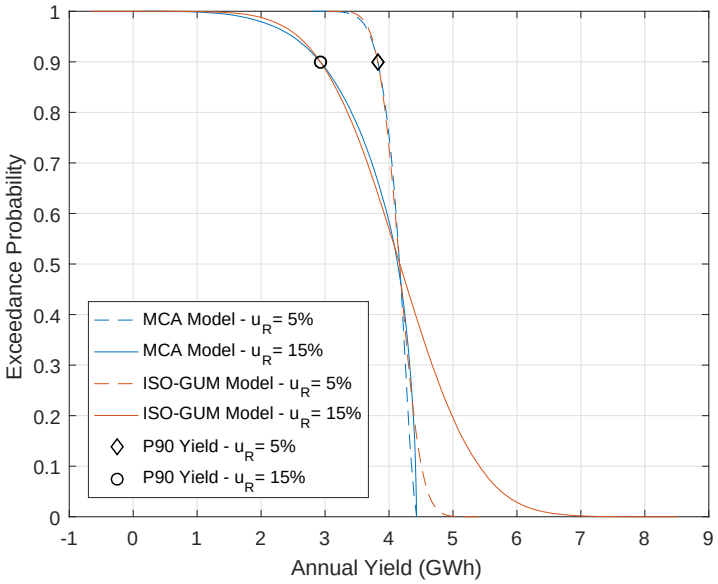

Figure 4.17: Annual yield uncertainty distributions due to resource uncertainty of 5% (dotted lines) and 15% (solid lines) for reference tidal project. The ISO-GUM results are derived with the custom c_v approach of using the P90 of u_R for linearisation, as shown in Figure 4.16. Therefore the $u_R = 5\%$ case uses a c_v derived using the function represented with the dotted red line in Figure 4.16a and the $u_R = 15\%$ case relates to Figure 4.16b. Note the reduction in P90 yield difference compared to the results in Figure 4.10 which use a generically representative $\pm 2\%$ perturbation for linearisation.

Table 4.12: Example project characteristics (OREC, 2015*b*) and resulting ISO-GUM overestimate using custom c_v

Project	**Description**	$\mathbf{u_R}$(%)	$\mathbf{u_L}$(%)	**ISO-GUM overestimate (%)**
A1 Single turbine	1x 28 day ADCP record, warranted availability and turbine performance	2.24	1	-0.2
A2 5-turbine array, minimal data	1x 28 day ADCP record, 2D hydrodynamic modelling, validated power curve, minimum performance and availability warranty	11.42	6.16	-0.29
A3 5-turbine array, moderate data	As A2, but with 3D CFD modelling of resource and wake interactions	10.25	5.79	-0.17
A4 5-turbine array, maximum data	As A3, but 90 day ADCP record and additional 30 day deployments for model validation	4.25	5.79	0.05
A5 10-turbine array	As A4, but larger turbine distance from ADCP location and blockage effects significant	4.25	6.3	0.07

4.7 Skewed Distributions

All individual input uncertainties in the comparisons so far are assumed to be Gaussian but this is not always a physically correct assumption. MCA was used to compare the effect of varying skew in the loss uncertainties to identify the significance of the Gaussian assumption required for ISO-GUM. A skew in the combined loss uncertainty will only be notable if a small number of the underlying uncertainties (4a-4f in Table 4.2) are dominantly skewed because the combined distribution will tend towards Gaussian otherwise. An extreme scenario, where one skewed distribution is assumed to be the only loss uncertainty, was modelled for a conservative comparison. A range of PERT distributions with increasing skew and with a common mode and range, representative of availability uncertainty, were used for the analysis (Figure 4.18).

The skewed u_L distribution results in a reduction in the P90 yield relative to the symmetrical case (Figure 4.19) for a given u_R. The reduction increases with skewness as the low end tail gets longer, but no strong relation with respect to the resource uncertainty level is observed. The difference observed is relatively small even for the most skewed distribution when compared to the differences in P90 yield observed in the earlier comparisons. Therefore, with the exception of projects with very low resource uncertainties (where ISO-GUM is accurate), the error due to assuming a symmetrical loss uncertainty distribution will be secondary to the magnitude of the error due to assuming linearity of the resource-yield function.

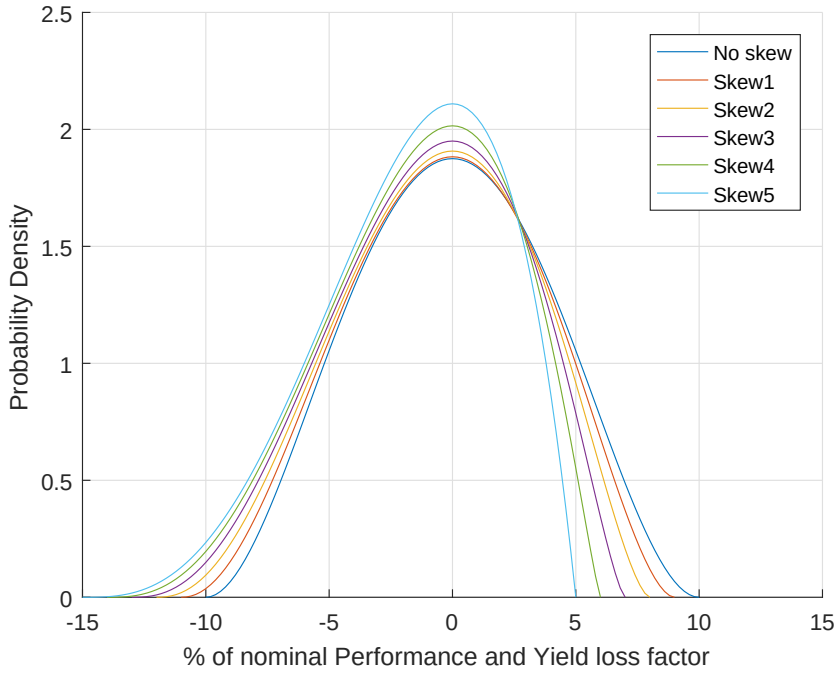

Figure 4.18: Range of skewed distributions used to represent skew in u_L

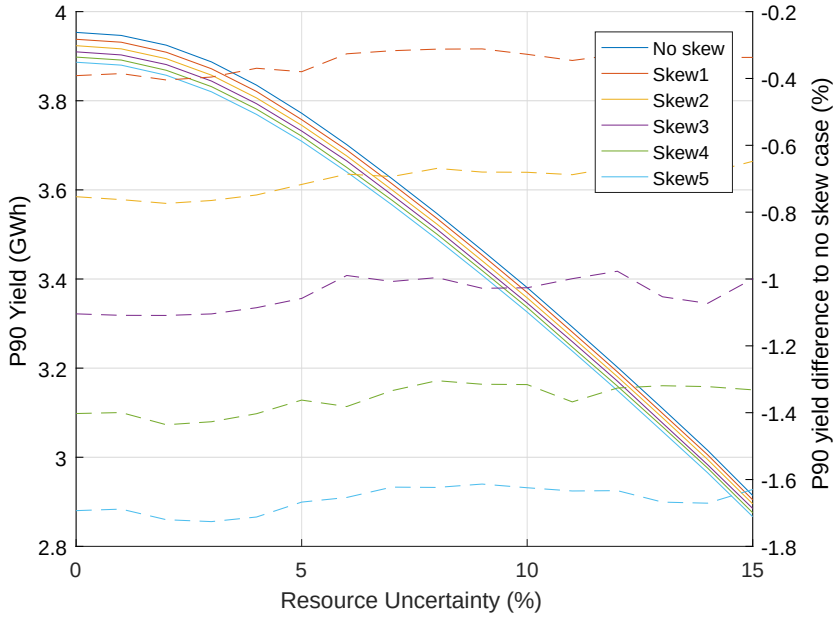

Figure 4.19: Effect of skewed u_L on P90 yield (solid line) and resultant difference relative to symmetrical u_L (dotted line), derived using MCA.

4.8 Discussion

The key assumptions in ISO-GUM are discussed below with consideration of the results presented and in comparison to MCA.

For a sufficiently large Monte Carlo sample size, n, the combined resource uncertainty, u_R, and the combined loss uncertainty, u_L, calculated using ISO-GUM and MCA will show excellent agreement under the independent and Gaussian distribution assumption. This can be observed in Figure 4.2 where the standard deviation of the empirical sum of the two independent distributions (i.e. MCA) is equal to the root sum square (i.e. ISO-GUM) of the two standard deviations ($\sqrt{1^2 + 1^2} = 1.41$). The uncertainty combination process is valid for both methods and the divergence in P90 yield observed in the results is due to the uncertainty propagation process.

In order to propagate the resource uncertainty into the resource-yield equivalent uncertainty, ISO-GUM effectively linearises the gradient between the perturbation factors to interpolate and extrapolate for resource deviations around the nominal assumption. Any strong non-linearity will result in inaccurate results because the fundamental assumption of a linear resource-yield function is violated. Also, ISO-GUM assumes that the combined annual yield uncertainty distribution is normally distributed to derive the P90 yield, but a non-linearity in the resource-yield function introduces a skew in the yield equivalent resource uncertainty distribution. The violation of the linear assumption therefore leads to further inaccuracy in the ISO-GUM results.

It is evident from Figure 4.9 that assuming a linear function between yield and resource for tidal turbines is not valid for the full range of resource uncertainties that may be encountered (although this is shown to be a reasonable approach for wind, in Figure 4.7). Considering a case with identical inputs, ISO-GUM

results can vary significantly depending on the perturbation used to derive c_v, and therefore to linearise the resource-yield function. Significant sensitivity is also shown to the site resource and turbine characteristics. The ISO-GUM results display a P90 yield error of at least 2% for all resource, power curve and c_v permutations tested here within a 4% to 11% resource uncertainty range (Figure 4.13). Crucially, the ISO-GUM error always leads to an overestimate in the P90 yield and gives an overly optimistic view of the investment risk. There is better agreement between ISO-GUM and MCA P50 yield results because the sensitivity to the non-linearity of the resource-yield function is low in the central case. However, ISO-GUM P50 error is also not in the conservative direction, and the error increases with increasing loss uncertainty.

The work presented here shows that it is not possible to recommend a generic perturbation level for linearisation that is valid for a wide range of uncertainties because the curvature of the resource-yield function is highly dependent on the nature of the resource frequency distribution (in relation to the performance curve) and the nature of the turbine power curve. Even if the shape of the function was known, some subjectivity is required to determine the optimal perturbation level with consideration of the curvature and uncertainty range of interest. These compounding issues with ISO-GUM lead to inconsistency in the methodology of different studies and is shown to be inherent in ISO-GUM in this study. Using MCA with a sufficiently high number of samples will provide a result very close to the analytical case irrespective of the non-linearity in the yield function or the uncertainty magnitude. This provides consistent results which can be interpreted at any interval of interest.

Given the above, it is also not possible to pragmatically estimate the magnitude of the ISO-GUM error for a given case because it depends on the net effect of the various parameters considered in the sensitivity analysis in Section 4.5 integrated over the annual velocity timeseries and the magnitude of uncertainties

under consideration. The unquantified exposure to error undermines confidence in ISO-GUM results, even for projects where the method may in fact be sufficiently accurate. This may be acceptable if the error gave results that were overly conservative but the opposite is true. The simplest method for accurately quantifying the ISO-GUM error is by comparison with MCA results. However, the ISO-GUM results are redundant if MCA results have been derived.

For calculating the P90 yield, errors much smaller than 2% can be achieved by using the P90 of the resource uncertainty under consideration as the perturbation to derive a custom c_v because this ensures that the linearisation captures the majority of the probability density. However, it is still difficult to precisely quantify the accuracy. Furthermore, the analysis has to be repeated for every percentile of interest given that a separate custom c_v is required. This method should be considered as a simple workaround solution rather than a physically accurate method.

Note that the generic c_v approach advocated in literature recommends using the average of a positive and negative perturbation about the nominal resource. However, the resource-yield function below the nominal resource is of interest when considering the P90 yield case. The gradient of the resource-yield function above and below the nominal resource is quite different, as seen in Figure 4.16. Including a positive perturbation gives equal weighting to the above nominal resource function during linearisation. If the P90 is of interest and a generic c_v must be used, it is recommended that the linearisation is carried out using a negative perturbation only.

The possibility to model skewed uncertainty distributions is an additional benefit of MCA. In general the effect of the skew on P90 yield will be small, but it can be significant if a small number of skews are dominant and the ISO-GUM c_v is otherwise accurate (i.e. low uncertainties). In particular, a combined uncertainty

distribution with a right skew will result in reduction in the P90 yield and therefore an overestimate is reported if the skew is neglected.

ISO-GUM is very inaccurate for assessing the high resource (optimistic) case because the linear model fails to represent the loss of yield due to high occurrence above the cut-out velocity. ISO-GUM therefore should not be used to consider the P10 yield or similar. There is a risk of misinterpreting ISO-GUM results if this limitation is not understood by the analyst as it is technically simple to extract a P10 yield, and may be valid approach for wind projects. Using MCA allows the optimistic scenarios to be appreciated as well as the pessimistic cases that form the basis of investment decisions.

ISO-GUM is practically simpler than MCA to implement and a spreadsheet tool is publically available (OREC, 2015*c*). MCA requires some specialist knowledge and/or software to construct the model and the computational requirement is also higher. However, the runtime for a sufficiently converged MCA simulation is still in the order of minutes on a standard desktop PC. Further efficiency gains can be achieved by calculating the annual yield using the frequency domain in Equation 4.2, if required.

4.9 Summary

A model is required to combine and propagate all the individual uncertainties that are present in a project's annual yield assessment to derive the total combined uncertainty on the annual yield estimate. The industry standard ISO-GUM method for propagation of annual yield uncertainties was compared to a MCA approach in this chapter. It was shown that the fundamental ISO-GUM assumption of a linear change in annual yield for small changes in resource is not accurate for tidal energy projects. This results in ISO-GUM overestimating the

P90 annual yield compared to MCA. The error increases with increasing resource uncertainty. Using a range of realistic test cases, it was shown that the error is likely to be significant for most real life projects, particularly at the early stage of the industry when uncertainties are high. A sensitivity analysis on various parameters affecting the linearity of the resource-yield function showed that it is difficult to determine the validity of the ISO-GUM method *a priori*. Confidence in ISO-GUM results is therefore undermined even in cases where the method is acceptable because the error cannot be quantified, but it has been shown that it can be significant. ISO-GUM was shown to be highly inaccurate for estimating the P10 yield due to the turbine cut-out effects not being accounted. MCA accounts for the non-linearities accurately by propagating distributions through the non-linear resource-yield function and thus estimates the P90 and the P10 yield correctly for all cases as long as a sufficiently high number of repetitions is used. Furthermore, it is possible to easily propagate non-symmetrical input distributions using MCA which is another ISO-GUM limitation.

Chapter 5

Financial Uncertainty Analysis

5.1 Introduction

Investors in energy projects have a range of potential technologies available for investment. The decision to invest in a particular technology or project is driven by a few major considerations. Johnstone et al. (2013) summarise the key considerations into 6 categories; the cost of electricity, responsiveness to demand, security of supply, resource availability, environmental impact and execution risk. As explained below, the cost of electricity is perhaps most critical for tidal energy projects because the other variables are either completely outside the control of a project developer, or at least largely uncontrolled in the near future.

Tidal energy is inherently unable to offer responsiveness to demand (in the absence of associated energy storage), but it does have the benefit of being highly predictable. It is an indigenous and abundant source in the UK (Carbon Trust, 2011*a*). The visual impact is small but the precise environmental impact is hard to quantify currently. The execution risk can be said to be high given the present lack of track record and experience. Therefore, as the most influential decision

factor, the financial performance of a project needs to be quantified robustly. The cost modelling process must be transparent and consistent to ensure confidence in the results.

The results of cost modelling, as with any type of modelling, have uncertainties associated with it. Understanding the uncertainties is important because a project with a low cost of energy and high uncertainties may be less investable than a lower uncertainty project with a higher energy cost. The uncertainties arise from the quality of the input data and the assumptions leading to the estimation of the Capital Expenditure (CapEx), Operational Expenditure (OpEx), plant performance and availability.

Chapter Outline

The aim of this chapter was to improve confidence in financial modelling uncertainty analysis.

A generic tool to model the financial performance of a tidal energy project with comprehensive uncertainty analysis using Monte Carlo analysis (MCA) was developed. The tool was then applied to a case study project and compared to other common methods for uncertainty analysis.

Note that the tool is sufficiently generic that it can equally be applied to a wave energy project, but this chapter refers only to tidal energy applications given the scope of the thesis.

5.2 Financial Analysis Theory

The fundamental principles required for cost of energy calculations and cash flow analyses are outlined in this section.

5.2.1 Time Value of Money

The concept of time value of money underpins all financial considerations that require an investment at the present time in order to benefit from a return on investment (ROI) at some point in the future. This is because any investment is made at the opportunity cost of an alternative option, such as immediate expenditure or interest accrual. It is for this reason that receiving £100 today is preferable to receiving the same £100 at some point in the future. In other words, the future value (FV) of the cash is greater than the present value (PV). In order for an investment to be a worthwhile endeavour, the ROI must at least be greater than the risk-free rate (Peirson et al., 2011). The risk-free rate is a theoretical interest rate which represents a guaranteed rate of return (Damodaran, 2008). A 12 month US Treasury bond is an example of a risk-free asset because the default risk can be assumed to be zero (Damodaran, 2008).

The process of calculating the FV from a PV and vice versa is called 'compounding' and 'discounting', respectively, as defined in Equations 5.1 and 5.2.

$$FV = PV \times (1 + r)^n \tag{5.1}$$

$$PV = \frac{FV}{(1 + r)^n} \tag{5.2}$$

where n is the number of accounting periods and r is the discount rate. The discount rate may be equal to the risk-free rate. Alternatively, when comparing

a competing investment opportunity with comparable risks, it is set to equal the expected rate of return from the alternative investment. This is also known as the hurdle rate. The hurdle rate is higher than the risk-free rate because investors accept some risk in order to access a potentially higher rate of return (Tucker, 2013; Deloitte, 2014).

Equation 5.2 can be expanded to calculate the net present value (NPV) of a series of payments and receipts over a prolonged period (cashflow) using:

$$NPV = \sum_{n=0}^{T} \frac{FV_n}{(1+r)^n} \tag{5.3}$$

where FV_n is the net cashflow in the n^{th} period and T is the total number of periods.

5.2.2 Levelised Cost of Energy

The PV of a project's costs and yield can be used to calculate the levelised cost of energy (LCOE):

$$\text{LCOE} = \frac{\text{CapEx} + PV(\text{OpEx}) + PV(\text{Decommissioning})}{PV(\text{Yield})} \tag{5.4}$$

LCOE is a useful metric that allows different projects of any technology type to be compared. It is not the most effective metric for informing investment decisions for specific projects because it does not consider the project's revenue and cashflow. As a result, a project's cost of finance is also not included in the LCOE. Note that the LCOE is very sensitive to the discount rate assumed (Visser and Held, 2014). A discount rate between 8 and 15% has been suggested for the marine energy industry, depending on the level of perceived risk in the investment (Davey et al., 2009; Carbon Trust, 2006*b*).

5.2.3 Discounted Cash Flow Analysis

An investment decision must be based on an understanding of the likely ROI. This requires a discount cash flow (DCF) analysis to consider the timings and values of the money paid and received over the life of the project (Fight, 2005). The typical cash outflows for tidal energy projects are CapEx, OpEx, tax, interest and decommissioning costs. Typical cash inflows are revenue, grants and financing. There are many variations in project financing arrangements leading to a wide range of possible methods and assumptions for modelling the financial performance. The description below is a succinct summary of the most common methods found in practice for modelling renewable energy projects in the UK.

Earnings Before Interest, Tax, and Debt Amortisation

The earnings before interest, tax and debt amortisation (EBITDA) is a project's net earnings. In the case of a tidal energy project, this typically includes the projection of expenditure and revenues on an annual basis (Equation 5.5). The revenue is directly linked to the project's energy yield. In the case of projects supported by the UK's contract for difference (CfD) regime, the revenue is a product of the agreed strike price and the yield for the first 15 years of operation, after which the project sells its electricity without any subsidies (DECC, 2013).

$$\text{EBITDA}_n = \text{CapEx}_n + \text{OpEx}_n + \text{Decommissioning Cost}_n + \text{Revenue}_n \quad (5.5)$$

where n is the accounting period number. Note that all cash inflows are positive and outflows are negative, in conformance with standard accounting conventions.

Interest

It is likely that tidal energy projects will be financed using a mixture of debt and equity funding in the near future, in a similar fashion to most offshore wind projects (Roberts, 2014). For example, the first commercially financed tidal energy project in the world, MeyGen, was funded with a 46:54 ratio of debt to equity (MeyGen, 2014). The debt provider is rewarded for their investment by payment of interest on the borrowed funds whilst the equity provider effectively shares the project's profit in proportion to their ownership of the project (Groobey et al., 2010).

The financing received is modelled as a cash injection to the project's cashflow at the start of the project's construction and the debt is repaid over a fixed term via periodic repayments of the borrowed principal and accrued interest. There are two main types of debt amortisation schedules; straight line and mortgage style (Figure 5.1) (Fight, 2005). Straight line amortisation requires the borrowed principal amount to be repaid on a pro-rata basis with the interest paid regularly on the outstanding amount, leading to a reduction in total payment in each subsequent period. On the other hand, a mortgage style amortisation involves predetermined fixed periodic payments consisted of a varying proportion of principal and interest, as shown in Figure 5.1.

Tax

The corporate tax required to be paid is dependent on the project's profitable performance. The profit for tax purposes in a given accounting period is not equal to the profit observed in the cashflow for that period (sum of EBITDA and interest). This is because the depreciating value of assets over time and any previous cumulative losses provide a shield to the project's tax obligations.

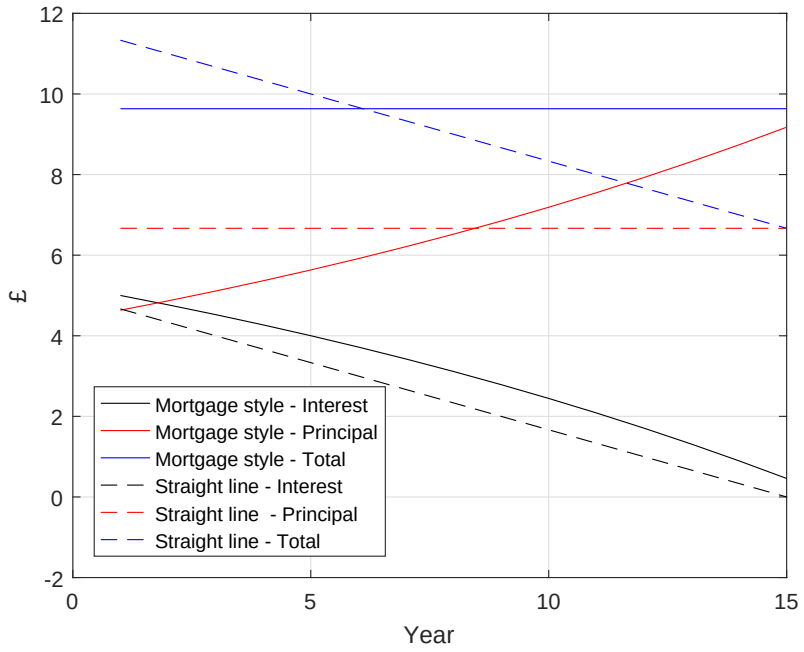

Figure 5.1: Amortisation of a £100 loan over 15 years at 5% annual interest rate using straight line and mortgage style debt amortisation schedule.

The depreciation can be calculated using the straight line or reducing balance method. The former depreciates the value of the assets linearly over the life of the asset whereas the latter calculates the depreciation proportional to the remaining book value of the assets. The rate of depreciation is determined by the type of asset and is defined in the UK by the Government's capital allowance mechanism. A longer term asset, such as a tidal energy farm, qualifies for a 8% annual depreciation rate (Gov.uk, 2016). The amount of depreciation in an accounting period can be used to offset the taxable profit to reduce the tax burden.

A project's previous losses are allowed to accumulate to further provide a tax shield. Tax is only paid after all accumulated losses have been offset tax free.

Nominal and Real Terms

Inflation affects the comparison of present costs to future costs because prices are anticipated to change in line with changes in inflation. This is separate to the concept of PV and FV, which is concerned with discounting future costs due to the opportunity cost in investing at the present time. Costs that are adjusted for inflation are referred to as real values whereas unadjusted costs are known as nominal values (Tucker, 2013). Assuming a positive inflation rate, future nominal values will be higher than real values. In the context of modelling cashflow, the costs can be modelled in real or nominal terms as long as a real or nominal discount rate is used respectively when calculating the PV. The relation between the real and nominal discount rate is defined using Fisher's equation (Cooper and John, 2011):

$$1 + r_n = (1 + r_r)(1 + i) \tag{5.6}$$

where r_n and r_r are the nominal and real discount rate respectively and i is the expected inflation rate.

Investment Decision Metrics

The purpose of the DCF analysis is to reduce the complex time varying financial performance of a project into simple metrics that can be used to make investment decisions. The three most commonly used metrics are net present value (NPV), internal rate of return (IRR) and debt service coverage ratio (DSCR) (Fight, 2005).

As defined in Equation 5.3, the NPV represents the total, discounted value of the project. A positive NPV represents a project that provides a positive return over its lifetime at the assumed discount rate.

The discount rate required to achieve a NPV of zero is called the IRR. This is a key metric used by equity investors to determine the profit margin in an investment and to compare it to other opportunities. It is highly sensitive to the timing of the cash flow (HM Treasury, 2013). It is most appropriate for cashflows with a large upfront investment followed by surpluses during subsequent periods. It should be noted that multiple IRRs may be possible if a project alternates between positive and negative cashflows (McKinsey & Co, 2017). It is also possible for a cashflow to result in non-real IRR values in highly unprofitable projects. Another limitation of IRR is that it is expressed in percentages which may make a small project appear attractive in comparison to a larger project even though the NPV of the latter is greater.

The IRR to a debt provider is equal to the interest rate, provided the loan is amortised as scheduled. The DSCR is of more interest to a debt provider as it is the ratio of free cashflow available (EBITDA + tax) to the debt service charges (principal repayment + interest) due in each accounting period. A high DSCR implies a healthy cashflow in terms of the debt obligation. Any periods where the DSCR is lower than 1 represents a scenario where the project is not able to repay the due amounts from its net income.

5.3 Review of Marine Energy Cost Models

A number of cost models for marine energy projects are available in the public domain. There are differences in techniques, sophistication and assumptions depending on the intended use of the model. However, each model has a process

to estimate CapEx, OpEx and yield. There are also different approaches for modelling the DCF and for uncertainty analysis. The differences in these processes can be used to categorise and evaluate the main marine energy cost models available. A succinct comparison is presented in Table 5.1 and a general discussion of the models is provided below. Note that some models are wave energy specific, but the comparison is still valid because the cost modelling procedure for wave and tidal energy projects is comparable.

The models estimate the installation CapEx separately from the cost of hardware and services. Most models estimate the total CapEx by simply summing user provided values for subcategories of procurement and installation CapEx. This approach can introduce significant uncertainty to the calculated LCOE depending on the source of the cost information. There is considerable variation in the CapEx estimation procedure for the models assuming a more complex approach. In general, hardware costs are calculated from material and labour costs as suggested in Carbon Trust (2006*a*), whereas installation costs are calculated based on modelling of the marine operations. There is no standard breakdown of CapEx cost categories, but convergence towards a high level breakdown as per the Equimar protocol is observable (Myers et al., 2010).

Table 5.1: Comparative summary of characteristics of existing marine energy cost models. Note that level of detail is highly redacted to allow a simple comparison, but further details on model assumptions can be found in Table 5.2

Model	**Reference**	**CapEx**	**OpEx**	**Yield**	**DCF**	**Uncertainties**
Carbon Trust	Carbon Trust (2006*a*)	Simple[1]	Simple[2]	Simple[2]	No	Deterministic[3]
Black and Veatch	Proprietary model[23]	Simple[1]	Simple[4]	Simple[2]	Yes	Probabilistic[5]
Bureau Veritas	Mcauliffe et al. (2015)	Simple[1]	Complex[6]	Mixed[7]	No	Probabilistic[8]
Aalborg University	Fernandez et al. (2014)	Complex[9]	Simple[4]	Complex[10]	Yes[11]	Simple[12]
TE-UBC	Li et al. (2011)	Simple[1]	Complex[13]	Complex[14]	No[15]	No
Exceedence	Alcorn (2016)	Simple[1]	Simple[1]	Complex[10]	Yes	Simple[16]
Maynooth	Teillant et al. (2012)	Complex[17]	Complex[18]	Complex[10]	Yes	No
de Andres et al	de Andrés et al. (2015)	Pragmatic[19]	Simple[4]	Complex[20]	Yes[11]	Probabilistic[20]
DTOcean	DTOcean (2016)	Flexible[21]	Flexible[21]	Flexible[21]	No	No
Sandia Lab	Neary et al. (2014)	Complex[22]	Complex[22]	Complex[22]	Yes	Qualitative

OpEx is estimated by summing user provided values for various O&M cost categories, as a % of CapEx or through modelling of failures, weather windows and vessel operations. The first two methods, as with the similar CapEx approach, has a large scope for introducing significant uncertainties from poor input information. The final method, which is more comprehensive, requires significant modelling simplifications. Device specific models require less simplification than generic O&M models. In general, estimating OpEx accurately is difficult until some experience is gained by the industry.

The yield estimates are either a simple multiplication of user specified rated capacity, load factor and other losses such as availability, transmission losses etc., or calculated from resource data (flow velocities) and power performance data (power curve and losses).

All models, with the exception of Li et al. (2011), adopt the NPV approach to discount future cash flows when estimating LCOE as recommended by the generic cost modelling best practice guidance in Visser and Held (2014). Some models include a DCF analysis with considerations of factors such as taxes, interest rates, subsidies, grants and debt in order to calculate IRR, but there is a divergence in the number of factors included within the different models, as noted in Table 5.2.

Whilst many authors acknowledge the large uncertainties present in the results, only a basic consideration of uncertainties is undertaken in practice, if at all. Deterministic best and worst cases point estimates are a common means of representing the likely variations. Some models adopt a probabilistic approach, but it is very limited as noted in Table 5.2. A stakeholder survey on approaches to cost modelling in the industry notes that “A need for improving risk assessment is perceived. Suggestions are made to apply stochastic approaches to consider uncertainties” (Ricci et al., 2009).

Table 5.2: Further details of marine energy cost model characteristics

Ref.	Description
1	Sum of user specified costs
2	From rated capacity, load factor and losses
3	Pessimistic/Base/Optimistic
4	% of user specified CapEx
5	MCA of uncertainties predefined by model depending on data source
6	Failures from RAM analysis, Monte Carlo Analysis of O&M ops
7	User input yield is combined with availability from RAM analysis
8	MCA with only 1000 simulations and standard deviation of 10% used
9	Structure costs from material usage, rest are user provided costs.
10	From power performance and resource data
11	No tax or financing costs included
12	% performance uncertainty only, relative to TRL
13	Failures and O&M modelled, unclear how
14	Hydrodynamic model to calculate array interactions, unclear how
15	LCOE calculated without discounting
16	Parametric sensitivity analysis and single degree of freedom goalseek
17	Hardware and installation CapEx from manufacturing and deployment
18	Costed from hourly rates, cost of parts and vessels
19	Time domain calculation as outlined in (De Andrés et al., 2013)
20	Interannual resource uncertainty only considered
21	Varying from user defined values to detailed calculation from basics
22	Based on detailed design calculations for a reference project
23	Discussed further in Section 5.4

5.4 Existing Black and Veatch Tool Description

An existing cost modelling tool was used as the basis for further development for this study. The capabilities and limitations of the tool are outlined in this section. A detailed description is not included as it is a proprietary tool developed by Black and Veatch (BV) for a commercial project. However, sufficient information is provided to fully support the narrative.

Comprehensive documentation with details of the existing tool's functions, limitations and bugs was not available as the existing tool is a draft version and the authors of the original work are no longer with the company. As such, the capabilities and limitations of the tool had to be inferred pragmatically from the available draft spreadsheet and manual, and bugs had to be identified logically.

5.4.1 Critical Appraisal of Existing Tool

The tool is based in Microsoft Excel and has a comprehensive uncertainty analysis capability by using a commercially available plug-in for MCA called Palisade @Risk. The user defines central values for each input variable. Also, the user is required to select a description from a preset list that best describes the level of uncertainty in the specified central value. For example, CapEx items have four associated options ranging from 'Based on prototype' to 'Based on order'. Proprietary definitions of the size and shape of distributions representing the uncertainty associated with each preset option for each input variable are used to produce random samples for input variables for MCA. The uncertainty bands are not presented here to protect the commercial confidentiality and because knowledge of the precise banding is not necessary to understand the tool's capabilities. The input distributions are used to conduct a probabilistic DCF analysis using MCA to derive the output distributions using the theory outlined

in Section 5.2. A breakdown of tool inputs is presented in Figures 5.2-5.3. The main tool outputs are distributions representing the project's LCOE, IRR and NPV.

5.4.2 Tool Limitations

A number of limitations of the existing tool were identified. The limitations can be categorised as follows; inherent in the structure of the tool architecture, related to the use of Microsoft Excel as the tool platform and result of human error in tool design (bugs).

Structural Limitations

- Input variables must be defined according to the rigid categorisation prescribed by the model. For example, the CapEx breakdown for a given project might not be split into the 6 CapEx sub-categories required by the tool and would therefore need a pragmatic re-categorisation;
- Uncertainty definitions associated with input variables are preset and categorised into predetermined uncertainty bands. A real project may not fit any of the available uncertainty descriptions;
- Modular structure not possible.

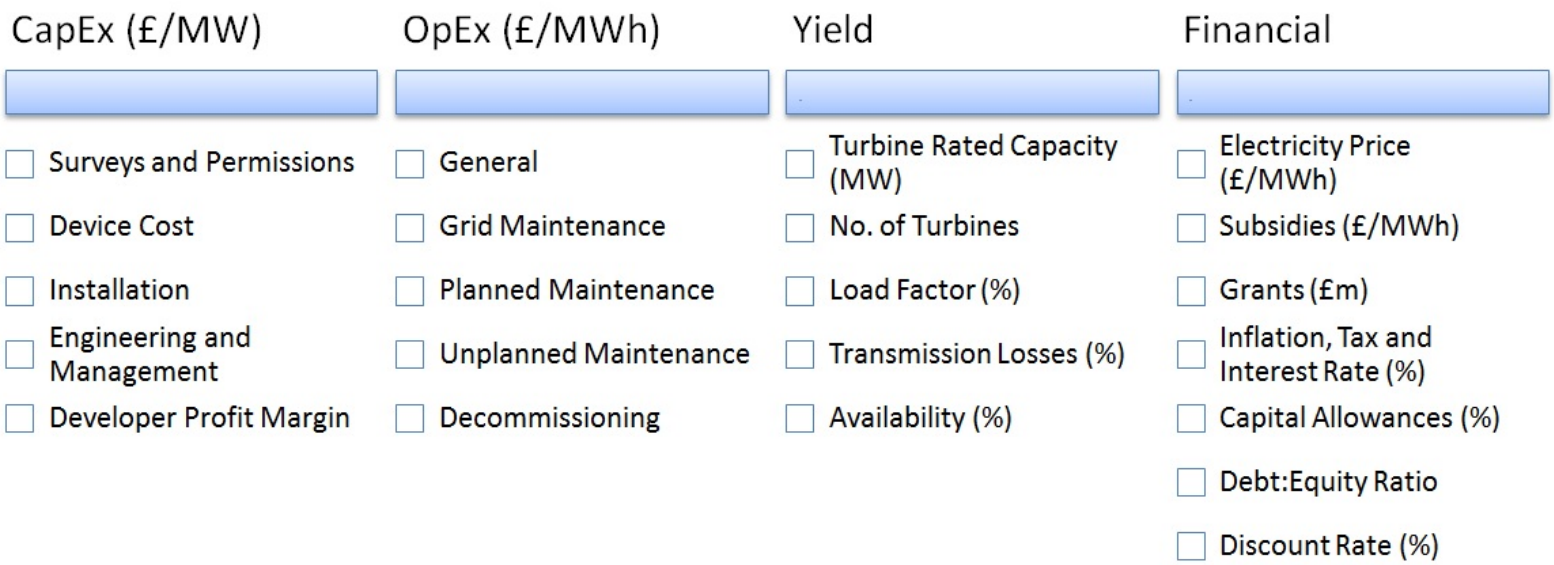

Figure 5.2: List of high level to existing tool. Variables with further subcategories are shown in Figure 5.3.

Figure 5.3: Breakdown of input categories for variables in Figure 5.2 that have further subcategories.

Platform Limitations

- Commercial license for Palisade @Risk plug-in required to be purchased (£1000-1700) (Palisade Corporation, 2017*a*);
- Model runtime is relatively high and increases non-linearly with added complexity due to the time taken in initialising the inputs. In its existing form, the model took approximately 2.5 minutes to run a simulation with 10,000 iterations;
- Very high memory requirement for large simulations;
- Access to intermediate model data is not straightforward, making in depth analysis difficult;
- It is easy for a user to accidentally delete or overwrite equations;
- Difficult to understand the logic, identify and fix bugs in long Excel equations, and further development adds to the existing complexity.

Tool Bugs

Many bugs in the existing tool were identified. In order to avoid listing specific tool functions, a generically comprehensible list is presented by categorising the bugs as follows:

- Incorrect uncertainty bands applied to variables: A number of input variables are defined by the user by specifying P5/P50/P95 values, but are read into @Risk as P10/P50/P90 values;
- Inconsistent treatment of units: Certain OpEx variables are defined in £/MW and others are defined in £/MW/year, but during summation all are treated as £/MW/year;

- Incorrect cell references: There are many instances where incorrect cells are referred to for mathematical operations;

- Double accounting: In one case, a loss factor is applied twice;

- Inconsistency in inflation of cash flow line items: Inflation is not applied to two revenue streams whereas all other cashflow items are inflated appropriately.

The effect of correcting the bugs is discussed in Section 5.5.5.

5.4.3 Rationale for Further Development

Based on an understanding of the tool's capabilities, limitations and bugs highlighted in the previous section, it was determined that it would be beneficial to convert the existing tool into Mathworks MATLAB. This would allow for a more computationally efficient tool with a modular architecture suitable for addition of further functionalities.

The development was carried out in two phases. The first phase, tool v1, was a direct translation of the existing Excel tool with no additional capabilities. The Excel logic was initially replicated in MATLAB exactly, including the bugs, to allow the translation to be verified. Corrections to known bugs were then implemented in MATLAB. Note that this approach was preferred over correcting the bugs in Excel before translating to MATLAB in order to preserve the original Excel spreadsheet as an unaltered reference point. Finally, tool v2 was developed to address the functional limitations of existing tool and to extend its capabilities.

5.5 Tool v1

The overall structure and logic of the MATLAB model is described below. Only one process was added in the development which was not a direct translation of the Excel tool. This was required due to limitations inherent in MATLAB functions (as described in Section 5.5.2). A verification of the model translation, convergence testing and correction of the known bugs is also presented. As before, the list of input variables is not provided to protect commercial confidentiality, but this does not prevent the functionality of the tool from being understood.

5.5.1 Model Logic

The model logic is illustrated in Figure 5.4 and the function of each script is as follows:

- 'master.m' sequentially initiates each of the model scripts;
- 'inputs.m' loads user provided central values and uncertainty categories to global workspace;
- 'errorBands.m' loads model definitions of error bands and distribution type associated with each uncertainty category for each variable to global workspace;
- 'preProcessing.m' prepares user inputs for use by model;
- 'initiateCreateDist.m' calls 'createDist.m' for each variable in model with the information required to produce a distribution that correctly represents the uncertainty in that variable;
- 'createDist.m' creates a MATLAB distribution object and produces a random sample from that distribution each time it is called;

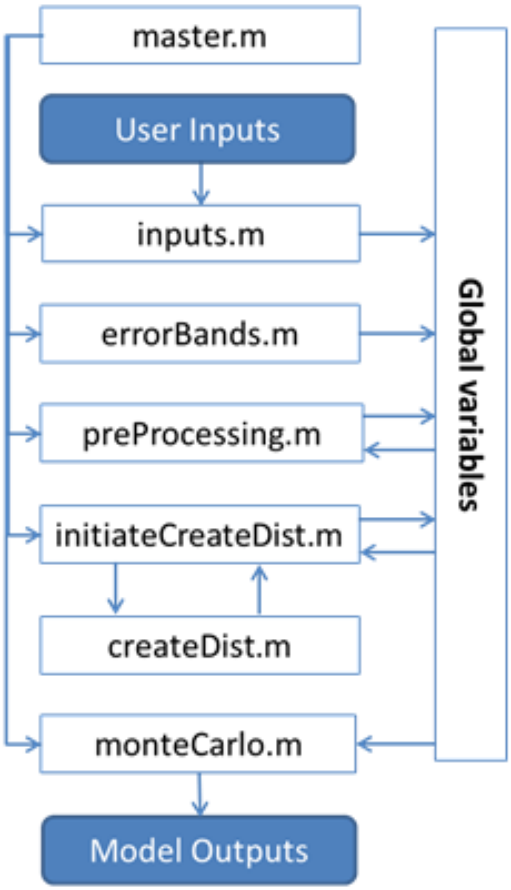

Figure 5.4: Flowchart of MATLAB Tool v1 model logic

- 'monteCarlo.m' combines the input distributions using the appropriate functions to conduct the probabilistic DCF analysis to produce the output distributions.

5.5.2 Percentile Transformation Algorithm

The existing @Risk model allows the user to assign uncertainty to variables using triangular and PERT distributions defined by P0/P5/P10 and P100/P95/P90 values. However, MATLAB requires these distributions to be specified by minimum and maximum values only. It is important to retain the percentile

based definition capability because it can be difficult to estimate accurately the minimum and maximum values, particularly for highly skewed distributions with long tails, because it requires estimating an almost impossible occurrence. It is more intuitive to estimate the P5/P95 or P10/P90, i.e. unlikely, but quite possible outcomes. No existing solution to transform the low and high percentile of a triangular or PERT distribution into the corresponding minimum/maximum value was found within built-in MATLAB functions or on the Mathworks file exchange community forum. Whilst it is simple to derive the n^{th} percentile from known minimum/maximum values, the analytical transformation of a n^{th} percentile to the minimum/maximum is not trivial (University of Texas, 2017). Therefore an empirical solution was developed to perform this process. It is loosely based on the methodology outlined by Buchsbaum (2012).

Palisade @Risk has an analytical solution to this problem, but it is a proprietary algorithm that is not accessible. An empirical solution can be fitted to the @Risk analytical solution for an arbitrary distribution domain. The distribution domain is the difference between the two percentiles used to define a distribution. The results can then be scaled to any user defined distribution domain using the empirical formulae. This method allows the transformation from P5 and P95 or P10 and P90 to minimum and maximum to be carried out entirely in MATLAB after a one-off derivation of the empirical equations using @Risk. It exploits the observation that the percentiles for a given distribution scale linearly with a change in domain size. If the minimum or maximum of a distribution and the percentile of interest (e.g. P5) is known, then the minimum or maximum of the same distribution at a different scale can be derived from knowledge of the same percentile in that scale. The process is explained in detail below.

Derivation of Empirical Solution

The derivation was first carried out for triangular and PERT distribution domains such that the P5 = 1 and P95 = 0. Distributions with mode ranging from 0 to 1 in increments of 0.05 were defined in @Risk with a constant P5 and P95 of 1 and 0, respectively. This covers the full spectrum of valid distribution shapes that meet the arbitrary domain constraint (P5=1, P95=0), with the change in mode representing a change in skew (Figure 5.5).

The analytical minimum and maximum values for each distribution were exported from @Risk. A best line was fitted through a plot of the minimum and mode and the maximum and mode using LabFit software (Figure 5.6). LabFit is a curve fitting software that uses non-linear regression and has a database of over 200 different functions with up to 4 parameters (LabFit, 2017). This process was also repeated for distributions such that P10 = 1 and P90 = 0. The fitted functions, presented in Table 5.3 and Table 5.4, relate the minimum and maximum to the mode when P5 = 1 and P95 = 0 or P10 = 1 and P95 = 0. This provides sufficient information to calculate the minimum and maximum for a triangular or PERT distribution of any scale if the P5/P10 and P95/P90 are known in that scale.

Note that LabFit uses the reduced chi squared parameter to determine the best fitting function from its extensive database (LabFit, 2017). An excellent fit is observed for all 8 functions, as seen in Figure 5.6 and Tables 5.3 and 5.4.

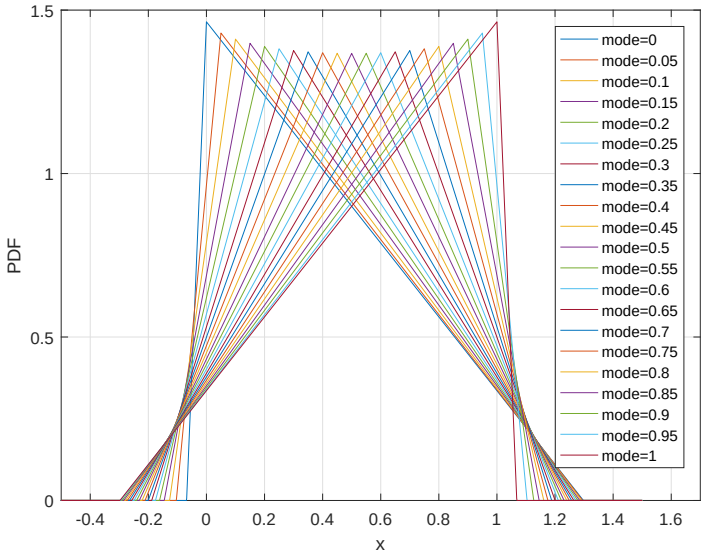

(a) Triangular Distribution

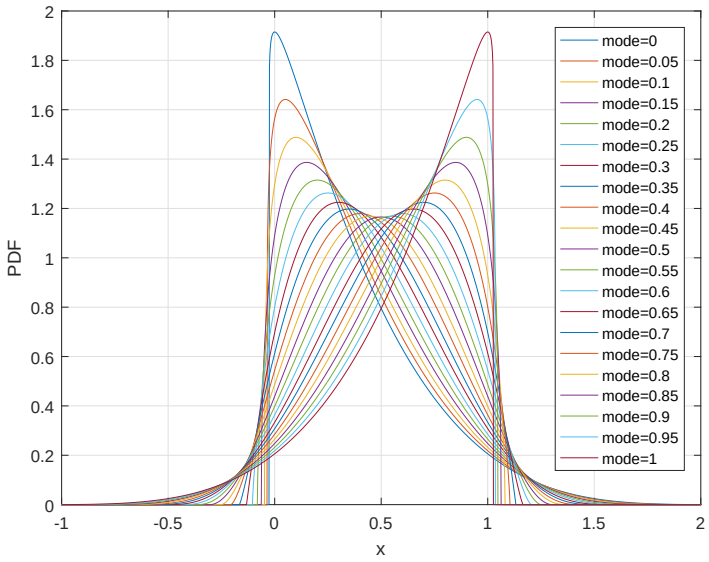

(b) PERT Distribution

Figure 5.5: Range of distributions used for empirical derivation of the relation between mode and minimum/maximum for known P5 and P95 values. Note that the common factor in the above plots is that P5=1 and P95=0 for all distributions.

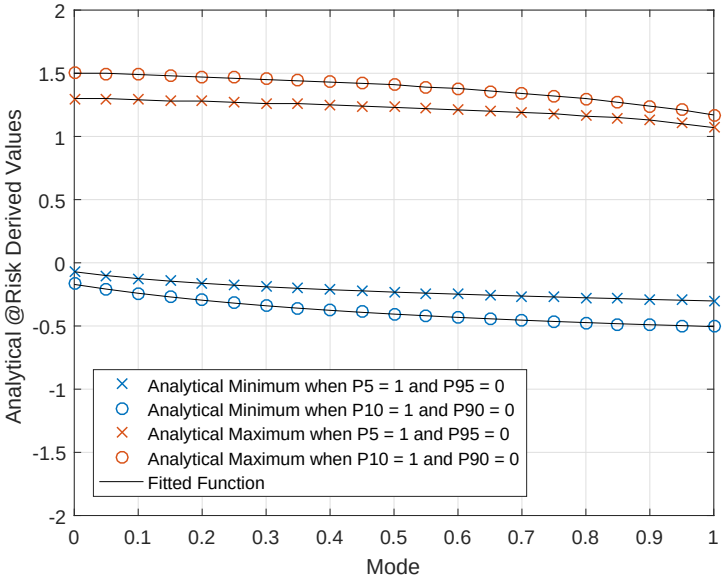

(a) Results for triangular distribution. The fitted functions are defined in Table 5.3.

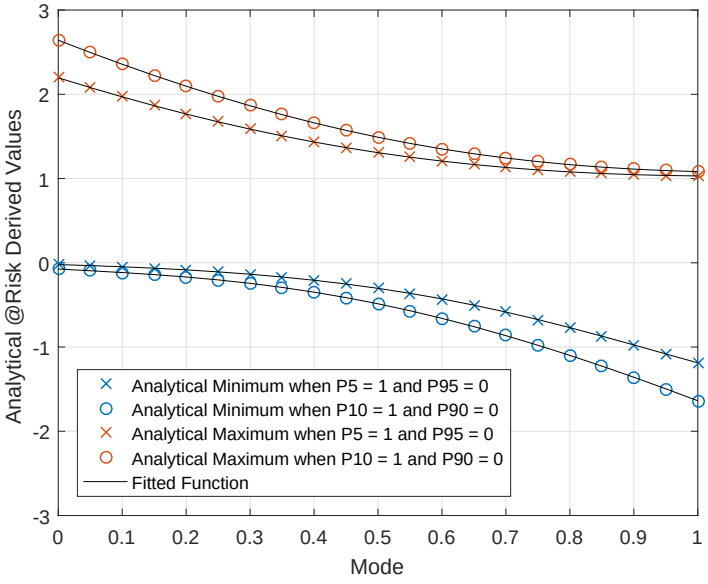

(b) Results for PERT distribution. The fitted functions are defined in Table 5.4.

Figure 5.6: Fitting functions to analytical minimum and maximum values derived using @Risk for the range of distributions defined in Figure 5.5, and also the equivalent distributions where P10 = 1 and P90 = 0.

Table 5.3: Empirical equations derived for calculating the minimum and maximum values from mode in the arbitrary domain for a triangular distribution. Note that Y is the minimum/maximum value and X is the mode in the arbitrary domain.

	P5 = 1, P95 = 0		**P10 = 1, P90 = 0**	
	Min	Max	Min	Max
Eqn.	$Y = \frac{A+X}{(B+CX)} + DX$	$Y = (A + BX)^C + D$	$Y = \frac{X}{(A+BX)} + C$	$Y = \sqrt{A - B(X - C)^2} + DX^2$
Red. ChiSq.	3.40E-06	2.14E-06	6.04E-06	5.98E-06
A	0.08904	0.057388	-1.2573	2.3066
B	-1.2577	-0.05301	-1.7421	0.99019
C	-3.5637	0.24919	-0.17122	-0.20845
D	-0.07577	0.81099		0.24342

Table 5.4: Empirical equations derived for calculating the minimum and maximum values from mode in the arbitrary domain for a PERT distribution. Note that Y is the minimum/maximum value and X is the mode in the arbitrary domain.

	P5 = 1, P95 = 0		**P10 = 1, P90 = 0**	
	Min	Max	Min	Max
Eqn	$Y = \frac{A}{1+Be^{CX}} + D$	$Y = \sqrt{A - B(X-C)^2} + DX$	$Y = \frac{A+X}{B+CX^2} + DX$	$Y = \sqrt{A - B(X-C)^2} + DX$
Red. ChiSq.	1.07E-05	5.30E-06	9.53E-07	9.94E-06
A	-2.2335	3.9407	-0.02769	5.3304
B	37.717	-5.3145	0.37273	-7.4297
C	-3.8234	0.4072	0.29969	0.47124
D	0.036232	-1.3791	-3.0841	-1.6397

Scaling of Empirical Solution to User Defined Domain

The process, which can be applied for a triangular or PERT distribution is as follows:

1. Scale the P5 or P10 (P_{low}), mode (P_{mode}) and P90 or P95 (P_{high}) in the user defined distribution domain to the arbitrary domain equivalent values, P'_{low}, P'_{mode} and P'_{high}, respectively. Note that P'_{low} and P'_{high} will, by definition, always scale down to 1 and 0, respectively, for this domain.

$$P'_x = \frac{P_x - P_{high}}{P_{low} - P_{high}} \tag{5.7}$$

   where $P_x = P_{low}$, P_{mode} or P_{high}.

2. Substitute the value of P'_{mode} in the appropriate equation in Tables 5.3 and 5.4 to calculate the corresponding minimum and maximum value in the arbitrary domain.

3. Scale minimum and maximum value in the arbitrary domain back to the original user defined domain. The mode in the user domain is already known as it is one of the inputs to the calculation.

$$x = x'(P_{low} - P_{high}) + P_{high} \tag{5.8}$$

   where x is the minimum or maximum value in the user defined domain and $x' = x$ in the scaled domain.

A worked example demonstrating the process above is presented in Appendix A. Also, the resultant distribution is compared to an @Risk derived distribution.

Validation

Any difference in minimum/maximum values calculated using this method and the @Risk analytical values is a result of the error in the distribution fitting for that particular value of P'_{mode}. The scaling of the parameters using Equations 5.7 and 5.8 does not introduce additional errors as the percentiles scale linearly in proportion to the change in domain scale.

Figures 5.7 and 5.8 show the error between empirical and @Risk analytical minimum and maximum values for each of the 8 empirical relations in Tables 5.3 and 5.4. Note that the error is expressed as a percentage of the distribution scale, i.e. maximum minus minimum. The magnitude of the percentage error is fixed regardless of the change in scale of the domain. Also note that the fitting error is unlikely to reduce if more analytical points are used. This is because the process was carried out for half the number of data points and the results very nearly identical. The same equations were fitted for all cases and all empirical constants were identical to two decimal points. This implies that enough data points exist at half the resolution to derive the converged solution. The statistical significance of errors of this magnitude on the resultant output distributions is considered in Section 5.5.4.

Limitations

The empirical relations derived using this method are limited to distributions that are defined by specifying the P5/P10 and P95/P90 values. Additional equations will be required to be derived manually for each additional user specific percentile required, e.g. P15 and P85. However, it is considered that the current capability is sufficient for most cases and additional derivations are not anticipated to be required.

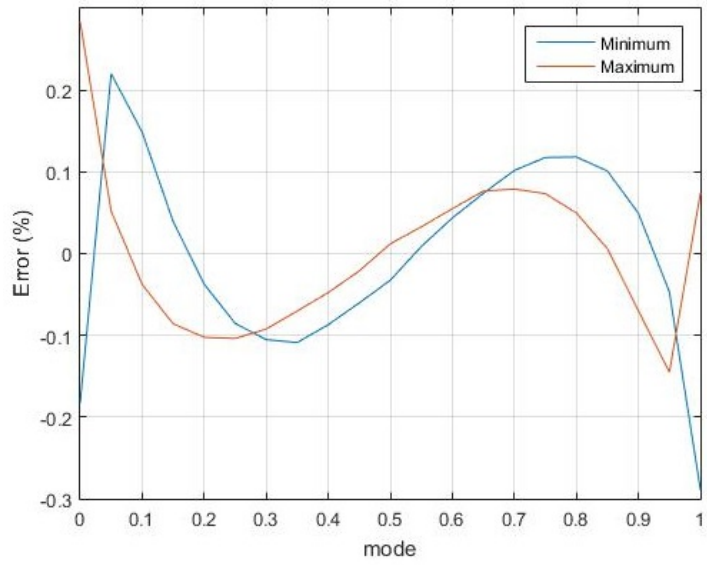

(a) Distribution defined by P5/P95

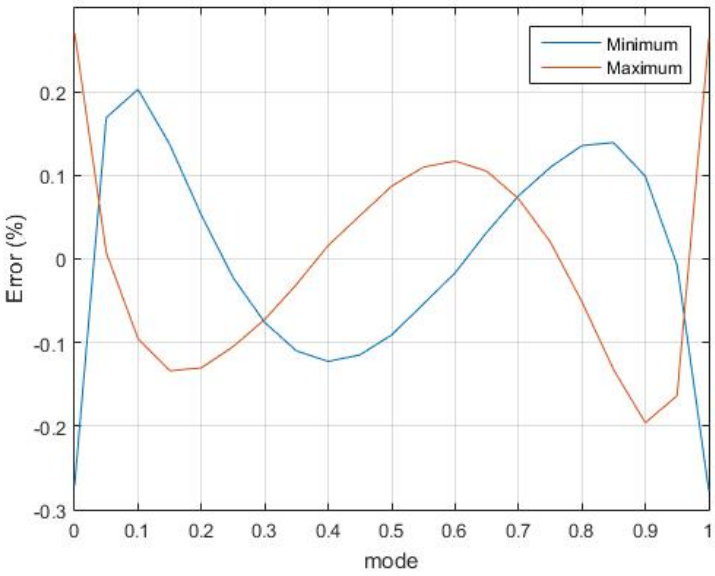

(b) Distribution defined by P10/P90

Figure 5.7: Error in minimum and maximum values for triangular distributions derived using empirical transformation compared to @Risk analytical solution. Note that the error is expressed as a percentage of the distribution scale and is invariant with magnitude of distribution domain.

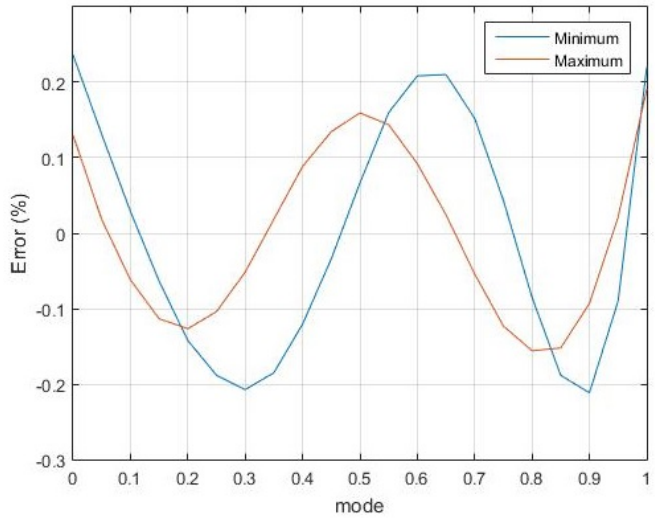

(a) Distribution defined by P5/P95

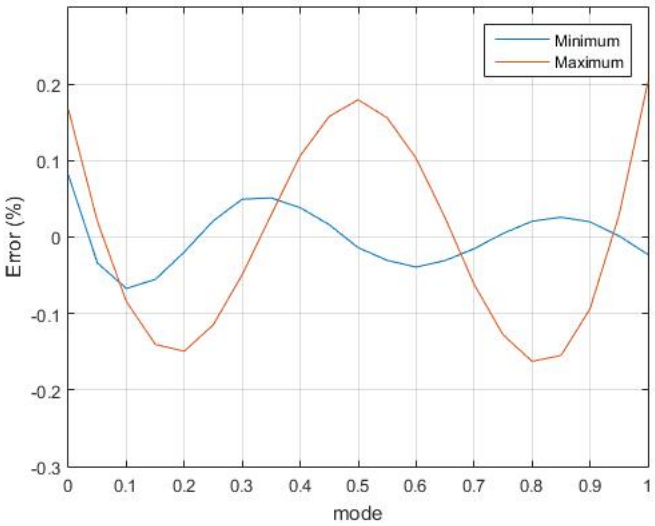

(b) Distribution defined by P10/P90

Figure 5.8: Error in minimum and maximum values for PERT distributions derived using empirical transformation compared to @Risk analytical solution. Note that the error is expressed as a percentage of the domain scale and is invariant with magnitude of distribution domain.

The empirical relations derived are limited to cases where $P_{min} < P_{mode} < P_{max}$. This means that extremely one sided distributions where the mode lies very close to the minimum/maximum value cannot be defined validly using this approach. However, such distributions are most intuitively defined by specifying the minimum or maximum values and therefore this approach is not required in that case anyway.

As shown in Figures 5.7 and 5.8, an error of up to ± 0.3% of the domain scale is possible when using these derivations depending on where the distribution specified by the user lies on the arbitrary domain scale. Even the maximum error is reasonably small and considered acceptable for MCA applications. This assertion is confirmed quantitatively in Section 5.5.4.

5.5.3 Convergence Testing

The mean and standard deviation of LCOE and IRR were used as the variables to test convergence. The number of simulations was increased exponentially from 150 to 450,000 in 17 increments. 10 repetitions were performed at each interval to test stability in results. The simulation time at each interval was also recorded. Note that the test was carried out using pragmatically assumed model inputs and does not represent any real project. The results are presented in Figure 5.9. 10000 simulations is deemed to be an appropriately large sample size with consideration of stability of results and practical computation time. Note that the MATLAB model is in the order of 5 times quicker than the existing Excel model.

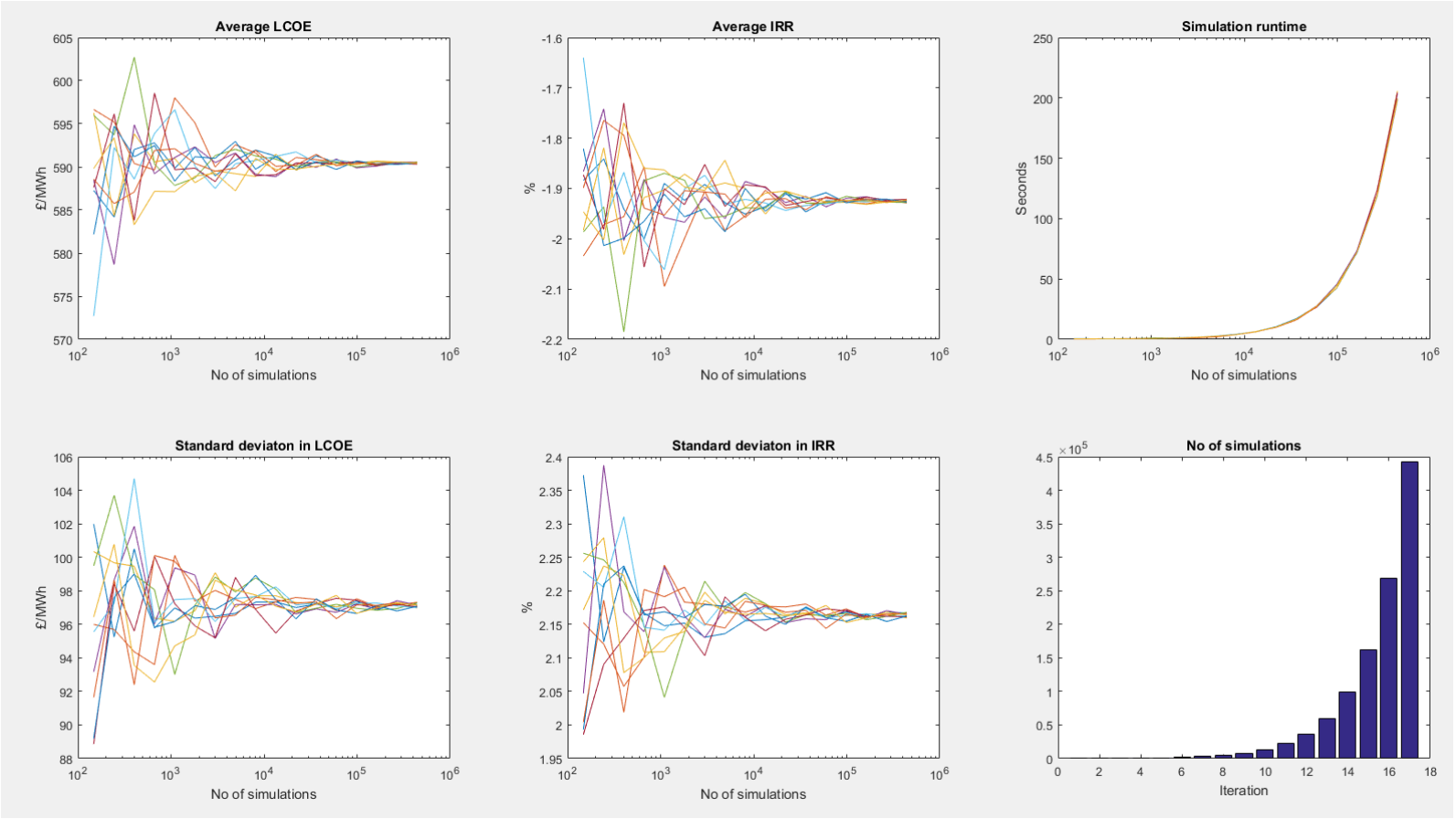

Figure 5.9: Convergence test results for tool v1. The test is carried out for increasing numbers of simulations and repeated 10 times for each simulation size. The repetitions are shown as lines of different colours.

5.5.4 Model Verification

The general approach to the verification was to compare distributions for a number of test variables derived from the existing Excel model and the translated MATLAB model when initiated with identical inputs. 95 intermediate variables were selected for comparison in this verification. This approach was chosen over analysing only final outputs such as LCOE and IRR because it gives more visibility of small errors that might otherwise be masked or cancelled out during summation. More specifically, the verification was carried out in the following two phases.

Seeded MCA without percentile transformation

An accurate translation from Excel to MATLAB can be proved if both models produce numerically identical results for each of the test variables. However, there are two issues that prevent this comparison to be made. Firstly, in order to produce numerically identical outputs, both models must generate numerically identical random samples for all input variables. This can be achieved by using a fixed seed for the random number generator (RNG) used to sample input distributions for MCA in Excel and MATLAB (Thomopoulos, 2013). In practice, it was found that a fundamental difference in the independent RNG algorithms in Excel and MATLAB prevented numerically identical samples to be drawn for PERT distributions even when the distribution parameters and seed were identical. It was possible to produce identical samples from triangular distributions with a fixed seed so the issue applies to PERT distributions only. The analysis proving this issue is discussed next.

It is expected that random samples produced in Excel and MATLAB for distributions with identical defining parameters seeded with the same fixed seed would be numerically identical. In practice, this was found to be true for

triangular distributions but not for Pert distributions, a special case of Beta distribution. The following studying investigates the underlying reason for this in order to identify a workaround.

The reason for this observation could have been that the same numbers are generated, but in a different sequence, resulting in a concurrent numbers not being the same. To test this, the samples were arranged in ascending order and plotted on a scatter plot to visualise the correlation (Figure 5.10). A perfect correlation is observed for the triangular distribution sample but this is not the case for the Beta (Pert) distribution sample, therefore indicating that the numbers are not identical irrespective of the sequence.

In Excel and Matlab the random numbers are sampled from a distribution by first generating a random number between 0 and 1. In Excel this number is then multiplied by the inverse cumulative distribution function (ICDF) of the respective distribution. It was not clear if the MATLAB random number generator (RNG) follows the same approach so the next test was to check if this was the case. If not, then Excel and MATLAB cannot be expected to produce identical samples with the same initial seed because the underlying method of random number generation is different. The Excel sample sequence is multiplied by the cumulative distribution function (CDF) to calculate the initial random number between 0 and 1 calculated by Excel. The same CDF is multiplied by the MATLAB sequence also to see if the same sequence of numbers between 0 and 1 is reached. A mismatch indicates that MATLAB has a differing method to convert the random numbers from 0 to 1 to sample values from the chosen distribution. The results in Figure 5.11 show that Excel and MATLAB have the same approach for triangular distributions but not for Pert. This explains the initial observation of seeded random sampled from Pert distributions not matching. Given this fundamental difference, it is concluded that no simple

workaround can be implemented to allow both RNGs to produce numerically identical samples.

Secondly, the percentile transformation algorithm outlined in Section 5.5.2 introduces a small numerical error. Therefore, the seeded MCA verification is carried out with all model inputs represented with triangular distributions and specified using minimum and maximum values to bypass the two issues preventing the comparison to be made.

The numerical comparison is made by finding the maximum difference between concurrent pairs of data in the Excel and MATLAB outputted distributions for each test variable, i.e. comparing n^{th} values from each distribution sample. The average maximum absolute difference across all 95 validation variables was found to be 4.20×10^{-6} and the maximum across all variables was 6.23×10^{-4}. Whilst the expectation was a zero difference, the small differences can be explained by the fact that the definitions of the distribution limits are subtly different due to rounding difference.

Probabilistic comparison with/without percentile transformation

The previous test does not allow verification of the script responsible for generating PERT distributions because numerically identical seeded MCA samples from Excel and MATLAB could not be produced for the Beta based distribution. The Excel and MATLAB models were initiated with a random seed and the inputs were represented using a mixture of triangular and PERT distributions. Given the random seed, there is no expectation of concurrent values from Excel and MATLAB samples to be comparable and the verification must be done statistically. The Two Sample Kolmogorov-Smirnov (KS) test was used for this purpose. The Two Sample KS test is a non-parametric test used to determine whether two

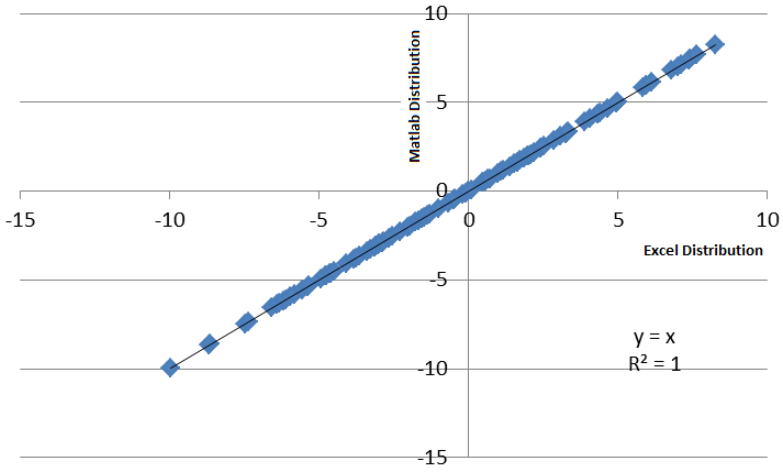

(a) Triangular Distribution

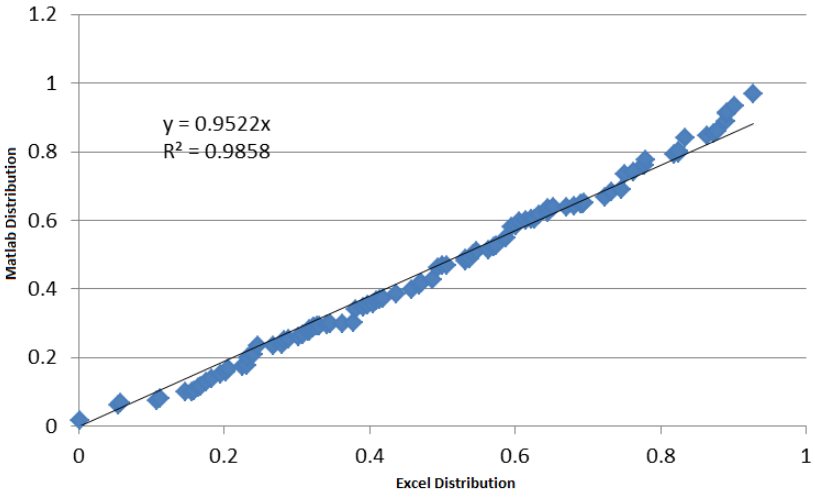

(b) Pert Distribution

Figure 5.10: Scatter plot of identical distributions sampled using the same fixed seed in Excel and MATLAB in order to compare numerical equivalence of the two samples. Note that both samples are arranged in ascending order to remove the effect of difference in sequencing of the numbers.

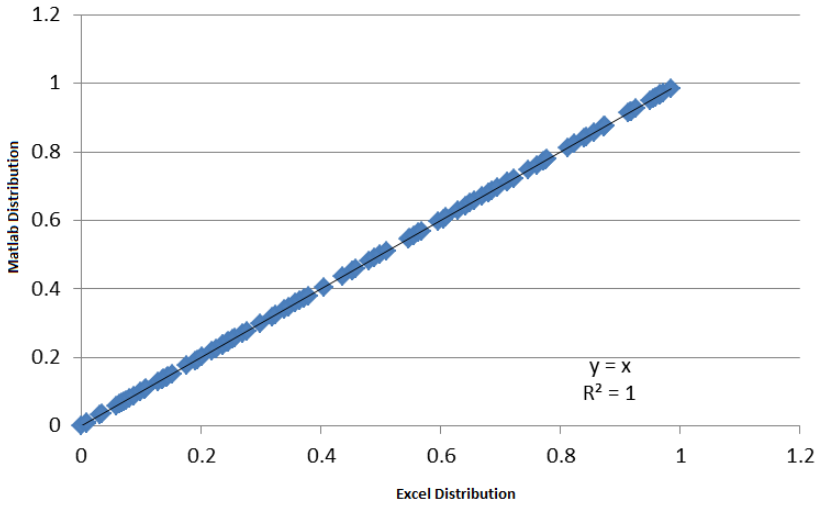

(a) Triangular Distribution

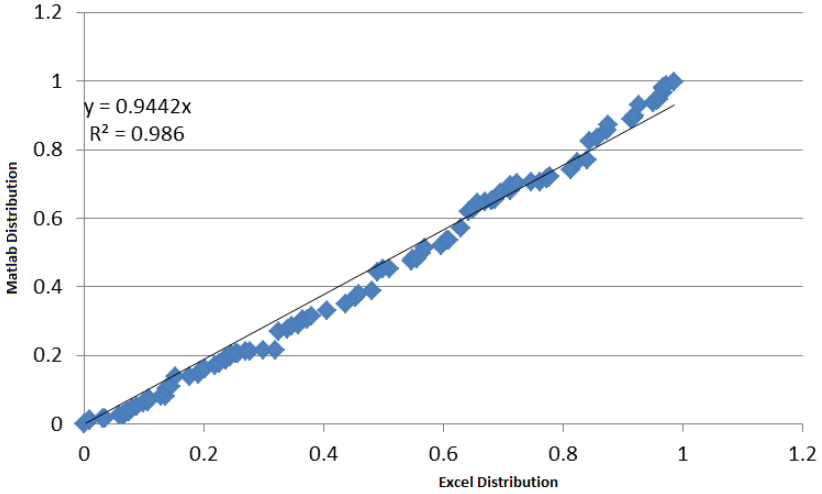

(b) PERT Distribution

Figure 5.11: Comparison of random samples generated from a common distribution with a fixed seed in Excel and MATLAB. Note that the distributions are scaled to a range between 0 and 1 by multiplying it by the CDF.

samples are drawn from the same underlying distribution (MIT, 2006). The null hypothesis was that the Excel and MATLAB model outputted distributions for each test variable are from the same continuous distribution. Note that the KS test was carried out for all variables with and without the percentile transformation algorithm (Section 5.5.2) implemented to test the statistical significance of the error introduced by its inclusion. The null hypothesis was accepted for all 95 variables in both cases at the 5% significance level.

5.5.5 Effect of Correcting Existing Tool Bugs

A comprehensive comparison of results before and after removing the bugs is not presented for a number of reasons. Firstly, many of the bugs were human errors leading to discrepancies of several orders of magnitudes (e.g. unit errors) and the results were not always physically sensible. Also, the number of bugs included in a calculation depends on the model settings so one particular set of results can be significantly less accurate than another set that bypasses most of the major bugs. As such, no inference could be made about the improvement in accuracy based on a few test cases, given the very large number of combinations of possible model settings.

Nonetheless, Figure 5.12 shows one example of the difference in LCOE distribution produced by the MATLAB model before and after correction of the bugs noted in Section 5.4.2. Note that both models are initiated using the same set of arbitrarily defined inputs for this illustration. There is a significant aggregate effect on the results as the distribution mode changes from approximately £575/MWh to £775/MWh and the shape of the distribution is also considerably altered.

A validation of the tool v1 after correcting the bugs was not possible because the rigid input structure makes it difficult to initiate a different model with the same

input conditions. It is also not strictly required because tool v1 was simply a starting point for the development of tool v2, which is the intended outcome. A validation of the tool v2 is presented in Section 5.6.

5.6 Tool v2

The focus of development of v2 of the tool was to introduce features that enable it to be applied to real projects that may be encountered in commercial practice. The v1 tool was restricted to somewhat idealised projects due to the rigidity in its input structure, some simplifying assumptions and relatively simple analytics of the model data. This section describes the development of additional capabilities, the tool structure and model validation.

5.6.1 Additional Capabilities

Flexible Inputs

A major limitation preventing the first version of the tool from being widely applicable to commercial projects was a requirement for CapEx and OpEx to be defined according to a predefined breakdown structure into sub-categories and a further detailed breakdown within the sub-categories. Whilst the breakdown was logical and comprehensive, real commercial projects are highly unlikely to

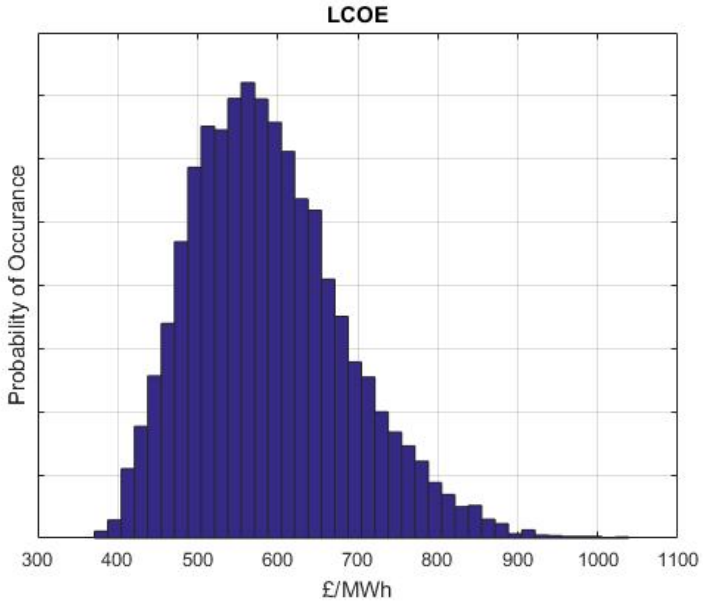

(a) Before correcting bugs

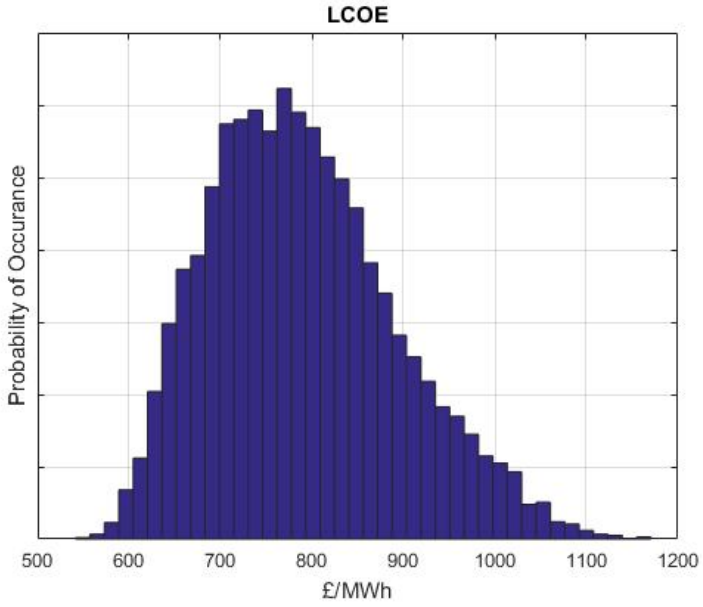

(b) After correcting bugs

Figure 5.12: Comparing LCOE output distribution from MATLAB model before and after correction of bugs carried forward from existing Excel tool

conform to that precise breakdown structure. For example, tool v1 requires the cost of the Power Take-off Unit (PTO) to be specified based on the cost of subcomponents such as seals, bearings, gearbox etc. and the also requires an uncertainty distribution to be attributed to each subcomponent cost. In reality, a project developer may have a contract for the supply of the entire PTO or turbine. The only way to process such a project in tool v1 would be to subjectively break down the cost and uncertainties into the required sub-categories. This step not only adds unnecessary labour time, but also introduces scope for inaccuracy and inconsistency between different projects because it is not easy to accurately subdivide a distribution such that the sum of the divided distributions results in the original distribution. Therefore, the capability to accept a fully flexible input structure for CapEx and OpEx was added to allow the user to divide and subdivide costs and uncertainty distributions as appropriate for the project under consideration.

Sensitivity Analysis

A deterministic and probabilistic sensitivity analysis function was added to the tool to allow the most critical variables to be identified. In general, the sensitivity analysis process is carried out by changing the value of one variable whilst keeping all other variables constant and calculating the resultant LCOE and IRR. This is repeated for every model variable. In the deterministic mode, the value of each sensitivity analysis variable is altered by a user defined (deterministic) percentage above and below the central value. In the probabilistic mode, the value is altered by one standard deviation of the uncertainty distribution attributed to that particular variable. As a result, the deterministic sensitivity analysis helps to identify the key systematic risks without consideration of the probability of occurrence, whereas the probabilistic sensitivity analysis identifies the key project risks with respect to probabilities. For example, a project where the CapEx

contributes to a large proportion of the LCOE will result in CapEx being a dominant variable in the deterministic analysis, but if there is very low uncertainty in the CapEx estimate then the probabilistic sensitivity analysis may show other variables to be more significant to LCOE because the variance is low. This is illustrated further in the case study in Section 5.7.

Other New Capabilities

Several other new capabilities were added to the tool in order to make it capable of representing variations likely to be observed in real projects and to make the tool more useable:

- Yield Degradation: A percentage loss factor to represent annual plant power performance degradation over time;
- OpEx Escalation: A percentage escalation factor to represent increasing maintenance cost over time;
- Decommissioning Funding Mechanism: Choice of 4 mechanisms; lumpsum at start, lumpsum at end, full life accrual and mid-life accrual. The lumpsum mechanisms capitalise the decommissioning fund from the cashflow at the start or end of the project life on a lumpsum basis, whereas the accrual mechanisms draw down from the cashflow annually on a pro-rata basis from the start or middle of the project's life;
- Refit CapEx: Allows the user to specify any in-life capital expenditure, such as a planned mid-life major rehaul;

- Cost Input Basis: Allows user to specify CapEx items on a relative or absolute basis, i.e. £/MW or £/project. OpEx items can be specified in £/MWh, £/MW or £/project per year. Costs may be specified in £s, £10,000s or £millions;

- Annual/Average Availability: The percentage availability may be specified separately for each year or as a lifetime average availability. The implication of these two options is expanded in Section 5.7.

5.6.2 Model Structure

A simple Microsoft Excel based graphical user interface (GUI) is provided to allow the user to enter the model inputs (Figure 5.13). For each variable, there is an option to specify the uncertainty by choosing a triangular or PERT distribution and the P0/P5/P10 and P100/P95/P90 value. The input variables are split into 4 categories; CapEx, OpEx, yield and financial. The structure of the CapEx and OpEx inputs is flexible as described in Section 5.6.1 and the breakdown of CapEx, OpEx and decommissioning cost is entirely user controlled. The yield and financial inputs required, as well as the key model outputs are shown in Figure 5.14.

Note that all intermediate line items such as revenue, tax, free cashflow etc. are accessible manually if required.

The model logic is illustrated in Figure 5.15 and the function of each script is as follows:

- 'master.m' sequentially initiates the following scripts and allows the user to specify options such as whether to run the model in deterministic or

probablistic mode, whether to run sensitivity analysis and whether to plot charts of results automatically;

- 'User Inputs' is the Excel spreadsheet that is used as the GUI;
- 'readInputs.m' reads the Excel inputs sheet and sequentially initiates the createInputStructure subroutine with the appropriate user values for CapEx, OpEx, yield and financial inputs;

	A	B	C	D	E	F	G	H
1	Input Cost Order of Magnitude		£k					
2	Relative or Absolute Costs?		Capacity Relative (per MW/yr)			Add Sub Levels		
3								
4	**Level**	**Component**	**Sublevels to Add**	**Value**	**Distribution**	**%ile Limits**	**Low %ile**	**High %ile**
5	*1*	*General*	*3*	*n/a*				
6	1.1	Licenses	0	5	Pert	P5/P95	2%	2%
7	1.2	Insurance	0	70	Pert	P5/P95	2%	2%
8	1.3	Monitoring	0	20	Pert	P5/P95	2%	2%
9	*2*	*Maintenance*	*2*	*n/a*				
10	2.1	Planned Maintenance	0	150	Pert	P5/P95	5%	5%
11	2.2	Unplanned Maintenance	0	150	Pert	P5/P95	15%	30%
12	*3*	*Decommissioning*	*0*	*0*	*n/a*			

CapEx Inputs | OpEx Inputs | Yield Inputs | Financial Inputs

Figure 5.13: Screenshot of model input GUI. This illustration shows the OpEx input sheet. Similar sheets for CapEx, yield and financial parameters allow all user input values and corresponding uncertainty distributions to be specified through this Excel interface. Note that there are no predefined fields for CapEx and OpEx inputs because a flexible user defined breakdown structure is permitted. The data in Column A, 'Level', informs the model of the categorical relationships between the list of variables.

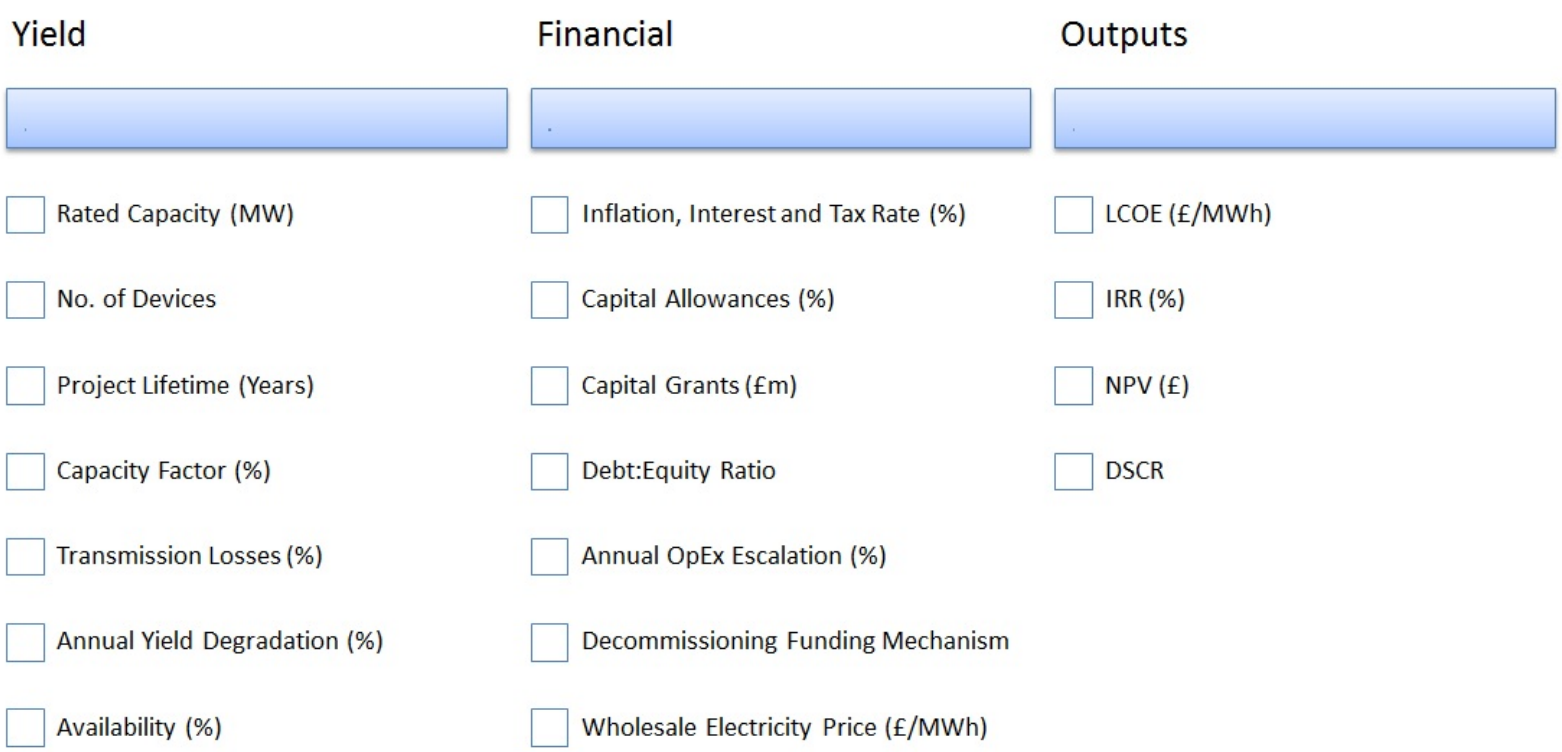

Figure 5.14: List of v2 tool inputs

- 'createInputsStructure.m' uses input values to define distribution objects for each input variable. A recursive loop allows an unstructured sub-categorisation of CapEx and OpEx items. For example, CapEx can be split into 2 sub-categories, one of which may have 4 sub-categories itself whereas the other has none;

- 'createDist.m' is called for each distribution object created by the parent script to generate a random sample for MCA;

- 'monteCarlo.m' combines input distributions using the appropriate functions to produce the output distributions;

- 'sumStructure.m' is called to sum the structure containing CapEx and OpEx sub-categories to produce a distribution of the total CapEx and OpEx;

- 'preProcessing.m' prepares user inputs for use by the monteCarlo script;

- 'sensitivityAnalysis.m' initiates the monteCarlo script for each variable with the central value replaced by the sensitivity analysis value. Note that the script is run statically so no MCA takes place, it is simply a deterministic DCF analysis to calculate LCOE and IRR using the perturbed input values.

5.6.3 Model Logic

The overall aim of the model is to reduce the user inputs into values for CapEx, OpEx and yield. Equation 5.4 can then be solved to derive the LCOE, and the free cashflow can also be derived to calculate the IRR. The derivation of these values is described in detail below. Note that the logic is repeated for each MCA simulation in order to provide the output distributions.

The CapEx is calculated by simply summing all cost components specified by the

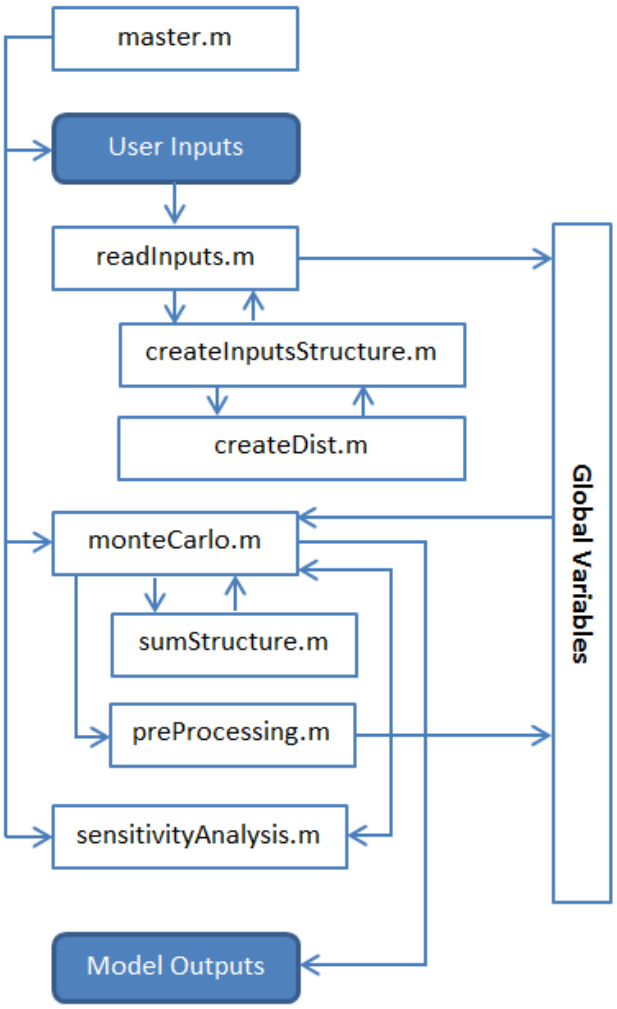

Figure 5.15: Flowchart of MATLAB Tool v2 model logic

user:

$$\text{CapEx} = \text{CapEx}_1 + \text{CapEx}_2 + \cdots + \text{CapEx}_n \tag{5.9}$$

Where $CapEx_n$ is the n^{th} user specified cost component. Since the CapEx is an upfront expenditure, it is already specified in its present value in nominal terms so an explicit adjustment for inflation is not required.

The OpEx is calculated by simply summing all OpEx subcomponents specified by the user:

$$\text{OpEx} = \text{OpEx}_1 + \text{OpEx}_2 + \cdots + \text{OpEx}_n \tag{5.10}$$

Where $OpEx_n$ is the n^{th} user specified OpEx subcomponent. Since the OpEx is an ongoing expenditure over the project's life, an explicit adjustment is required to specify it in nominal terms for each project year as follows:

$$\text{Nominal Cost} = \text{Real Cost} \times (1 + InflationRate)^t \tag{5.11}$$

Where t is the future time period the cost is being adjusted for.

The annual yield is calculated by multiplying the user specified capacity factor, total installed capacity, availability and losses by the hours in a year. Sufficient information is now available for solve the Equation 5.4, noting that the present value of the future OpEx and yield must be used (Equation 5.3).

Next, the free cashflow is constructed using the newly derived CapEx and OpEx cashflows in conjunction with the user specified financial inputs such as electricity price, tax and depreciation rates and project finance structure.

The subsidy and wholesale electricity price assumptions are used in conjunction with the annual yield to calculate the project's revenue in real terms:

$$\text{Revenue} = (\text{Subsidy} + \text{Wholesale Price}) \times \text{Annual Yield} \tag{5.12}$$

The EBITDA is calculated by substituting the results from Equations 5.9-5.12 into Equation 5.5.

Next, the mortgage style debt repayment structure described in Section 5.2.3 is used to calculate the principal and interest payments due through the lifetime of the project. Similarly the tax due in each year is calculated using the capital allowance and straight line depreciation methods described in Section 5.2.3.

Finally, the free cashflow can be derived as follows:

$$\text{Free Cashflow} = \text{EBITDA} + \text{Tax} + \text{Interest} + \text{Principal Repayment} \quad (5.13)$$

Note that the model follows standard accounting conventions whereby a positive value is a cash inflow and a negative value is an outflow. Therefore tax, interest and principal repayment will always be negative terms.

5.6.4 Tool Validation

As highlighted in Section 5.3, no other DCF analysis model with full MCA capability could be found in the public domain. A full validation of the tool is therefore not possible. However, a leading industry techno-economic model, called Exceedence Finance, is capable of deterministic DCF analysis. Both models were initiated with identical inputs and found to produce an identical output cashflow. This is strong evidence for the validity of the MATLAB tool's DCF analysis logic because it was developed entirely independent from the Exceedence tool logic. Note that it is not possible to publish the resultant data due to the terms of the license used to access the software. Whilst this comparison only validates the model logic deterministically, it should be noted that the probabilistic verification in Section 5.5.4 proved the validity of the tool's MCA logic relative to the leading

MCA software package, Palisade @Risk. A high level of confidence in the accuracy of the tool's outputs is therefore achieved.

5.7 Case Study

5.7.1 Introduction

A realistic pilot tidal array financed with a mixture of debt, equity and grants was used as a case study to demonstrate the functions of the tool. The results of the stochastic MCA uncertainty analysis are compared to the simpler deterministic methods described in Section 2.4.1. The simple deterministic method is referred to as Method 1 in the following text, and the probability weighted deterministic method is referred to as Method 2. MCA is referred to as Method 3.

5.7.2 Model Inputs

The assumptions used to define the project are summarised in Tables 5.5 to 5.8. Note that the input values are derived mostly from data found in the literature, but engineering judgement was used where necessary, and is specified in Tables 5.5-5.8. Further modelling assumptions are:

- Project has entered procurement contracts for the hardware, but has not entered the construction phase so the CapEx uncertainty is largely attributed to the construction phase;
- Project is constructed in 1 year with power output beginning at the start of the next year;

- Mortgage style debt amortization (Groobey et al., 2010);
- Capital allowances and reducing balance depreciation is used to derive tax obligation (Gov.uk, 2016);
- 100,000 Monte Carlo simulations used for all analyses;
- PERT distributions with limits as defined in Tables 5.5 to 5.8 used to represent uncertainty in all model variables.

Note that the LCOE and IRR values used are representative, but the accuracy of the values is not of primary importance for this study because the difference in results using different methods (for constant inputs) is of interest.

Table 5.5: Breakdown of CapEx inputs and uncertainty assumptions. Note that the total CapEx is taken from OES (2016) and converted from USD to GBP using an exchange rate of 1.53. This is the average rate for the year to 31/03/2016. The split between CapEx categories is taken from Carbon Trust (2006*a*) and the uncertainty distributions are defined pragmatically to represent a project that has completed procurement, but installation is incomplete.

Variable	**Value (£k/MW)**	**P5**	**P95**
Project Development	482	2%	5%
Hardware	See breakdown below		
Device	2700	2%	5%
Moorings And Foundation	770	2%	5%
Grid Connection	770	2%	5%
Installation	1156	2%	15%

Table 5.6: Breakdown of OpEx inputs and uncertainty assumptions. Note that the total OpEx is taken from OES (2016) and converted from USD to GBP using an exchange rate of 1.53. This is the average rate for the year to 31/03/2016. The split between OpEx categories is taken from Carbon Trust (2006*a*) and the uncertainty distributions are defined pragmatically to represent relatively high uncertainty in unplanned maintenance

Variable	**Value (£k/MW)**	**P5**	**P95**
General	See breakdown below		
Licenses	5	2%	2%
Insurance	72	2%	2%
Monitoring	21	2%	2%
Maintenance	See breakdown below		
Planned Maintenance	150	5%	5%
Unplanned Maintenance	145	15%	30%
Decommissioning	0	n/a	n/a

Table 5.7: Breakdown of yield inputs and uncertainty assumptions

Variable	**Value (units)**	**P5**	**P95**	**Comments**
Rated Capacity	2 MW			n/a
No Of Turbines	5			n/a
Lifetime Of Project	25 years			n/a
Capacity Factor	35%	9%	9%	Value from OES (2016), uncertainty from OREC (2015*b*)
Resource Uncertainty	n/a	17%	17%	Uncertainty from OREC (2015*b*)
Availability	96%	2%	15%	Value from OES (2016), pragmatic uncertainty

Table 5.8: Breakdown of financial inputs and uncertainty assumptions

Variable	**Value (units)**	**P5**	**P95**	**Comments**
Inflation Rate	2%	20%	20%	Government inflation target, pragmatic uncertainty
Interest Rate	6%	10%	10%	Value from Visser and Held (2014), pragmatic uncertainty
Tax Rate	20%	n/a	n/a	UK Corporate tax rate in 2016
Capital Allowances	8%	n/a	n/a	UK special pool rate capital allowance (Gov.uk, 2016)
Capital Grants	25% of CapEx	n/a	n/a	Pragmatic assumption
Debt Equity Ratio	40:60	n/a	n/a	Pragmatic assumption
Feed-in Tariff	£305/MWh	n/a	n/a	For first 15 years of project (DECC, 2013)
Loan Period	15 years	n/a	n/a	Pragmatic assumption
Discount Rate	10%	20%	20%	Based on literature review in Section 5.3
Wholesale Electricity Price	£84.54/MWh	25%	25%	Assumed to apply from year 16 onwards. From DECC (2012)

5.7.3 Results

The P5 and P95 of a distribution were considered as representing the pessimistic and optimistic case for LCOE in this analysis, respectively. Similarly, the P95 and P5 were considered pessimistic and optimistic for IRR, respectively. Therefore, the model was run in deterministic mode with all input variables fixed to their optimistic and pessimistic levels (P5/P95) to calculate the optimistic and pessimistic LCOE and IRR for the static analyses (Method 1 and 2). A central case using central inputs values was also modelled. Finally, a probabilistic simulation using empirical input distributions was run for MCA (Method 3).

Figures 5.16 and 5.17 show the pessimistic, central and optimistic LCOE and IRR values for the case study project resulting from the three uncertainty methods considered. The central LCOE value from the static analysis is 4% lower than the MCA P50 due to the skew in the distribution and corresponds to the MCA derived P62 LCOE (Figure 5.16b). The pessimistic and optimistic case results using Method 1 represent a scenario where each uncertain variable simultaneously assumes its extreme value and therefore represents a highly unlikely best/worst case rather than a reasonable optimistic/pessimistic view. This is the reason for the large disagreement with the MCA P5 and P95 values. Weighting the magnitude of the variation in proportion to its probability (Method 2) gives a closer agreement with MCA results, but an error is still present. Similar observations can also be made for the IRR results.

Figure 5.18 shows results of a sensitivity analysis to identify the variables that affect the LCOE and IRR most significantly. Some large differences can be observed in the sensitivity of the key variables under probabilistic and deterministic sensitivity analysis. The probabilistic sensitivity analysis used MCA to derive the variation in the LCOE and IRR resulting from a perturbation on the central value of a variable equal to 1 standard deviation of its uncertainty.

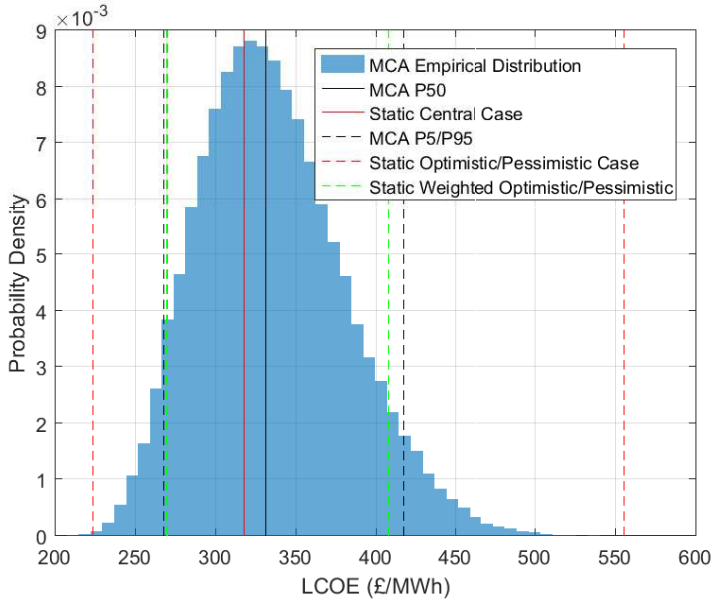

(a) LCOE Distribution Histogram

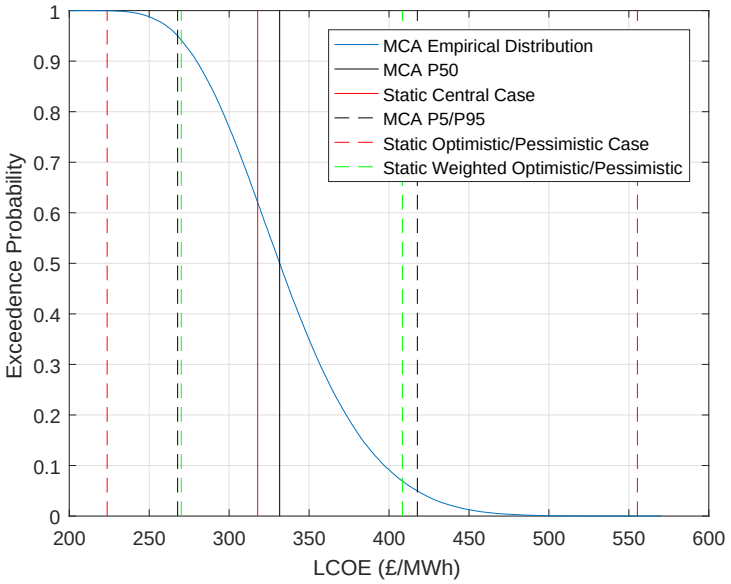

(b) LCOE Distribution ICDF

Figure 5.16: Comparing LCOE results derived using three different uncertainty analysis methods. The pessimistic/central/optimistic values from each analysis are overlaid as vertical lines.

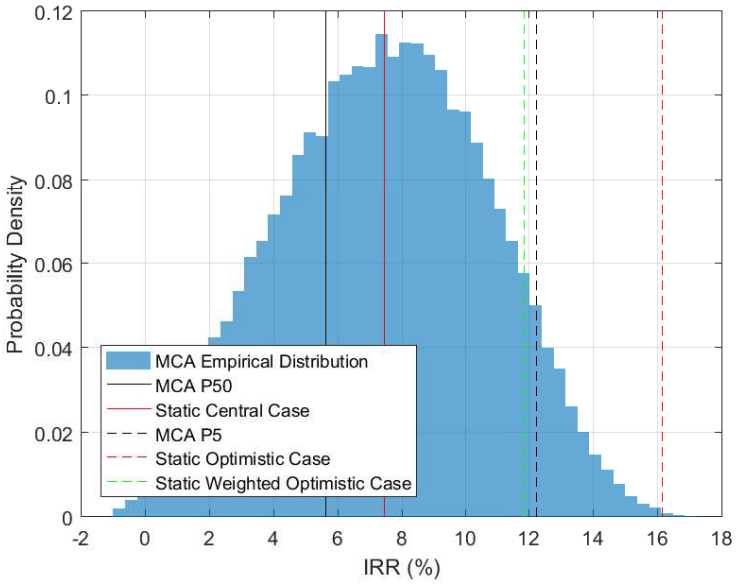

(a) IRR Distribution Histogram

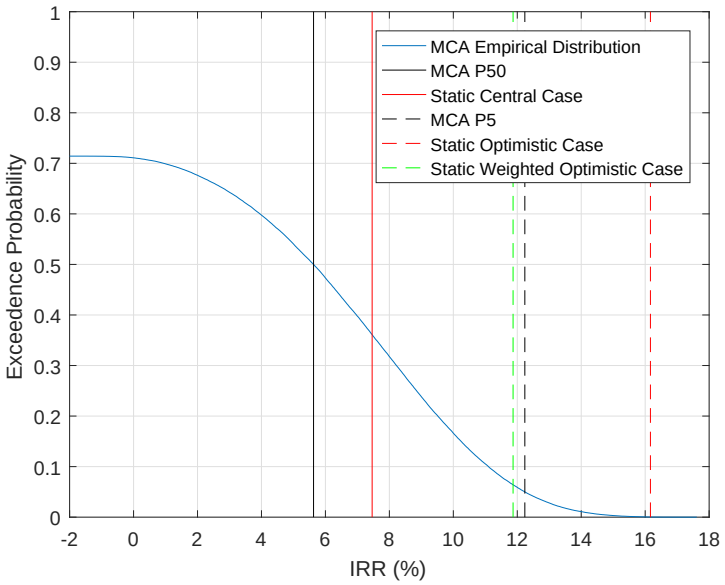

(b) IRR Distribution ICDF

Figure 5.17: Comparing IRR results derived using three different uncertainty analysis methods. The pessimistic/central/optimistic values from each analysis are overlaid as vertical lines. Note that the pessimistic IRRs are not real numbers and therefore not plotted.

The deterministic level sensitivity is derived from a uniform user specified 7.5% perturbation. The 7.5% perturbation is chosen pragmatically with consideration of the range of uncertainties prevalent in all the variables. The difference between the two methods is most apparent for CapEx, which is a very important factor to the project's finances, but has relatively small uncertainty in this case because the procurement phase is assumed to be complete. Conversely, the probabilistic sensitivity to resource uncertainty is greater than the deterministic sensitivity because a large amount of uncertainty is assumed for this project.

As seen in Table 5.1, there are a number of variations in modelling assumptions used by different authors. The implication of some common variations on the LCOE and IRR is presented in Figure 5.19. The variations tested are specified in Table 5.9.

The decommissioning cost has only a small effect because it has a low present value due to future discounting. The yield degradation and OpEx escalation are more significant because the LCOE and IRR are more sensitive to OpEx and yield, and with a higher present value. Modelling the tax and debt obligations does not affect LCOE because it does not consider project cashflow, but the effect on IRR is large. In general, the base case P95:P50 and P50:P5 ratios are maintained, thus indicating that the variations in the assumptions affect the P50, but not the relative uncertainty.

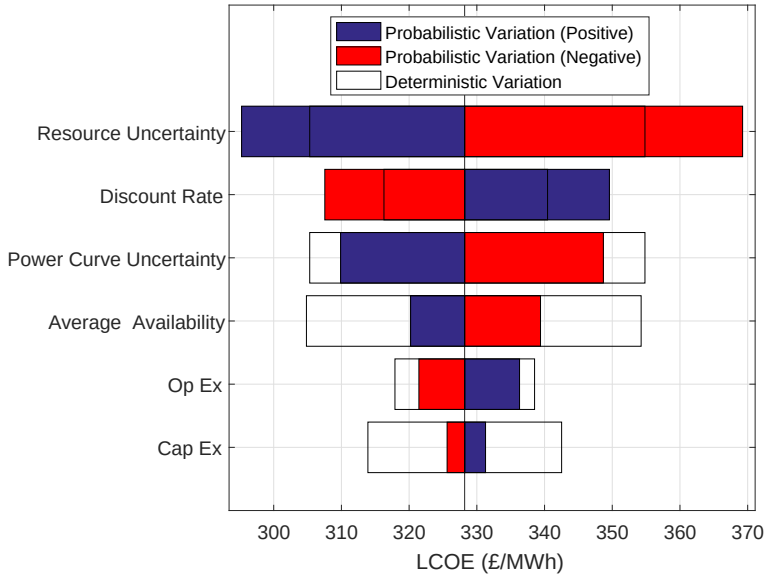

(a) LCOE Sensitivity

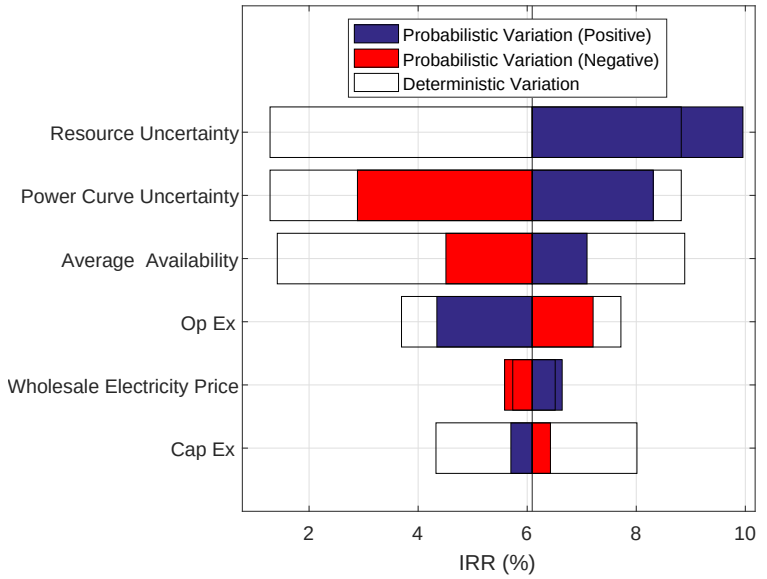

(b) IRR Sensitivity

Figure 5.18: Sensitivity of LCOE and IRR to changes in the model variables. Probabilistic sensitivity results are derived by perturbing each variable by $\pm$ 1 standard deviation of its uncertainty distribution whereas the deterministic sensitivity results are derived by perturbing each variable by $\pm$ 7.5%. Note that the negative perturbation on resource uncertainty results in a non-real IRR and is therefore not plotted. Also note that only the 6 most sensitive model variables are presented here.

Table 5.9: Breakdown of variations in central case parameters to test common modelling assumptions

Variable	Value (units)	P5	P95	Comments
Mid-life refit	50% of CapEx	25%	25%	Assume major marine operation for large component replacement in year 13. Values chosen pragmatically
Annual yield degradation	2% annually	5%	5%	Values adjusted pragmatically based on equivalent wind data in Staffell and Green (2014) and Wilkinson (2014)
Annual OpEx escalation	2% annually	15%	15%	Pragmatic judgement
Decommissioning - Lump sum at end	100k/MW	50%	50%	From Climate Change Capital (2010).
Decommissioning Continuous Accrual				
Decommissioning Midlife Accrual				
Decommissioning Ringfence Funds				
No debt/tax obligations	n/a	n/a	n/a	As assumed by several authors in Table 5.1

It is often necessary to use pragmatic judgement to specify the uncertainty on costs due to the lack of data (Maravas and Pantouvakis, 2013). It is important to note that assuming a certain magnitude of uncertainty on costs of subcomponents individually is not equivalent to the total cost being subject to the same magnitude of uncertainty. Figure 5.20 shows the difference in the uncertainty distribution of hardware costs for the case study project if one applies the uncertainty bands in Table 5.5 (P95 = -5%, P5 = 2%) separately to each of the three hardware subcomponents and if that uncertainty is assumed to apply to the total hardware cost instead. The total cost uncertainty is smaller when it is specified at the subcomponent level because it is assumed that the uncertainties are uncorrelated, thus the likelihood of all subcomponents being simultaneously and equally different in cost is small. The effect of this on the LCOE for the case study project is small because the project has a relatively low sensitivity to CapEx variations (Figure 5.18), but it is possible for it to be more significant for other projects.

Similarly, the implication of assuming an availability uncertainty on an annual basis rather than for an average value for the 25 year project lifetime is not intuitive, but important to understand. Figure 5.21 shows the reduced availability uncertainty over the project lifetime due to the independent and uncorrelated relation between the project availability over consequent years. Interestingly, there is very little effect on annual yield uncertainty compared to a case where the same error bands are applied to the project's lifetime availability instead (i.e. perfect correlation between years). This is because the net yield is also dependent upon the resource and loss uncertainty which cannot be assumed to be correlated. The case study project assumes high uncertainty on these parameters, but a project with lower uncertainty would result in a higher discrepancy. When these uncertainties are ignored, a large difference in annual yield uncertainty is

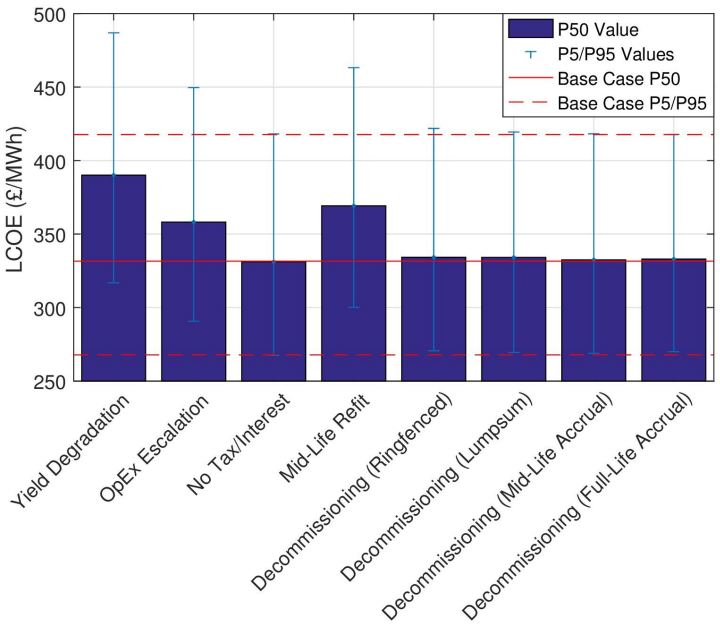

(a) LCOE Sensitivity

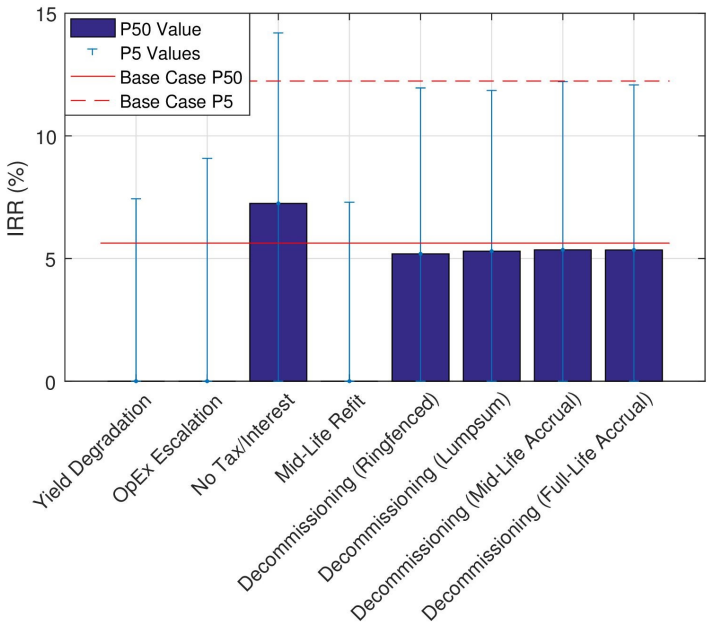

(b) IRR Sensitivity

Figure 5.19: Sensitivity of LCOE and IRR values to common variations in assumptions (Table 5.9). Note that all P95 and some P50 IRRs are not real numbers and therefore not plotted.

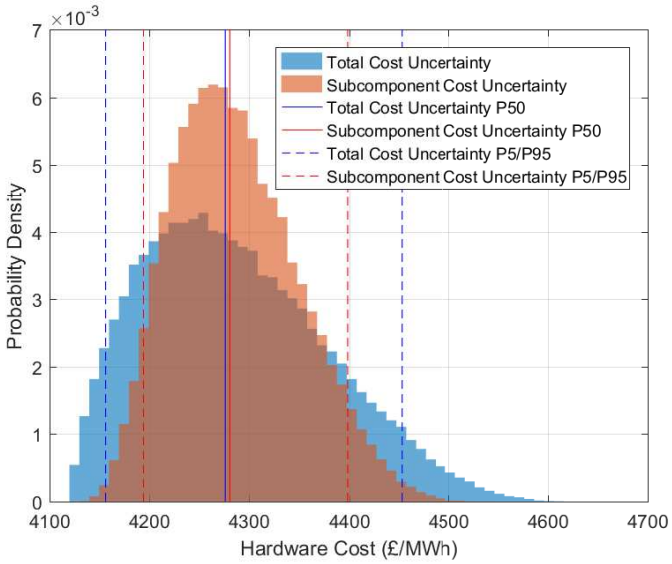

Figure 5.20: Effect of applying same uncertainty bands (P95 = -5%, P5 = 2%, as specified in Table 5.5) on hardware cost subcomponents and on total hardware costs.

observed depending on the correlation assumed between annual availability over time (Figure 5.21, secondary axis).

5.7.4 Discussion

The key observations in the results of the case study and its implications are discussed below.

It may be expected that a LCOE calculation based on P50 inputs would provide a P50 LCOE, but the central LCOE estimate from the static analyses is equivalent to the P62 of the MCA LCOE distribution for the case study project (Figure 5.16). This is because the distribution is skewed and the mode is therefore not equal to the median. LCOE distributions will generally be skewed, even if all input uncertainties are symmetrical, due to the division of the cost uncertainty distribution by the yield uncertainty equation (Equation 5.4). The P50 LCOE

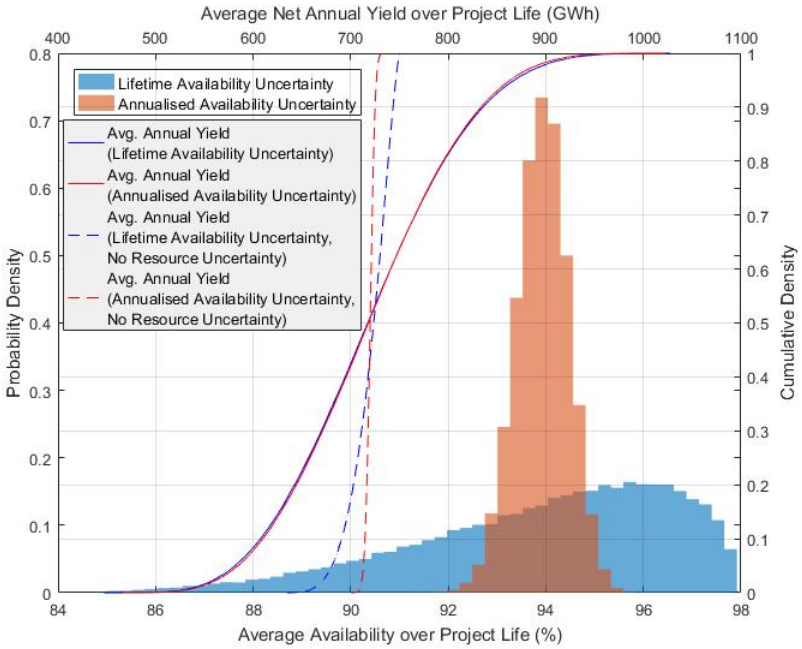

Figure 5.21: Effect of applying same uncertainty bands on annual availability and on project lifetime availability.

is of most interest to decision makers for understanding the central case so the overestimation of the static methods is a notable observation, particularly as it gives a non-conservative view. The static central estimate has to be interpreted as the mode of the LCOE distribution which will only be equal to the P50 if the distribution is symmetrical, but the difference will be increasingly significant as the skew increases. It is noted that none of the literature reviewed in Table 5.1 that utilises the static uncertainty analysis methods acknowledges this important point.

The limitations of the optimistic and pessimistic cases derived using the static methods must also be understood. The Method 1 results calculated using P5/P95 values for all variables can wrongly be interpreted without acknowledging that the LCOE represents an extremely unlikely case due to the independence of the uncertainties. Furthermore, without visibility of the LCOE distribution, as provided by MCA, it is difficult to interpret the LCOE at different percentiles. As

shown in Figure 5.16, Method 2 is reasonably accurate at estimating the P5/P95 LCOE when the model is solved using P5/P95 inputs. However, if a P10/P90 was then required for analysis, the model would need to be run again with all inputs at P10/P90. In cases where the uncertainty distributions are defined using expert judgement, there is likely to be an inconsistency between the results because it is difficult to pragmatically estimate values from a distribution at different percentiles accurately.

It is noted that all of the models reviewed in Table 5.1 that use deterministic uncertainty analysis adopt the Method 1 approach only. The probability weighted approach in Method 2 is used in various other sectors for applications such as sales forecasting, but no evidence of its application for marine energy cost modelling was found in literature (Azizuddin, 2013). The probability weighted deterministic outputs are more valuable practically than the Method 1 outputs which represent highly unlikely outcomes. Given that Method 2 is reasonably simple, it is recommended for all cases where the probabilities on the inputs can be defined. However, it is highlighted that the probability weighted outputs do not correspond exactly to the input percentiles. For the example in Figure 5.17, the output LCOE calculated using P5 inputs corresponds to the P7 LCOE, but the difference will be greater for distributions with higher skew. For final investment decision analysis, this type of unquantified error may be unacceptable.

MCA produces output distributions that can be used to derive consistently accurate results (assuming accurate inputs and a sufficiently high number of simulations) at any percentile of interest and skewness in the distributions is naturally accounted for. However, MCA relies on more detailed input information than the static analysis and Method 1 may be more suitable for projects where it is not possible to accurately define confidence intervals on the input parameters. MCA can be applied to any project with sufficiently rich input data for Method 2 and given the advantages of MCA, it should be the preferred method of analysis.

Whilst the computational burden for MCA is considerably larger than that for Method 2, it is still quite modest with a model runtime of approximately 30 seconds on a standard laptop computer.

The previous comments are made in relation to LCOE results, but they apply equally to IRR results also.

It is important to select the most appropriate of the two types of sensitivity analysis presented in Figure 5.18 because the results of the two methods can vary greatly. The deterministic sensitivity assumes a uniform uncertainty for all variables and therefore informs which factors provide the largest benefit from a given amount of uncertainty reduction, whereas the probabilistic sensitivity represents the biggest risks to a specific project with consideration of the various uncertainty levels defined for each parameter defining the project. The former method is most likely to be of interest for strategic analyses, whereas the latter is of interest to investors.

There are some parameters, such as yield degradation over time, affecting a project's financial performance that are very difficult to quantify at the current level of maturity of the sector, and are often neglected from analysis. However, it is physically representative to model them, albeit with a large uncertainty allocation. The sensitivity analysis in Figure 5.19 shows that annual yield degradation and mid-life refit are two commonly ignored parameters with a very significant impact on the case study project's financial metrics. Notable yield degradation has been identified in wind farm operational data (Staffell and Green, 2014). It is likely that tidal farms will suffer at least as much degradation given the similarities in the technology and the added factors such as biofouling and increased difficulty in access for maintenance. Similarly, it is not physically realistic to assume no major component rehaul for the 25 year project duration based on experience from the wind sector, especially considering the harsher environmental conditions

experienced by tidal turbines. For the case study project, including the yield degradation and mid-life refit results in a 18% and 12% increase in LCOE, respectively, and a 13% and 9% increase in the P5/P95 LCOE range.

The decommissioning cost is also commonly neglected in cost models. Figure 5.19 shows that there is little sensitivity to any of the decommissioning funding mechanisms. However, it may still be important to model the decommissioning cost, uncertainty and funding mechanism for an investment decision to determine the risk of defaulting on the project debt because it can lead to a negative cashflow in certain years. For example, the mid-life accrual model results in a less favorable DSCR than the full life accrual model for the latter years of a project because a lower proportion of the free cashflow is available to pay the debt service charges due to the higher decommissioning annuities. The project's cashflow in the final year cannot support the lumpsum payment of decommissioning at project completion and would lead to the project becoming insolvent. This is despite the LCOE and IRR being very similar to the accrual models which indicate a healthier cashflow and this highlights the need to properly model the timings of the decommissioning expense for an investment decision.

Figures 5.20 and 5.21 highlight the exposure to significant errors if uncertainties are defined subjectively without careful consideration. Assigning uncertainty bands to subcomponents of a variable that are independent and uncorrelated is clearly representing a different case to one where the same bands are applied directly to the total value of the variable. However, it is easy to make this assumption if the implication of summation of independent uncertainties is not appreciated. It is therefore recommended when subjectively assigning uncertainty distributions to inputs that due consideration is given to identify the subcomponent level at which it is most intuitive to assess the uncertainty.

5.8 Summary

There is a lack of standardisation in the cost modelling process for marine energy projects. Whilst the high uncertainty in results is acknowledged, a comprehensive analysis of the uncertainties is not generally performed. A highly flexible and generic cost modelling tool with probabilistic uncertainty analysis using MCA was developed to address these issues.

The tool was applied to a realistic tidal energy project to demonstrate its functions and highlight benefits provided compared to commonly used deterministic uncertainty analysis techniques. MCA was shown to provide unambiguous results which are consistently accurate, easy to interpret and can be queried to provide any confidence interval of interest.

The key uncertainties that have a large impact on the LCOE and IRR for the case study project were identified using a sensitivity analysis and it was shown that the results can vary significantly depending on whether a fixed perturbation magnitude is applied to each sensitivity test parameter (i.e. deterministic sensitivity analysis) or if the perturbation magnitude is varied depending on the uncertainty distribution representing the parameter (i.e. probabilistic sensitivity analysis). Finally, the sensitivity of the results to a number of commonly ignored parameters was studied. It was shown that commonly made assumptions, such as assuming no degradation in annual yield over time or assuming that no major rehaul of the turbines will be necessary for the duration of the project, have a significant impact on the P50 financial metrics. Ignoring decommissioning costs does not have a significant impact on the LCOE and IRR, but it is important to model the mechanism for funding the decommissioning phase because the timing of the cashflow can result in a default on the project's debt.

Chapter 6

Linking Yield and Financial Uncertainty Analyses

6.1 Introduction

Chapter 4 highlighted the difference in the annual yield uncertainty for a given project resulting from the use of ISO-guide to the expression of uncertainty in measurement (ISO-GUM) and Monte Carlo analysis (MCA) methods for uncertainty propagation. Chapter 5 presented a method to propagate uncertainties in a project's costs and yield through to the levelised cost of energy (LCOE) and internal rate of return (IRR). This chapter linked the two processes together to demonstrate the impact of the two yield uncertainty analysis methods on the uncertainty in investment metrics. This is more valuable to investors than knowing the inaccuracy in the P90 yield (as in Chapter 4) because it directly demonstrates the extent to which a project's P90 IRR varies if the less accurate yield uncertainty method is used, with all other parameters being equal.

6.2 Linked Modelling Methodology

In Section 5.7, the yield uncertainty was calculated from user specified values for capacity factor and resource uncertainty. In this chapter, this user specified yield uncertainty distribution was replaced by the distributions derived using the ISO-GUM and MCA methodologies outlined in Section 4.3. The cost and financial assumptions made earlier are kept constant and the detailed definitions of these assumptions can be found in the sections listed in Table 6.1. Several test cases are analysed to amplify the power of the results derived in Chapters 3 and 4. For each case, the resultant LCOE and IRR distributions are of interest for the comparisons because the difference observed is the ISO-GUM error. As before, the assumptions are intended to represent a realistic tidal energy project, but high accuracy in the input values was not a priority because the analysis is concerned with relative differences between ISO-GUM and MCA results.

Table 6.1: List of references to previous chapter sections where the defining parameters of the test case used in this analysis are specified.

Assumptions related to	**Defined/presented in**
Turbine	Figure 4.5a
Site Resource	Figure 4.5a
CapEx	Table 5.5
OpEx	Table 5.6
Financial	Table 5.8

All assumptions used to illustrate the two cases presented in Figures 4.10-4.11 were carried forward to calculate the impact on LCOE and IRR for the case study project analysed in Section 5.7. To remind, Figures 4.10-4.11 compare the annual yield uncertainty distributions for the reference tidal project using

MCA and ISO-GUM for different levels of resource uncertainties (u_R) and loss uncertainties (u_L). Therefore, comparisons between ISO-GUM and MCA were made for the following six combinations of u_R and u_L:

- Case 1: $u_R = 5\%$ and $u_L = 0\%$;
- Case 2: $u_R = 15\%$ and $u_L = 0\%$;
- Case 3: $u_R = 5\%$ and $u_L = 5\%$;
- Case 4: $u_R = 5\%$ and $u_L = 15\%$;
- Case 5: $u_R = 15\%$ and $u_L = 5\%$;
- Case 6: $u_R = 15\%$ and $u_L = 15\%$.

The difference in LCOE and IRR resulting from the use of MCA and ISO-GUM over the full range of resource uncertainties (u_R) and loss uncertainties (u_L) varying from 0% to 15% was also considered.

In order to assess the sensitivity of the relation between yield uncertainty and LCOE and IRR uncertainty with respect to variations in cost uncertainties, the analysis is repeated with CapEx and OpEx uncertainty reduced to 0% for the 6 case studies defined earlier.

Also, in order to assess the sensitivity of the relation between yield uncertainty and LCOE and IRR uncertainty with respect to variations in cost, the 6 cases above are repeated with CapEx and OpEx varied by $\pm 25\%$.

6.3 Results

Figures 6.1-6.3 show the LCOE and IRR distributions resulting from the analysis described in Section 6.2.

Note that this data is not directly comparable to the LCOE and IRR distribution in Figures 5.16b and 5.17b, respectively, despite all cost and financial parameters defining the project being the same in both cases. This is because the user specified yield uncertainty distribution used in Chapter 5 is replaced by the ISO-GUM and MCA derived yield uncertainty distributions (presented in Figures 4.10-4.11). The user defined yield uncertainty distribution is based upon a generically representative capacity factor and a pragmatic uncertainty assumption (Table 5.7). It was not chosen to accurately represent the reference tidal site and therefore has no direct relation to the turbine, site resource and uncertainty assumptions made to calculate the combined yield uncertainty distribution using ISO-GUM and MCA. It is noted that the lower LCOE and higher IRR in Figures 6.1-6.3 compared to Figures 5.16b and 5.17b is due to an approximately 5% higher capacity factor resulting from the turbine model and site resource assumed for the reference tidal project than the generic user specified assumption of 35% in Table 5.7.

The comparison pertinent to this analysis is between the LCOE and IRR distributions resulting from the ISO-GUM and MCA derived yield distributions, i.e. between the dotted lines or between the solid lines in Figures 6.1-6.3. Table 6.2 summarises the difference in P10 and P50 LCOE resulting from the use of ISO-GUM and MCA derived yield uncertainty distributions for each of the 6 cases being analysed. The P10 LCOE is compared instead of the P90 in order to be consistent with the analysis in Chapter 4, which also considers the conservative case (i.e. P90 yield). Similarly, Table 6.3 summarises the difference in IRR, but note that the P75 values are quoted because the P90 IRRs are non-real values when u_R is equal to 15%.

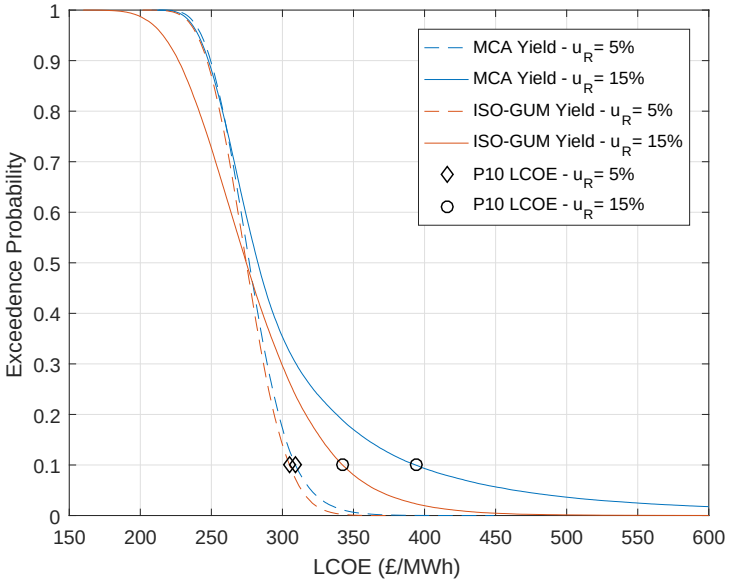

(a) Derived using yield distributions in Figure 4.10, i.e. $u_L = 0\%$

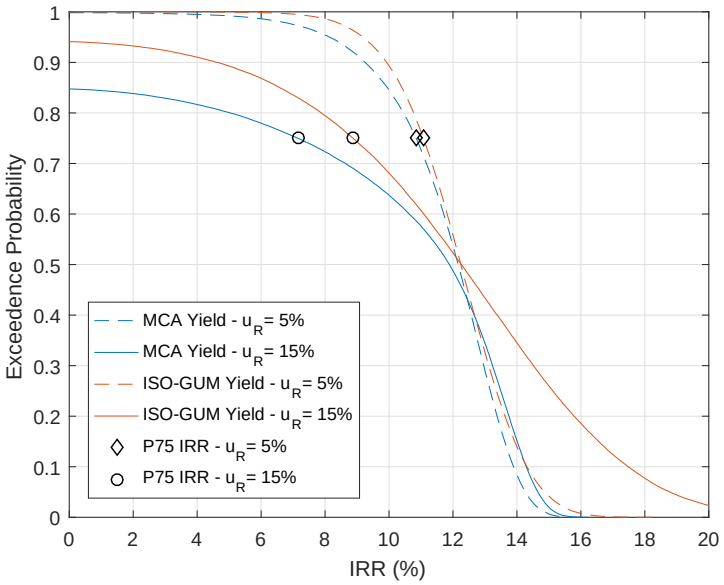

(b) Derived using yield distributions in Figure 4.10, i.e. $u_L = 0\%$

Figure 6.1: LCOE distributions calculated using assumptions in Table 6.1. This is related to the MCA empirical distribution in Figure 5.16b in that all cost and financial assumptions are constant, but the user specified yield distribution used for that illustration is replaced by the ISO-GUM and MCA derived yield distributions presented in Figure 4.10.

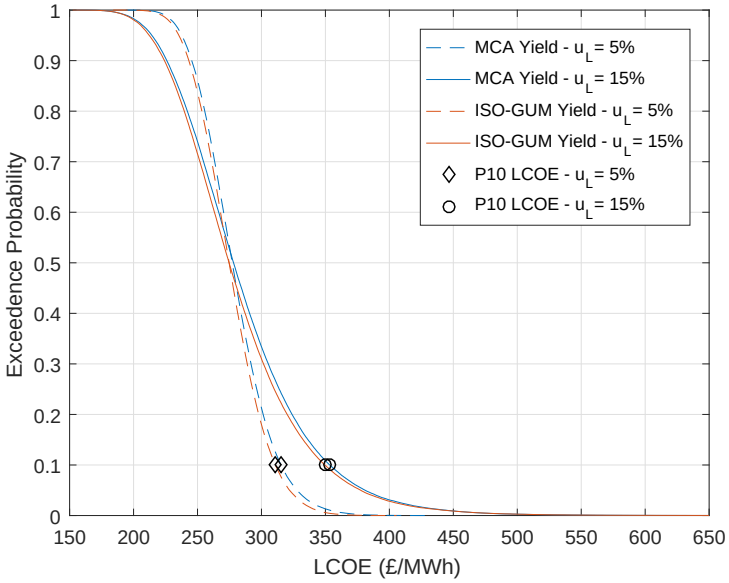

(a) Derived using yield distributions in Figure 4.11a, i.e. $u_R = 5\%$

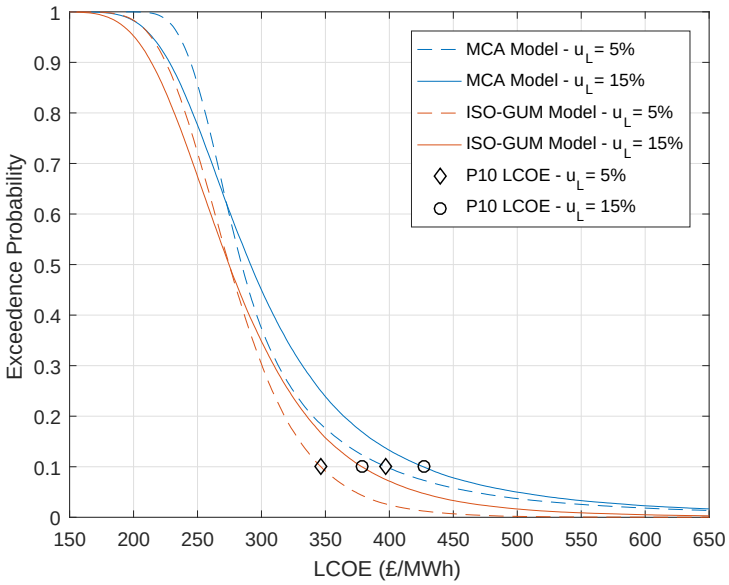

(b) Derived using yield distributions in Figure 4.11b, i.e. $u_R = 15\%$

Figure 6.2: LCOE distributions calculated using assumptions in Table 6.1. This is related to the MCA empirical distribution in Figure 5.16b in that all cost and financial assumptions are constant, but the user specified yield distribution used for that illustration is replaced by the ISO-GUM and MCA derived yield distributions presented in Figure 4.11.

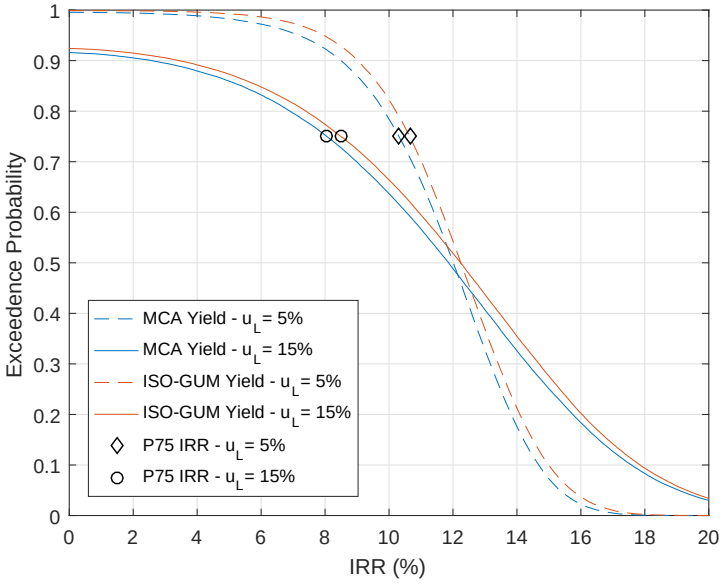

(a) Derived using the yield distributions in Figure 4.11a, i.e. $u_R = 5\%$

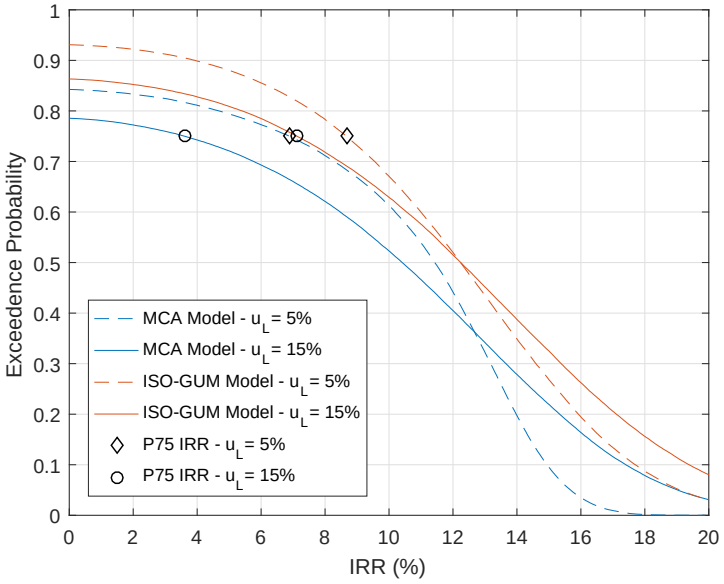

(b) Derived using the yield distributions in Figure 4.11b, i.e. $u_R = 15\%$

Figure 6.3: IRR distributions calculated using assumptions in Table 6.1. This is related to the MCA empirical distribution in Figure 5.17b in that all cost and financial assumptions are constant, but the user specified yield distribution used for that illustration is replaced by the ISO-GUM and MCA derived yield distributions presented in Figure 4.11.

Table 6.2: Difference in P10 and P50 LCOE distributions resulting from the difference in ISO-GUM and MCA derived yield uncertainty distributions. For reference, the equivalent yield differences are summarised in Table 4.6. Note that a positive value indicates that the MCA value is larger than the ISO-GUM value.

	P10 LCOE Difference		**P50 LCOE Difference**	
	u_R=5%	u_R=15%	u_R=5%	u_R=15%
u_L=0%	1.45%	13.06%	0.77%	2.88%
u_L=5%	1.36%	12.79%	0.88%	3.42%
u_L=15%	1.07%	11.26%	1.26%	5.78%

Table 6.3: Difference in P75 and P50 IRR resulting from the difference in ISO-GUM and MCA derived yield uncertainty distributions. For reference, the equivalent yield differences are summarised in Table 4.6. Note that a positive value indicates that the ISO-GUM value is larger than the MCA value. Also, note that the percentage point difference is shown for IRR, i.e. the arithmetic difference in percentage IRR.

	P75 IRR Difference		**P50 IRR difference**	
	u_R=5%	u_R=15%	u_R=5%	u_R=15%
u_L=0%	0.23%	1.61%	0.08%	0.38%
u_L=5%	0.34%	1.78%	0.24%	0.80%
u_L=15%	0.44%	3.52%	0.38%	1.83%

Figures 6.4 and 6.5 show the variation in ISO-GUM overestimate of LCOE and IRR across the full range of u_R and u_L being considered. This shows the impact of the differences in yield shown in Figure 4.12a propagated through to the final LCOE and IRR distributions.

Figures 6.6-6.8 correspond to the same analysis as that presented in Figures 6.1-6.3, with the exception that the uncertainties in the project CapEx and OpEx are assumed to be zero in order to separate the effect of cost uncertainties from the yield uncertainties. Tables 6.4 and 6.5 summarise the differences in P10 and P50 LCOE and P75 and P50 IRR respectively resulting from the use of ISO-GUM and MCA derived yield uncertainty distributions for each of the 6 cases being analysed.

Figures 6.9-6.14 correspond to the same analysis as that presented in Figures 6.1-6.3, with the exception that the uncertainties in the project CapEx and OpEx are varied by $\pm 25\%$ in order to analyse the effect of varying cost magnitudes. Tables 6.6, 6.7 and 6.8 summarise the differences in P10 and P50 LCOE and P75 and P50 IRR respectively resulting from the use of ISO-GUM and MCA derived yield uncertainty distributions for each of the 6 cases being analysed for the low and high cost assumption. Note that the P75 IRR values are non-real for the high cost case and are therefore not tabled.

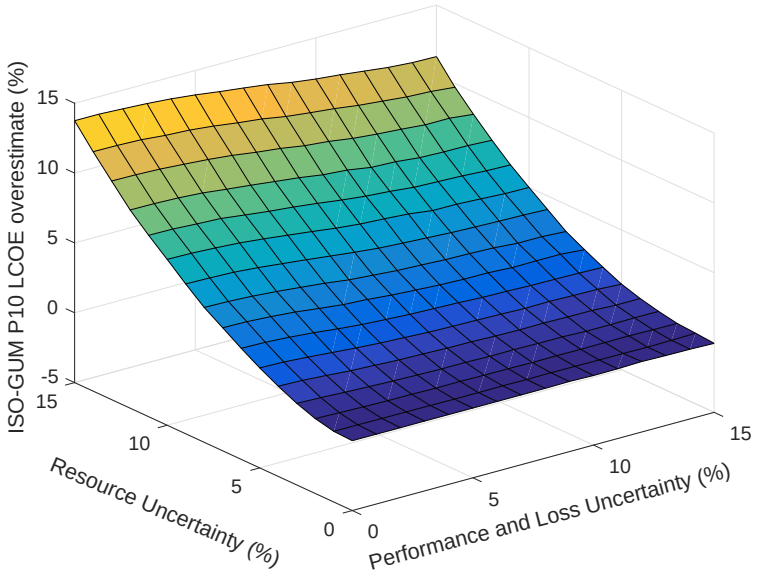

(a) P10 LCOE overestimate resulting from the use of ISO-GUM

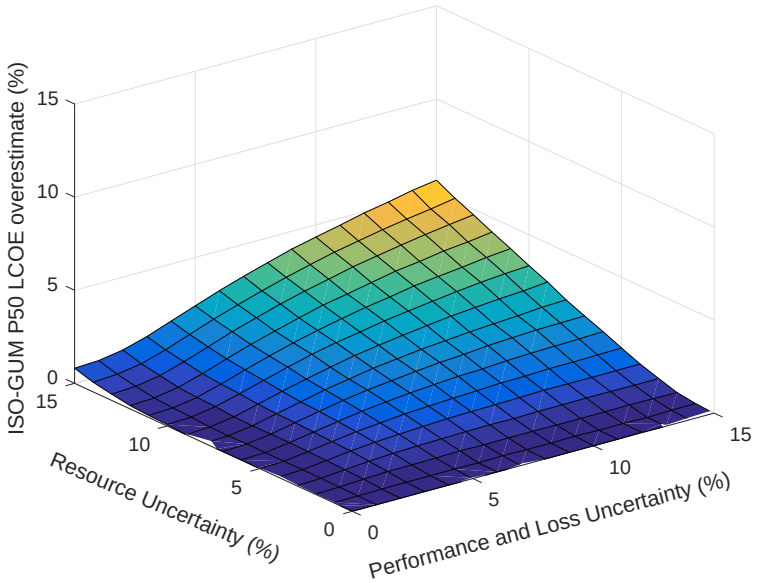

(b) P50 LCOE overestimate resulting from the use of ISO-GUM

Figure 6.4: Difference in P90 and P50 of LCOE distributions calculated using assumptions in Table 6.1 and the ISO-GUM and MCA derived yield distributions for a range of u_R and u_L.

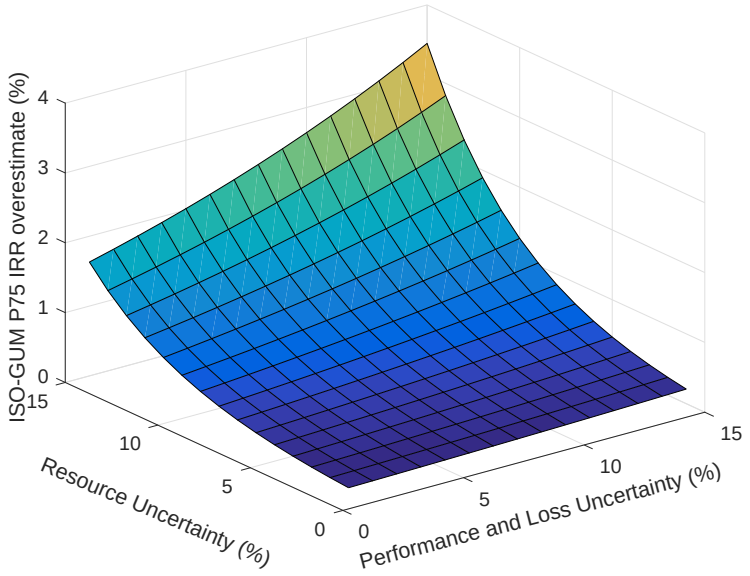

(a) P75 IRR overestimate resulting from the use of ISO-GUM

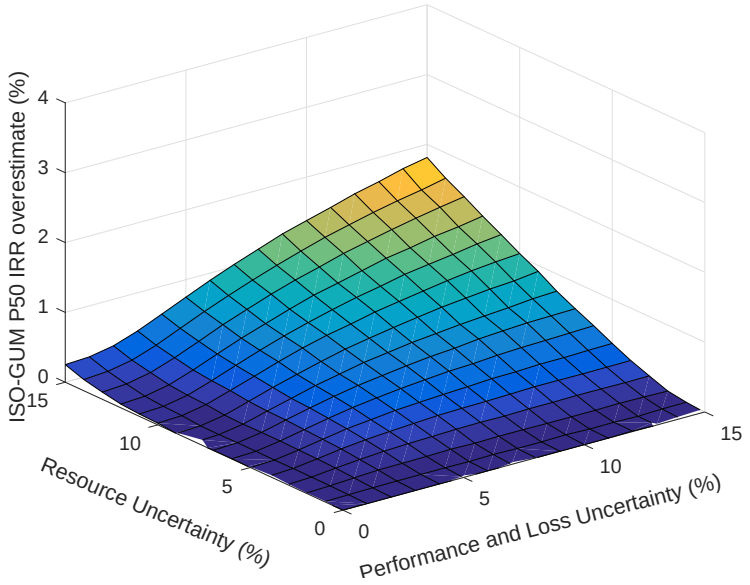

(b) P50 IRR overestimate resulting from the use of ISO-GUM

Figure 6.5: Difference in P75 and P50 of IRR distributions calculated using assumptions in Table 6.1 and the ISO-GUM and MCA derived yield distributions for a range of u_R and u_L. Note that the percentage point difference in IRR is shown, i.e. the arithmetic difference in percentage IRR.

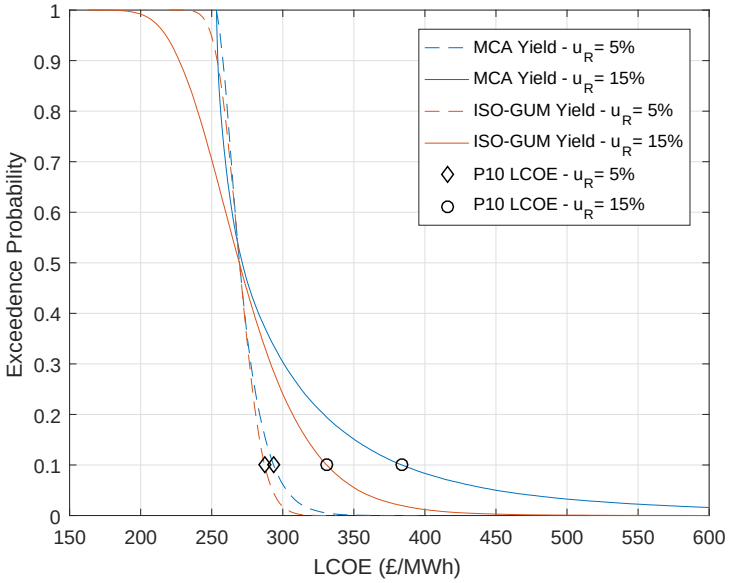

(a) Derived using yield distributions in Figure 4.10, i.e. $u_L = 0\%$

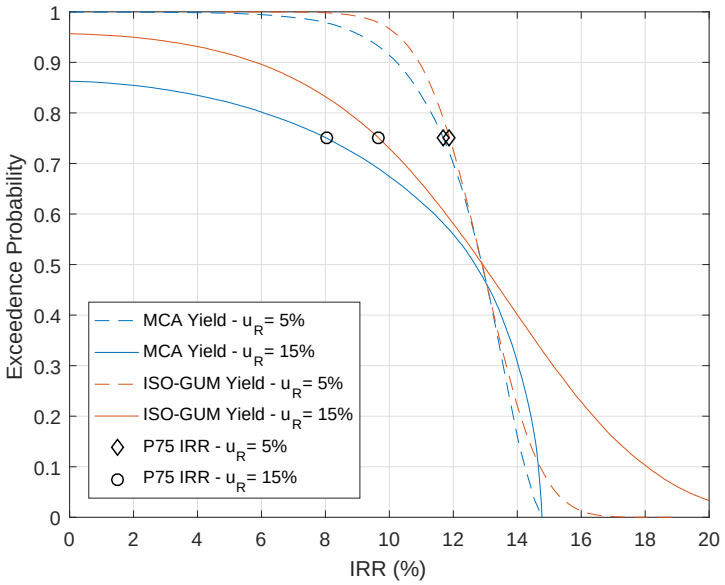

(b) Derived using yield distributions in Figure 4.10, $u_L = 0\%$

Figure 6.6: LCOE distributions calculated using assumptions in Table 6.1. This is related to the MCA empirical distribution in Figure 5.16b in that all cost and financial uncertainties are systematically reduced to zero, and the user specified yield distribution used for that illustration is replaced by the ISO-GUM and MCA derived yield distributions presented in Figure 4.10.

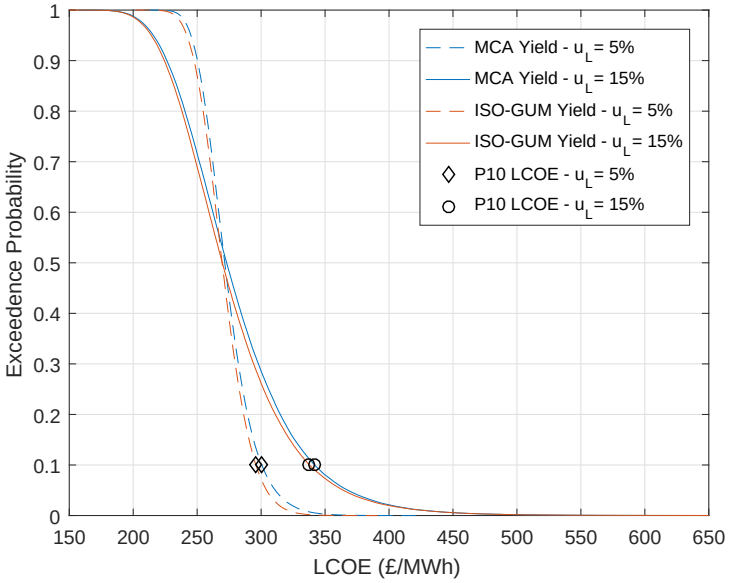

(a) Derived using yield distributions in Figure 4.11a, i.e. $u_R = 5\%$

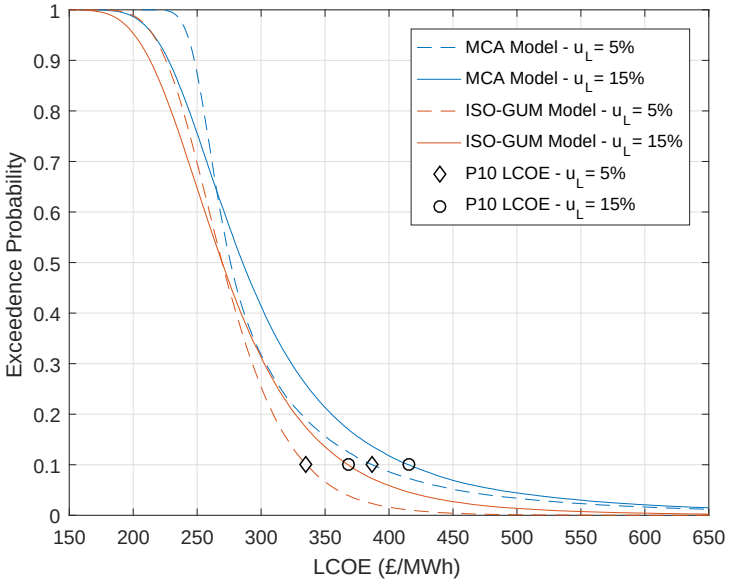

(b) Derived using yield distributions in Figure 4.11b, i.e. $u_R = 15\%$

Figure 6.7: LCOE distributions calculated using assumptions in Table 6.1. This is related to the MCA empirical distribution in Figure 5.16b in that all cost and financial assumptions are systematically reduced by zero, and the user specified yield distribution used for that illustration is replaced by the ISO-GUM and MCA derived yield distributions presented in Figure 4.11.

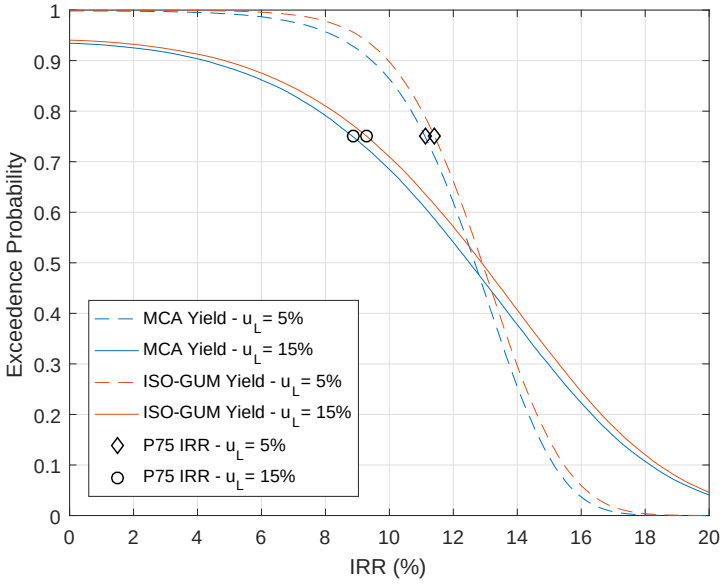

(a) Derived using the yield distributions in Figure 4.11a, i.e. $u_R = 5\%$

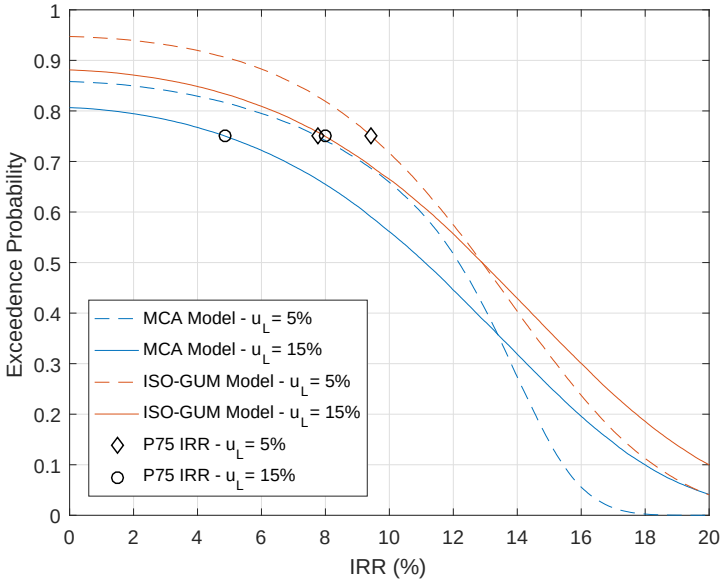

(b) Derived using the yield distributions in Figure 4.11b, i.e. $u_R = 15\%$

Figure 6.8: IRR distributions calculated using assumptions in Table 6.1. This is related to the MCA empirical distribution in Figure 5.17b in that all cost and financial assumptions are systematically reduced to zero, and the user specified yield distribution used for that illustration is replaced by the ISO-GUM and MCA derived yield distributions presented in Figure 4.11.

Table 6.4: Difference in P10 and P50 LCOE distributions resulting from the difference in ISO-GUM and MCA derived yield uncertainty distributions and no cost uncertainty assumptions. For reference, the equivalent yield differences are summarised in Table 4.6. Note that a positive value indicates that the MCA value is larger than the ISO-GUM value.

	P10 LCOE Difference		**P50 LCOE Difference**	
	u_R=5%	u_R=15%	u_R=5%	u_R=15%
u_L=0%	2.16%	13.78%	0.00%	0.77%
u_L=5%	1.55%	13.37%	0.76%	2.35%
u_L=15%	1.17%	11.38%	1.24%	5.62%

Table 6.5: Difference in P75 and P50 IRR resulting from the difference in ISO-GUM and MCA derived yield uncertainty distributions and no cost uncertainty assumptions. For reference, the equivalent yield differences are summarised in Table 4.6. Note that a positive value indicates that the ISO-GUM value is larger than the MCA value. Also, note that the percentage point difference is shown for IRR, i.e. the arithmetic difference in percentage IRR.

	P75 IRR Difference		**P50 IRR difference**	
	u_R=5%	u_R=15%	u_R=5%	u_R=15%
u_L=0%	0.20%	1.63%	0.00%	0.24%
u_L=5%	0.30%	1.69%	0.23%	0.73%
u_L=15%	0.45%	3.11%	0.38%	1.79%

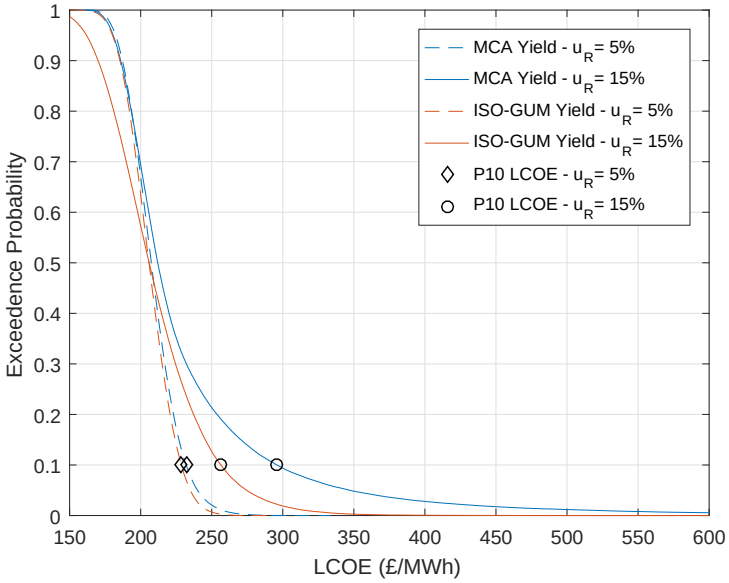

(a) Derived using yield distributions in Figure 4.10, i.e. $u_L = 0\%$

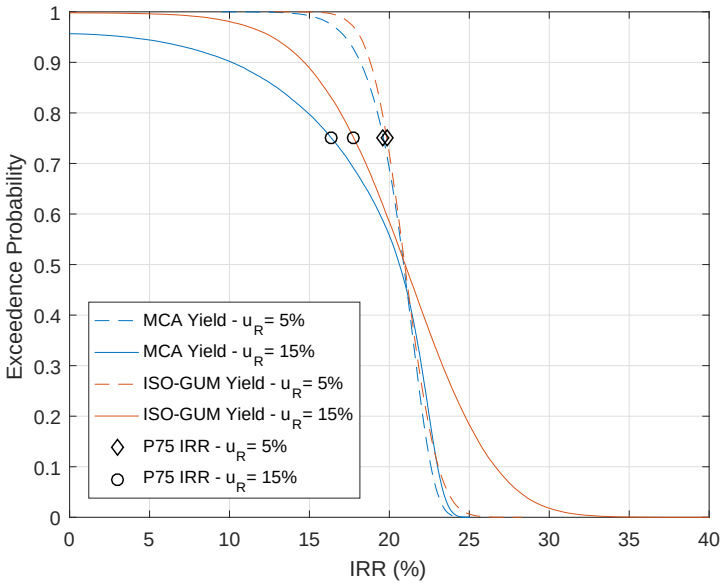

(b) Derived using yield distributions in Figure 4.10, $u_L = 0\%$

Figure 6.9: LCOE distributions calculated using assumptions in Table 6.1. This is related to the MCA empirical distribution in Figure 5.16b in that all cost and financial assumptions are systematically reduced by 25%, and the user specified yield distribution used for that illustration is replaced by the ISO-GUM and MCA derived yield distributions presented in Figure 4.10.

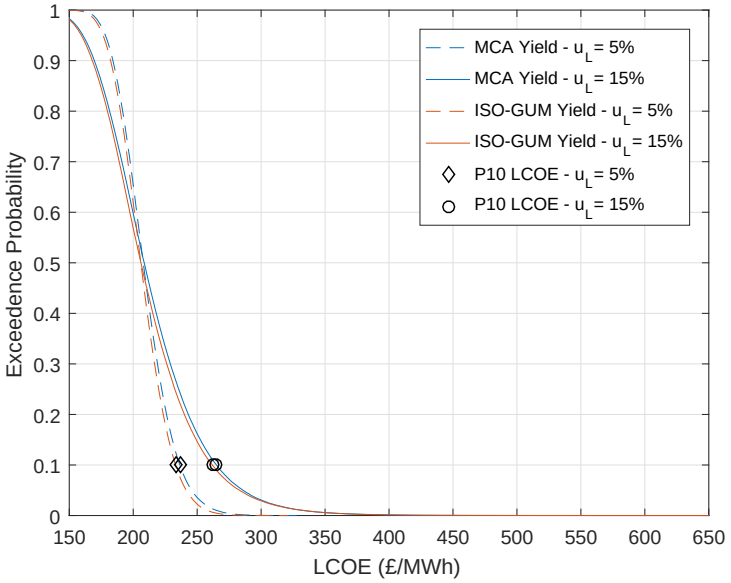

(a) Derived using yield distributions in Figure 4.11a, i.e. $u_R = 5\%$

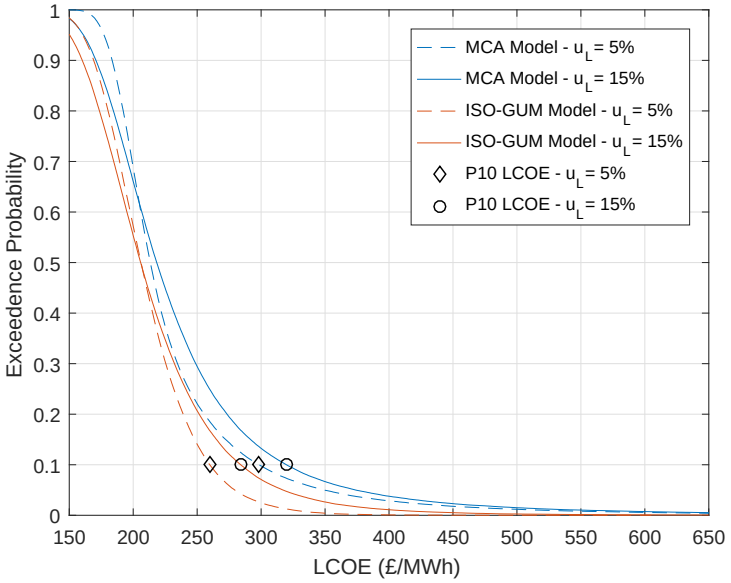

(b) Derived using yield distributions in Figure 4.11b, i.e. $u_R = 15\%$

Figure 6.10: LCOE distributions calculated using assumptions in Table 6.1. This is related to the MCA empirical distribution in Figure 5.16b in that all cost and financial assumptions are systematically reduced by 25%, and the user specified yield distribution used for that illustration is replaced by the ISO-GUM and MCA derived yield distributions presented in Figure 4.11.

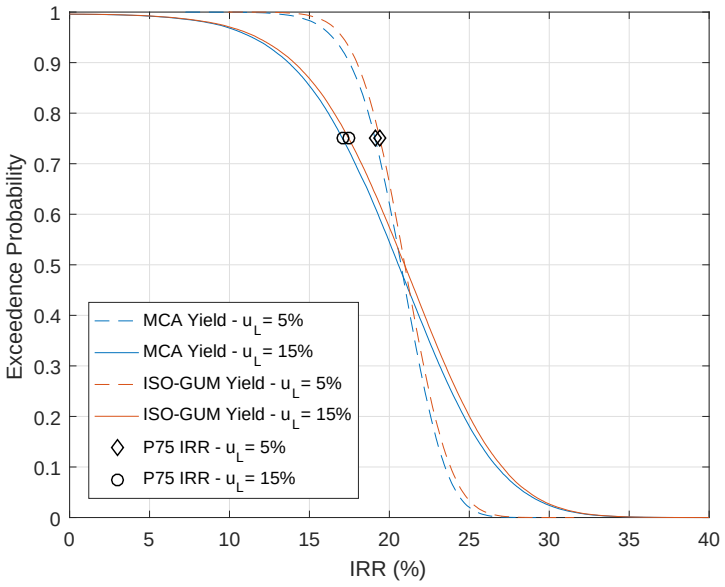

(a) Derived using the yield distributions in Figure 4.11a, i.e. $u_R = 5\%$

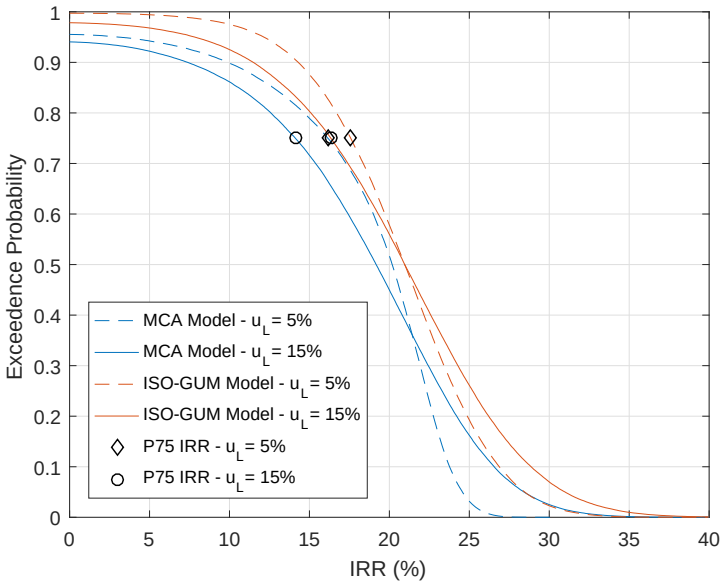

(b) Derived using the yield distributions in Figure 4.11b, i.e. $u_R = 15\%$

Figure 6.11: IRR distributions calculated using assumptions in Table 6.1. This is related to the MCA empirical distribution in Figure 5.17b in that all cost and financial assumptions are systematically reduced by 25%, and the user specified yield distribution used for that illustration is replaced by the ISO-GUM and MCA derived yield distributions presented in Figure 4.11.

Table 6.6: Difference in P10 and P50 LCOE distributions resulting from the difference in ISO-GUM and MCA derived yield uncertainty distributions and low cost assumptions. For reference, the equivalent yield differences are summarised in Table 4.6. Note that a positive value indicates that the MCA value is larger than the ISO-GUM value.

	P10 LCOE Difference		**P50 LCOE Difference**	
	u_R=5%	u_R=15%	u_R=5%	u_R=15%
u_L=0%	1.45%	13.3%	0.80%	2.84%
u_L=5%	1.39%	12.92%	0.92%	3.43%
u_L=15%	1.24%	11.16%	1.22%	5.75%

Table 6.7: Difference in P75 and P50 IRR resulting from the difference in ISO-GUM and MCA derived yield uncertainty distributions and low cost assumptions. For reference, the equivalent yield differences are summarised in Table 4.6. Note that a positive value indicates that the ISO-GUM value is larger than the MCA value. Also, note that the percentage point difference is shown for IRR, i.e. the arithmetic difference in percentage IRR.

	P75 IRR Difference		**P50 IRR difference**	
	u_R=5%	u_R=15%	u_R=5%	u_R=15%
u_L=0%	0.21%	1.40%	0.07%	0.36%
u_L=5%	0.29%	1.43%	0.23%	0.78%
u_L=15%	0.39%	2.29%	0.39%	1.78%

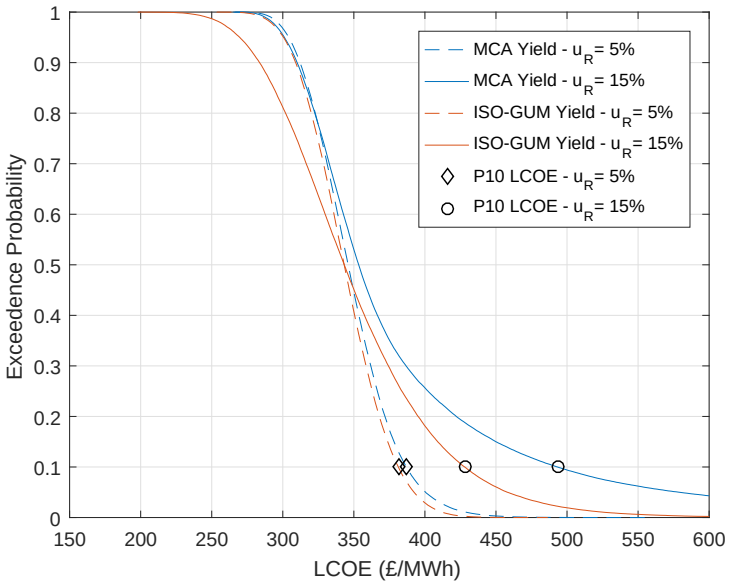

(a) Derived using yield distributions in Figure 4.10, i.e. $u_L = 0\%$

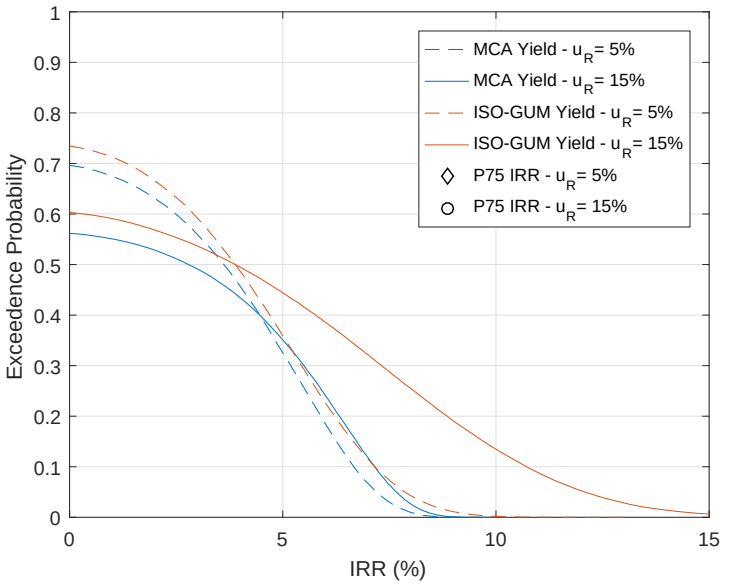

(b) Derived using yield distributions in Figure 4.10, $u_L = 0\%$

Figure 6.12: LCOE distributions calculated using assumptions in Table 6.1. This is related to the MCA empirical distribution in Figure 5.16b in that all cost and financial assumptions are systematically increased by 25%, and the user specified yield distribution used for that illustration is replaced by the ISO-GUM and MCA derived yield distributions presented in Figure 4.10.

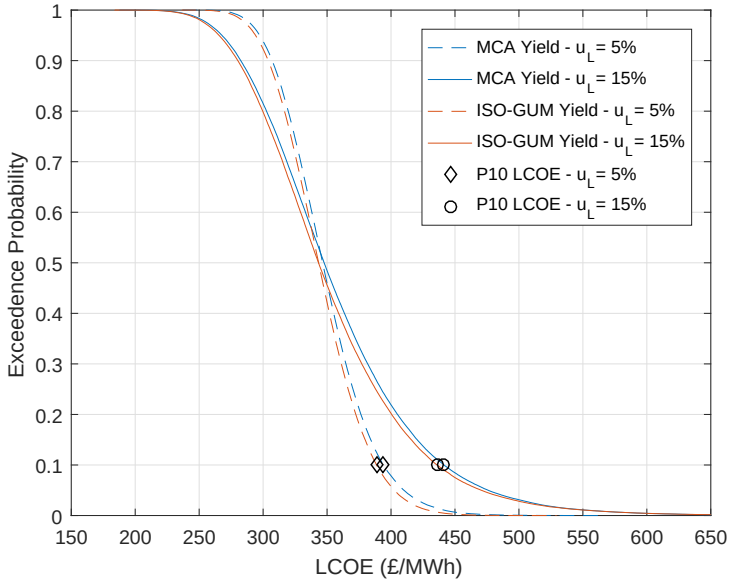

(a) Derived using yield distributions in Figure 4.11a, i.e. $u_R = 5\%$

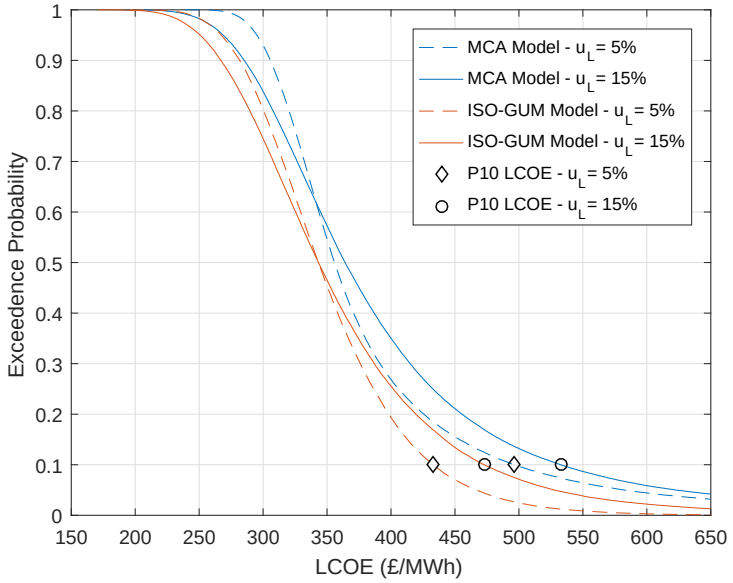

(b) Derived using yield distributions in Figure 4.11b, i.e. $u_R = 15\%$

Figure 6.13: LCOE distributions calculated using assumptions in Table 6.1. This is related to the MCA empirical distribution in Figure 5.16b in that all cost and financial assumptions are systematically increased by 25%, and the user specified yield distribution used for that illustration is replaced by the ISO-GUM and MCA derived yield distributions presented in Figure 4.11.

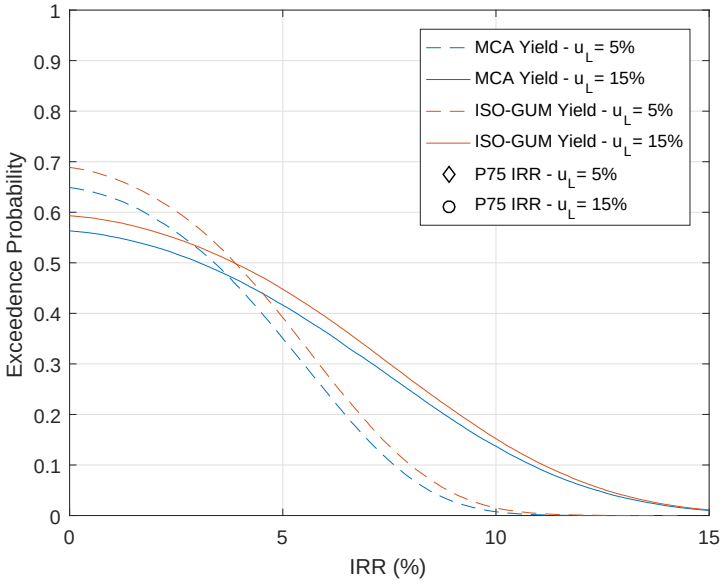

(a) Derived using the yield distributions in Figure 4.11a, i.e. $u_R = 5\%$

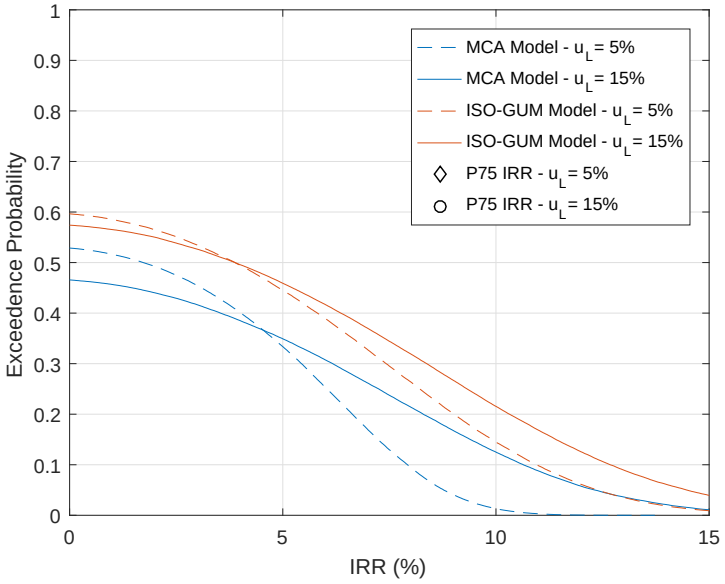

(b) Derived using the yield distributions in Figure 4.11b, i.e. $u_R = 15\%$

Figure 6.14: IRR distributions calculated using assumptions in Table 6.1. This is related to the MCA empirical distribution in Figure 5.17b in that all cost and financial assumptions are systematically increased by 25%, and the user specified yield distribution used for that illustration is replaced by the ISO-GUM and MCA derived yield distributions presented in Figure 4.11.

Table 6.8: Difference in P10 and P50 LCOE distributions resulting from the difference in ISO-GUM and MCA derived yield uncertainty distributions and high cost assumptions. For reference, the equivalent yield differences are summarised in Table 4.6. Note that a positive value indicates that the MCA value is larger than the ISO-GUM value.

	P10 LCOE Difference		**P50 LCOE Difference**	
	u_R=5%	u_R=15%	u_R=5%	u_R=15%
u_L=0%	1.45%	13.23%	0.80%	2.88%
u_L=5%	1.37%	12.77%	0.91%	3.52%
u_L=15%	1.23%	11.22%	1.25%	5.71%

6.4 Discussion

The analysis in the previous section provides the systematic response to ISO-GUM yield error. It not only converts the yield error into metrics that are more intuitive to decision makers (LCOE and IRR), but in doing so also highlights the relative importance of the yield error in the holistic chain of uncertainties. For example, a large yield error may be acceptable if the resultant impact on the IRR is acceptably small, or vice versa.

It was assumed in Section 4.4.3 that a 2% P90 yield error due to the use of ISO-GUM can be considered as a threshold beyond which the resulting error on the project's investment metrics would be too large to be acceptable. The P90 yield difference for the Case 1 combination of uncertainties is 1.85% (Table 4.6) and therefore just below this arbitrary threshold. This leads to a 0.24%, 0.34% and 0.53% difference in the P50, P75 and P90 IRRs, respectively. Note that these are percentage point differences (i.e. arithmetic difference in percentage IRRs).

Whilst these errors may seem small relative to the MCA P50 IRR of 12%, it should be noted that this is a low uncertainty case. The project would therefore be at an advanced stage of development and well understood, with a low tolerance for errors. It is also reiterated that all variables in the analysis are constant except for the yield uncertainty propagation method. Therefore, this error is entirely introduced through the use of ISO-GUM and can simply be avoided by using MCA. With this in mind, it is considered that the earlier assertion of 2% P90 yield error due to ISO-GUM being a reasonable threshold is acceptable.

The size of the error is considerably larger for the higher resource uncertainty cases (Case 3 and 4) due to the higher P90 yield errors. Whilst it is true that a project with 15% resource uncertainty may be at an early stage of development and therefore have a higher acceptance threshold for errors, the resultant LCOE and IRR errors are very large due to the non-linear divergence in the yield error with increasing resource uncertainty.

The differences in the P50 values are smaller but still notable. This suggests that the ISO-GUM method is not only inaccurate for assessing the lower likelihood conservative cases, but also the central (median) case. As with the P10/P90 comparisons, the difference is much smaller for the lower uncertainty cases, but these projects also have a correspondingly lower tolerance for avoidable errors.

Figures 6.4 and 6.5 show that the variation in impact of ISO-GUM error on the LCOE and IRR follows a similar profile to that of the ISO-GUM yield error (Figure 4.12a). This is to be expected as all inputs to the two comparisons are constant except the yield distributions. Furthermore, the relation between the two is roughly linear because no additional non-linearities are introduced in the cost model. As discussed in Chapter 4, there is a very high sensitivity to the magnitude of resource uncertainties and a small sensitivity to the performance and loss uncertainties. Also as previously discussed, the P50 yield error is comparatively

small and this is notable in the P50 LCOE and IRR error being significantly lower across the uncertainty range. There is a higher sensitivity of the P50 to increase in u_L than the P10. A large driver of the P10 error is the inaccurate ISO-GUM assumption of the combined uncertainty distribution being Gaussian, which affects the tail of the distribution more significantly than the median. The higher u_L results in a more Gaussian combined uncertainty distribution which results in the P10 discrepancy reducing. Since this affects the P50 much less significantly, the impact of increasing u_L is more visible on the P50. The maximum P75 IRR overestimate of c. 3.5% is quite extreme in relation to the median IRR of c. 12%. The error in P90 IRR would be even greater but in this instance no real IRR is possible for the P90 cashflow and is therefore not considered.

Figures 6.6-6.8 can be compared to Figures 6.1-6.3 because they demonstrate the same underlying analysis but one considers the combined cost and yield uncertainties whereas the other includes only the yield uncertainties. A decrease in the P10 LCOE and P90 IRR in absolute terms is observed when the cost uncertainties are assumed to be zero due to the resultant lower overall project uncertainty. There is no significant variation in the ISO-GUM LCOE or IRR error when compared to the earlier case where cost uncertainties are includes. However, a comparison of Table 6.4 with Table 6.2 shows that the P10 LCOE overestimate is higher when cost uncertainties are assumed to be zero whereas the P50 LCOE overestimate is lower. This is due to the combined uncertainty distribution being more Gaussian when additional uncertainties originating from the cost parameters are included due to the effects of the Central Limit Theorem. This favours the RSS P90, which is inaccurate due to false assumption of Gaussian combined uncertainty distribution, but the P50 is mostly unaffected. Since the assumption of no cost uncertainties is extreme and even in this case the impact of ISO-GUM accuracy is small in comparison to overall error magnitude, it can be deemed that

the cost uncertainties are a secondary consideration in the accuracy of ISO-GUM for uncertainty in financial metrics compared to the yield uncertainties.

Figures 6.9-6.14 can be compared to Figures 6.1-6.3 because they demonstrate the same underlying analysis but Figures 6.9-6.11 represent a low cost scenario whereas Figures 6.12-6.14 represent a high cost scenario, with a fixed yield uncertainty assumption. Again, a low sensitivity of the relative differences to the variation in cost magnitudes (with cost uncertainties constant) is observed despite quite large differences in LCOE and IRR due to the considerably improved/worsened cost assumptions. This re-enforces the view that the cost uncertainties are distinct from the yield uncertainties in relation to the magnitude of impact on financial metrics when ISO-GUM or MCA are used for yield uncertainty analysis. Therefore, the focus of the consideration of choice between ISO-GUM and MCA for yield uncertainty analysis must be based mostly of the factors discussed in Chapter 4 as the additional impact of cost uncertainties is low in relative terms.

The 2% P90 yield error determined in Chapter 4 is therefore still considered valid when consideration of its impact on LCOE and IRR under various assumptions related to the cost magnitudes and cost uncertainties.

The error in the ISO-GUM yield distributions leads to an overly optimistic view of a project's LCOE and IRR in all cases. This can lead to misinformed investment decisions being made. The inaccuracy is particularly noteworthy because it stems from the choice of uncertainty analysis method, and can be avoided relatively easily by using MCA.

6.5 Summary

The impact of the error in yield uncertainty distribution introduced through the use of ISO-GUM was propagated to uncertainty in a project's investment metrics. This isolates the effect of yield uncertainty analysis errors on LCOE and IRR errors, and allows informed decisions to be made on the acceptability of ISO-GUM for a given project. From consideration of 4 cases representing various combinations of project uncertainty levels, it was deemed that the assumption in Section 4.4.3 of a 2% P90 yield error as a threshold beyond which MCA should be used is acceptable. As shown in Chapter 4, it is difficult to quantify the ISO-GUM inaccuracy but the 2% threshold is likely to be exceeded in almost all realistic cases. This leads to investment decisions being made on overly optimistic expectations. The recommendation of the use of MCA for tidal energy yield uncertainty analysis is therefore maintained after consideration of the resultant impact on a project's investment metrics.

Chapter 7

General Discussion and Conclusions

7.1 General Discussion

7.1.1 Yield Uncertainty Analysis

The ISO-GUM method has been recommended for propagating tidal energy yield uncertainties in recent industry guidance documents, but no comprehensive evidence of its validity can be found in the literature. Based on an analysis of a typical tidal energy project, the fundamental ISO-GUM assumption of linear variation in annual yield with change in resource was shown to be not always valid. There is considerable non-linearity in the resource-yield function due to the rated and cut-out regions of the power curve not resulting in higher yields for higher velocities. A similar comparison for a typical wind project, where ISO-GUM is routinely used, showed a linear relation over the same range of resource variation. The higher concentration of the tidal resource close to the non-linear regions of a

typical tidal turbine power curve introduces significant non-linearity. It is evident why the ISO-GUM approach is widely adopted in the wind sector and it appears that, prior to this work, not enough consideration has been give to testing its validity for tidal energy applications.

The limited validity of the ISO-GUM linearity assumption results in an over-estimate in the P90 yield compared to the MCA derived value, which does correctly account for the non-linearity. The ISO-GUM P90 yield error was shown to increase with increasing resource uncertainty. Furthermore, the ISO-GUM P10 yield is highly inaccurate as the dramatic reduction in yield due to turbine cut-out is not accounted for. The P50 yield error was smaller in comparison, but this also increases with increase in resource uncertainty. MCA can accurately estimate any percentile of interest because it solves the resource-yield function explicitly.

The non-linearity of the resource-yield function varies between projects depending on the distribution of the resource and power curve. A sensitivity analysis on all parameters affecting the resource-yield function was carried out using values encompassing an extensive range of realistic projects. Considerable variation was observed in the result. Depending on the shape of the resource-yield function, it was shown that a maximum resource uncertainty between 4% and 11% gives a 2% P90 yield error, which was considered to be a threshold beyond which ISO-GUM is unsuitable. The logic underpinning the variation in resource-yield function shape is complex due to the large number of variables affecting it. It is not possible to deduce accurately *a priori* where in the 4-11% range a particular project fits based on an inspection of its defining characteristics. Qualitative observations can be made, however. For example, a turbine with a high rated velocity relative to the site resource is likely to be closer to a P90 yield error of 11% than 4%. However, considerable experience is required to make such pragmatic statements accurately and consistency between different analyses cannot be assured. MCA can be used accurately irrespective of the non-linearity of the resource-yield function and does

not require subjective judgement to determine its validity and accuracy on a case-by-case basis.

For a given resource-yield function, the ISO-GUM P90 yield error depends upon the magnitude of the resource uncertainty and the loss uncertainty, and also upon the arbitrary choice of resource perturbation range used to linearise the function. The ISO-GUM P90 yield error for all combinations of resource and loss uncertainties from 0% to 15% were visualised for a typical tidal project using a linearisation range of ±2%. Resource uncertainty greater than 5% was shown to give a minimum P90 yield error of 2% irrespective of the loss uncertainty. Considerable sensitivity to the choice of linearisation range was also observed. This is because the function is quite non-linear close to the central nominal yield point so small changes in the range results in a significantly different gradient being calculated. The optimal choice of linearisation range varies from project to project because it depends on the shape of the resource-yield function and applicable resource uncertainties. It is therefore not simple to determine the most accurate linearisation range, and an arbitrary selection is required in practice. An improvement on the arbitrary selection was suggested. This involves tailoring the linearisation range to the output percentile of interest because it closely captures the most probable range of resource variation being considered. Nonetheless, the residual error would still remain unquantified. MCA can be used accurately irrespective of the magnitudes of the resource and loss uncertainties. Also, it does not require the use any arbitrary or case specific linearisation assumptions.

Most realistic projects, and all early stage projects with high resource uncertainties, will result in an ISO-GUM P90 yield overestimate of greater than 2% leading to an overly optimistic view of a project's performance. Given the difficulty in deducing the non-linearity, confidence in ISO-GUM results is undermined even for projects where the method may be accurate because the error cannot be quantified. The simplest method for accurately quantifying the ISO-GUM error is to

compare it to MCA results. However, if MCA results are derived then ISO-GUM results are redundant anyway because MCA provides consistently accurate results that can be interpreted at any percentile of interest. MCA is therefore recommended for propagating uncertainties for all tidal energy projects.

The use of MCA also allows non-symmetrical input uncertainty distributions to be applied. However, it was shown through testing a range of cases that the impact on results is small, unless a small number of uncertainties are dominantly skewed.

7.1.2 Financial Uncertainty Analysis

Based on a literature review, it was concluded that there is a lack of standardisation in cost modelling methodology and assumptions for tidal energy projects. Furthermore, there is a lack of comprehensive quantification of uncertainty in LCOE and IRR estimates.

A generic, device agnostic discounted cash flow (DCF) analysis tool with flexible inputs and probabilistic uncertainty analysis using MCA was developed. The tool was applied to a realistic case study to demonstrate its functions and to compare results to simpler deterministic results.

A simple but rarely acknowledged observation is that the LCOE distribution is skewed and the mode is therefore different to the median. The most likely deterministic CapEx, OpEx and yield provides the most likely LCOE and IRR, but it is not equal to the P50 values. In the case study analysed, the modal LCOE is equal to the P62 and therefore there is a 38% chance of the LCOE being higher than the mode. This is a significant observation, and one that will affect most

projects because LCOE distributions will tend to be skewed due to the division of cost distributions by the yield distribution.

MCA provides a distribution which can be interpreted unambiguously because the visualisation allows non-technical decision makers to easily understand the likelihoods. Furthermore, any confidence interval of interest can be quantified.

A probability weighted deterministic method was outlined and applied to the case study project to simulate a pessimistic and optimistic case similar to the MCA P5 and P95. This was done by using the P5 and P95 input values and weighting them for their probability of occurrence. The resultant LCOE and IRR are not P5 and P95 values but reasonably close approximations. This approach allows a simple quantification of the pessimistic and optimistic case, but the exact percentiles cannot be quantified so it is not a statistically robust solution.

The difference between using deterministic and probabilistic sensitivity analysis on case study input parameters was shown. The more suitable of the two methods depends on the objective of the analysis. The probabilistic sensitivity analysis considers the project specific risks and is likely to be of interest to investors. The deterministic analysis assumes uniform uncertainties and therefore indicates key systematic risks. This information is more useful at a strategic level and therefore of interest to policy makers. It is not clear from literature that this difference is widely acknowledged and the use of a simple deterministic sensitivity analysis is common.

The sensitivity of the LCOE and IRR to some common variations in modelling assumptions was also tested. It is common to ignore parameters that are difficult to quantify, such as reduction in turbine performance over time leading to yield degradation and OpEx escalation. However, the LCOE and IRR were shown to be considerably sensitive to these parameters. As such, it was recommended that

such variables should be included in analyses, albeit with an appropriately high uncertainty. This is more physically representative than assuming no degradation. A low sensitivity to the decommissioning costs was shown. However, it is important to model the mechanism for funding decommissioning costs nonetheless because the timing of payments is important to assess whether a project can sustain its debt obligations throughout its life.

The use of MCA for financial modelling uncertainty analysis allows the impact of the ISO-GUM error in P90 yield to be quantified in terms of error on the LCOE and IRR by propagating the ISO-GUM and MCA derived annual yield uncertainty distributions. This was carried out for 4 combinations of resource and loss uncertainties. The lowest uncertainty case, which corresponds to a 2% P90 yield error, results in a 0.53 percentage point difference in P90 IRR. This is a significant difference in relation to the P50 IRR of 12%, and particularly with consideration that it stems entirely from the inaccuracy of ISO-GUM because all other parameters are constant. The difference is greater for the higher uncertainty cases. It is re-iterated that the ISO-GUM error provides an overly optimistic view. From an investment perspective, the error may be more tolerable if it were in the conservative direction. Given that this error can be eliminated simply by using MCA for the yield uncertainty analysis, it is considered an easy gain and the earlier assertion of a 2% P90 yield error being a threshold for ISO-GUM validity is considered reasonable.

7.2 Concluding Statements

7.2.1 Conclusions

The overarching general conclusion from this research is that MCA is an improved uncertainty analysis method compared to the approaches typically used in the industry for the applications considered. It avoids making unquantified assumptions by propagating distributions through the functional relationship. It leads to unambiguous and consistently accurate results, provided that a sufficiently large number of simulations is used.

MCA requires more computational resource and user expertise than the simpler methods considered. However, the MCA simulation run time is in the order of minutes on a standard laptop PC for all analyses presented here. This compares to a run time of a few seconds for the simpler methods. The higher computer time required is justified for all but the most basic of analyses given the considerable benefits provided by MCA. The small investment in software and/or user training required to use MCA can also be similarly justified.

The specific conclusions in relation to the objectives specified in Section 1.7.1 are presented below.

Yield Uncertainty Analysis

ISO-GUM was identified as the recommended method for tidal energy yield uncertainty analysis. Its limiting assumptions were appraised and no detailed analysis of its validity for tidal energy applications was found. MCA was identified as an alternative method which is not restricted by the same limiting assumptions. A MCA framework for tidal energy yield uncertainty propagation was developed

and the resulting combined annual yield uncertainty distributions were compared to ISO-GUM outputs for a wide range of realistic projects. ISO-GUM was found to overestimate the P90 yield by at least 2%, but often much greater than that, for most realistic cases. This was due to the ISO-GUM assumption of a linear resource-yield function and a Gaussian combined yield uncertainty distribution being inaccurate. MCA was therefore recommended for tidal energy yield uncertainty analysis, and a modification of the standard ISO-GUM method was also offered as a simpler solution with a reduced but still unquantified error.

Overall, the aim of improving confidence in yield uncertainty analysis was achieved by demonstrating MCA as a consistently accurate method compared to the currently recommended ISO-GUM method.

Financial Performance Uncertainty Analysis

A lack of comprehensive uncertainty analysis was noted in a review of existing marine energy cost models, with deterministic or simple stochastic methods being used most commonly. A highly flexible generic cost modelling tool was developed with detailed DCF analysis and comprehensive stochastic uncertainty analysis using MCA. The LCOE and IRR uncertainties were derived for a realistic case study project using MCA and deterministic methods. Significant differences between the results were observed in the quantitative value of the results, and also the practical value. This is because MCA provides quantified intervals which correctly account for skews in the distributions. MCA was therefore recommended for tidal energy financial performance uncertainty analysis, and a probability weighted deterministic method was also suggested as a simpler solution with improved results.

Overall, the aim of improving confidence in financial uncertainty analysis was

achieved by two means; demonstration of MCA as a consistent and unambiguous method with scope for interesting analytics (such as probabilistic sensitivity analysis), and by highlighting simple, but not widely appreciated nuances of uncertainty analysis (such as modal LCOE not being equal to median LCOE).

7.2.2 Contribution to Knowledge

The contributions to knowledge resulting directly from this thesis are:

- Currently recommended method (ISO-GUM) for yield uncertainty analysis was shown to significantly overestimate P90 yield for almost all realistic tidal energy projects, which leads to investment decisions being based on overly optimistic yield performance expectations;
- A range within which ISO-GUM may be valid was quantified;
- An alternative method (MCA) was shown to be more accurate;
- An adaptation to the recommended ISO-GUM methodology was suggested and tested for increased ISO-GUM accuracy if the use of MCA is not possible;
- Empirical algorithm developed to derive a distribution's minimum and maximum values based on user specified P5/P95 and P10/P90 values. This has been shared on the Mathworks File Exchange Community page (Shah, 2017);
- Improved awareness of limitations and possible false interpretations of deterministic cost uncertainty analyses. Added benefits of stochastic approach, such as the ability to conduct probabilistic sensitivity analyses, were also highlighted;

- The significance of commonly used cost modelling assumptions, such as assuming no turbine degradation over time, was quantified;
- The impact of error in P90 yield was quantified in terms of error in P90 LCOE and IRR.

7.2.3 Industrial Impact

In addition to the impact to the wider industry through the contributions to knowledge, several commercial benefits have been provided to the sponsoring company, Black and Veatch, as a result of this research project.

The DCF analysis tool with probabilistic uncertainty analysis developed through this research significantly enhances the company's capabilities in cost modelling for renewable energy projects. It avoids the cost of purchasing external software. More importantly, the use of in-house tools removes the 'black box' associated with proprietary software and gives more control to the company over its use. Also, no other marine energy cost modelling software, to the author's knowledge, offers the flexible MCA uncertainty analysis capability. This provides the company with a competitive advantage when bidding for work. The benefits of stochastic uncertainty analysis are appreciated by the company and a previous project required a time consuming manually iterative workaround in Microsoft Excel in the absence of such a tool. The tool provides a versatile and repeatable process that will also result in time savings in the future. Finally, the tool may be commercialised directly as a standalone software for sale, in addition to providing services through its internal use.

In addition to the direct usage of the tool, the knowledge gained through this research has also been used to commercial benefit. The experience gained through the tool development was used to produce a similar stochastic tool for

construction budget contingency analysis for a commercial client. The knowledge gained through the detailed comparisons of ISO-GUM and MCA was used in the company's capability statement in bids for work in different applications to yield uncertainty analysis.

7.2.4 Limitations and Further Work

It is assumed throughout the thesis that the uncertainty on each relevant parameter is accurately known. Quantification of the uncertainty is a process fraught with difficulties and is a source of uncertainty in itself. However, the intended end use of the tools and methodologies developed in this project is for consultancy projects where it is routine to apply expert judgement and pragmatic adjustments in the absence of appropriate data to quantify uncertainties. It is therefore considered appropriate to exclude the uncertainty quantification from the scope.

It is also implicitly assumed that the functional relationships between the input and output variables of the uncertainty analysis are physically accurate representations. Whilst not strictly a limitation of the methodologies analysed, it is highlighted that an inaccuracy in the functional model will yield poor results irrespective of the quality of the uncertainty analysis method used. This is true for results of any model and is considered separate to the present aim of improving uncertainty analysis.

MCA is able to propagate fully or partially correlated input uncertainties. The impact of such a consideration in relation to the assumption of independent and uncorrelated uncertainties would be interesting, although it is unlikely to be used in industry at this early stage of development because large datasets would be required to quantify correlations. For comparison, the independent

and uncorrelated assumption is also commonly used in the more developed wind energy sector (Derrick, 2009).

It is likely that the ISO-GUM linearity assumption is also inaccurate for wave energy projects. The industry guidance recommends ISO-GUM equally for wave and tidal energy projects. A similar comparison to that in Chapter 4, but for wave energy projects is considered to be of interest for the wave energy sector.

The MCA framework permits further development to propagate bin-wise uncertainty in a power curve through to the annual yield uncertainty as an alternate to user specified uncertainty in capacity factor. However, such a capability is also considered unlikely to be commercially useful in the near future because data on bin-wise uncertainty in a power curve is not generally available.

It is intended that the DCF tool used for financial uncertainty analysis will be continuously developed. The following additional functions are considered to be most desirable for the next version of the tool and are noted for further work:

- Allow empirical distributions to be associated with input variables where the data is available to support this;
- Account for inter annual variation in resource based on tidal phasing. This can have a significant impact on the IRR compared to an analysis that makes the physically incorrect assumption that there is no time dependency on prevalent site resource (Stock-Williams et al., 2013);
- Allow quarterly accounting of the cashflow. This allows CapEx expenditure to be split across the construction period and also for revenue in construction to be modelled;
- Allow tracking of a project over time in order to record the reduction in uncertainties as the project progresses through the development cycle.

References

ABPmer, The Met Office and Proudman Oceanographic Laboratory (2008), *Atlas of UK Marine Renewable Energy Resources: Technical Report*, Department for Business, Enterprise & Regulatory Reform, London.

Albatern (2017), 'Wave energy - Albatern'. [Accessed December 31st, 2017]. **URL:** *http://albatern.co.uk/wave-energy/*

Alcorn, R. (2016), 'Exceedence Finance Manual'. [Available on request from software provider].

Ash, R. B. (2008), *Basic Probability Theory*, Dover Publications, Mineola, New York.

Atlantis Resources (2017), 'MeyGen Phase 1A Approaches 400MWh of Generation'. [Accessed June 2nd, 2017]. **URL:** *https://www.atlantisresourcesltd.com/2017/03/23/meygen-phase-1a-approaches-400mwh-generation/*

Azizuddin, A. (2013), *Siebel Forecasting Guide*, Pothi Publishing, Bengaluru.

Azpurua, M. A., Tremola, C. and Paez Barrios, E. (2011), 'Comparison of the Gum and Monte Carlo Methods for the Uncertainty Estimation in Electromagnetic Compatibility Testing', *Progress In Electromagnetics Research B* **34**, 125–144. doi: 10.2528/PIERB11081804.

Baruah, P., Eyre, N., Qadrdan, M., Chaudry, M., Blainey, S., Hall, J. W., Jenkins, N. and Tran, M. (2014), 'Energy system impacts from heat and transport electrification', *Proceedings of the ICE - Energy* **167**, 139–151. doi: 10.1680/ener.14.00008.

Bastidas-arteaga, E. and Soubra (2015), 'Reliability Analysis Methods', *ALERT Doctoral School 2014 - Stochastic Analysis and Inverse Modelling* pp. 53–77.

BEIS (2016*a*), 'Digest of United Kingdom Energy Statistics 2016'. London: Department for Business Energy & Industrial Strategy. Retrieved from: https://www.gov.uk/government/statistics/digest-of-united-kingdom-energy-statistics-dukes-2016-main-chapters-and-annexes.

BEIS (2016*b*), *Energy and Climate Change Public Attitude Tracker*, Department for Business, Energy & Industrial Strategy, London.

Bertrand-Krajewski, J., Ribeiro, A., Almeida, M., Sun, S. and van den Broeke, J. (2011), 'Evaluation of uncertainties in measurements', *PREPARED Enabling Change* p. 45.

Bloomberg (2014), 'Marine Power May Suffer More Casualties After Siemens Tidal Sale'. [Accessed June 2nd, 2017]. **URL:** *https://www.bloomberg.com/news/articles/2014-12-05/marine-power-may-suffer-more-casualties-after-siemens-tidal-sale*

Bloomberg New Energy Finance (2017*a*), *2017 Update on Wave and Ocean Thermal - Bobbing along*, BNEF, London.

Bloomberg New Energy Finance (2017*b*), *H1 2017 Global LCOE Update*, BNEF, London.

Boon, J. D. (2004), *Secrets of the Tide: Tide and Tidal Current Analysis and Applications, Storm Surges and Sea Level Trends*, 1st edn, Woodhead Publishing.

Borthwick, A. G. L. (2016), 'Marine Renewable Energy Seascape', *Engineering* **2**(1), 69–78. doi: 10.1016/J.ENG.2016.01.011.

Buchsbaum, P. (2012), 'Modified Pert Simulation'. [Accessed June 2nd, 2017]. **URL:** *http://www.greatsolutions.com.br/images/BetaEng.pdf*

Carbon Trust (2006*a*), *Cost Estimation Methodology - The Marine Energy Challenge approach to estimating the cost of energy produced by marine energy systems*, London.

Carbon Trust (2006*b*), *Future Marine Energy - Results of the Marine Energy Challenge: Cost competitiveness and growth of wave and tidal stream energy*, London: Author.

Carbon Trust (2011*a*), *Accelerating Marine Energy - The potential for cost reduction - insights from the Carbon Trust Marine Energy Accelerator*, London.

Carbon Trust (2011*b*), *UK Tidal Current Resource and Economics Study*, London.

Clayton, R. (2016), Tidal Energy Yield Uncertainties: Learning from the Wind Industry, *in* '6th International Conference on Ocean Energy', Edinburgh.

Climate Change Capital (2010), *Offshore Renewable Energy Installation Decommissioning Study*, London.

CNBC (2017), 'OPEC reaches agreement to cut oil production to 32.5 million barrels a day: Oil ministers'. [Accessed December 31st, 2017]. **URL:** *http://cnb.cx/2EnIpeS*

Codiga, D. L. (2011), 'Unified Tidal Analysis and Prediction Using the UTide Matlab Functions', p. 59. doi: 10.13140/RG.2.1.3761.2008.

Committee on Climate Change (2016), *UK climate change action following the Paris Agreement*, London.

Cooper, R. and John, A. (2011), *Macroeconomics, Theory through Applications*, Flatworld.

Couto, P. R. G., Damasceno, J. C. and Oliveira, S. P. (2013), 'Monte Carlo Simulations Applied to Uncertainty in Measurement', *Theory and Applications of Monte Carlo Simulations* pp. 27–51. doi: 10.5772/53014.

Cowan, G. (1998), *Statistical Data Analysis*, Vol. 1. doi: 10.1017/CBO9781107415324.004.

CRAN-R (2018), 'Deterministic Sensitivity Analysis'. [Accessed February 11nd, 2018]. **URL:** *https://cran.r-project.org/web/packages/heemod/vignettes/fsensitivity.html*

Damodaran, A. (2008), What is the riskfree rate? A Search for the Basic Building Block, Technical report, Stern School of Business, New York University.

Davey, T., Harrison, G. P. and Stallard, T. (2009), *Procedures for Economic Evaluation*, EquiMar - Deliverable D7.2.1. Online report: http://www.equimar.org/equimar-project-deliverables.html.

De Andrés, A. D., Guanche, R., Armesto, J. A., Del Jesus, F., Vidal, C. and Losada, I. J. (2013), 'Time domain model for a two-body heave converter: Model and applications', *Ocean Engineering* **72**, 116–123. doi: 10.1016/j.oceaneng.2013.06.019.

de Andrés, A. D., Guanche, R., D-Simal, P., Vidal, C. and J.Losada, I. (2015), Uncertainties on the techno-economic feasibility assessment of wave energy projects, *in* '11th European Wave and Tidal Energy Conference', Nantes, pp. 1–10.

DECC (2011), *UK Renewable Energy Roadmap*, Department of Energy and Climate Change, London.

DECC (2012), *Updated Energy & Emissions Projections - Annex J - Total Capacity*, Department of Energy and Climate Change, London.

DECC (2013), *Consultation on the draft Electricity Market Reform Delivery Plan Annex B : Strike price methodology*, Department of Energy and Climate Change, London.

Deloitte (2014), *Establishing the investment case Wind power*, London.

Derrick, A. (2009), Uncertainty - The Classical Approach, *in* 'American Wind Energy Association Windpower Conference', Chicago.

DNV KEMA (2013), *Framework for the Categorisation of Losses and Uncertainty for Wind Energy Assessments*, Arnhem.

Dobos, a., Gilman, P. and Kasberg, M. (2012), P50/P90 Analysis for Solar Energy Systems Using the System Advisor Model, *in* '2012 World Renewable Energy Forum', Denver.

DTOcean (2016), 'DTOcean User Manual'. [Accessed June 2nd, 2017]. **URL:** *https://setis.ec.europa.eu/dt-ocean/download/file/fid/21*

Du, X. (2005), 'First Order and Second Reliability Methods', *University of Missouri - Rolla* . Online report: http://web.mst.edu/ dux/repository/me360/ch7.pdf.

Economist (2010), 'And now, the electricity forecast'. [Accessed June 2nd, 2017]. **URL:** *http://www.economist.com/node/16295634*

Ellison, S. L. R. and Williams, A. (2012), *Quantifying Uncertainty in Analytical Measurement*, Eurachem/CITAC, Olomouc.

EMEC (2014), *EMEC Data Guidelines (Guide 033-01-01 20141009)*, Stromness.

Energy UK (2016), *Pathways for the GB Electricity Sector to 2030*, London.

European Commission (2015), *The Paris Protocol A blueprint for tackling global climate change beyond 2020*, Brussels.

European Environment Agency (2016), *World final electricity consumption by region in the Baseline Scenario*, Copenhagen.

Eurostat (2017), 'Energy Dependence'. [Accessed December 31st, 2017]. **URL:** *http://bit.ly/2lxyMBL*

Fernandez, J., Peter, J., Helstrup, N. E. and Fernández-chozas, J. (2014), 'User guide COE Calculation Tool for Wave Energy Converters'.

Fight, A. (2005), *Introduction to Project Finance*, Vol. 3446, Elsevier/Butterworth-Heinemann, Amsterdam. doi: 10.1016/B978-075065905-5.50001-5.

Financial Times (2017), 'UK pipeline shutdown sends energy prices soaring'. [Accessed December 31st, 2017]. **URL:** *http://on.ft.com/2C4atSZ*

Garrad Hassan (2001), *Scotland's Renewable Resource 2001: Volume I - The analysis*, Bristol.

Geer, T. (2015), An Advanced Understanding of the Impact of Deviations in Turbine Performance, *in* 'European Wind Energy Conference', Paris, pp. 1–19.

Goldstein, M. (2016), Uncertainty Quantification for Complex Physical Systems, *in* 'Uncertainty Analysis in Energy Systems Seminar', Edinburgh.

Gov.uk (2016), 'Work out your capital allowances - GOV.UK'. [Accessed June 2nd, 2017]. **URL:** *https://www.gov.uk/work-out-capital-allowances/writing-down-allowances*

Groobey, C., Pierce, J., Faber, M. and Broome, G. (2010), 'Project Finance Primer for Renewable Energy and Clean Tech Projects', *Wilson Sonsini Goodrich & Rosati* .

Ha, Y.-C., Her, J.-Y., Lee, S.-J. and Lee, K.-J. (2014), 'Comparison of ISO-GUM and Monte Carlo Method for Evaluation of Measurement Uncertainty', *Transactions of the Korean Society of Mechanical Engineers. B* **38**, 647–656.

Haahr, M. and Cherry, D. (1999), *Introduction to Randomness and Random Numbers*, random.org.

Hansen, N. R. (2005), Probability Theory and Statistics, Technical Report November, University of Copenhagen.

Harvard University (2007), *A Summary of Error Propagation*, Cambridge.

Hicks, S. (2006), *Understanding tides*, National Oceanic and Atmospheric Administration, Maryland.

HIE (2016), *Marine Energy : Key Steps to Maintain a Great British Success Story*, Inverness.

HM Treasury (2013), *Guidance Note : the Use of Internal Rates of Return in PFI Projects*, London.

Holický, M. (2013), *Introduction to Probability and Statistics for Engineers*, Springer. doi: 10.1007/978-3-642-38300-7.

IEC (2005), *Wind Turbines. Part 12-1, Power Performance Measurements of Electricity Producing Wind Turbines*, Geneva.

IEC (2013), *Technical Specification IEC/TS 62600-200 - Marine energy - Wave, tidal and other water current converters - Part 200: Electricity producing tidal energy converters - Power performance assessment*, Geneva.

IEC (2015), *Technical Specification IEC/TS 62600-201 Marine energy - Wave, tidal and other water current converters - Part 201: Tidal energy resource assessment and characterisation*, Geneva.

IHO (2008), *Standards for Hydrographic Surveys*, 5th edn, International Hydrographic Organisation, Monaco.

IHO (2013), *Principles of Tides and Water Levels*, International Hydrodynamic Organisation, Monaco.

IRENA (2014), *Tidal Energy Technology Brief*, International Renewable Energy Agency, Abu Dhabi.

Iyer, A. S. (2011), New Methodologies and Scenarios for Evaluating Tidal Current Energy Potential, PhD thesis. **URL:** *http://www.era.lib.ed.ac.uk/handle/1842/6182*

JCGM (2008*a*), *Evaluation of measurement data - Guide to the expression of uncertainty in measurement*, Joint Committee for Guides in Metrology, Sevres.

JCGM (2008*b*), *Evaluation of measurement data Supplement 1 to the Guide to the expression of uncertainty in measurement Propagation of distributions using a Monte Carlo method*, Joint Committee for Guides in Metrology, Sevres.

Johnstone, C. M., Pratt, D., Clarke, J. A. and Grant, A. D. (2013), 'A techno-economic analysis of tidal energy technology', *Renewable Energy* **49**, 101–106. doi: 10.1016/j.renene.2012.01.054.

KPMG (2017), 'CFD Allocation Round Two - Results that will blow you away'. Online report: https://home.kpmg.com/uk/en/home/insights/2017/09/cfd-allocation-round-2-results-that-will-blow-you-away.html.

Krewitt, W., Nienhaus, K., Klebmann, C., Capone, C., Stricker, E., Graus, W. and Supersberger, N. (2009), 'Role and Potential of Renewable Energy and Energy Efficiency for Global Energy Supply'.

Kutney, T., Karsten, R. and Polagye, B. (2013), Priorities for Reducing Tidal Energy Resource Uncertainty, *in* '10th European Wave and Tidal Energy Conference', Aalborg, pp. 1–11.

LabFit (2017), 'LabFit Help Files'. [Accessed June 2nd, 2017]. **URL:** *http://zeus.df.ufcg.edu.br/labfit/help.htm*

Lackner, M., a.L. Rogers and Manwell, J. (2007), 'Uncertainty analysis in wind resource assessment and wind energy production estimation', *45th AIAA Aerospace Sciences Meeting and Exhibit* pp. 1–16. doi: doi:10.2514/6.2007-1222.

Leete, S., Xu, J. and Wheeler, D. (2013), 'Investment barriers and incentives for marine renewable energy in the UK: An analysis of investor preferences', *Energy Policy* **60**, 866–875. doi: 10.1016/j.enpol.2013.05.011.

Li, Y., Lence, B. J. and Calisal, S. M. (2011), 'An integrated model for estimating energy cost of a tidal current turbine farm', *Energy Conversion and Management* **52**, 1677–1687. doi: 10.1016/j.enconman.2010.10.031.

Loucks, D. P., van Beek, E., Stedinger, J. R., Dijkman, J. P. and Villars, M. T. (2005), 9 Model Sensitivity and Uncertainty Analysis, *in* 'Water Resources Systems Planning and Management: An Introduction to Methods, Models and Applications', 1st edn, Unesco, pp. 254–290. doi: ISBN: 92-3-103998-9.

Magnusson, S. E. (1997), *Uncertainty analysis : Identification , Quantification and Propagation*, Lund Institute of Technology, Lund.

Maravas, A. and Pantouvakis, J.-p. (2013), 'Guidelines for Modelling Time and Cost Uncertainty in Project and Programme Management', *Physics Procedia* **74**, 203–211. doi: 10.1016/j.sbspro.2013.03.045.

Mcauliffe, F. D., Macadré, L.-m., Donovan, M. H., Murphy, J. and Lynch, K. (2015), Economic and Reliability Assessment of a Combined Marine Renewable Energy Platform, *in* '11th European Wave and Tidal Energy Conference', Nantes.

McKinsey & Co (2017), 'Internal Rate of Return: A cautionary Tale'. [Accessed

June 2nd, 2017]. **URL:** *http://www.mckinsey.com/business-functions/strategy-and-corporate-finance/our-insights/internal-rate-of-return-a-cautionary-tale*

MEASNET (2009), *Evaluation of Site Specific Wind Conditions, Version 1*, Madrid.

MeyGen (2014), '£51 million MeyGen Financial Close Completed'. [Accessed June 2nd, 2017]. **URL:** *http://www.meygen.com/2014/09/51-million-meygen-financial-close-completed/*

MeyGen (2017), 'Lessons Learnt from MeyGen Phase 1a Part 1/3 : Design Phase'. Online report: http://www.waveandtidalknowledgenetwork.com/ItemDetails.aspx?id=34192.

MIT (2006), *Kolmogorov-Smirnov Test*, Statistics for Applications, Massachusetts Institute of Technology. Cambridge.

Mortensen, N. G. and Jørgensen, H. E. (2013), Comparative Resource and Energy Yield Assessment Procedures (CREYAP) Pt . II, *in* 'EWEA Technology Workshop Resource Assessment', Dublin.

Myers, L. E., Retzler, C., Pizer, D. and Gardner, F. (2010), *Device Classification Template*, EquiMar - Deliverable D5.2. Online report: http://www.equimar.org/equimar-project-deliverables.html.

NASA (2015), *Appendix G : Cost Risk and Uncertainty Methodologies*, NASA Cost Estimating Handbook, Washington D.C.

Natural Power (2015), *Energy Yield Assessments and Validation Studies*, Glasgow.

Neary, V. S., Previsic, M., Jepsen, R. a., Lawson, M. J., Yu, Y.-H., Copping, A. E., Fontaine, A. a. and Hallett, K. C. (2014), 'Methodology for Design and Economic Analysis of Marine Energy Conversion (MEC) Technologies', *Sandia National Laboratories* .

NOAA (2018), 'Tides and Currents - Harmonic Constituents'. [Accessed February 18nd, 2018]. **URL:** *https://tidesandcurrents.noaa.gov/harcon.html?id=9410170*

Ó'Catháin, M. (2012), Towards increased confidence in wave and tidal energy production estimates, *in* '4th International Conference on Ocean Energy', Dublin.

Ó'Catháin, M., Carnus, T. and Stock-Williams, C. (2013), Wave & Tidal Energy Production Estimates : Converting Resource Uncertainties into Energy Uncertainties, *in* '10th European Wave and Tidal Energy Conference', Vol. 4, Aalborg.

Ocean Energy Europe (2017), *Ocean Energy Project Spotlight - Investing in Tidal and Wave Energy*, Brussels.

OES (2016), *Annual Report 2015*, Ocean Energy Systems, Paris.

OES (2017), *Annual Report 2016*, Ocean Energy Systems, Paris.

Open University (1989), *Waves, tides, and shallow-water processes*, Pergamon Press, in association with the Open University, Milton Keynes, England.

OREC (2015*a*), *Framework for the Categorisation of Losses and Uncertainty for Wind Energy Assessments*, Offshore Renewable Energy Catapult, Blyth.

OREC (2015*b*), *Wave and Tidal Energy Yield Uncertainty - Reference Document*, Offshore Renewable Energy Catapult, Blyth.

OREC (2015*c*), *Wave and Tidal Energy Yield Uncertainty - Spreadsheet Tool*, Offshore Renewable Energy Catapult, Blyth.

OREC (2015*d*), *Wave and Tidal Energy Yield Uncertainty Literature Review*, Offshore Renewable Energy Catapult, Blyth.

Palisade Corporation (2010), *Guide to Using @Risk: Risk Analysis and Simulation Add-In for Microsoft Excel*, Ithaca.

Palisade Corporation (2017*a*), 'Palisade Corporation'. [Accessed June 2nd, 2017]. **URL:** *https://www.palisade.com/risk/*

Palisade Corporation (2017*b*), 'Risk Analysis: What Is It and When to Use Deterministic & Stochastic Risk Analyses?'. [Accessed June 2nd, 2017]. **URL:** *http://www.palisade.com/risk/risk_analysis.asp*

Parliament of the United Kingdom (2008), 'Climate Change Act 2008', *HM Government, London* .

Pawlowicz, R., Beardsley, B. and Lentz, S. (2002), 'Classical tidal harmonic analysis including error estimates in MATLAB using TDE', *Computers and Geosciences* **28**(8), 929–937. doi: 10.1016/S0098-3004(02)00013-4.

Peirson, Brown, Easton, Howard and Pinder (2011), Chapter 7 Risk and Return, *in* 'Business Finance', 11th edn, McGraw-Hill, pp. 168–206.

Poyry (2014), *Levelised costs of power from tidal lagoons*, Poyry, Sweden.

Pugh, D. T. (1987), *Tides, Surges and mean sea-level*, Vol. 5, John Wiley & Sons. doi: 10.1016/0264-8172(88)90013-X.

Raychaudhuri, S. (2008), 'Introduction to Monte Carlo simulation', *2008 Winter Simulation Conference* pp. 91–100. doi: 10.1109/WSC.2008.4736059.

RD Instruments (2011), *Acoustic Doppler Current Profilers Principles of Operation: A Practical Primer*, California.

RenewableUK (2013), *Wave and Tidal Energy in the UK: Conquering Challenges , Generating Growth*, London.

RenewableUK (2017), *Export Nation - A year in wind, wave and tidal exports*, London.

ReNews (2016), 'UK sets £290m CfD budget'. [Accessed June 2nd, 2017]. **URL:** *http://renews.biz/104850/uk-sets-290m-cfd-budget/*

Ricci, P., Lopez, J., Villate, J. and Stallard, T. (2009), *Summary of attributes of cost models used by different stakeholders*, EquiMar - Deliverable D7.1. Online report: http://www.equimar.org/equimar-project-deliverables.html.

Roberts, D. G. (2014), Project Finance for Ocean Energy : Issues to Consider, *in* '5th International Conference on Ocean Energy', Halifax.

Rosenblatt, M. (1952), 'Remarks on a Multivariate Transformation', *Annals of Mathematic Statistics* **23**, 470–472.

Seguro, J. V. and Lambert, T. W. (2000), 'Modern estimation of the parameters of the Weibull wind speed distribution for wind energy analysis', *Journal of Wind Engineering and Industrial Aerodynamics* **85**(1), 75–84. doi: 10.1016/S0167-6105(99)00122-1.

Shah, S. (2017), 'Percentile transform for Monte Carlo sampling (calculate min and max from p5/p95 or p10/p90)'. [Accessed June 2nd, 2017]. **URL:** *http://bit.ly/2pPu4iC*

Shermon, D. (2016), Cost Risk Analysis (CRA) and Schedule Risk Analysis (SRA) explained, *in* 'Palisade EMEA Risk Conference', Edinburgh.

SI Ocean (2013), *Ocean Energy: Cost of Energy and Cost Reduction Opportunities*, Brussels.

Smith, A., Smith, C. and Stewart, M. (2017), 'Financing Tidal Power in a post MeyGen Era'. Online Webinar by Tidal Energy Today on 5th September 2017.

Smith, R. (2014), *Uncertainty Quantification, Theory, Implementation, and Applications*, Society for Industrial and Applied Mathematics.

Staffell, I. and Green, R. (2014), 'How does wind farm performance decline with age?', *Renewable Energy* **66**, 775–786. doi: 10.1016/j.renene.2013.10.041.

Stiven, T., Couch, S. J. and Iyer, A. S. (2011), Assessing the impact of ADCP resolution and sampling rate on tidal current energy project economics, *in* 'OCEANS 2011 IEEE', Santander, pp. 1–10. doi: 10.1109/Oceans-Spain.2011.6003659.

Stock-Williams, C., Parkinson, S. and Gunn, K. (2013), An Investigation of Uncertainty in Yield Prediction for Tidal Current Farms, *in* '10th European Wave and Tidal Energy Conference', Aalborg.

Sudman, S. (1976), *Applied sampling*, Academic Press, New York.

Sullivan, T. (2015), *Introduction to Uncertainty Quantification*, Vol. 63, Springer Series in Applied Mathematics. doi: 10.1007/978-3-319-23395-6.

Teillant, B., Costello, R., Weber, J. and Ringwood, J. (2012), 'Productivity and economic assessment of wave energy projects through operational simulations', *Renewable Energy* **48**, 220–230. doi: 10.1016/j.renene.2012.05.001.

The Crown Estate (2012), *UK Wave and Tidal Key Resource Areas Project - Summary Report*, London.

The World Bank (2012), *Green Infrastructure Finance*, Washington, D.C.

Theodorou, D., Meligotsidou, L., Karavoltsos, S., Burnetas, A., Dassenakis, M. and Scoullos, M. (2011), 'Comparison of ISO-GUM and Monte Carlo methods for the evaluation of measurement uncertainty: Application to direct cadmium measurement in water by GFAAS', *Talanta* **83**(5), 1568–1574. doi: 10.1016/j.talanta.2010.11.059.

Thomopoulos, N. T. (2013), *Essentials of Monte Carlo Simulation: Statistical Methods for Building Suimulation Models*, Springer, New York. doi: 10.1007/978-1-4614-6022-0.

Tucker, J. (2013), *QFinance: The Ultimate Resource*, 4th edn, Bloomsbury.

Uihlein, A. and Magagna, D. (2016), 'Wave and tidal current energy - A review of the current state of research beyond technology', *Renewable and Sustainable Energy Reviews* **58**, 1070–1081. doi: 10.1016/j.rser.2015.12.284.

UK Trade & Investment (2015), UK Offshore Wind: Opportunities for trade and investment, Technical report, London.

University of Bristol (2015), 'Tidal Theory'. Online report: www.bris.ac.uk/depts/union/.../PROJECT/TIDAL

University of Texas (2017), 'Analytical Point Estimates'. [Accessed June 2nd, 2017]. **URL:** *http://bit.ly/2s551xr*

Uusitalo, L., Lehikoinen, A., Helle, I. and Myrberg, K. (2015), 'An overview of methods to evaluate uncertainty of deterministic models in decision support', *Environmental Modelling and Software* **63**, 24–31. doi: 10.1016/j.envsoft.2014.09.017.

Vestas (2015), 'Vestas 2MW Platform Datasheet'. [Accessed June 2nd, 2017]. **URL:** *http://bit.ly/1Q8dtMT*

Visser, E. and Held, A. (2014), *Methodologies for estimating Levelised Cost of Electricity (LCOE) Implementing the best practice LCoE methodology of the guidance*, Ecofys, Utrecht.

Walker, A. (2011), *The Future of Marine Renewables in the UK*, Royal Academy of Engineering, London.

Wicklin, R. (2013), *Simulating Data with SAS*, SAS Institute, North Carolina.

Wilkinson, M. (2014), Long-term Performance of Wind Farms, *in* 'EWEA Technical Workshop', Malmo.

World Energy Council (2016), *World Energy Resources: Marine Energy*, London.

Wyatt, S. (2014), Financing marine energy: The role of innovation in reducing risk, *in* '5th International Conference on Ocean Energy', Halifax.

Yang, J.-Z., xi Li, G., Wu, B.-z., Gong, J.-z. and Wang, J. (2014), 'Comparison of GUF and Monte Carlo methods to evaluate task-specific uncertainty in laser tracker measurement', *Journal of Central South University* **21**(10), 3793–3804. doi: 10.1007/s11771-014-2364-y.

Appendix A

Worked Example of Percentile Transformation Algorithm

The process described in Section 5.5.2 is demonstrated using an example below. Let the user defined inputs be:

$P5(P_{low}) = 25$, Mode $(P_{mode}) = 10$, $P95(P_{high}) = 5$, Distribution = Pert

Using Equation 5.7:

$P'_{low} = 0$, $P'_{mode} = 0.25$, $P'_{high} = 1$

Using Table 5.4:

$x' = -0.107849641$ and 1.67315242 for minimum and maximum, respectively.

Using Equation 5.8:

$x = 2.843007$ and 38.46305 for minimum and maximum, respectively.

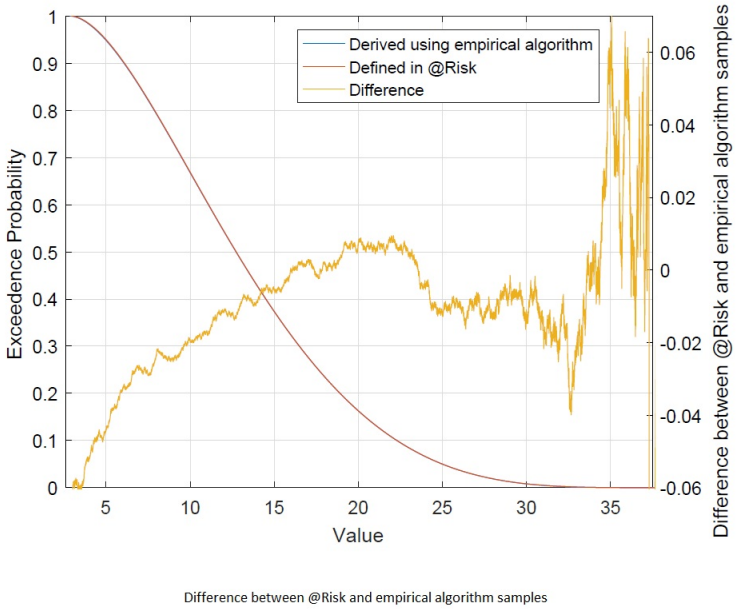

Figure A.1: Comparing histogram of 10000 random samples produced from the empirical and @Risk analytical values of minimum and maximum for a distribution defined by a P5, mode and P95 of 5, 10 and 25 respectively.

The difference in random samples drawn from distributions defined using the analytical and empirical values is very small (Figure A.1).

Appendix B

Publications

This chapter lists all publications resulting from this research project. URL links to papers, presentations and posters are provided, where possible.

B.1 Journal Paper (In Review)

- Shah, S., Buckland, H., Thies, P.R., Bruce, T. (Unpublished), 'Comparison of Yield Uncertainty Propagation Methods for Tidal Energy', *International Journal of Marine Energy.*

B.2 Conference Papers

- Shah, S., Buckland, H., Thies, P.R., Bruce, T. (2016), 'Combining Tidal Energy Yield Estimates', *in* '3rd Asian Wave and Tidal Energy Conference', Singapore [Available at http://bit.ly/2rrfSCr];

- Shah, S., Buckland, H., Cohen, C., Thies, P.R., Bruce, T. (2017), 'De-Risking Marine Energy Project Development Through Improved Financial Uncertainty Analysis' *in* '36th International Conference on Ocean, Offshore and Arctic Engineering', Trondheim [Available at http://bit.ly/2rhtP1q];

- Shah, S., Buckland, H., Cohen, C., Thies, P.R., Bruce, T. (2017), 'Comparison of Yield Uncertainty Propagation Methods for Tidal Energy' *in* '2nd IDCORE Symposium', Edinburgh [Available at http://bit.ly/2qMNndY - Presentation only];

- Shah, S., Buckland, H., Cohen, C., Thies, P.R., Bruce, T. (2017), 'Minimising Marine Energy Risk by Understanding Uncertainties' *in* 'All Energy Conference', Glasgow [Available at http://bit.ly/2ssdmID - Presentation only].

B.3 Conference Posters

- Shah, S., Couch, S., Thies, P.R., Bruce, T., Iyer, A. (2015), 'De-risking tidal energy project development through improved uncertainty analysis' *in* 'RenewableUK Wave and Tidal Energy Conference', Glasgow [Available at http://bit.ly/2srWG4l];

- Shah, S., Buckland, H., Thies, P.R., Bruce, T. (2016), 'Choosing failure rate behaviour models for reliability assessments' *in* '5th International Conference for Ocean Energy', Edinburgh [Available at http://bit.ly/2rSAFOP];

- Shah, S., Buckland, H., Thies, P.R., Bruce, T. (2016), 'Techno-economic risk modelling for marine energy projects using Monte Carlo analysis' *in* '1st IDCORE Symposium', Edinburgh [Available at http://bit.ly/2qN9vVq].

B.4 Other

- Shah, S. (2016), 'Percentile transformation algorithm Tech Note', Published on MathWorks File Exchange Community [available at http://bit.ly/2pPu4iC].

—